

COMPUTATIONAL CIVIL ENGINEERING 2004

F. Paulet-Crainiceanu, C. Ionescu, H. Barbat

editors



EDITURA SOCIETĂȚII ACADEMICE "MATEI - TEIU BOTEZ"

Iasi, 2004

International Symposium

“Computational Civil Engineering 2004”

Iași, România, June 11, 2004



F. Paulet-Crainiceanu, C. Ionescu, H. Barbat
Editors



EDITURA SOCIETĂȚII ACADEMICE "MATEI-TEIU BOTEZ"
Iași, 2004

"Computational Civil Engineering. 2004", International Symposium
Iași, România, June 11, 2004
F. Paulet-Crainiceanu, C. Ionescu, H. Barbat
Editors

Descrierea CIP a Bibliotecii Naționale a României

Computational civil engineering - 2004 / ed.: Fideliu

Păuleț-Crăiniceanu, Constantin Ionescu, Horia Barbat. -
Iași : Editura Societății Academice "Matei-Teiu Botez",
2005

Bibliogr.

ISBN 973-7962-50-8

I. Păuleț-Crăiniceanu, Fideliu (ed.)

II. Ionescu, Constantin (ed.)

III. Barbat, Horia (ed.)

004:624

Table of Contents

1. Păuleț-Crăiniceanu, F., Ionescu, C. Methods and Achievements in Computational Civil Engineering	3
2. Bonett, R., Barbat, Al.H., Pujades, L.G., Lagomarsino, S., Penna, A. Capacity Curves for Unreinforced Masonry Buildings	11
3. Lantada, M.N., Pujades, L.G., Barbat, Al.H., Seismic Risk Scenarios for Barcelona, Spain	22
4. Petzek, E., Băncilă, R., Kosteas, D. The Determination of Crack Growth Rate for Old Riveted Steel Bridges	35
5. Bakule, L., Paulet-Crainiceanu, F., Rodellar, J. Mitigation of Seismic Vibrations of a Benchmark Cable Bridge Using Structural Active Control	45
6. Dima, A., Răcănel, I.,R. Checks of the Tubular Joints and Structural Elements for the “Romexpo” Pavilion Dome	55
7. Răcănel, I.,R., Dima, Al. Dynamic Analysis of the “Romexpo” Pavilion Dome Using a 3D Finite Element Model	64
8. Răcănel, C. Asphalt Mixtures Creep Susceptibility	72
9. Bârsan, E., Ignat, C. The Compact Method from Analysis of Water Distribution Systems	80
10. Bârsan, E., Ignat, C. Monitoring of Water Distribution Systems for Minimization of Energetic Costs	87
11. Bârsan, E., Ignat, C. Analysis of Water Distribution Networks by a Technical-Economic Method	95
12. Bârsan, E., Ignat, C. Development of a Existed Water Supply Network Methodology for Sizing and/or Rehabilitation of Water Distribution Systems	110
13. Bârsan, E., Ignat, C. Methodology for Sizing and/or Rehabilitation of Water Distribution Systems	120
14. Bârsan, E., Ignat, C. Simulation of Water Distribution Systems on Extended Period of 24 Hours	132
15. Nicuță, A., Ursache, F. Considerations Regarding the Reological Analysis of the Failure Mode, Specifically to Clays	140
16. Vlad, I., Blagoi, O. Alternative Approaches for Analysis of Elastic Thick Plates Resting on Pasternak and Winkler Foundations	145
17. Budescu, M., Ciongradi, I., Roșca, O. Theoretical and Experimental Studies of a Class of Steel Roof Profiles	155

18. Comisu, C.C., Ionescu, C. Metodologia de investigare analitico-experimentală și de identificare în concept dinamic a tablierelor de poduri. Studii de caz (in Romanian)	166
19. Diaconu, D., Ibanescu M. Analysis of a Multilayered Wall to Fire Action Based on Thermal Insulation Criterion	179
20. Vrabie, M. Issues Regarding the Effect of the Supporting Medium on the Bending Vibrations of Beams	186
21. Babor, T.D., Rotaru, A. Fault Trees	194
22. Babor, T.D., Rotaru, A. Unitary Methodology of Investigation	202
23. Roșca, O. On the Solution of the Stiff Systems of Equations	210
24. Chițan, V.E., Ștefan, D. Inelastic Time–History Analysis of One Degree of Freedom System under Seismic Motions	221
25. Rotaru, A., Babor, T.D. Deformability Analysis of Rock for Homogeneous and Discontinuous Multi-Crack Masses	229
26. Rotaru, A., Babor, T.D. Stability Coefficients versus Stability Evaluation Using Finite Element-Neural Network Hybrid Algorithms for Earth Slopes Analysis	242
27. Luca, S., Pastia, C., Florea, V. Design Criteria of Tuned Mass Damper for Vibration Control of Multi-Degree of Freedom Structures	243
28. Pastia, C., Covatariu, D., Luca, S.G. Design Decisions of a Control System for a Single-Degree-of-Freedom Structure from Energy Balance Point of View	251
29. Köllő, G., Ciotlăuș, M. Probleme specifice privind stabilitatea căii fără joante (in Romanian)	259

METHODS AND ACHIEVEMENTS IN COMPUTATIONAL CIVIL ENGINEERING

Fideliu PAULET-CRAINICEANU¹, Constantin IONESCU²

Abstract

In Civil Engineering as in all other engineering domains, Computational Civil Engineering plays an important role. This is shown by the large diversity of computations involved in solving common and advanced problems that arise in this area of human activity. The International Symposium “Computational Civil Engineering 2004” is an example of the importance researches, scholars and engineers give to the use of computers and computer methods in their professional life. This paper is mainly a review of the work involved in the papers submitted to the above mentioned symposium. The spectrum of this work is so large that the review could only partially reflect the tremendous and dynamical labor included in contributions to the symposium.

1. Computational Civil Engineering, Infrastructure of Civil Engineering Work

The topics involved by Computational Civil Engineering show large diversity. The papers submitted to the International Symposium “Computational Civil Engineering 2004” are covering almost all the subdomains in Civil Engineering and, therefore, implies that Civil Engineering is using computational work as an important part of its infrastructure for research and practical operation.

In [1], a group of scientists, R. Bonett, Al.H. Barbat, L.G. Pujades, S. Lagomarsino and A. Penna, study unreinforced masonry buildings typical for Eixample district of Barcelona. They develop a structural analysis procedure based on finite element non-linear macro-elements for describing masonry walls. Using Monte-Carlo simulations for obtaining mechanical proprieties of the materials, seismic capacity curves of the studied buildings have been issued. Two seismic demand spectra were employed: one deterministic, corresponding to the greater earthquake expected in the city of Barcelona, and another having 10% probability of being exceeded in a period of 50 years. A computer program, TreMuri, is the tool for modeling the building in the case-study. The generated capacity curves generally correspond to the first mode of vibration of the structure, based on the assumption that the fundamental mode of vibration contains the predominant response of the structure. Conclusions are revealing that the unreinforced masonry buildings of the studied district of Barcelona could suffer heavy damage for a

¹ Assoc. Prof., Ph.D., “Gh.Asachi” Technical University of Iasi, fideliu@ce.tuiasi.ro

² Prof., “Gh.Asachi” Technical University of Iasi cionescu@ce.tuiasi.ro

ground motion with characteristics similar to those of the seismic demand scenarios expected. Therefore, the authors are recommending the retrofit of buildings of the analyzed type.

The researches presented in [2] are in the line with the previous one and is studying possible scenarios for the city of Barcelona in case of major earthquakes. The authors, N. Lantada, L.G. Pujades¹ and A.H. Barbat, are developing an integrated Geographical Information System (GIS) application that estimates the risk scenarios. Two main methodologies are adopted: one is based on European Macro-seismic Scale (EMS-98) and vulnerability indices, and the second one is based on fragility curves. A beta distribution describes the damage probability distribution of the vulnerability index associated to each building. The presented application is paving the way for emergency plans of the city by mapping the buildings, census areas, neighborhoods and districts of Barcelona for hazard, vulnerability and damage. These colored maps show a six-grade scale of possible degradations: no damage, slight damage, moderate damage, substantial to heavy damage, very heavy damage and destruction. The presented Figures reveal that in Zone II of the city more than 50% of high rise buildings could suffer moderate to severe damages.

E. Petzek, R. Băncilă, and D. Kosteas, [3], deal with the problem of safety and remaining service life assessment for the existing bridges. More specific, the researches are focused on the behavior of the old riveted steel bridges. A new approach, based on fracture mechanics principles, is proposed for determination of the crack growth. This method offers the possibility for establishing the rate of propagation of cracks and, consequently, the time period in which the structure is still safe for use. Two steps are involved: based on failure assessment diagrams, the final acceptable dimensions of defects are obtained and, based on fatigue evaluation analysis, the remaining service life (number of cycles remaining until fracture takes place) of the structure is computed. Experimental tests on an old riveted bridge over Mures River were conducted and allowed the validation of the theory.

Structural active control is the topic of [4]. The authors, L. Bakule, F. Păuleț-Crăiniceanu, and J. Rodellar, present a methodology for controlling structure based on optimal control theory. Matrices from the index to be minimized are deduced from energy considerations. Reduced controller is determined based on gramians. At the same time the minimization index suffer the same kind of reduction as the controller. A flowchart is showing the main steps for obtaining the feedback matrix. The application of the method is an a cable-stayed bridge that is the subject for an international benchmark. Computations are showing good results for the method.

Paper in reference [5] proves that even with the help of modern computational methods, the analysis of steel structures remains very complex. In particular, the building of "ROMEXPO" Pavilion Dome in Bucharest, Romania, is investigated.

The finite element model is composed from 32 steel truss semi-arches with triangular cross section and also 32 shell elements. Two main combinations of actions are used. The authors, Al. Dima and I.R. Răcănel, consider static actions as the dead load, wind action with both pressure and suction, and snow load with symmetrical and asymmetrical distribution. Then checks for resistance of the joints to compression/tension, penetration, and of the nominal stress are performed. Also stability checks are performed. Additional in-house software was used. The conclusions are showing that the allowable limit was not surpassed but, some elements are close to the buckling limit.

Dynamic analysis of the same dome from [5] is presented in [6]. I.R. Răcănel and Al. Dima, detail the data concerning this building raised between 1962 and 1964 after the dome roof has been destroyed by a snow storm in 1961. In-situ inspection was also performed in order to clarify details missing from the available documentation for this 93.5 m diameter building. The finite element model has a total of 7536 joints, 15360 truss elements and 32 shell elements. Dynamic analysis was performed in two forms: eigenvector analysis and Ritz-vector analysis. Authors conclude about the plus of stiffness introduced by some added cables and concrete structure. It is also revealed that the third mode of vibration is a general torsional one and the first two modes of vibration can play an important role in the seismic response of the studied structure.

The asphalt mixtures creep susceptibility of two types of tested asphalts is determined through the use of p ratio and recovery coefficient by C. Răcănel in reference [7]. The static uniaxial compression creep test type is envisioned. Samples from BA16 classical asphalt mixture and MASF16 stone mastic asphalt are employed. Temperature from 23 to 60 degrees Celsius, a pressure of 174 kPa and a compression-decompression 60 minutes time were used. Results show the dependence of the strain on the temperature. However, it is underlined that the viscoelastic response of the material is non-linear and also that p ratio and recovery coefficient are indicators for establishing the quality of asphalt mixture.

A series of six papers [8-13] written by the same authors, E. Bârsan and C. Ignat, demonstrates how prolific a cooperation between an engineer and a mathematician is. The first paper, [8], presents a method for the analysis of the water distribution systems. Three main steps are followed: construction of the node-pipeline incidence matrix (NPIM), obtaining the initial distribution of flow rates by Gauss-Jordan method, and quasi-orthogonalization of the NPIM for application of the Newton-Raphson procedure that corrects the flow rates. An 18 nodes water supply network is used for application of the method.

In [9], a computer assisted monitoring system for water distribution systems is exposed. Optimization of the costs for pumping is related to the supplying flow rate and the pumping head. The method establishes the pumping flow rate by minimization of maximum flow rate, hydraulic calculation of the network and

setting of the pumping head by minimization of reference piezoelectric head. The application considers a system composed from pumping station, network with 22 nodes and an inflow/draining tank.

Water distribution network analysis is also the topic for paper [10]. This time, a combined economical and technical approach is used for dimensioning the network. Mathematically, this is transposed into a non-linear programming problem employing Lagrange procedure for determining the flow rates and head losses, i.e. a summing of Kirchhoff's law and economic conditions imposed to the network. The exemplification of the method is done on a eight nodes water supplying network.

The case of updating existing water networks is the main topic of paper [11]. The method consists in the assurance of energy conservation on independent loops. Corrections to the rate flow and dimensioning are iteratively performed. A computer program is developed and an example on a network is shown.

In [12], a nonlinear iterative genetic algorithm for rehabilitation and dimensioning of water distribution systems is proposed. The optimization is done for an objective function changing according to the imposed restrictions. Two computer program versions based on that algorithm are issued. A version is accepting modifications of the pipes and the other take into consideration the possibility of doubling the pipes. The presented methodology permits automatic specification of modification or replacement that can be done and the evaluation of costs for the proposed solutions. A study case with an 18 nodes water network is illustrating the strategy.

E. Bârsan and C. Ignat, in [13], are dealing with the problems involved by the analysis of behavior of water network system during a 24 hour period. This analysis is permitting the monitoring of hydraulic parameters in the distribution network, tanks and pumps. The simulations establish hourly the inflow or outflow in or from tanks, volume and water level in tanks, flow rates and heights of pumping stations, pipeline flow rates and node piezometric heads between maximum and minimum consumption level for every hour of the day. An application with 22 nodes, two pump stations and a water tank compounding a water network system is presented.

The reference [14] is treating reological aspects of the failure mode specific to clays. The authors, A. Nicuță and F. Ursache, are mainly stressing on the dependency of clays resistance on time, or long lasted time resistance. Experimental work is employed. Tests with length of 6 months and 1 year were performed on three different clays at a constant stress, for determination of the time to failure. Conclusions are showing that the proposed methodology is effective.

The effects of shear and normal pressure in plates is studied in the paper [15]. The authors, I. Vlad and O. Blagoi are dealing with numerical solutions for the problem of thick plates resting on a bi-modulus Pasternak subgrade and compare them with solutions obtained by Finite Element Analysis and with solutions for the case of a plate resting on Winkler

foundation. The application performed presents the particular solutions for a rectangular plate with clamped boundary, for the case of a hinged rectangular plate and for a semi-elliptical plate. Conclusions show that all the models used have some domain of applicability and researchers or engineers should carefully chose a model in function of the parameters discussed in this work.

M. Budescu, I.P. Ciongradi and O.V. Roșca study the behavior of three steel sheet made roof profiles under gravity loads, [16]. Their analysis is mainly experimental and is carried out observing codes specifications. A special designed stand was buit for this study. The testing procedure consisted of several repeated loading-unloading cycles. The loading-unloading cycles pointed out the lack of permanent strain for maximum displacements below specific limits. One of the specimen from each tested profile class was loaded until collapse. For some profiles, local buckling of the edge ribs was the cause of collapse. As a consequence, the assembly technique of the steel sheet edges becomes very important, as is pointed out by conclusions.

C. C. Comisu, C. Ionescu propose a combined analytical and experimental methodology for investigating the bridges decks. The methodology is integrating also the concept of dynamical identification of bridges decks and can be applied to old and new bridges, too. The main point is to experimentally obtain the dynamic characteristics of the bridges and, based on them, important judgments on the structural state can be withdrawn. At the same time, prediction on the structure’s evolution can be issued. Analytical work is used for setting the experimental, *in-situ*, work. A case study, on a bridge with damaged supports, is employed for testing the methodology.

A non-stationary analysis of the conductive heat transfer through Finite Element Method is the topic of a paper, [18], written by D. Diaconu and M. Ibanescu. A computer program was made for this type of analysis, based on step by step direct integration technique solver. The studied case is of a non-structural wall exposed to fire. The wall consists of two layers of glass fiber reinforced plaster and, between them, a mineral wool layer. The research establishes the evolution of temperature inside the wall, if a fire occurs at one side. All the scenario is corresponding to a ISO standard. For the wall in study, an important reserve of temperature is found.

M. Vrabie is presenting results from researches conducted on the effect of the supporting medium on the bending vibrations of beams, [19]. It is observed that vibrations of beams laid on Winkler elastic medium are significantly influenced by a series of characteristics of the support-medium. Variation of those characteristics lead to a differential equation of the deformed axis with variable coefficients. Therefore numerical solutions, using Galerkin approach for Finite Element Method is proposed. Conclusions are showing that, from engineering practical point of view, results with good approximations can be obtained. Also, it is stated that the proposed methodology can be extended to vertical members of buildings’ foundations.

In order to analyze the faults that are affecting the performance of buildings, D. Babor and A. Rotaru propose the fault tree concept, [20]. This concept is described along with diagnosis tree and, for practical application, an expert system including fault tree philosophy is employed. Therefore the authors are showing the elements of this expert system recommended for diagnosis of buildings states: knowledge base, fuzzy logic manager, explanation mechanism, user/computer interface.

The same authors as above are dealing with investigation methodology concepts envisioning a unified approach in defect and degrading dynamic identification and prediction [21]. After presenting the procedure for investigation and detecting any *symptoms* of anomalies, the work is focused on cause determination. The last operation has to answer to questions as: what caused the defect? (or technique-oriented descriptions); who caused the defect? (or liability-oriented descriptions); how did the defect originate? (or system-oriented descriptions). An example about moisture problems in buildings is illustrating the procedure. Next, the paper is detailing the procedure's next steps: origin of causes and decay process and maintenance. Conclusions point out that the presented methodology can be efficient in preventive maintenance planning.

Numerical methods in Engineering constitute the domain for the paper [22]. The author, O. Rosca is analyzing the complexity of efficiency involved by solving *stiff* first order differential system of equations. A stiff system consists from two components: one with a fast dynamic behavior and the other with slow dynamic.. A generalization of the Runge-Kutta method (Rosenbrock method) and a generalization of the Bulirsch-Stoer method (Bader and Deuflhard extrapolation method) are explained. MATLAB and SIMULINK is used to model the application chosen for exemplification and comparisons. This application refers to a single degree of freedom dynamic system in free damped motion. Results and conclusions show the importance of using appropriate solver for efficiency and convergence of solutions.

V.E. Chițan and D. Ștefan are dealing with complex parametrical non-linear response of structures under earthquake and dynamic loads, [23]. Parameters taken into account are: the type of action (eight seismic actions and sine action into the range 0.1 to 2.0s period), natural period (0.5 to 2.0 s), damping, hysteretic loop and so on. The presented results show non-linear displacements, velocity and acceleration time-history response diagrams for the single degree of freedom system. Also hysteretic damping-force and force displacements diagrams are shown and commented. Additional results for different types of response spectrums are presented.

In [24], A. Rotaru and T.D. Babor study the deformability of rock mass through the use of the Homogenized Multi-Crack Model. In this model all cracks are parallel and present in an isotropic and linear elastic medium. The effectiveness of the proposed model is estimated by applying a 2-Dimensional Displacement Discontinuity Method. The paper presents the way the constraint stress and effective compliance is estimated. Also, a theoretical background of the failure simulation of rock masses by discontinuous deformation analysis is shown. Conclusions underline that the researched method is promising but still needs further improvements.

The same two authors, A. Rotaru and T.D. Babor, use the Finite Element Method and Neural Network for studying earth slopes stability. The paper firstly focuses on the problem of modeling mechanical systems with neural network and, in particular, to apply the method the soil mechanics. Details as training the neural network are revealed. Then the approach for including the neural network into the finite element method is presented. This hybrid method is then applied to soil and for the estimation of stability of earth slopes. The numerical example is an 10 m depth soil excavation. A mesh consisting of 250 nodes and 216 rectangular elements is used. The obtained results show good agreement with real cases and thus is validating the hybrid proposed method.

S. Luca, C. Pastia and V. Florea analyze the design criteria that lead to effectiveness of passive tuned mass dampers located in buildings subjected to seismic actions [26]. For multi-degree of freedom systems, attachment of tuned mass dampers to structural system is mathematically expressed both in classical and state space form. Then an application on a three degree of freedom structure is studied. Frequency response and seismic response of the structure show important mitigations due to passive devices. However, as conclusions underline there are actions that can lead to equal or even to greater responses.

Reference [27] is dealing with an energy analysis for passive, semi-active and active controlled structural systems. The authors, C. Pastia, D. Covatariu and S.G. Luca firstly present the way the energy balance takes place into structures with control devices under seismic loads. A case study for a simple single degree of freedom system structural model submitted to El Centro earthquake is presented. Decomposition of time-history responses energy is showing and commented in detail. The computational tool used for analysis is MATLAB and SIMULINK. Conclusions are showing that implementation of passive, semi-active or active control into a structure is a complex problem that involves many parameters and experimental work should also be employed.

In [28], G. Kollo and M. Ciotlăuș are studying the jointless railway track behavior on high temperatures. They show that, in the rail tensions could appear because of high temperatures and the result is a phenomenon with spontaneous character and damaging effects on the safety of the circulation. The resistance of the track at transversal displacement and the rail stability in the horizontal plane especially in curves are analyzed. Calculus of involved parameters and examples are illustrating the complexity of research methodology.

2. Conclusions

Computations and computational methods in Civil Engineering are important aspects of Civil Engineering domain. This determines that the International Symposium “Computational Civil Engineering 2004”, the second in a row of scientific meetings on this topic, to exhibit its necessity as a tool for exchanging knowledge and for getting together specialists involved in computation and use of computers for solving their problems.

References (11 pts bold, 12 pts before, 6 pts after)

1. Bonett, R., Barbat, Al.H., Pujades, L.G., Lagomarsino, S., Penna, A., Capacity Curves for Unreinforced Masonry Buildings, *Proceedings of the International Symposium “Computational Civil Engineering 2004”, Iași, Romania, June 11, 2004*, editors: F. Paulet-Crainiceanu, C. Ionescu, H. Barbat, Academic Society “Matei-Teiu Botez” Iasi Publishing House, 2004, ISBN 973-7962-50-8, pp.11-21
2. Lantada, M.N., Pujades, L.G., Barbat, Al.H., Seismic Risk Scenarios for Barcelona, Spain, *idem*, pp.22-34
3. Petzek, E., Băncilă, R., Kosteas, D., The Determination of Crack Growth Rate for Old Riveted Steel Bridges, *idem*, pp.35-44
4. Bakule, L., Paulet-Crainiceanu, F., Rodellar, J., Mitigation of Seismic Vibrations of a Benchmark Cable Bridge Using Structural Active Control, *idem*, pp.45-54

5. Dima, A., Răcănel, I.R., Checks of the Tubular Joints and Structural Elements for the “Romexpo” Pavilion Dome, *idem*, pp.55-63
6. Răcănel, I.,R., Dima, Al., Dynamic Analysis of the “Romexpo” Pavilion Dome Using a 3D Finite Element Model, *idem*, pp.64-71
7. Răcănel, C., Asphalt Mixtures Creep Susceptibility, *idem*, pp.72-79
8. Bârsan, E., Ignat, C., The Compact Method from Analysis of Water Distribution Systems, *idem*, pp.80-86
9. Bârsan, E., Ignat, C., Monitoring of Water Distribution Systems for Minimization of Energetic Costs, *idem*, pp.87-94
10. Bârsan, E., Ignat, C., Analysis of Water Distribution Networks by a Technical-Economic Method, *idem*, pp.95-109
11. Bârsan, E., Ignat, C., Development of a Existed Water Supply Network Methodology for Sizing and/or Rehabilitation of Water Distribution Systems, *idem*, pp.110-119
12. Bârsan, E., Ignat, C., Methodology for Sizing and/or Rehabilitation of Water Distribution Systems, *idem*, pp.120-131
13. Bârsan, E., Ignat, C., Simulation of Water Distribution Systemso Extended Period of 24 Hours, *idem*, pp.132-139
14. Nicuță, A., Ursache, F., Considerations Regarding the Reological Analysis of the Failure Mode, Specific to Clays, *idem*, pp.140-144
15. Vlad, I., Blagoi, O., Alternative Approaches for Analysis of Elastic Thick Plates Resting on Pasternak and Winkler Foundations, *idem*, pp.145-154
16. Budescu, M., Ciongradi, I., Roșca, O., Theoretical and Experimental Studies of a Class of Steel Roof Profiles, *idem*, pp.155-165
17. Comisu, C.C., Ionescu, C., Metodologia de investigare analitico-experimentală și de identificare în concept dinamic a tablierelor de poduri. Studii de caz, *idem*, pp.166-178 (in Romanian)
18. Diaconu, D., Ibanescu M., Analysis of a Multilayered Wall to Fire Action Based on Thermal Insulation Criterion, *idem*, pp.179-185
19. Vrabie, M., Issues Regarding the Effect of the Supporting Medium on the Bending Vibrations of Beams, *idem*, pp.186-193
20. Babor, T.D., Rotaru, A., Fault Trees, *idem*, pp.194-201
21. Babor, T.D., Rotaru, A., Unitary Methodology of Investigation, *idem*, pp.202-209
22. Roșca, O., On the Solution of the Stiff Systems of Equations, *idem*, pp.210-220
23. Chițan, V.E., Ștefan, D., Inelastic Time–History Analysis of One Degree of Freedom System under Seismic Motions, *idem*, pp.221-228
24. Rotaru, A., Babor, T.D., Deformability Analysis of Rock for Homogenous and Discontinuous Multi-Crack Masses, *idem*, pp.229-235
25. Rotaru, A., Babor, T.D., Stability Coefficients Versus Stability Evaluation Using Finite Element-Neural Network Hybrid Algorithms for Earth Slopes Analysis, *idem*, pp.236-242
26. Luca, S., Pastia, C., Florea, V., Design Criteria of Tuned Mass Damper for Vibration Control of Multi-Degree of Freedom Structures, *idem*, pp.243-250
27. Pastia, C., Covatariu, D., Luca, S.G., Design Decisions of a Control System for a Single-Degree-of-Freedom Structure from Energy Balance Point of View, *idem*, pp.251-258
28. Kollo, G., Cioflăuș, M., Consideratii privind stabilitatea caii sudate fara joante, *idem*, pp. 259-266 (in Romanian)

CAPACITY CURVES FOR UNREINFORCED MASONRY BUILDINGS

Ricardo Bonett¹, Alex H. Barbat², Luis G. Pujades², Sergio Lagomarsino³ and
Andrea Penna⁴

Abstract

The area of the Eixample district of Barcelona has an important historical, architectural and cultural value and covers approximately 750 hectares of the city. Most of its residential buildings have a unreinforced masonry structure, are high, have an average age of 100 years and have been designed and built without the consideration of any earthquake resistant criterion. In addition to this, they have some particular features, typical for the constructive techniques of the city at that time, which have been identified as potential damage sources. To evaluate the expected seismic performance of these buildings, a typical six-story unreinforced masonry building was modeled. The building was designed and constructed in 1882 and contains details which are typical of that constructive period of the Eixample district. The dynamic behavior was studied by means of a structural analysis procedure which uses macro elements to model the masonry panels. This model describes the nonlinear in-plane mechanical behavior of the panels and assesses the expected damage in masonry buildings due to earthquakes. Monte Carlo simulation has been used to take into account the uncertainties in the mechanical properties of the materials. In this way, the mean seismic capacity curves of the building and the corresponding standard deviations have been obtained. The results obtained will be used in studying the seismic performance of the unreinforced masonry buildings of the Eixample District.

1. Introduction

The emblematic zone of the central district of Barcelona, Spain, denominated “Eixample”, was designed in the middle of the nineteenth century. This urban area has an important historical, architectural and cultural value and covers approximately 750 hectares of the city. The most representative typology of this district corresponds to unreinforced masonry buildings (URM) which are incorporated into numerous almost square blocks, denominated “islands”. The construction of these buildings took place between 1860 and 1940, with 25 buildings in average for each block. They were designed only to vertical static loads, without any consideration of seismic design criteria, because they were built

¹ Professor, National University of Colombia, Medellin, Colombia

² Professor, Technical University of Catalonia, Barcelona, Spain

³ Professor, University of Genoa, Genoa, Italy

⁴ Research Professor, University of Pavia, Italy

previous to the first seismic design code of Spain. All of the existing URM buildings in this area already have exceeded their life period and only one small part of them are new, reinforced concrete buildings.

The slabs of these buildings are wooden, or are made of reinforced concrete or steel (according to the building period) with ceramic ceiling vaults. Due to the greater height of the first floors of these buildings, almost all of them have soft first floors. Moreover, due to the need of bigger commercial areas in the first floors, cast iron columns were used instead of masonry walls, what reduces even more the stiffness of the buildings. Therefore, it can be supposed intuitively that the seismic vulnerability of these buildings is high.

Recently researchers of the Seismological Section of the Cartographic Institute of Catalonia (ICC) re-evaluated the seismic hazard of Barcelona, approaching the problem from two points of view: one deterministic and the other probabilistic [1]. Two types of demand spectra were generated: 1) one that corresponds to the greater earthquake expected in the city (determinist case) and 2) other that corresponds to the earthquake having a 10 percent of probability of being exceeded in a period of 50 years, that is, a seismic hazard scenario with a return period of 475 years (probabilistic case). These two demand spectra supposed an important contribution to the definition of the seismic hazard and require the evaluation of the seismic performance of the URM buildings for this new form of defining the seismic demand. The N2 method proposed by Fajfar [2] is used with this aim. Starting from the obtained spectral displacement demand and using the damage states proposed by Calvi [3] for URM structures, the damage degree and consequently the building performance level are determined.

The mechanical properties of the materials used to build the structures of the Eixample were determined empirically during many years and therefore they have associated a high uncertainty. In the particular case of the building chosen to represent this typology, only the expert's opinion was available. In order to overcome this lack of information, the Monte Carlo's simulation technique is used. The main parameters defining the mechanical characteristics of the model are defined as random variables. These variables are generated starting from their probability distribution functions, which are characterized by means of a mean value and a covariance. This simulation process allows describing the behavior of a group of buildings with similar geometric characteristics. The simulation process allows studying the influence of the uncertainties in the structural parameters on the evaluation of the seismic performance level.

2. Structural typology

The typical Eixample URM building which has been studied has six stories, brick walls of 30 cm for the façade walls and 15 cm in the other walls. The two first floors have metallic beams and ceramic ceiling vaults simply supported on metallic

main beams and cast iron columns. Rubble is placed on the upper part of the vaults and above it there is a lime mortar layer and the pavement. For the other stories, the slab is made of wooden beams which support the ceramic ceiling vaults. At the basement and ground floors, the masonry bearing walls of the upper part of the structure are supported on metallic main beams which, in turn, are supported on cast iron columns. The columns are supported on a die, which is supported on the masonry foundation, being this a type of connection a very deformable one.

In the Eixample zone there are 8989 buildings, 6160 (that is a 69%) corresponding to URM buildings with the same typology as the described one. Therefore, this six-story URM building constructed in 1882, with details which are typical for that constructive period in the Eixample district, has been chosen for a detailed study aimed to provide information for the evaluation of the seismic behavior of all the buildings of the district having this typology.

The distribution in plant of the building is approximately rectangular (18.9 m × 24.5 m) and it has a central squared patio and two lateral ones. In elevation, the building shows certain irregularities, such as: cast iron columns at the ground floor, masonry bearing walls directly supported on metallic main beams, which, in turn, are supported on the mentioned columns. Therefore, there is a considerable variation of the stiffness with the height of the structure, which reduces the seismic capacity of the structure and can produce a mechanism of collapse due to the presence of a soft floor.

3. Model of the building

TreMuri program has been used for modeling the considered building type. The program was developed by Galasco, Lagomarsino and Penna [4], it is based on a macro elements model to represent the masonry walls and considers the structural damage by means of constitutive models that have been calibrated from the observed dissipation mechanisms in real cases. The model considers the overturning phenomenon, which is modeled by an elastic contact at both sides of the macro element. The shear cracking is described through a component of an inelastic deformation which takes into account the damage and friction effects. The global behavior of the masonry walls, considering holes such as windows and doors, is obtained by means of an adequate assembling of the macro elements, using masonry piers as well as lintels.

The macro elements model is based on an assemblage of shear walls connected each to other and with their corresponding floor slab. The experience shows that shear and overturning damages are localized, usually, at certain wall zones, while other zones remain almost undamaged. This observation permits to model walls by using deformable macro elements that can suffer damages and rigid elements which represent the wall parts which remain undamaged.

Figure 4 shows the three substructures in which a macro element is subdivided: A lower layer ① and an upper one ③, in which the bending and axial effects are predominant. Finally, a central part ② of the element which suffers shear deformations and does not show any evidence of axial or bending deformations. A complete cinematic model should take into account the three degrees of freedom for each node i and j , that is: the axial displacement w , the horizontal displacement u and the rotation φ . There are two degrees of freedom for the central zone: the axial displacement δ and the rotation ϕ (see Figure 1).

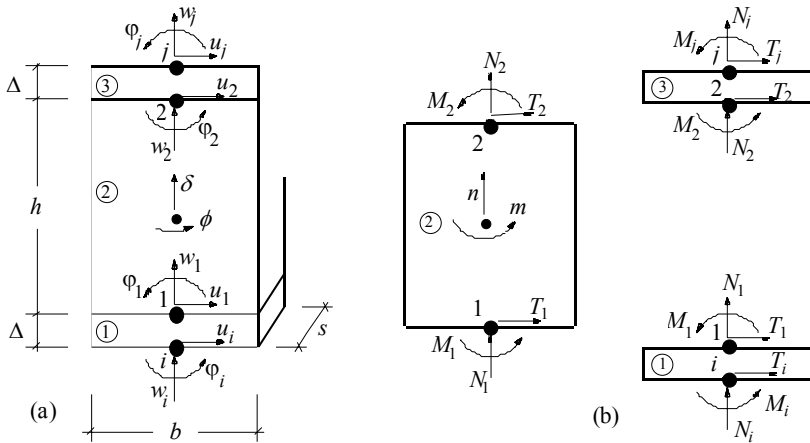


Figure 1. Cinematic model for the macro element [6].

Thus, the kinematics is described by an eight degrees of freedom vector, $\mathbf{a}^T = \{u_i, w_i, \varphi_i, u_j, w_j, \varphi_j, \delta, \phi\}$, which is obtained for each macro element. It is assumed, for this model, that the extremities have an infinitesimal width ($\Delta \rightarrow 0$).

The overturning mechanism, which may occur due to the fact that the material does not resist traction stresses, is modeled by means of a lateral elastic contact between the interfaces ① and ③. The constitutive equations between the kinematics variables w , φ and the correspondent static quantities n and m are linear and uncoupled until the limit condition $m/n \leq b/6$, when the cross section is smaller than the entire zone subjected to compression. The following equations are obtained for substructure ①:

$$N_i = kA(\delta - w_i) + N_i^* \quad (1)$$

$$M_i = \frac{1}{12} kAb^2(\varphi_i - \phi) + M_i^* \quad (2)$$

where $A = s \cdot b$ corresponds to the transversal section of the panel. The inelastic contribution N_i^* and M_i^* are obtained from the unilateral perfect elastic contact condition:

$$N_i^* = \frac{-k \cdot A}{8|\varphi_i - \phi|} \left[|\varphi_i - \phi| b + 2(\delta - w_i) \right]^2 H \left(\left| e_i \right| - \frac{1}{6} b \right), \quad (3)$$

$$M_i^* = \frac{k \cdot A}{24(\varphi_i - \phi)|\varphi_i - \phi|} \left[(\varphi_i - \phi) b - (\delta - w_i) \right] \left[|\varphi_i - \phi| b + 2(\delta - w_i) \right]^2 H \left(\left| e_i \right| - \frac{1}{6} b \right) \quad (4)$$

where $H(\bullet)$ is the Heaviside's function.

The shear response of the panel is expressed considering a uniform shear deformation distribution $\gamma = (u_i - u_j) / h + \phi$ in the central part ② of the element and imposing a relationship between the kinematic quantities u_i , u_j , ϕ and the shear stress $T_i = -T_j$. The cracking damage is usually localized on the diagonals, where the displacement occurs along the joints and is described by an inelastic deformation component, which is activated when Coulomb's friction limit condition is reached. Starting from the effective shear deformation corresponding to layer ② and being G the elastic shear module, the constitutive equations can be expressed as [5]

$$T_i = \frac{GA}{h} (u_i - u_j + \phi h) + T_i^* \quad (5)$$

$$T_i^* = -\frac{GA}{h} \frac{c\alpha}{1+c\alpha} \left(u_i - u_j + \phi h + \frac{h}{GA} f \right) \quad (6)$$

where the inelastic component T_i^* takes into account the friction stress force f , opposite to the sliding mechanism, and involves a damage parameter α and a non-dimensional coefficient c which controls the inelastic deformation. According to this model, the friction plays the role of an internal variable governed by the following limit condition [5]:

$$\Phi_S = |f| - \mu \cdot N_i \leq 0 \quad (7)$$

where μ is the friction coefficient. These constitutive equations can describe the variation of the resistance of the panel due to changes in the axial forces $N_j = -N_i$. The damage and its effects upon the mechanical characteristics

of the panel are described by the damage variable α which increases according to failure criterion [4]

$$\Phi_d = Y(S) - R(\alpha) \leq 0, \quad (8)$$

where $Y = \frac{1}{2}cq^2$ is the rate of the energy release due to the damage; R is the strength function and $S = \{t \ n \ m\}^T$ is the internal force vector. Assuming R as a function increasing with α up to the critical value $\alpha_C = 1$ and decreasing for higher values of α , the model can describe the stiffness degradation, the strength degradation and pinching effect.

The complete constitutive model of the macro element can be expressed in the following finite way:

$$Q = Ka + Q^* \quad (9)$$

where $Q^* = \{T_i^* \ N_i^* \ M_i^* \ T_j^* \ N_j^* \ M_j^* \ N^* \ M^*\}$ contains the nonlinear terms which are evaluated by means of the equations of the evolution of the damage variable α and the friction f . Finally K is the elastic stiffness matrix:

$$K = \begin{bmatrix} GA/h & 0 & 0 & -GA/h & 0 & 0 & 0 & -GA \\ 0 & kA & 0 & 0 & 0 & 0 & -kA & 0 \\ 0 & 0 & kAb^2/12 & 0 & 0 & 0 & 0 & -kAb^2/12 \\ -GA/h & 0 & 0 & GA/h & 0 & 0 & 0 & GA \\ 0 & 0 & 0 & 0 & kA & 0 & -kA & 0 \\ 0 & 0 & 0 & 0 & 0 & kAb^2/12 & 0 & -kAb^2/12 \\ 0 & -kA & 0 & 0 & -kA & 0 & 2kA & 0 \\ -GA & 0 & -kAb^2/12 & GA & 0 & -kAb^2/12 & 0 & GAh + kAb^2/6 \end{bmatrix} \quad (10)$$

The nonlinear terms N^* and M^* are defined by means of the following equation:

$$N^* = N_j^* - N_i^*; M^* = -M_j^* - M_i^* + T_i^* h \quad (11)$$

The macro element shear model is a simplification of a more complex continuous model [6] whose parameters are directly correlated with mechanicals properties of the masonry elements. The parameters of the macro model should be considered as representative for an average behavior. In addition to its geometrical characteristics, the macro element is defined by using the following six parameters: The shear modulus G , the axial stiffness K , the shear strength of the masonry f_{vq_0} , the non-dimensional coefficient which controls the inelastic deformation c , the

global friction coefficient f and the factor β which controls the pinching. The last factor is defined both for columns and lintels.

4. Macro element model for the studied building of the Example

Figure 2 shows a three-dimensional view and in plant of the model used for the representative building of the Example. The model is defined by 8 walls in the x direction (walls M1 to M8) and 6 walls in the y direction (walls M9 to M14). Each wall has been modeled as an assemblage of piers, lintels and frame elements (in some cases) connected to the nodes of the model by means of rigid joints. All the nodes have 5 degrees of freedom (3 displacement components and 2 rotation components corresponding to the axes x and y) except the base nodes of the model. The slabs have been modeled as an orthotropic finite elements diaphragm, defined by 3 or 4 nodes connected to the three-dimensional nodes of each level. A main analysis direction is identified, which is characterizes by a Young’s modulus E_1 and the direction perpendicular to this one is characterized by a Young’s modulus E_2 . Figure 3 shows the macro element model corresponding to walls 1 and 2.

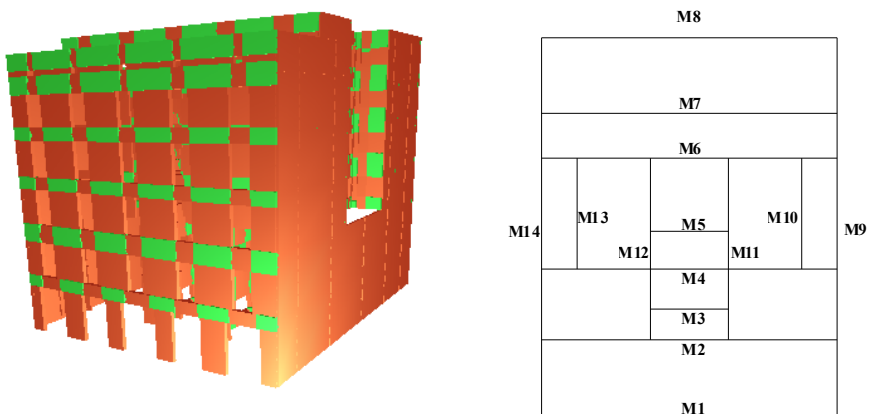


Figure 2. Three-dimensional model of the analyzed typical building of the Example.

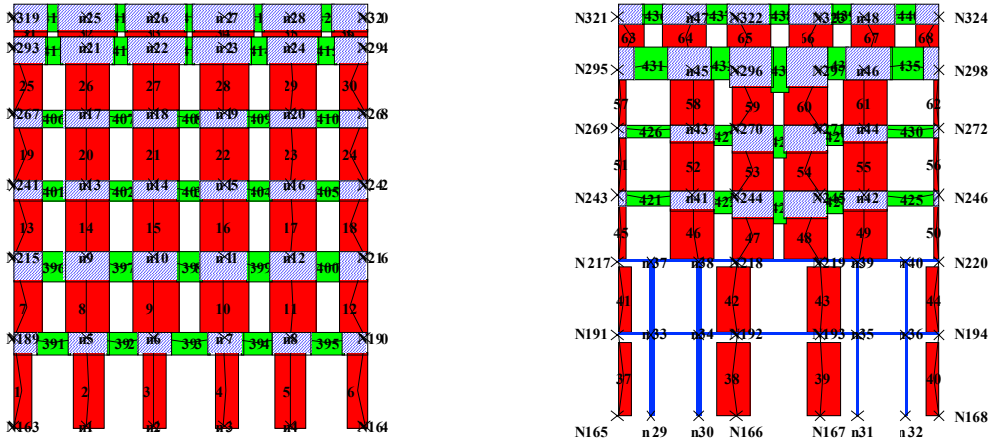


Figure 3. Macro element model for walls 1 and 2.

In order to analyze the constructive system of the URM buildings of the Eixample, it is necessary to have a good knowledge on the materials used in building their main elements. The bricks are the basic material of these buildings, being used widely in walls, stairs and slabs. The typical dimensions of the used bricks are of 30 cm \times 15 cm and with thicknesses varying between 3 cm and 11 cm and were until the beginning of the XXth century. Later, mechanical systems were used, what improved considerably their compactness. Lime mortar was used in the constructive process of the buildings of the Eixample. The wide use of this material is associated to constructive tradition, to consumption habits and, apparently, to its strength which was considering adequate at that period.

In this work, probability distribution functions, *pdf*, are used to define the most important parameters of the model. These functions are characterized by a mean value and a covariance. The definition of the mean value of each parameter has been defined using the opinion of experts, who provided sufficient information for defining a model. Nevertheless, due to the subjective character of this information, the main parameters have been considered as random variables with their uncertainties. The most important mechanical properties of the materials used in the analysis of the building of the Eixample are:

Masonry: Young's modulus of the wall $E = 2.10 \cdot 10^9$ N/m²; Shear modulus $G = 0.7 \cdot 10^9$ N/m²; Shear strength $\tau = 1.0 \cdot 10^5$ N/m²; Pinching factor for the piers $\beta_p = 0.5$; Pinching factor for the lintels $\beta_d = 0.05$.

Cast iron columns: Young's modulus $E_s = 2.10 \cdot 10^{11}$ N/m²; Specific weight $\gamma_s = 7850$ kg/m³.

Concrete columns: Young's modulus $E_h = 2.8 \cdot 10^9$ N/m²; Specific weight $\gamma_h = 2500$ kg/m³.

Slabs: Young’s modulus in the main direction $E_1 = 4.20 \cdot 10^9 \text{ N/m}^2$; Young’s modulus in the orthogonal direction $E_2 = 4.20 \cdot 10^7 \text{ N/m}^2$; Shear modulus $G = 0.4 \cdot 10^9 \text{ N/m}^2$.

Among all these characteristics, those shown in Table 1 have been defined as random variables because they have an important influence on the structural response of this one type of buildings. The normal probability distribution function has been used for the three variables, where the mean value of each parameter corresponds to the values proposed by experts. The covariance has been defined in such a way to cover the range of the possible values of each parameter.

Table 1. Probability distribution functions, median values and covariance of the random variables.

Parameter	fdp	Mean	Covariance
Young’s modulus E	Normal	$2.1 \cdot 10^9 \text{ N/m}^2$	0.3
Shear strength τ	Normal	$1.0 \cdot 10^5 \text{ N/m}^2$	0.3
Pinching factor β_p	Normal	0.5	0.3

5. Capacity curve

The capacity curve generally corresponds to the first mode of vibration of the structure, based on the assumption that the fundamental mode of vibration contains the predominant response of the structure. In the case of the analyzed building, a force distribution was established corresponding to the bending modal shape oriented along the y axis. Therefore, the walls 9, 10, 11, 12, 13 and 14 are involved in the analysis (see Figure 6). However, for the sake of simplicity, the loads only will be applied to the walls 9 and 14, which are really provides the greater stiffness in that direction.

The capacity curve is obtained performing a pushover analysis with this load pattern. This curve describes the relationship between base shear and the roof displacement of an equivalent single degree of freedom model, characterized by the period and the modal mass of the third mode of vibration. The response of the model of the typical URM building is defined by means of the capacity curves obtained by means of the Monte Carlo simulation technique. Thus, 100 samples for each variable were generated and a structural model was defined for each sample group. One hundred capacity curves were thus obtained. The advanced computational tool STAC [7] has been used in the simulation process. Figure 4 shows to the capacity spectra corresponding to the mean value and to the corresponding standard deviations. This type of the representation shows the sensitivity of these analysis methods to the uncertainties in the structural parameters.

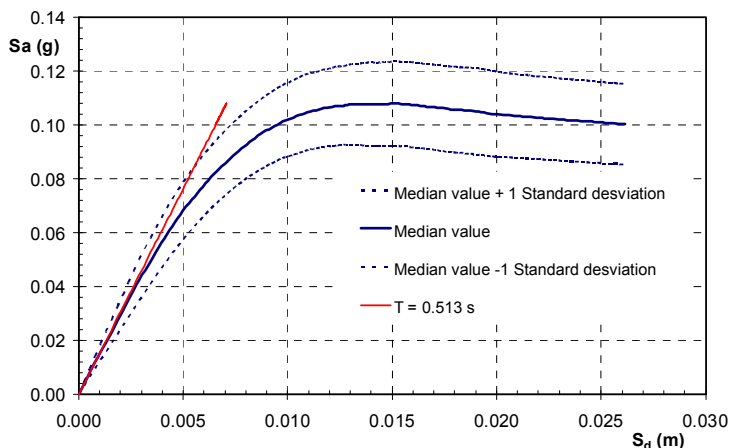


Figure 4. Median, median + 1σ , median - 1σ capacity spectra.

6. Conclusions

The seismic behaviour of an unreinforced masonry building, typical for the Eixample area of Barcelona, Spain, has been analyzed by means of a structural model which uses macro elements for the masonry panels. Monte Carlo simulation has been performed to take into account the uncertainties in the mechanical properties of the materials. Mean seismic capacity curves have been obtained for the building as well as their standard deviations. It can be stated that the unreinforced masonry buildings of the Eixample could suffer heavy damage for a ground motion with characteristics similar to those of the seismic demand scenarios expected in Barcelona. Therefore, the seismic behavior of the buildings having this typology should be retrofitted in order to improve their seismic performance.

Acknowledgments

This work has been partially sponsored by the Spanish Ministry of Science and Technology and with FEDER funds (projects: 2000-1740-C05-01/RIES, REN 2001-2418-C04-01 y REN2002-03365/RIES) and by the European Commission (RISK-UE Project, contract EVK4-CT-2000-00014).

References

1. Irizarry J., Goula X. y Susagna, T. Analytical formulation for the elastic acceleration-displacement response spectra adapted to Barcelona soil conditions. Technical Report, Instituto Cartografico de Cataluna, Barcelona, 2003.

2. Fajfar, P. and Gaspersic, P. “The N2 method for the seismic damage analysis of RC buildings”. *Earthquake Engineering and Structural Dynamics* 1996, 25: 23-67.
3. Calvi, M. C. “A displacement-based approach for vulnerability evaluation of classes of buildings, *Journal of Earthquake Engineering* 1999, 3 (3): 411-438.
4. Galasco, M., Lagomarsino, S. y Penna, A. TREMURI Program: Seismic Analyser of 3D Masonry Buildings, Universidad de Genoa, 2002.
5. Brencich, A. and Lagomarsino, S. “A macroelement dynamic model for masonry shear walls”, *Computer Methods in Structural Masonry-4*, edited by G.N.Pande, J. Middleton and B. Kralj, 1998.
6. Gambarotta, L. and Lagomarsino, S. “A microcrack damage model for brittle materials”. *International Journal Solids and Structures* 1993, 30: 177-198.
7. STAC program. “Stochastic análisis computational”, International Center for Numerical Methods in Engineering (CIMNE), Barcelona, 2002.
8. Lagomarsino, S. and Penna, A. “Guidelines for the implementation of the II level vulnerability methodology. WP4: Vulnerability assessment of current buildings. RISK-UE project: An advanced approach to earthquake risk scenarios with application to different European towns”, 2003.

SEISMIC RISK SCENARIOS FOR BARCELONA, SPAIN

N. Lantada¹, L. G. Pujades¹ and A. H. Barbat²

Summary

An integrated GIS application is developed by using ArcView GIS software (Lantada [1]), in order to estimate risk scenarios for different seismic intensities and response spectra in Barcelona, Spain. Two seismic hazard scenarios are considered. The risk analysis of individual residential buildings is performed according to two methodologies developed within the RISK-UE Project of the European Commission RISK-UE [2]. The first methodology is based on the EMS-98 building typologies (Grünthal [3]) and vulnerability indices, the second one is based on fragility curves. Both methods are applied to the most representative residential building typologies of Barcelona, namely unreinforced masonry and reinforced concrete buildings. In the vulnerability index method, the specific residential buildings of Barcelona are classified in different classes characterized by a similar seismic behaviour. An average vulnerability index is associated to each building typology. This index is refined on the basis of behaviour modifiers, linked to the number of stories, the year of construction, irregularity in height, the position of the building within the aggregate and differences in the height between adjacent buildings. The damage probability distribution, corresponding to the vulnerability functions, is described by a beta distribution, characterized by a mean damage grade parameter, which is related to the vulnerability index and intensity by means of a single empirical equation. In the fragility curves method, we use specific fragility curves and Damage Probability Matrices, developed for the same two buildings typologies. The ability of GIS tools to store, manage, analyse, and display the large amount of spatial and tabular data involved in this study allows mapping hazard, vulnerability and damage at different levels: buildings, census areas, neighbourhoods and districts. Selected results, consisting of scenarios obtained for the seismic risk of Barcelona, Spain, are finally given. These results will be useful for preparing emergency plans for the city.

1. Introduction

Barcelona is the political and economical capital of Catalonia and the second city of Spain after Madrid. It is situated on the northeast coast of Spain and it concentrates a big percentage of the total population of the region (1.505.325 inhabitants in 2001). The city is located in a moderate seismic hazard area

¹ Geotechnical Engineering and Geosciences Department, Technical University of Catalonia, Barcelona, Spain.

² Structural Mechanics Department, Technical University of Catalonia, Barcelona, Spain.

according to the Spanish seismic code (NCSE-02 [4]). However, most of its buildings were built between 1860 and 1940 with an unreinforced masonry structure, prior to the first Spanish Seismic Code, and show a high vulnerability. Moreover, it is well known today that the use of this structural typology is not adequate in a seismic area and that their seismic resistant retrofit is difficult and expensive.

Barcelona is organized into 10 districts: Ciutat Vella, Eixample, Sants-Montjuïc, Les Corts, Sarrià-Sant Gervasi, Gràcia, Horta-Guinardó, Nou-Barris, Sant Andreu and Sant Martí. Each district is subdivided into a number of neighbourhoods, with a total number of 38. All the available data have been integrated into a Geographic Information System (GIS), which in this case was ArcView GIS software (ESRI) (Lantada [1]). The data inventory for the buildings included in this study is composed of 63536 units (87 % of total buildings in the city), and information about their year of construction, structural typology and number of floors is available.

2. Seismic hazard

In spite of the fact that Barcelona is located in a moderate seismic zone, the seismic hazard of the city has been intensively studied in the last ten years. The seismic scenarios here considered corresponds to a deterministic case and represents the maxima historical earthquakes that affected Barcelona. The seismic action will be modelled in terms of EMS-92 intensity and by using response and demand spectra. Local effects are included in the final seismic hazard maps. The basis Intensity is increased by half intensity units while response or demand spectra are modified by means of amplification factors, which have been calculated by using the transfer functions developed by Cid [5]. Figure 1 shows the hazard maps. In the intensity case, the map reflects the proximity of the source, which is assumed to be at about 30 km. For the spectral values case the contribution of two historical earthquakes has been combined and we have considered average response spectra for each of the four zones (Irizarry [6]). The S_a values in the right side map in Figure 1 are the maxima S_a values which correspond to the period range between 0.1 and 0.22 s.

3. Vulnerability index methodology

Traditionally, the methodologies used in Italy by GNDT (National Group for Defence from Earthquake) identify the existing building typologies within the studied area and define their class of vulnerability (i.e. A, B, C) (Giovinazzi [7]). For each of vulnerability class, the relationship between intensity and damage may be defined by using Damage Probability Matrices (DPM). Alternatively, vulnerability functions, correlating damage factor (relationship between the cost of the repair intervention and the value of the structure) with

the Peak Ground Acceleration (PGA) of the expected seismic input, can also be used to obtain the damage (Corsanego [8]).

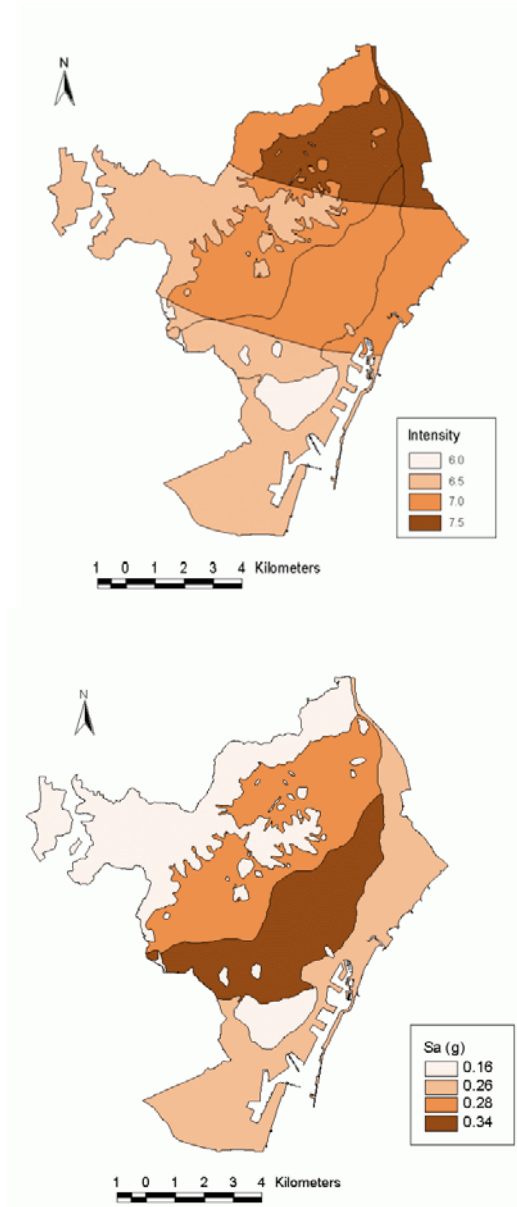


Figure 1. Deterministic seismic hazard scenarios, including local soil effects in intensity and spectral values terms S_a .

According to the GNDT methodology, the specific buildings of Barcelona are classified in different groups characterized by a similar seismic behaviour. All the buildings belonging to each typology are cast within the most probable class. The six vulnerability classes denoted by A to F are arranged in a decreasing vulnerability order, according to the EMS-98 intensity scale (Grunthal [3]). Vulnerability indices V_I are assigned to the most representative typologies of the city. Their values are arbitrary, since this index represents only a score that quantifies the seismic behaviour of the building. However the vulnerability index ranges between 0 and 1, being its value close to 1 for the most vulnerable buildings and close to 0 for the buildings with high seismic resistance (i.e. high-code structural design) (Giovinazzi [9]).

A first refinement of this average initial vulnerability index is performed by taking into account the age of the building. The building stock is grouped in 6 age categories by considering reasonable time periods in function of the existence of seismic codes in Spain and its level, as well as other specific construction features.

Further refinements of the vulnerability index V_I come from other behaviour modifiers, which are used to evaluate a global vulnerability index of each building, as follows:

$$V_I^{building} = V_I^{class} + \sum_{j=1}^n Vm_j \quad (1)$$

where V_I^{class} is the vulnerability index corresponding to the category of the building, Vm_j is a vulnerability factor or a behaviour modifier and $V_I^{building}$ is the final vulnerability index of the building. These Vm_j modifiers in equation (1) are different for isolated and aggregate buildings.

For isolated buildings we consider the following 4 modifiers: number of floors, irregularity in height, length of the façade and state of preservation. For building in aggregates we take into account the effects due to the different heights of adyacent buildings and the effects due to the position of the building in the aggregate (i.e. corner, header, or intermediate)

Concerning the damage, the methodology recognizes a no-damage state, labelled as *None* and five damages states, termed as *Slight*, *Moderate*, *Substantial to Heavy*, *Very Heavy* and *Destruction*. A sort of mean damage grade (μd) permits to completely characterize the expected damage for a building, known its vulnerability and for a given intensity. Equation (2) relates μd , intensity and the vulnerability index.

$$\mu_D = 2.5 \left[1 + \tanh \left(\frac{I + 6.25 \cdot V_I - 13.1}{2.3} \right) \right] \quad (2)$$

Damage probability matrices, can be then easily obtained by assuming that the damage probability follows a beta probability density function (PDF)

$$PDF: P_\beta(x) = \frac{\Gamma(t)}{\Gamma(r)\Gamma(t-r)} \frac{(x-a)^{r-1} (b-x)^{t-r-1}}{(b-a)^{t-1}} \quad a \leq x < b \quad (3)$$

In our case a is set to 0 (*None* damage state) and b is 6 (*Destruction* damage state). The parameter t affects the scatter of the distribution and its value is fixed to 8 in order the beta distribution to be similar to the binomial distribution. EMS-98 indicates that the damage distribution of a building follows a binomial distribution. (see also Giovinazzi [9]). Finally parameter r is given as a function of μ_d in the following equation.

$$r = t(0.007\mu_D^3 - 0.0525\mu_D^2 + 0.2875\mu_D) \quad (4)$$

Then, the probability that the damage be less or equal to a damage grade $P_\beta(k)$ is obtained by integrating $P_\beta(k)$ in equation (3) between 0 and the k -damage grade. Finally probability of occurrence of the state damage k , p_k is obtained as follows:

$$p_k = P_\beta(k+1) - P_\beta(k) \quad (5)$$

Figure 2 shows an example of the construction of p_k values for the case $\mu_d=2$.

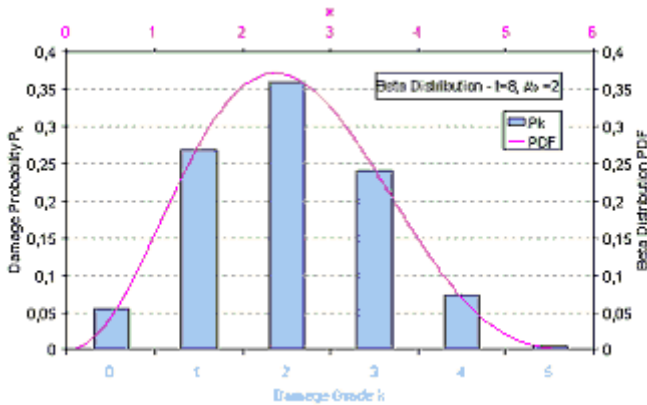


Figure 2. Evaluation of probabilities of each damage state (see explanation in the text).

All the collected data, vulnerability indices and damage factors have been used to build up a GIS application. We have used ArcView GIS. In this way, we may obtain detailed damage scenarios for each area or district and for any seismic intensity.

4. Fragility curves methodology

A more advanced method to analyse earthquake risk is based on the capacity-demand analysis and fragility curves. Of course, the application of this technique requires more information about the seismic action and buildings, because its application requires performing dynamic analyses of the buildings, in order to obtain the capacity and demand spectrum, which is based on the response spectrum. As said before, most of the residential buildings of Barcelona are reinforced concrete and masonry buildings. In order to apply this advanced methodology to Barcelona, specific fragility curves for low rise, mid rise and high rise, reinforced concrete and unreinforced masonry buildings have been developed (Moreno [10]). Obtaining the performance point for each analysed typology, allows obtaining the corresponding probabilities p_k .

This methodology considers building fragility curves for four damage states based on FEMA [11] and denoted as: *Slight*, *Moderate*, *Severe* and *Complete*. In fact, *Severe* damage state here, comprises *Substantial* and *Very Heavy* damage states in the previous methodology. Each fragility curve is assumed to follow a lognormal distribution and therefore may be characterized by a median and a standard deviation (β_{DSi}) value of seismic hazard parameter (i.e. S_a or S_d). For example, given the spectral displacement, S_d , the probability of being in, or exceeding a given damage state, DS, is modelled as:

$$P[DS > DS_i / S_d] = \Phi \left[\frac{1}{\beta_{DSi}} \ln \left(\frac{S_d}{\overline{S_d}_{DSi}} \right) \right] \quad (6)$$

where $\overline{S_d}_{DSi}$ is the median value of spectral displacement at which the building reaches the threshold of the damage state, DS , β_{DSi} is the standard deviation of the natural logarithm of spectral displacement of damage state, DS , and Φ is the standard normal cumulative distribution function. The subscript i , represents the damage state, from slight ($i=1$), to collapse ($i=4$).

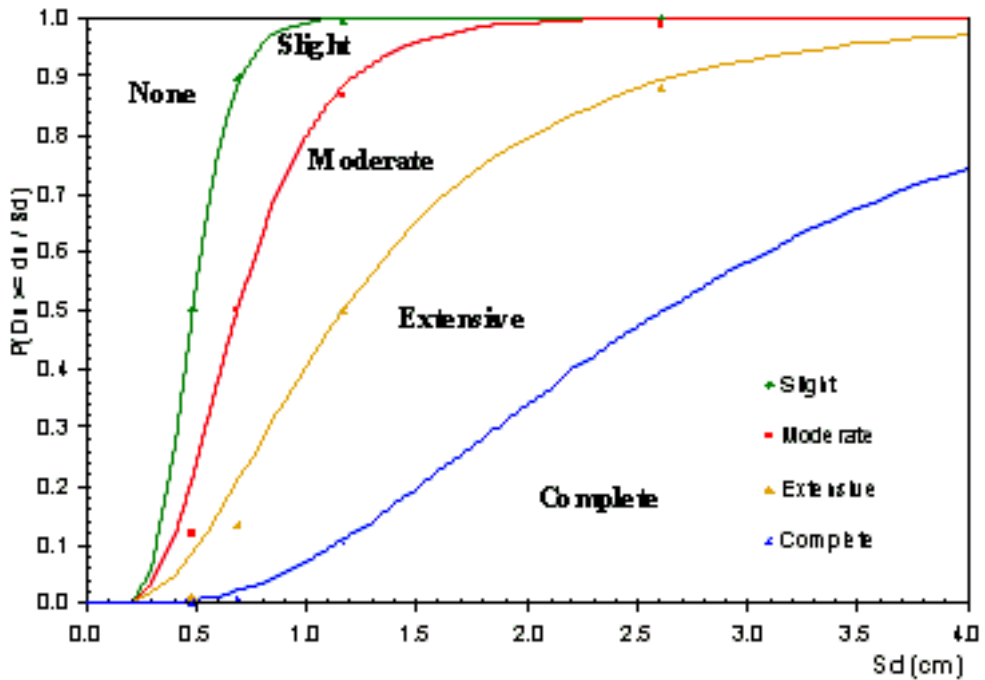


Figure 3. Fragility curves for M3.3 high-rise buildings of Barcelona (Moreno [10]).

	Zone	None	Minor	Moderate	Severe	Collapse	DS _m
Low-Rise	1	0,950	0,037	0,011	0,002	0,000	0,066
	2	0,737	0,189	0,063	0,009	0,001	0,349
	3	0,917	0,061	0,018	0,003	0,001	0,109
	R	1,000	0,000	0,000	0,000	0,000	0,001
Mid-Rise	1	0,003	0,166	0,399	0,353	0,079	2,339
	2	0,121	0,384	0,289	0,189	0,017	1,598
	3	0,273	0,364	0,215	0,139	0,009	1,247
	R	0,623	0,193	0,105	0,076	0,003	0,642
High-Rise	1	0,003	0,145	0,389	0,371	0,092	2,404
	2	0,135	0,388	0,281	0,178	0,018	1,556
	3	0,307	0,369	0,195	0,120	0,009	1,155
	R	0,647	0,205	0,086	0,059	0,003	0,566

Table 1. Probability damage matrices for masonry buildings (deterministic scenario).

Therefore, to calculate the probabilities from function Φ in equation (6), it is necessary to define \overline{Sd}_{DS_i} and β_{DS_i} for each damage state. Fragility curves usually are represented in a coordinate system whose abscissas are i.e. the spectral displacement (Sd) and whose ordinates are the conditional probabilities that a particular damage state is met ($P[DS=DS_i]$) or exceeded ($P[DS>DS_i]$). Figure 3 shows an example. By crossing the capacity and demand spectra of a given building, we find the performance point, getting the Sa or Sd of this building when it suffers the considered seismic action. Then from each fragility curve corresponding to a specific structural typology and elevation of the building, it is possible to obtain the probabilities of occurrence for each damage state. In this way, we are able to construct the damage probability matrices. Table 1 summarizes the distribution of probability for each damage state, for masonry buildings and for each zone. The last column in Table 1, has the meaning of mean expected damage state, and is analogous to μd in the vulnerability index method. This is computed by the equation:

$$DS_m = \sum_{i=0}^4 DS_i * P[DS_i] \quad (7)$$

According to this equation, for example a value $DS_m=1.3$ indicates that the most probable structural damage state of the corresponding building, ranges between *slight* and *moderate* states, being more probable the *slight* damage state. Thus, DS_m is a weighed average of different damage DS_i states where the probability to reach it, $P[DS_i]$, is the weigh. Again, this sort of average damage state, permits to plot seismic damage scenarios, by using a single parameter. Of course, alternative maps, may plot the spatial distribution of the probability of occurrence for a determined damage state, it's to say, $P[DS_i]$ for a given i .

5. Seismic risk scenarios

The process of obtaining the final seismic risk scenarios according to the vulnerability index methodology is: the behaviour modifiers are first calculated and associated with the vulnerability index of each building. The deterministic seismic hazard map in terms of intensity (see Figure 1, left side map) and the map with information on the buildings are then overlaid in the GIS. The result is a new map with information on the seismic zone where the buildings are located. Finally, the mean damage grade is calculated by using equation (2) in order to obtain the damage scenario. We have adopted a graduated color scale to represent the 0 to 5 damage states. Namely: *No damage*-white, *Slight*-green, *Moderate*-yellow, *Substantial to Heavy*-Orange, *Very Heavy*-red and *Destruction*-black). In the same way, the damage scenarios corresponding to the analysis based on the fragility curves methodology are obtained by overlaid, in the GIS, the corresponding deterministic seismic hazard map in terms of spectral values (see, right side map in

Figure 1) and building map with information about their typologies. The information on damage probability matrices for each typology (see Table 1) is then associated in this final map. In this case the graduation of colors of the legend for each damage state from 0 to 4 are: *No damage-white*, *Slight-green*, *Moderate-yellow*, *Severe-red* and *Complete-black*.

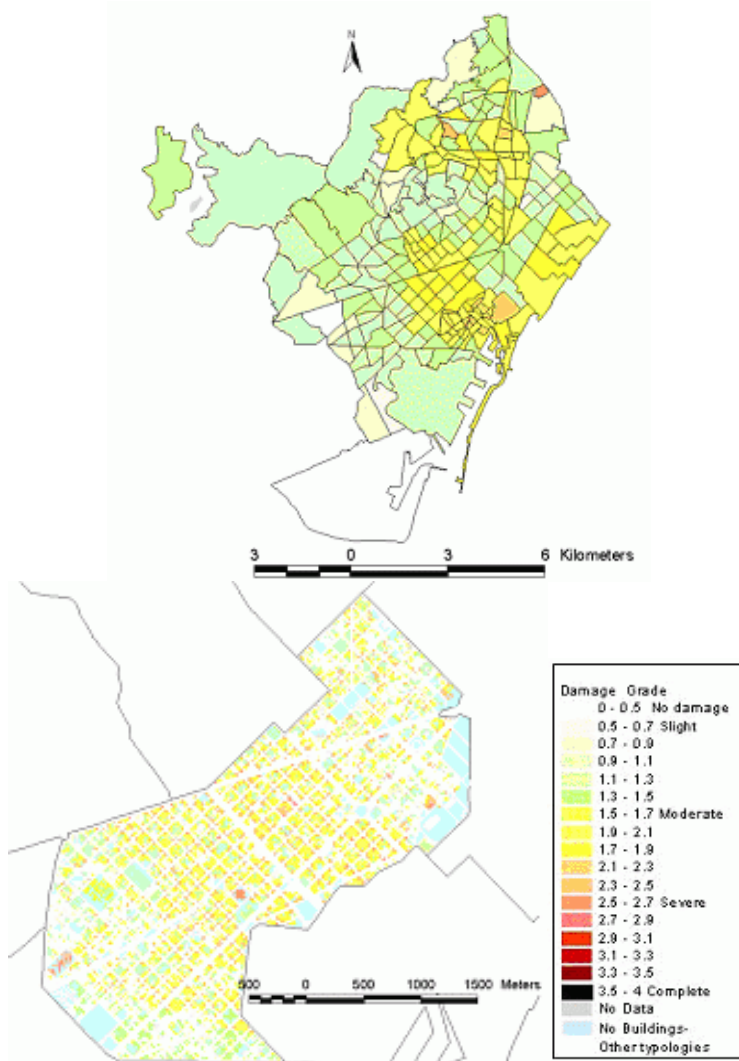


Figure 3. Damage scenario for census areas. A detail of the Eixample district is standed out (Vulnerability index Method).

Figures 3 and 5 show the obtained seismic risk scenarios. We can see how the expected damage for a relatively low seismic intensity is relatively high. About

50% percent of high rise masonry buildings located in Zone II would present a damage state between *moderate* and *severe* (see also Table 1). This fact might be due to the high vulnerability of this typology. On the other hand we can see how the damage follows a radial pattern from downtown, in the center of the city, to the outskirts of Barcelona. This fact may be due to the history evolution of the city, with old masonry buildings concentrated downtown and in the first city expansion represented by the Eixample district. It is also possible to see the influence of the nearness of the earthquake in the case analyzed in Figure 3 (see also Figure 1).

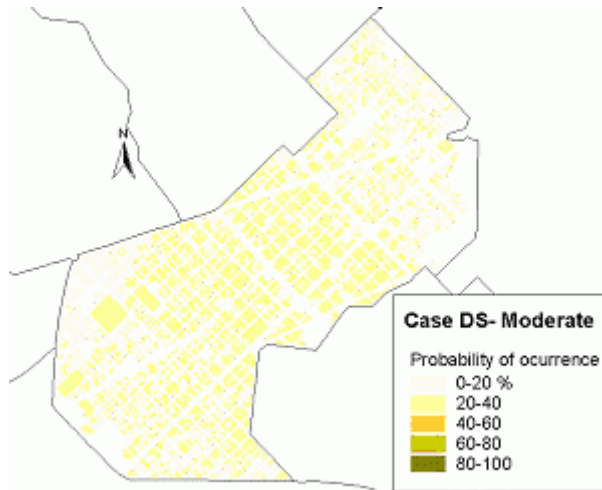


Figure 4. Probabilities of the *moderate* damage state in the Eixample District. (Fragility curves method)

Both maps of figures 3 and 5 show a single value: the mean expected damage state for each building. Of course, we may also map other specific scenarios as for example, for each damage state, we may plot its probability spatial distribution. When doing this, we have maintained the same color-scale used in Figures 3 and 5, to identify each damage state, but the differences in the probabilities are now represented by different tones of the same color. An example of these damage state probability maps is shown in Figure 4 for a *moderate* damage state in the Eixample district. It must be noted that most of the buildings in this district are old unreinforced, high-rise buildings (more than 70%), and all of them are inside Zone II. So, according to values in Table 3, the occurrence probability of the *moderate* damage state is about 28% (light-middle yellow in Figure 4).

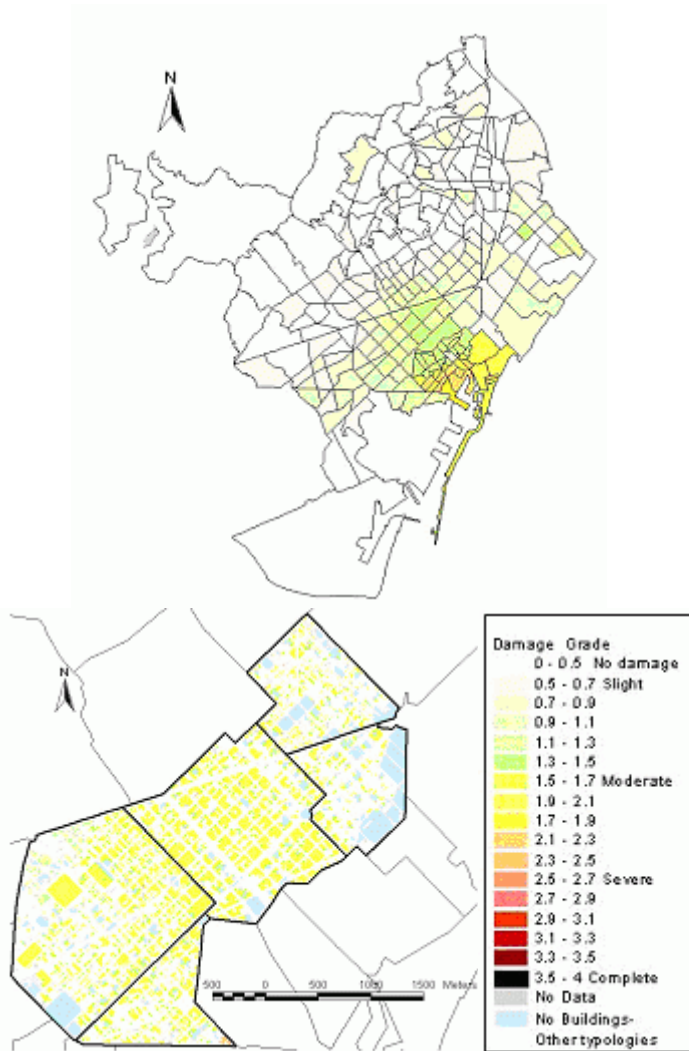


Figure 5. Damage scenario for census areas. A detail of the Eixample district is standed out (Fragility curves Method).

6. Discusion and conclusions

In this paper we have implemented a GIS tool to obtain seismic risk scenarios in urban areas and we have analysed the case of Barcelona (Spain). Really it has been possible because of the great amount of information available about the seismic hazard of the city and the typology, age and other characteristics of almost the complete stock of buildings of the city. Our tool easily admits two methods. In the

first one the seismic action is considered by means of e.g. EMS intensity and the fragility of the buildings is modelled by vulnerability indices. The second method uses fragility curves and requires determining the S_a or S_d parameters, in order to get the damage state probabilities, and therefore, it requires the computation of fragility curves, the capacity and demand spectra, and, finally the performance point. Therefore the first method requires less information and admits rough simplifications about both the seismic input and the vulnerability of the buildings. The second one is more advanced but requires more information about the seismic action (we really need response spectra) and about the buildings. Both the fragility curves and the capacity spectra require detailed structural plans and other design and construction details. Therefore, we feel that the results obtained by using the second method are more reliable. In spite of the differences in the results shown in figures 3 and 5, both methods provide excellent results, showing an excellent correlation with the main features of the built-up environment of the city. It is clear in both cases that a city, like Barcelona, located in a low to moderate hazard region has paid no attention to the seismic performance of their buildings, and therefore it is expected a high seismic vulnerability and a considerable risk. In fact the expected damage for a VI EMS intensity earthquake would be close to the damage that seismic intensity scales anticipate for a VII intensity grade.

Acknowledgements

The civil protection department of the Barcelona Municipality has provided most of the information and data used in this study. Sonia Giovinazzi and Sergio Lagomarsino, at the University of Genoa, have developed the methodology and guidelines of the vulnerability index method we have applied here. This work has been partially supported by the European Community Risk-UE project (Contract N. EVK4-CT-2000-00014) and Science and Technology Ministry of Spain (Contracts N. REN2000-1740-C05-01 RIES, REN2001-2418-C04-01/RIES and RSN2002-03365/RIES).

REFERENCES

1. Lantada, N. and Nuñez, M.A., Sistemas de Información Geográfica. Prácticas con ArcView. Politext. Barcelona: Edicions UPC, 2002. 1-226.
2. RISK-UE, E.C.R.-U.P., Advanced methodology for seismic risk scenarios with applications in European cities (RISK-UE). (Contract N. EVK4-CT-2000-00014). 2003.
3. Grunthal, G., European Macroseismic Scale 1998: Cahiers du centre Européen de Géodynamique et Séismologie. Vol. 15. Luxemburg: G. Grünthal, 1998.
4. NCSE-02, Norma de Construcción Sismorresistente Española. Parte General y de Edificación, Comisión Permanente de Normas Sismorresistente, Real Decreto 997/2002 del 27 de septiembre de 2002, Boletín Oficial del Estado,

- 244, viernes 11 de Octubre de 2002. Ministerio de Fomento, 1994: 35898-35987.
5. Cid, J., Susagna, T., Goula, X., Chavarria, L., Figueras, S., Fleta, J., Casas, A., and Roca, A., Seismic Zonation of Barcelona Based on Numerical Simulation of Site Effects. *Pure Applied Geophysics*, 2001. 158.
 6. Irizarry, J., Goula, X., and Susagna, T., Seismic Hazard Assesment for the City of Barcelona. *Institut Cartogràfic de Catalunya: Barcelona*, 2002: 95.
 7. Giovinazzi, S. and Lagomarsino, S. A methodology for the vulnerability analysis of built-up areas. in X National Conference on Earthquake Engineering. *Potenza (Italy)*, 2001
 8. Corsanego, A. and Petrini, V., Evaluation criteria of seismic vulnerability of the existing building patrimony on the national territory, *Seismic Engineering*. Vol. 1, 1994. 16-24.
 9. Giovinazzi, S. and Lagomarsino, S., WP04:Guidelines for the implementation of the I level methodology for the vulnerability assessment of current buildings. *Risk-UE Project: Genoa (Italy)*, 2002.
 10. Moreno, R., Lantada, N., Bonett, R., Barbat, A.H., and Pujades, L.G., WP4: Vulnerability assessment of current buildings. Capacity and Fragility of the Barcelona's residential buildings. *CIMNE: Barcelona*, 2003: 14.
 11. FEMA., HAZUS 99 Estimated annualised earthquake losses for the United States. *Federal Emergency Management Agency (FEMA): Washington*, 2000.

THE DETERMINATION OF CRACK GROWTH RATE FOR OLD RIVETED STEEL BRIDGES

Edward PETZEK¹, Radu BĂNCILĂ², Dimitris KOSTEAS³

Abstract

The paper refers to the problems in the field of evaluation of the safety against fatigue.

The majority of existing railway steel bridges that have been built at the turn of the last century are riveted structures. Many of these bridges are still in operation after damages, several phases of repair and strengthening.

The problem of these structures is the assessment of the present safety for modern traffic loads and the remaining service life.

Replacement with new structures raises financial, technical and political problems.

The calculation of remaining fatigue life is normally carried out by a damage accumulation calculation (theory Palmgren – Langer – Miner). However, in many cases this method does not provide satisfactory results.

Along with the classical method of damage accumulation, a new approach based on the fracture mechanics principles is proposed.

The method of fatigue assessment for structural elements with defects was developed basing on the possibility of modelling, on the propagation rate of crack dimensions under fatigue loads and with the help of known laws. The method is founded on the recommendations of the BS 7910:1999 applied for old riveted steel bridges. It can also be applied for other bridge structures, which contain defects.

After a general presentation, a study concerning the determination of the crack growth rate is included in the paper.

¹ Ass. Prof. PhD. Eng., Technical University „Politehnica” of Timișoara, Romania
epetzek@ceft.utt.ro

² Prof. PhD. Eng., Technical University „Politehnica” of Timișoara, Romania
rbancila@ceft.utt.ro

³ Prof. PhD. Eng., Technical University of München, Germany, DimitrisKosteas@lrz.tu-muenchen.de

1. Introduction

The majority of railway existing steel bridges that have been built at the turn of the last century are riveted structures. Many of these old bridges have been repaired or strengthened after being damaged. “*No structure is build to last an eternity.*” The safety of these bridges for modern traffic loads throughout their remaining service life needs to be considered.

The calculation of remaining fatigue life is normally carried out by a damage accumulation calculation (theory Palmgren – Langer – Miner).

The cumulative damage caused by stress cycles will be calculated; failure criteria will be reached.

$$D = \sum \frac{n_i}{N_i} \leq 1 \quad (1)$$

However, in many cases this method does not provide satisfactory results; consequently a complementary method based on fracture mechanics is proposed.

The presence of cracks in structural elements modifies essentially their fracture behaviour. Fracture, assimilated in this case as crack dimensions growth process under external loadings, will be strongly influenced by the deformation capacity of the material. This capacity is reflected by the two fracture modes observed in practice, namely: the ductile and the brittle fracture. It is considered in practice that the structural element loses its safety in operation at the appearance of a crack. Fracture mechanics offer a tool for the assessment of crack propagation rate and, implicitly, of the time period in which the cracked structural element can be exploited under safe conditions.

The life prediction methodology is conceived as an advanced, complete analysis of structural elements containing fatigue defects, being founded on fracture mechanics principles and containing two steps [1]; namely one of determination of defects' acceptability with the help of Failure Assessment Diagrams and of determination of final acceptable values of defect dimensions; this is followed by a second step which in fact represents a *fatigue evaluation of the analysed structural elements* basing on the present stress history recorded on the structure, on the initial and final defect dimensions and the FM parameters, namely the material characteristics **C** and **m** from the Paris relation (crack growth under real traffic stress) and further on the exact determination of the number of cycles **N** needed in order that a fracture take place, respectively the determination of the remaining service life of the structural elements (years, months, days).

2. Fatigue crack propagation and crack propagation laws

The method of fatigue assessment for structural elements with defects was developed basing on the possibility of modelling, on the propagation rate of crack dimensions under fatigue loads and with the help of known laws. The method is

founded on the recommendations of the BS 7910:1999 applied for old riveted steel bridges. It can also be applied for other bridge structures, which contain defects.

In the present state of knowledge it is generally accepted that the fatigue failure of materials is a process containing three distinct steps: (1) initiation of defect (crack), (2) crack propagation in material, (3) separation through complete failure of the material in two or more pieces. Practically, the safety service life of an element under fatigue conditions can be expressed as follows:

$$N_f = N_i + N_p \tag{2}$$

N_i = number of cycles necessary for the initiation of the defect (crack)

N_p = number of cycles necessary for the propagation of the defect until the occurrence of failure

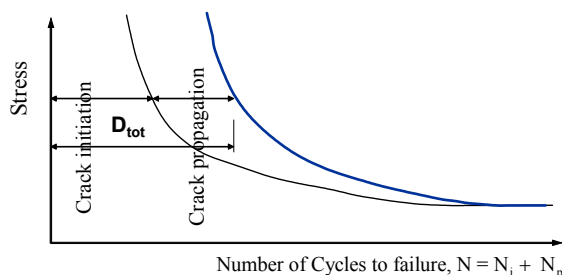


Figure 1 Fatigue life of structural elements

For a good description of the fatigue crack propagation the following influencing factors must be taken into account:

- Structure geometry
- Defect (crack) geometry
- Material properties
- Rate and frequency of loading
- Temperature and environment

The evaluation of crack propagation conditions can be accomplished with the help of characteristic values, which are founded on fracture mechanics concepts: material toughness expressed by the stress intensity factor K or J integral value and the crack growth rate da/dN (crack growth for each load cycle). A relation of the following type can express the crack growth rate:

$$\frac{da}{dN} = f(\Delta K, R, H) \tag{3}$$

da/dN - crack extension for one load cycle

ΔK - stress intensity range, established basing on the stress range $\Delta\sigma$;

$$\Delta K = K_{max} - K_{min}$$

R - stress ratio $R = \frac{\sigma_{min}}{\sigma_{max}}$; H - indicates the history dependence.

The crack growth rate da/dN , defined as a crack extension da obtained through a load cycle dN (it can also be defined as da/dt , in which case the crack extension is related to a time interval), represents a value characteristic of the initiation phases respectively the stable crack propagation. It has been experimentally observed that the connection between the crack growth rate and stress intensity factor variation represents a suitable solution for the description of the behaviour of a metallic material containing a crack, as in the case of steel. In a logarithmic graphical representation of the crack growth rate da/dN versus the stress intensity range ΔK a curve as the one in the following figure is obtained.

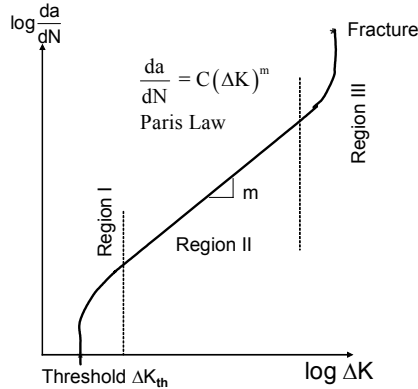


Figure 2 Logarithmic representation of the fatigue crack growth in steel

In the technical literature a large number (over 60) of crack propagation rate laws can be found. These crack propagation equations can be divided into three groups [3] by taking into account the parameters they contain:

$$a) da/dN = C_1 f_1(a); \quad b) da/dN = C_2 f_2(\Delta\sigma); \quad c) da/dN = C_3 f_3(\Delta K) \quad (4)$$

a – crack length;

ΔK – stress intensity factor range;

N – number of cycles;

C_i cu $i = 1...3$ – material parameters;

$\Delta\sigma$ - stress range;

f_i cu $i = 1...3$ – functions.

Obviously, the existing formulas have different degrees of complexity including more or less parameters. Beyond doubt, the equations belonging to group c) are the most valuable, as the use of fracture mechanics parameters offers a series of advantages. These advantages base on the fact that within fracture mechanics a well defined relation between the material parameters – stress – dimension and geometry of the defect has been established.

3. Application of fatigue crack propagation data

The most important equation of group c) is the Paris and Erdogan law:

$$da_1 = C \cdot \Delta K^m \quad \Delta K = K_{\max} - K_{\min} = Y(\sigma_{\max} - \sigma_{\min})\sqrt{\pi a} \quad (5)$$

The calculation of the structural elements' remaining service life can be done basing on the Paris law, more precisely by the integration of this law:

$$N = \int_0^N dN = \int_{a_0}^{a_{crit}} \frac{da}{C \cdot \Delta K^m} \quad (6)$$

N - number of stress cycles necessary in order that the crack extends from its initial dimension a_0 to the critical value a_{crit} , where failure occurs;

a – crack length;

C, m – material constants from the crack propagation law;

ΔK – stress intensity factor range.

This integral can be numerically calculated by taking into account a critical detail knowing the crack values (initial and critical), basing on the following relation:

$$N = \int_{a_0}^{a_{crit}} \frac{da}{C \cdot \Delta \sigma^m \cdot Y^m \cdot (\pi a)^{-m/2}} \quad (7)$$

The number of cycles N_{ij} obtained with the help of relation (7) represents the remaining service life of the detail, by regarding the initial length a_0 up to the critical length a_{crit} , by admitting a stable crack propagation.

The critical crack value can be calculated basing on the K criterion respectively on the J or $CTOD$ criterions or with the help of the failure assessment diagram [1].

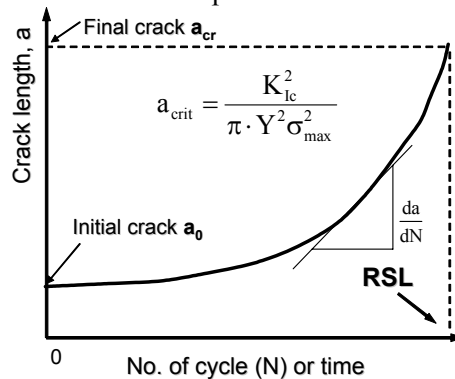


Figure 3 Principles for determining the remaining service life

4. Measurement of fatigue crack growth rates

The C and m material constants from the Paris law are experimentally determined by fracture mechanical tests. In this sense in most cases compact specimens $C(T)$, three point bended specimens $SEN(B)$ and middle central panels $M(T)$ are used; see figure 4. Such a standard which describes the test methods for the determination of the crack growth rate is the American Standard ASTM E 647 (*Standard Test Method for Measurement of Fatigue Crack Rates*).

The procedure for the determination of crack growth rate in metallic materials bases on the use of specimens containing a fatigue defect (crack). This precrack has a well established length and is placed at the top of the machined notch. The precracked specimens are then tested at a fatigue cycle; during the test the crack

length extension is measured according to the number of cycles which correspond to these extensions. Basing on the recordings the curve crack length extension versus applied number of cycles is drawn. With the help of these curves the crack propagation rate da/dN is determined by using one of the standard methods: secant method or incremental polynomial method.

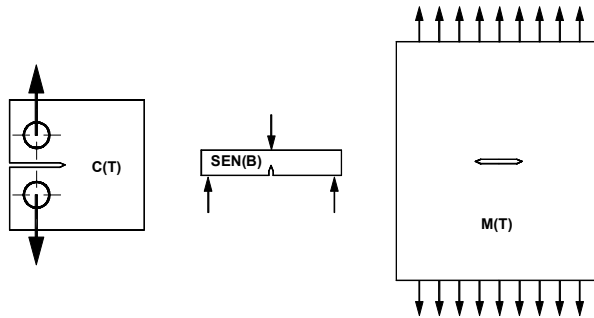


Figure 4 Generally used specimen for crack propagation tests

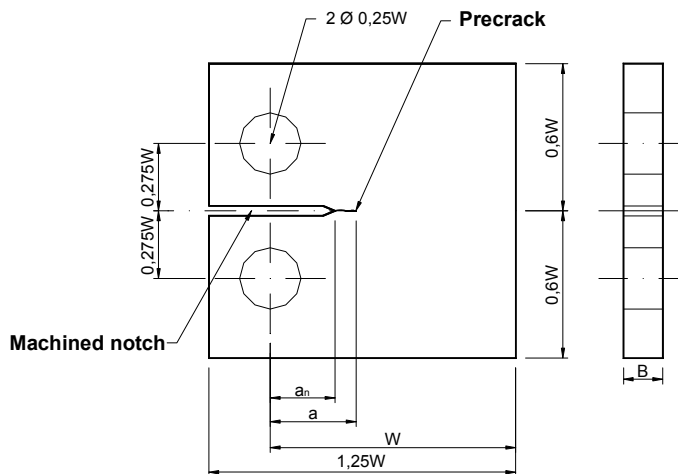


Figure 5 Standard Compact – Tension Specimen

The necessary apparatus for the performing of the test is composed of the following:

- ✓ *Grips and fixtures for specimens* – depending on the specimen type. For C(T) specimens a clevis and pin assembly is used at both ends of it so that the specimen is allowed to rotate in plane while it is loaded. The proportions of the fixtures are given in terms of the main specimen dimensions and are included in the standard.
- ✓ *The testing machine* – it has to be chosen so that the stress distribution is symmetrical to the specimen notch. The load cell in the test machine should be

verified in accordance with Practices E 4 and Practice E 407 and the testing should be conducted so that both ΔP and P_{max} are controlled to within $\pm 2\%$ throughout the test.

- ✓ *Measurement of crack length* – this has to be done as a function of elapsed cycles by means of a visual technique or an equivalent one (see figure 6) capable of resolving crack extensions of 0,10 mm or 0,002W (the greater of the two values). For visual measurements the polishing of the test area of the specimen and the use of indirect lighting in the resolution of the crack tip is needed. It is recommended that the recordings be done without interrupting the tests. The measurements of the crack lengths have to be performed at intervals so that the da/dN data are distributed almost equally to ΔK . The measurement intervals are recommended in the standard depending on the specimen type. For example for the C(T) specimen:

$$\Delta a \leq 0,04W \text{ for } 0,25 \leq a/W \leq 0,40 \tag{8}$$

$$\Delta a \leq 0,02W \text{ for } 0,40 \leq a/W \leq 0,60 \tag{9}$$

$$\Delta a \leq 0,01W \text{ for } a/W \geq 0,60 \tag{10}$$

It is recommended to chose a minimum Δa of 0,25 mm. However, situations may appear where the Δa needs to be reduced bellow 0,25 mm in order to obtained at least five (da/dN , ΔK) data points in the near-threshold regime.

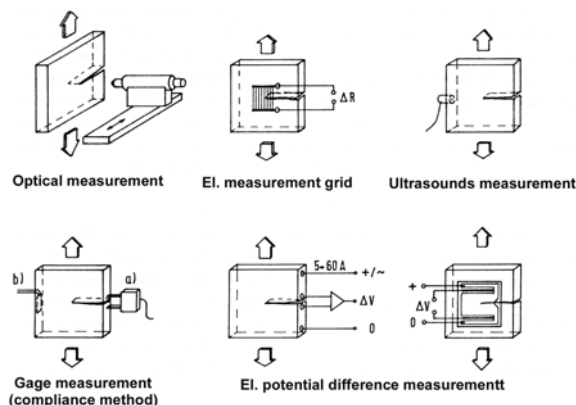


Figure 6 Measurement of crack length

5. Experimental tests

The authors performed such experimental test to determine the crack growth rate for an old riveted bridge [4]. The subject of this experimental program has been the old railway steel bridge in Arad. The bridge was built in 1912 and situated on the main line Timișoara – Arad, crossing the Mureș River (for details see [1, 4], and it was dismantled in the autumn of 2000. This structure has been chosen because specimens could be sampled from most stressed elements also because many other similar structures, build in the same period are still in operation.

For these tests, which were performed in accordance with ASTM E647-93, compact specimens C(T) (thickness 8 mm) have been used. They have been sampled from the stringers, cross girders and main girder – lower chord (all these main structural elements have been taken from span 3 of the bridge).



Figure 7 Stringer, cross girder and main girder pieces

Sixteen specimens have been prepared and they were divided into five series, according to the sampling place; see table 1.

Test type	Reference Standard	Structural element / Sampling place	No. of samples	Sample marking
Measurement of fatigue crack growth rate	ASTM E647-93	Stringers – flange	3	LT: 1,18,19
		Cross girder – flange	4	QT: 6,7,16,17
		Main girder – lower chord	4	HT: 24,25,26,27
		Stringers – web	3	LT-St: 36,37,38
		Cross girder – web	3	QT-St: 45,46,47

Table 1 Test samples

The dimensions of the samples have been established according to the specifications of the reference standard and are presented in the following figure.

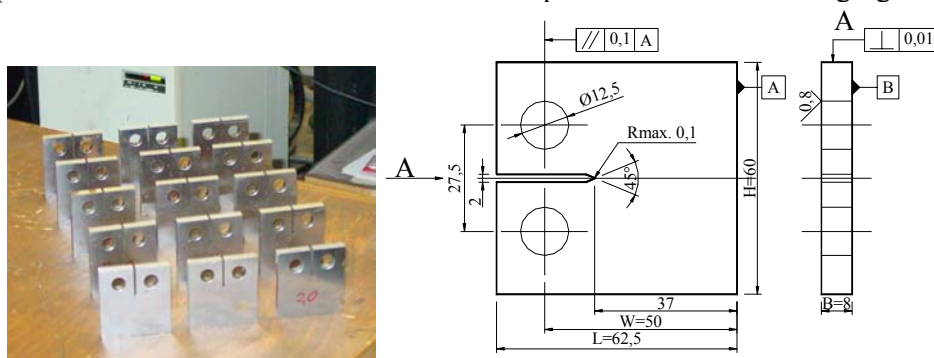


Figure 8 Test samples and dimension

It should be mentioned here that the test have been performed in the laboratory of the Technical University of Munich.

The main steps of the experimental program include:

- Step 1 – The specimen preparation
- Step 2 – Fatigue precracking of samples
- Step 3 – The fatigue test
- Step 4 – Computing and interpretation of results

The test apparatus used in this step is the following:

- Clevis and pin assembly for fixing and loading the C(T) specimen.
- Precracking machine – Instron +/- 100 kN with digital counter of load cycles.
- Optical device – microscope Periplan 20x.
- Supplementary light source.

The determination of the crack growth length is performed by means of the a – N curves within the experimental tests, in accordance with the incremental polynomial method, recommended in Appendix IX of the ASTM 647-93.

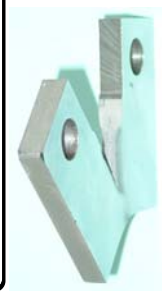
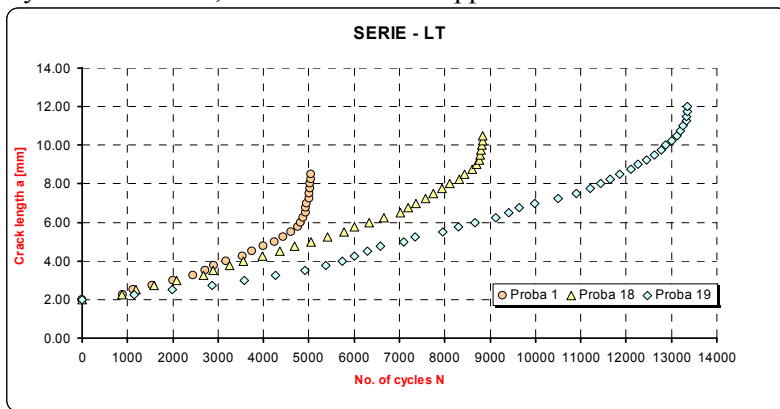


Figure 9 Test acquisition data for stringers (LT)

The final results are presented in the following table.

Nr.	Locul de prelevare	Spec.	Material constants (experimental value)	
			C	m
1	Stringers - Flange LT-G	CT 1	2.2008E-11	3.1454E+00
2		CT 18	7.9268E-09	2.0537E+00
3		CT 19	1.0731E-07	1.5610E+00
4	Cross girders - Flange QT-G	CT 16	5.2610E-11	3.0082E+00
5		CT 7	3.5506E-09	2.2374E+00
6		CT 6	1.0626E-07	1.6069E+00
7	Main girder - lower chord HT-UG	CT 24	2.5920E-10	2.6692E+00
8		CT 25	2.2860E-09	2.2687E+00
9		CT 26	2.3290E-10	2.6480E+00
10	Stringers - web LT-St	CT 36	5.0021E-15	4.7629E+00
11		CT 37	5.6573E-15	4.7340E+00
12		CT 38	-3.7558E-18	6.0158E+00
13	Cross girders - web QT-St	CT 45	1.0866E-30	1.1348E+01
14		CT 46	6.9089E-18	5.8764E+00
15		CT 47	1.7480E-19	6.5922E+00

Table 2 C and m test results

6. Conclusions

The determination of material constants C and m offer a major advantage because, due to the fact, that they characterise the real state of the fatigued material that corresponds to the sampling moment, all problems connected to the establishment of loading history (necessary for the classical safety evaluation) of the analysed bridge are eliminated. Furthermore, in some situations, this loading history can be traced only with great approximation, that is then introduced into the life prediction calculus. The results have been used in a modern life prediction methodology based on fracture mechanics principles and which is presented in [1].

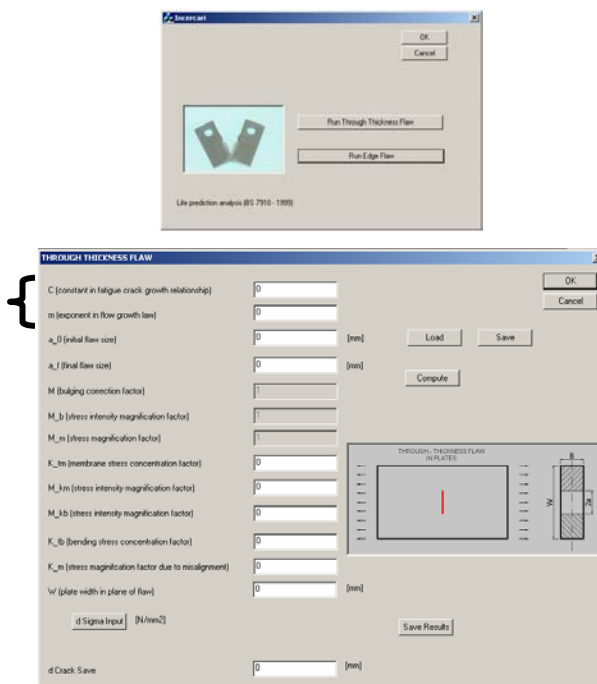


Figure 10 Life prediction program

References

1. Petzek, E., „*Siguranța în exploatare și reabilitarea podurilor metalice*”, Ed. Mirton, Timișoara, 2004.
2. * * *, BS 7910:1999, „*Guide on the Methods for Assessing the Acceptability of Flaws in Metallic Structures*“, British Standards Institution, London, 1999.
3. Czoboly, E., „*Fatigue Crack Propagation*”, EMAS Ltd. U.K., 5th IFMASS, p. 103-116, Belgrade, 1989.
4. Kosteas, D., Băncilă, R., Petzek, E., „*Die Methodik zur Bestimmung der Restsicherheit am Beispiel bestehender Stahlbrücken in Rumänien*“, Versuchsbericht nr. 052/LME, München, 2002.

MITIGATION OF SEISMIC VIBRATIONS OF A BENCHMARK CABLE BRIDGE USING STRUCTURAL ACTIVE CONTROL

Lubomir BAKULE¹, Fideliu PĂULEȚ-CRĂINICEANU², José RODELLAR³

Abstract

In Structural Active Control, Civil Engineering is facing challenges that involve integration with knowledge and specialists from electronics, automatic control, computer science, robotics, new materials, etc. At the same time, practical applications are still too expensive.

For most researchers in this field a solution to challenges is to create analytical models aiming to be applied for important structures subjected to strong natural actions. Then, comparisons between strategies can show ways to continuations of researches. Small scale experiments could also be employed, if budgets are available.

Optimal Active Control is used in this paper for showing a procedure to minimize the energy of a structure submitted to earthquake actions. The centralized presented strategy is easing the choice for the parameters and limits the degree of arbitrariness in imposing them. Attention is given to using reduced state models. The system reduction is based on controllability and observability gramians. The reduced state procedure is applied both to the system and to the weighting matrices. This makes the procedure original.

The control method is verified on a FEM model of the cable-stayed bridge given by an international benchmark. External actions are three important strong earthquake acceleration records. The process noise and the measurement benchmark requirements are included within the discrete-time approach.

The application is showing the way the design was performed. Results are judged based on the benchmark performance indexes. Conclusions show that the controlled system is competitive. Stresses, bending moments, forces, displacements, velocities, and accelerations are kept into allowable limits.

1. Introduction

Since its beginning, [1], Structural Control has been growing in a fast pace as a subject contributing with means to alleviate the effects of harming loads. Last years have shown a stress on researches about active control of large structures with many active devices. Optimal control has been used in [2] and [3] in a centralized

¹ Dir.Res., Inst. Info.Theory & Automation, Acad. Sci., Prague, e-mail: bakule@utia.cas.cz

² Associate Prof., Faculty of Civil Engrg. and Arch. Iasi., e-mail: fideliu@ce.tuiasi.ro

³ Prof., Dept. de Matem. Appl. III, UPC, Barcelona, e-mail: jose.rodellar@upc.edu

setting. Decentralized controllers have been proposed in [4], [5] and [6]. Also, sliding mode control has been analyzed as a method to cope with uncertainties [7].

In the context of optimal control, an energy-based method for choosing the weighting parameters was developed [8]. The method is very convenient because it implies a simple way to set the control parameters. Using this method, it is possible to control large structures using many devices and, in this way, the efficiency and reliability of the control are highly increased. Then other authors adopted similar energy-based control strategies [9].

The international benchmark control problem for seismic response of cable-stayed bridges is used [10] to prove the efficiency of the proposed strategy. For this goal, the full state methodology for tuning the weighting control matrices is set up in order to adapt it to the needs of canonical modal transformation and model reduction procedures [11], [12].

Therefore, realistic simulations with few measurement devices and reduced order estimator are performed. Discrete-time simulations take into account process noise and the measurement noise. The results are compared with the benchmark sample control strategy. Results show good behavior of the proposed control methodology according to a set of evaluation criteria established by the benchmark.

2. Problem Statement

The objectives of this study are specified as follows:

1. To present the LQG control design for reduced order global systems.
2. To apply this theoretic approach on the cable-stayed bridge benchmark, i.e. to perform the control design and to evaluate the simulation results.

3. Solution

It consist of two parts: Reduced order LQG methodology and Benchmark control design and simulations.

Reduced Order LQG Methodology

Optimal active control is a time domain strategy that is appropriate for controlling the response of structures subjected to strong earthquakes. The strategy allows minimizing the induced structural energy [13].

In Structural Control, the state equation of motion for a n degree of freedom controlled system under seismic action is:

$$\dot{\mathbf{x}}(t) = \mathbf{A}\mathbf{x}(t) + \mathbf{B}\mathbf{u}(t) + \mathbf{h}\ddot{x}_g(t), \quad \mathbf{x}(0) = \mathbf{x}_0 \quad (1)$$

where $\mathbf{x}(t)$ is the $2n$ -dimensional state, and \mathbf{A} , \mathbf{B} are appropriate matrices.

Setting the control actions as $\mathbf{u}(t) = -\mathbf{K}\mathbf{x}(t)$, the goal of the method is to obtain the feedback gain matrix \mathbf{K} to minimize a performance index J defined by

$$J = \frac{1}{2} \int_0^{\infty} [\mathbf{x}'(t)\mathbf{Q}\mathbf{x}(t) + \mathbf{u}'(t)\mathbf{R}\mathbf{u}(t)] dt \quad (2)$$

where \mathbf{Q} and \mathbf{R} are weighting matrices, $2n \times 2n$ -dimensional and $m \times m$ -dimensional, respectively; and m is the number of the actuators. Minimization of the performance criterion (2) implies to solve the Riccati equation

$$\mathbf{P}\mathbf{A} - \mathbf{P}\mathbf{B}\mathbf{R}^{-1}\mathbf{B}'\mathbf{P} + \mathbf{A}'\mathbf{P} + \mathbf{Q} = \mathbf{0} \quad (3)$$

Then, the control gain matrix is $\mathbf{K} = \mathbf{R}^{-1}\mathbf{B}'\mathbf{P}$.

Appropriate settings can be found for the full states-based matrices \mathbf{Q} and \mathbf{R} . For example, if $\mathbf{Q} = \text{diag}(\mathbf{K}_1, \mathbf{M}_1)$, then the first term in the brackets of Equation (2) is an energy expression and therefore Equation (2) leads to minimization of the energy of the structural response. Matrix \mathbf{R} can be set as $\mathbf{R} = r\mathbf{I}$, where \mathbf{I} is the identity matrix and r is a scalar, the unique parameter to be determined [13].

Usually, only few measurements are available. In this case, the output of the system, \mathbf{y} , is expressed through a second equation complementing the state-space model, in the form:

$$\begin{cases} \dot{\mathbf{x}} = \mathbf{A}\mathbf{x} + \mathbf{B}\mathbf{u} + \mathbf{h}\ddot{x}_g \\ \mathbf{y} = \mathbf{C}\mathbf{x} + \mathbf{D}\mathbf{u} \end{cases} \quad (4)$$

where \mathbf{C} is a $p \times 2n$ measurement matrix and \mathbf{D} is the $p \times m$ matrix showing the influence of the control forces on the output.

A first step to avoid the inconvenience of using all states is to apply a canonical transformation $\mathbf{x}_c = \mathbf{T}_c\mathbf{x}$ or $\mathbf{x} = \mathbf{T}_c^{-1}\mathbf{x}_c = \mathbf{P}_c\mathbf{x}_c$ based on the eigenvector matrix $\mathbf{P} = \mathbf{T}_c^{-1}$. This way, the system (4) takes the new form:

$$\begin{cases} \dot{\mathbf{x}}_c = \mathbf{A}_c\mathbf{x}_c + \mathbf{B}_c\mathbf{u} + \mathbf{h}_c\ddot{x}_g \\ \mathbf{y} = \mathbf{C}_c\mathbf{x}_c + \mathbf{D}\mathbf{u} \end{cases} \quad (5)$$

where $\mathbf{A}_c = \mathbf{P}^{-1}\mathbf{A}\mathbf{P}$, $\mathbf{B}_c = \mathbf{P}^{-1}\mathbf{B}$, $\mathbf{C}_c = \mathbf{P}^{-1}\mathbf{C}$, and $\mathbf{h}_c = \mathbf{P}^{-1}\mathbf{h}$.

The second step, based on controllability and observability gramians [14, 15], is to use a state coordinate transformation matrix $\bar{\mathbf{T}}$ applied to the system (5), i.e., $\bar{\mathbf{x}} = \bar{\mathbf{T}}\mathbf{x}_c$. The resulting system is a balanced system:

$$\begin{cases} \dot{\bar{\mathbf{x}}} = \bar{\mathbf{A}}\bar{\mathbf{x}} + \bar{\mathbf{B}}\mathbf{u} + \bar{\mathbf{h}}\ddot{\mathbf{x}}_g \\ \mathbf{y} = \bar{\mathbf{C}}\bar{\mathbf{x}} + \mathbf{D}\mathbf{u} \end{cases} \quad (6)$$

where $\bar{\mathbf{A}} = \bar{\mathbf{T}}\mathbf{A}_c\bar{\mathbf{T}}^{-1}$, $\bar{\mathbf{B}} = \bar{\mathbf{T}}\mathbf{B}_c$, $\bar{\mathbf{C}} = \mathbf{C}_c\bar{\mathbf{T}}^{-1}$, and $\bar{\mathbf{h}} = \bar{\mathbf{T}}\mathbf{h}_c$. If only the first most significant q states are retained for the structural response, the system (6) can be rewritten in the form:

$$\begin{cases} \begin{Bmatrix} \dot{\bar{\mathbf{x}}}_1 \\ \mathbf{0} \end{Bmatrix} = \begin{bmatrix} \bar{\mathbf{A}}_{11} & \bar{\mathbf{A}}_{12} \\ \bar{\mathbf{A}}_{21} & \bar{\mathbf{A}}_{22} \end{bmatrix} \begin{Bmatrix} \bar{\mathbf{x}}_1 \\ \bar{\mathbf{x}}_2 \end{Bmatrix} + \begin{Bmatrix} \bar{\mathbf{B}}_1 \\ \bar{\mathbf{B}}_2 \end{Bmatrix} \mathbf{u} + \begin{Bmatrix} \bar{\mathbf{h}}_1 \\ \bar{\mathbf{h}}_2 \end{Bmatrix} \ddot{\mathbf{x}}_g \\ \mathbf{y} = \begin{bmatrix} \bar{\mathbf{C}}_1 & \bar{\mathbf{C}}_2 \end{bmatrix} \begin{Bmatrix} \bar{\mathbf{x}}_1 \\ \bar{\mathbf{x}}_2 \end{Bmatrix} + \mathbf{D}\mathbf{u} \end{cases} \quad (7)$$

where $\bar{\mathbf{x}}_1$ are the states to be retained, a q -dimensional vector. $\bar{\mathbf{x}}_2$ are the states to be eliminated, $\bar{\mathbf{x}}_2 = -\bar{\mathbf{A}}_{22}^{-1}\bar{\mathbf{A}}_{21}\bar{\mathbf{x}}_1 - \bar{\mathbf{A}}_{22}^{-1}\bar{\mathbf{B}}_2\mathbf{u} - \bar{\mathbf{A}}_{22}^{-1}\bar{\mathbf{h}}_2\ddot{\mathbf{x}}_g$. This way, the reduced state system is:

$$\begin{cases} \dot{\mathbf{x}}_r = \mathbf{A}_r\mathbf{x}_r + \mathbf{B}_r\mathbf{u} + \mathbf{h}_r\ddot{\mathbf{x}}_g \\ \mathbf{y} = \mathbf{C}_r\mathbf{x}_r + \mathbf{D}_r\mathbf{u} + \mathbf{h}_y\ddot{\mathbf{x}}_g \end{cases} \quad (8)$$

where: $\mathbf{A}_r = \bar{\mathbf{A}}_{11} - \bar{\mathbf{A}}_{12}\bar{\mathbf{A}}_{22}^{-1}\bar{\mathbf{A}}_{21}$, $\mathbf{B}_r = \bar{\mathbf{B}}_1 - \bar{\mathbf{A}}_{12}\bar{\mathbf{A}}_{22}^{-1}\bar{\mathbf{B}}_2$, $\mathbf{h}_r = \bar{\mathbf{h}}_1 - \bar{\mathbf{A}}_{12}\bar{\mathbf{A}}_{22}^{-1}\bar{\mathbf{h}}_2$, $\mathbf{C}_r = \bar{\mathbf{C}}_1 - \bar{\mathbf{C}}_2\bar{\mathbf{A}}_{22}^{-1}\bar{\mathbf{A}}_{21}$, $\mathbf{D}_r = \mathbf{D} - \bar{\mathbf{C}}_2\bar{\mathbf{A}}_{22}^{-1}\bar{\mathbf{B}}_2$, $\mathbf{h}_y = -\bar{\mathbf{C}}_2\bar{\mathbf{A}}_{22}^{-1}\bar{\mathbf{h}}_2$, and $\mathbf{x}_r = \bar{\mathbf{x}}_1$.

Therefore, for the system (8), the index to be minimized is:

$$J = \frac{1}{2} \int_0^{t_f} [\mathbf{x}'_r \mathbf{Q}_e \mathbf{x}_r + \mathbf{u}' (\mathbf{R} + \mathbf{R}_e) \mathbf{u} + 2\mathbf{x}'_r \mathbf{N}_e \mathbf{u}] dt \quad (9)$$

where $\mathbf{A}_e = \begin{bmatrix} \mathbf{I} & -\bar{\mathbf{A}}_{22}^{-1}\bar{\mathbf{A}}_{21} \end{bmatrix}$, $\mathbf{B}_e = \begin{bmatrix} \mathbf{0} & -\bar{\mathbf{A}}_{22}^{-1}\bar{\mathbf{B}}_2 \end{bmatrix}$, $\mathbf{N}_e = \mathbf{A}'_e (\bar{\mathbf{T}}^{-1})' \mathbf{P}'_c \mathbf{Q} \mathbf{P}_c \bar{\mathbf{T}}^{-1} \mathbf{B}_e$, $\mathbf{Q}_e = \mathbf{A}'_e (\bar{\mathbf{T}}^{-1})' \mathbf{P}'_c \mathbf{Q} \mathbf{P}_c \bar{\mathbf{T}}^{-1} \mathbf{A}_e$, and $\mathbf{R}_e = \mathbf{B}'_e (\bar{\mathbf{T}}^{-1})' \mathbf{P}'_c \mathbf{Q} \mathbf{P}_c \bar{\mathbf{T}}^{-1} \mathbf{B}_e$.

Note that, because of the above transformations, Equation (9) is an approximation of the Equation (2). The corresponding Riccati equation is then:

$$\mathbf{P}\mathbf{A} - (\mathbf{P}\mathbf{B} + \mathbf{N}_e)(\mathbf{R} + \mathbf{R}_e)^{-1}(\mathbf{B}'\mathbf{P} + \mathbf{N}'_e) + \mathbf{A}'\mathbf{P} + \mathbf{Q}_e = \mathbf{0} \quad (10)$$

and the gain matrix is expressed by: $\mathbf{K} = (\mathbf{R} + \mathbf{R}_e)^{-1}(\mathbf{B}'\mathbf{P} + \mathbf{N}'_e)$.

For real applications, the model from Equation (8) can be adapted into the form:

$$\begin{cases} \dot{\mathbf{x}}_r = \mathbf{A}_r \mathbf{x}_r + \mathbf{B}_r \mathbf{u} + \mathbf{h}_r \ddot{\mathbf{x}}_g + \mathbf{G} \mathbf{w} \\ \mathbf{y}_m = \mathbf{C}_r \mathbf{x}_r + \mathbf{D}_r \mathbf{u} + \mathbf{h}_y \ddot{\mathbf{x}}_g + \mathbf{H} \mathbf{w} + \mathbf{v} \end{cases} \quad (11)$$

where \mathbf{w} and \mathbf{v} are the process noise and the measurement noise vectors respectively; \mathbf{G} and \mathbf{H} are distribution matrices and \mathbf{y}_m is the measured output vector.

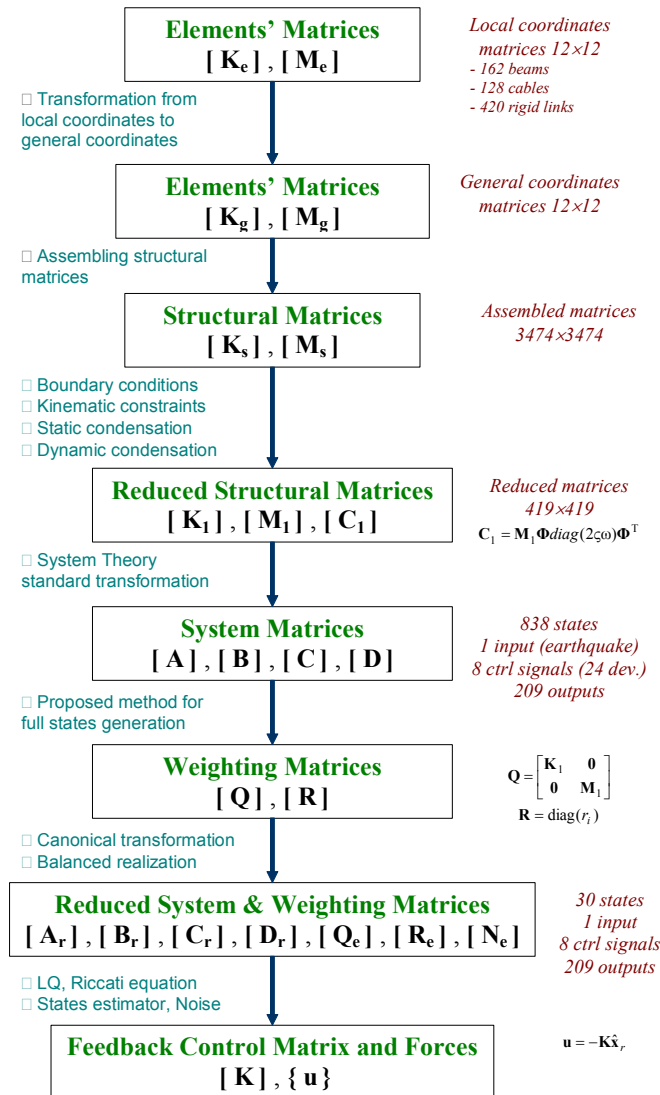


Figure 1. Overview of the proposed procedure and application to benchmark (right column)

The states of the system (11) can be estimated from the measured outputs using for example a Kalman filter [16]:

$$\dot{\hat{\mathbf{x}}}_r = \mathbf{A}\hat{\mathbf{x}}_r + \mathbf{B}\mathbf{u} + \mathbf{L}(\mathbf{y}_m - \mathbf{C}_r\hat{\mathbf{x}}_r - \mathbf{D}_r\mathbf{u}) \quad (12)$$

where $\hat{\mathbf{x}}_r$ is the vector of estimated states and \mathbf{L} is the filter gain matrix deduced from solving also a Riccati equation. Then the control forces are: $\mathbf{u} = -\mathbf{K}\hat{\mathbf{x}}_r$.

All the procedure shown above is formulated in continuous time. The application in the next section is using the discrete time version of the method as the practice requires. A time delay between the computation of control forces and their application is also considered. Supposing a time delay equal to the sampling time, Δt , the control forces are applied at the time, t_{i+1} . This is one step after the real measuring time, t_i , when the measurement vector, $\mathbf{y}_{m,i}$, was obtained.

Benchmark Control Design and Simulations

The control procedure previously described (Figure 1) is applied to the model of a cable-stayed bridge, Cape Girardeau over Mississippi River, that is the object of a benchmark problem [10]. Figure 2 shows the diagram of the conceptual control system imposed by the benchmark and a FEM model of the bridge with the instrumentation proposed on it is shown in Figure 3.

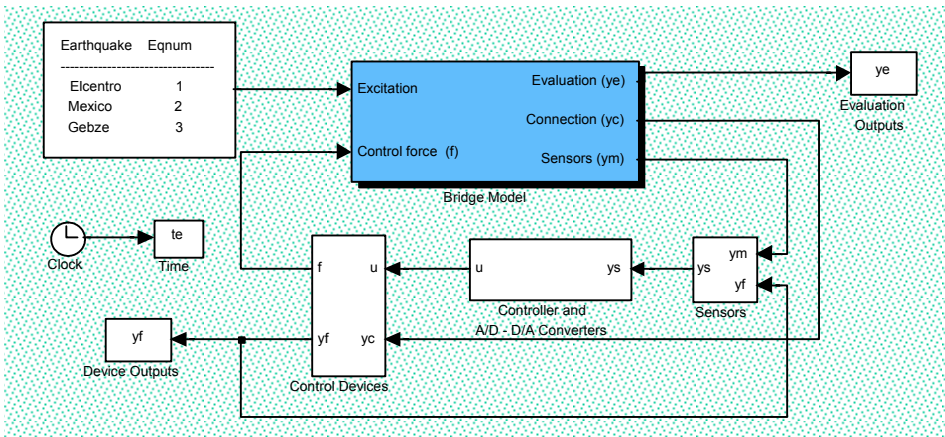


Figure 2. Conceptual control system of the benchmark problem

The main span of the bridge is 350.6 m with the side spans of 142.7 m in length. It has a total of 128 cables that connect the 29.3 m wide deck with the towers, 100 m and 105 m tall.

Figure 4 shows the Response Spectrums, 3% Damping, the of the three applied actions, El-Centro NS, 1940, Mexico City, 1985, and Gebze NS, 1999, (right).

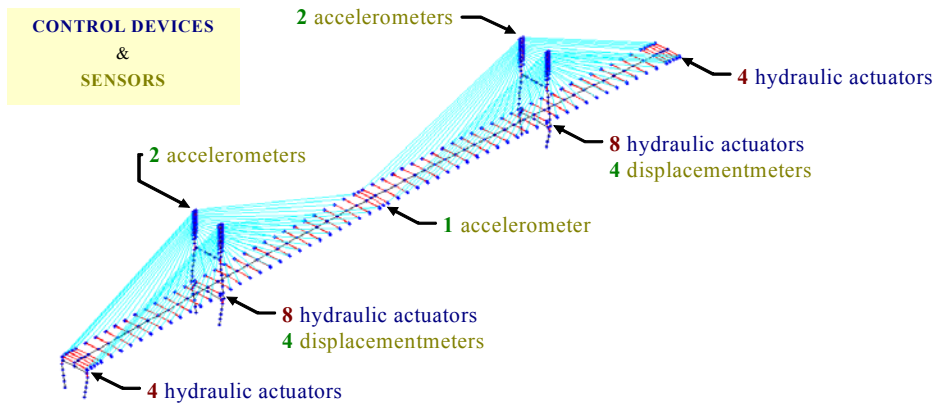


Figure 3. FEM model of the bridge and the instrumentation

Statical reduction of the initial FEM model leads to a 419 dynamical degrees of freedom system. The system is reduced to a system with 30 states, as it is done in the benchmark sample scheme, for reasons of comparisons. The whole strategy is shown by the diagram in Figure 1.

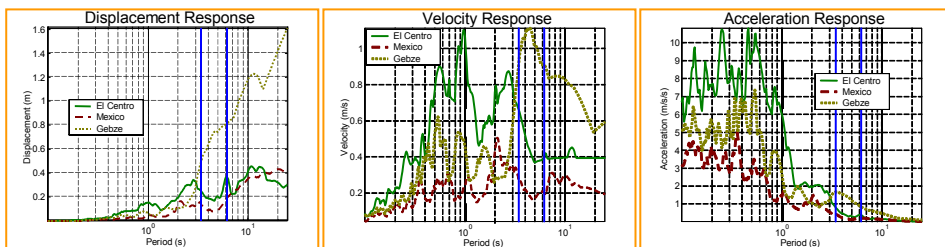


Figure 4. Comparison of the Response Spectrums, 3% Damping (El Centro NS 1940, Mexico City NS 1985, Gebze NS 1999)

For the digital implementation, continuous to discrete-time signal converters are included. Four longitudinal direction accelerometers are placed on the tops of the towers and one is located in the mid span. Four sensors measuring displacements were located between the towers and the deck [10], see Figure 3.

To evaluate and compare the results of the proposed control strategies, the benchmark establishes 18 performance criteria. First six criteria refer to peak responses; the criteria from seven to eleven are related to normed responses, while the criteria twelve to eighteen are concerned to control strategy.

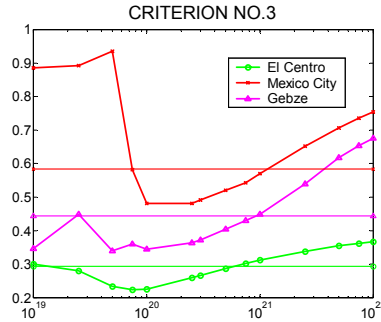


Figure 5. Criterion no.3 as a function of r

In order to choose a suitable value for the weighting matrix \mathbf{R} , based on a unique scalar r , comparisons between the responses or criteria have been performed. For this application, in the case of non-predictive control option, the scalar r took 14 different values within the interval $[1.0e19, 1.0e22]$. As an example of the design strategy, in Figure 5 the variation of the criterion number three (relative, maximum overturning moment for towers) as a function of the scalar r is presented. The values of these criteria given in the benchmark sample solution are also presented (as horizontal lines of the same type) for comparison. It can be seen a non-constant behavior of the results (values of criteria). In addition, this behavior is still a function of the three external actions (earthquakes), so different in content and effects.

Following the previous paragraphs' ideas, Table 1 shows a numerical comparison for the different results obtained for the first 15 criteria under the selected values for r . For each of the three earthquake actions there are shown two different columns with criteria values. The case at left refers to the benchmark given sample control (as the base of comparison). The case at the right refers to applying the strategy proposed in the section above, with $r = 1.0e20$. As a general idea, the proposed strategy is better than the benchmark example.

4. Conclusions

The previous results in [11], [12] are further improved for the need of more realistic applications. The weighting matrix \mathbf{Q} tuning is done on energy-based procedure for the full state system. Since the measurements and the estimators cannot assure the knowledge or approximation of too many states, a reduced order model is employed [14, 15]. The matrix \mathbf{Q} is reduced following similar transformations, as the system itself. A finite element model of a bridge proposed as a benchmark problem for structural control under seismic actions [10] is used for application. The discrete-time simulations include the requirements on the

process noise and the measurement noise. Good behavior of the controlled system according to the benchmark evaluation criteria set is noted and discussed.

Table 1. Comparison of results from benchmark and proposed application

Criteria	No Control	El Centro Earthquake	Mexico Earthquake	Gebze Earthquake			
J ₁	1.0000	0.3868	0.3111	0.4582	0.5289	0.4540	0.3930
J ₂	1.0000	1.0681	0.9618	1.3693	1.9527	1.3784	1.1285
J ₃	1.0000	0.2944	0.2249	0.5836	0.4821	0.4434	0.3443
J ₄	1.0000	0.6252	0.6021	0.6140	0.6010	1.2246	0.9447
J ₅	0.8029	0.1861	0.1799	-	-	-	-
J ₅	0.1481	-	-	0.0775	0.0598	-	-
J ₅	0.3832	-	-	-	-	0.1481	0.1250
J ₆	1.0000	1.2006	0.9903	2.3317	2.1423	3.5640	2.7958
J ₇	1.0000	0.2257	0.3910	0.3983	1.2238	0.3231	0.7172
J ₈	1.0000	1.1778	3.7022	1.2118	8.6430	1.4371	7.0297
J ₉	1.0000	0.2665	0.2359	0.4192	0.4769	0.4552	0.4277
J ₁₀	1.0000	0.8813	0.8352	1.1067	1.9712	1.4570	1.7293
J ₁₀	0.0867	0.0280	0.0201	-	-	-	-
J ₁₁	0.0225	-	-	0.0103	0.0079	-	-
J ₁₁	0.0423	-	-	-	-	0.0171	0.0133
J ₁₂ *10 ³	-	1.5887	0.0020	0.5744	0.0020	1.7145	0.0020
J ₁₃	-	0.7883	0.6502	1.1742	1.0789	1.9541	1.5329
J ₁₄ *10 ³	-	2.7011	0.0038	1.7523	0.0038	7.3689	0.0094
J ₁₅ *10 ⁴	-	4.2871	0.0006	2.3343	0.0005	6.9492	0.0009
J ₁₆	-	24	24	24	24	24	24
J ₁₇	-	9	9	9	9	9	9
J ₁₈	-	30	30	30	30	30	30

Acknowledgements

This work was supported in part by the ASCR under Grant A2075304, by the CNCSIS under Grant 33371-542-04, and by the CICYT under Grant DPI2002-04018-C02-01.

References

1. Yao, T.P.J., Concept of structural control. *Journal of Structural Division*, vol. 98 (St7), 1972.

2. Păuleț-Crăiniceanu, F., *Active Control Approach for Long Span Bridge Responses to Strong Earthquakes*, Ph.D. Thesis, Yokohama National University, Yokohama, 1997.
3. Schemann, A.G. and Smith, H.A., Vibration control of cable-stayed bridges. *Earthquake Engineering and Structural Dynamics*, vol. 27, 1998.
4. Achkire, Y. and Preumont, A., Active tendon control of cable-stayed bridges. *Earthquake Engineering and Structural Dynamics*, vol. 25, 1996.
5. Magaña, M.E. and Rodellar, J., Nonlinear decentralized active tendon of cable-stayed bridges. *Journal of Structural Control*, vol. 5, 1998.
6. Bakule, L. Păuleț-Crăiniceanu, F., Rodellar J., Decentralized control design for a cable-stayed bridge benchmark. *Proceedings of the 2002 American Control Conference*, Anchorage, Alaska, USA, 2002.
7. Luo, N., de la Sen, M., Rodellar, J. and Magaña, M.E., Decentralized sliding mode control of a two-cable stayed bridge. In Holnicki, J. and Rodellar, J., editors, *NATO ARW Workshop on Smart Structures*, Kluwer Academic, Dordrecht, 1998.
8. Păuleț-Crăiniceanu, F., Seismic response control of long cable-stayed bridges. *Proceedings of the Second World Conference on Structural Control*, vol. 2, John Willey & Sons, Chichester, 1999..
9. Wong, K.F.K. and Yong, R., Effectiveness of structural control based on control energy perspectives. *Earthquake Engineering and Structural Dynamics*, vol. 30, 2001.
10. Dyke, S.J., Bergman, L.A., Turan, G. and Caicedo, J.M., Benchmark control problem for seismic response of cable-stayed bridges. <http://wusceel.cive.wustl.edu/quake>, 2000.
11. Păuleț-Crăiniceanu, F., Rodellar J., and Monroy C., Control Settings and Performance Analysis of an Optimal Active Control Method for Cable Bridges, *ECCM-2001, 2nd European Conference on Computational Mechanics*, CD-ROM Datacomp, Cracow, Poland, 2001.
12. Păuleț-Crăiniceanu, F., Rodellar J., Optimal seismic response control of a long span cable-stayed bridge for a benchmark problem. *Engineering Construction and the Environment*. Matei-Teiu Botez, Iasi, 2003.
13. Păuleț-Crăiniceanu, F., Structural active control for buildings and bridges in seismic areas. *Proceedings of the International Conference on Advanced Problems in Vibration Theory and Applications, ICAPV2000*, Science Press, Beijing, 2000.
14. Kailath, T., *Linear Systems*. Prentice-Hall, Englewood Cliffs, 1980.
15. Inman, D.J., *Vibration with Control, Measurement, and Stability*. Prentice Hall, Englewood Cliffs, 1989.
16. Bryson, A.E. and Ho, Y.C., *Applied Optimal Control*, John Wiley & Sons, New York, 1975.

CHECKS OF THE TUBULAR JOINTS AND STRUCTURAL ELEMENTS FOR THE “ROMEXPO” PAVILION DOME

Alexandru DIMA¹, Ionuț Radu RĂCĂNEL²

Abstract

In this paper are presented some results for resistance checks of tubular joints and stability checks for the structural elements of the “ROMEXPO” pavilion dome in Bucharest. All these results come from a expert survey carried out in the Steel Bridges Department of the Faculty of Railways, Roads and Bridges in Bucharest during the year 2003.

The structure has been built for the first time in 1961 in the solution single layer dome, through adapting a structure which was developed for the first time in Brno, the Czech Republic. After the collapse of the structure caused by a asymmetrical snow concentration in the winter of the year 1961, the dome was rebuilt between 1963-1964, using another solution, consisting in truss arches made from circular hollow sections.

At that time, the behaviour of the whole structure, after the collapse, has been studied on reduced scale models (1:10). The sectional stresses used in the checks of the structural elements are obtained using simplified calculation models and methods and no particular checks for the tubular joints are performed.

Today, the development of hardware and software for structural analysis allow to consider a large number of hypotheses for the behaviour of structures. Also, the evolution of the standards and norms for concrete and steel structures suggest many actions and combinations of actions which are not tacked into account at the moment when the “ROMEXPO” pavilion dome was built.

Even with the help of these modern computational methods, the analysis of the steel structure of the dome still remain very complex. The sectional stresses used to perform all the checks presented in this paper are obtained from a three dimensional static analysis carried out with a general purpose finite element software, SAP 2000. Following the international prescriptions which are allowed in Romania for the verification of the structures made from hollow sections, at the Department of Steel Bridges, some verification software are developed. In this manner the resistance of tubular joints and the stability of the structural elements of the dome according the actual norms could be performed.

¹ Assistant Professor Alexandru DIMA, Ph. D, Technical University of Civil Engineering Bucharest, e-mail: adima@cfdp.utcb.ro

² Lecturer Ionuț Radu RĂCĂNEL, Ph. D, Technical University of Civil Engineering Bucharest, e-mail: ionut@cfdp.utcb.ro

1. Description of the finite element model

The steel structure of the dome of “ROMEXPO” pavilion exhibition consist in 32 truss semi-arches, with a triangular cross section. The structural elements of those arches are circular hollow sections connected directly at joints through weld. In the key stone all semi-arches are connected through a ring, which has a cross sections made from riveted plates and angles. Also, in the upper zone of the semi-arches, these are connected through a bracing system. At the bottom part, between the arches exists skylights and two rings around the dome. This two rings are executed as truss girders, made from circular hollow sections and having also a triangular cross section similar to the semi-arches. In the skylights zone, a bracing system consisting in Φ 35 mm crossing tensioned steel cables was considered at the design moment, but at this time these cables does not exist in the structure.

Tacking into account the complexity of the structure a space finite element model has been built using a general purpose finite element program, SAP 2000. Following the structure of the dome and his geometry, from the finite element library of the structural analysis program, the frame element has been chosen. The curved structural elements of the dome are also modeled using straight frame elements, but the number of segments is increased automatically by the program in order to minimize the difference between the subtense of the circle and the circular curve.

The Frame element uses a general, three-dimensional, beam-column formulation which includes the effects of biaxial bending, torsion, axial deformation, and biaxial shear deformations. For each frame element different cross-sections, local axes and end releases can be defined. The definition of particular local axes is necessary to respect the orientation in space of the element and his cross section characteristics. All the elements are considered as rigid connected at joints, the rigidity of each joint resulting from the rigidity of each frame element which comes to the node. For each frame element a number of 4 (four) output stations is considered. These output stations are the points where the program computes and display the results.

For the central ring of the dome, in the zone of the semi-arches key stone, 32 shell elements with four nodes are used (figure 1b).

The Shell element is a three- or four-node formulation that combines separate membrane and plate-bending behaviour. The four-joint element does not have to be planar. The membrane behaviour uses an isoparametric formulation that includes translational in-plane stiffness components and a rotational stiffness component in the direction normal to the plane of the element. The plate bending behaviour includes two-way, out-of-plane, plate rotational stiffness components and a translational stiffness component in the direction normal to the plane of the element. By default, a thin-plate (Kirchhoff) formulation is used that neglects transverse shearing deformation. Also, a thick-plate (Mindlin/Reissner)

formulation which includes the effects of transverse shearing deformation can be chosen.

In this finite element model, combined membrane-shell behaviour is considered. For each shell element, local axes are defined, in order to respect the space orientation of the element and the correct definition of the element thickness.

The whole space finite element model of the dome includes 7536 joints, 15360 frame elements and 32 shell elements. A general view of the discrete model is presented in figure 1a. In figure 1b, the discrete model of the central ring and his connections with arches, is shown.

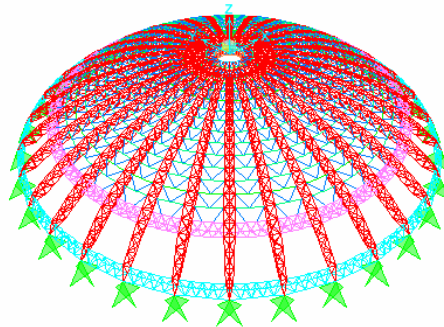


Figure 1a – Finite element model of the steel dome

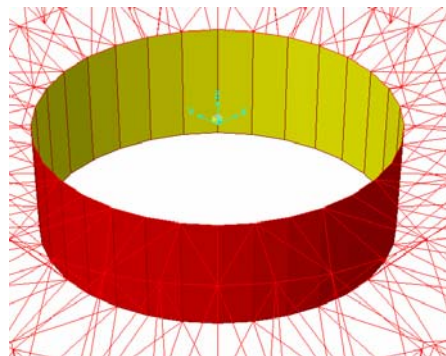


Figure 1b – Detail with the discrete model of the central ring

The dome is made from steel OL37 and in the analysis program the behaviour of the material was considered to be linear elastic. The elasticity modulus of the steel is $E=210000 \text{ N/mm}^2$ and Poisson's coefficient is 0.3.

2. ACTIONS AND COMBINATIONS OF ACTIONS ACTING ON THE DOMES STRUCTURE

For the static analysis of the steel dome, in order to obtain the sectional stresses to check the resistance of tubular joints and the stability of structural elements, according to actual romanian norms for structures, the following actions are considered:

- the self-weight of the structure (G), computed by the analysis program, using the geometry of each structural element and the mass density of the material
- wind action (V), with both effects, pression/suction
- snow load (Z), having both symmetrical and asymmetrical distribution.

All these actions are considered as forming the fundamental group of actions and two calculation hypotheses are tacked into account:

Hypothesis A1:

$$n_d \cdot G + n_g \cdot (n \cdot V + n \cdot Z_{n/ns}) \quad (1)$$

Hypothesis A2:

$$n \cdot G + n_g \cdot (n_d \cdot V_{su} + n \cdot V_p + n \cdot Z_{s/ns}) \quad (2)$$

where

G, V, Z are the actions symbols;

n_d and n are the coefficient to multiply de actions for the favorable or unfavorable effect respectively;

n_g is the coefficient for grouping of actions;

s/ns are subscripts which help to choose the maximal sectional stress from two snow loading situations, symmetrical or unsymmetrical;

su, p are subscripts for the effect of suction and pression of wind loading.

All the loads coming from the hypotheses presented above are introduced into discrete model as concentrated joint loads. Through the static analysis, the sectional stresses for all the structural elements has been computed. For the most important elements in the dome structure, having the biggest values for axial force or bending moment, values obtained through a sort made by de analysis program, some checks have been performed. The final values of the sectional stresses used in resistance and stability checks are obtained according to the two hypotheses presented above.

The sectional stresses diagrams (axial force N , bending moment in plane 1-2, M_{33} , bending moment in plane 1-3, M_{22}) for the self-weight load of the steel dome are presented in figure 2a, b, c.

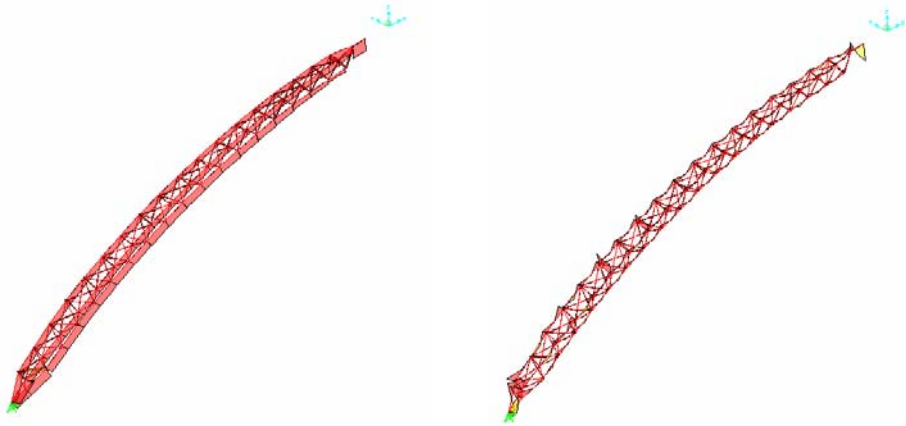


Figure 2a – Axial force N diagram for Semi-arch number 1 Figure 2b – Bending moment M_{33} diagram for semi-arch number 1

Semi-arch number 1

diagram for semi-arch number 1

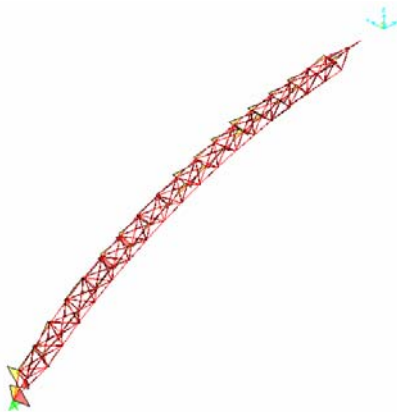


Figure 2c – Bending moment M_{22} diagram for semiarch number 1

3. RESISTANCE CHECKS FOR TUBULAR JOINTS AND STABILITY CHECKS FOR STRUCTURAL ELEMENTS

3.1 Resistance checks for tubular joints

For tubular joints of the steel dome, the resistance checks have been performed according to the norms used in the steel offshore design made from hollow

sections. According to the norms accepted in Romania for the offshores checks the following verification criteria are used:

- a) Geometrical condition for the check of the tubular joints for compression and tension:

$$F_{yb}(\gamma \sin \theta) / F_{yc}(11 + 1.5\beta) \leq 1 \quad (3)$$

where:

F_{yb}, F_{yc} - yield stress limit of the steel for brace and chord respectively
 $\gamma = D/2T$; $\beta = d/D$; $r = t/T$ – the parameters of the joint with D, d - chord diameter and brace diameter respectively; T, t – chord and brace thickness;
 θ - the brace angle (measured from the chord)

- b) Check condition for the penetration of the tubular joint through the shear of the main tube (chord):

b.1 Check of the penetration stress:

$$v_p = (rf \sin \theta) / \beta \leq v_{pa} = Q_q Q_f (F_{yc} / 0.6\gamma) \quad (4)$$

where:

v_p, v_{pa} – punching shear and punching shear capacity respectively
 Q_q, Q_f – design factors according to joint and load type

- b.2 Check of the penetration stresses resulting from the combination of the bending moments in the braces plane (MP) and normal to the braces plane (MNP):

$$\left[v_p(MP) / v_{pa}(MP) \right]^2 + \left[v_p(MNP) / v_{pa}(MNP) \right]^2 \leq 1 \quad (5)$$

- b.3 Check of the combination of the penetration stresses coming from axial sectional stress, bending moment in braces plane (MP) and bending moment in a plane normal to the braces plane (MNP):

$$v_p(N) / v_{pa}(N) + 2 / \pi \arcsin \{ [v_p(MP) / v_{pa}(MP)]^2 + [v_p(MNP) / v_{pa}(MNP)]^2 \}^{1/2} \leq 1 \quad (6)$$

- c) Check condition of the tubular joint for the nominal stress in brace:

c. 1 Check of the stresses in the brace:

$$\begin{aligned}
 N &\leq N_a = Q_q^N Q_f^N F_{yc} T^2 / (1.7 \sin \theta) \\
 MP &\leq MP_a = Q_q^{MP} Q_f^{MP} F_{yc} T^2 / (1.7 \sin \theta) \\
 MNP &\leq MNP_a = Q_q^{MNP} Q_f^{MNP} F_{yc} T^2 / (1.7 \sin \theta)
 \end{aligned}
 \tag{7}$$

where:

N_a, MP_a, MNP_a – axial, bending moment in the braces plane and normal to the braces plane capacity

c.2 Check for the combination of the bending moment in the braces plane and normal to the braces plane:

$$[MP/MP_a]^2 + [MNP/MNP_a]^2 \leq 1
 \tag{8}$$

c.3 Check for the combination of the axial stresses N and bending moments in the braces plane MP and normal to the braces plane MNP:

$$N/N_a + 2 / \pi \arcsin\{[MP/MP_a]^2 + [MNP/MNP_a]^2\}^{1/2} \leq 1
 \tag{9}$$

3.2 Stability (buckling) checks for structural elements

According to the norm GERMANISCHER LLOYD, Section 3, the relationship for the structural elements, subjected to an axial force N and to a bending moment coming from $M = (MP^2 + MNP^2)^{1/2}$, is:

$$(\gamma \cdot N) / (\chi \cdot N_p) + \beta(\gamma \cdot N) / M_p + \Delta_n \leq 1
 \tag{10}$$

where:

- N_p, M_p - plastic compression resistance force and plastic resistance bending moment respectively;
- χ - reduction factor for flexural buckling (according to buckling curves);
- $\Delta_n = 0.25 \cdot \chi^2 \cdot (N_p \cdot \gamma_m) / N_e$, with N_e = Euler buckling force

4. RESULTS AND CONCLUSIONS

In order to perform resistance checks for tubular joints and stability checks for the structural elements of the steel dome, some computation software were developed at the Steel Bridges Department of the Faculty of Railways, Roads and Bridges. These programs are: “NodK.exe” for joints having “K” form and “NodT-Y.exe” for joints having “T” or “Y” form. The program “flambaj” was very useful to check the structural elements for stability.

The sectional stresses are computed with the help of SAP 2000 program for two situations: the steel dome having crossing tensioned steel cables Φ 35 mm in the skylight zone and the case of the structure without these cables. After the sort of the structural elements, only those having the biggest values for the sectional stresses are verified.

To perform the resistance check of tubular joints, the node number 1775 is chosen. For the stability check of the structural elements two frames element are chosen: 5064 and 5221. The selected elements and joint are shown in the figure 3.

For the tubular joints that have been checked, the allowable limit presented in relationships (4)-(9) is not exceeded.

For the stability checks, according to the relationship (10) the obtained results are:

- a) for the structure without tensioned steel cables in the skylight zone:
 - element 5064: $(\gamma \cdot N)/(\chi \cdot N_p) + \beta(\gamma \cdot N)/M_p + \Delta n = 1.179 > 1$
 - element 5221: $(\gamma \cdot N)/(\chi \cdot N_p) + \beta(\gamma \cdot N)/M_p + \Delta n = 1.006 > 1$
- b) for the structure with tensioned steel cables in the skylight zone:
 - element 5064: $(\gamma \cdot N)/(\chi \cdot N_p) + \beta(\gamma \cdot N)/M_p + \Delta n = 1.026 > 1$
 - element 5221: $(\gamma \cdot N)/(\chi \cdot N_p) + \beta(\gamma \cdot N)/M_p + \Delta n = 0.831 < 1$

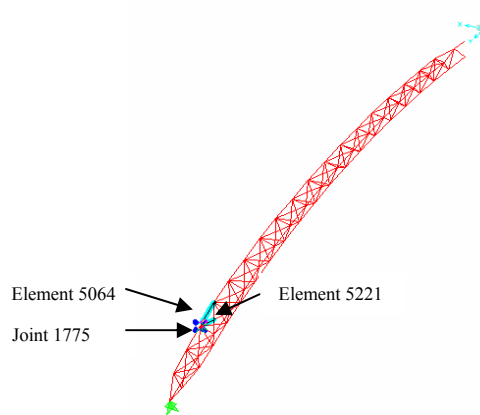


Figure 3 – Tubular joint and structural element selected to be checked

According to this results it can be concluded that no problems concerning the resistance of tubular joints exists. From stability point of view, some structural elements are near to the them buckling limit. A solution to decrease the value of the axial stresses and bending moments, which can produce the buckling phenomena, can be the reintroduction of the stiffening tensioned steel cables Φ 35 mm in the skylight zone of the dome, which at this moment are not present in the structure.

5. REFERENCES

1. ***, API RP 2A-LRFD – Load and Resistance Factor Design (Edition 1993).
2. ***, API RP 2A-WSD – Recommended Practice for Planning, Designing and Constructing Fixed Offshore Platforms – working Stress Design (Edition 1993).
3. ***, GERMANISCHER LLOYD – Rules for Classification and Construction, Offshore Technology (Edition 1999).
4. Computers and Structures Inc., SAP 2000 – Reference Manual, 2003.
5. S.C. Consis Proiect S.R.L., Steel dome of the “ROMEXPO” pavilion – technical expert appraisal, 2003.

**DYNAMIC ANALYSIS OF THE “ROMEXPO” PAVILION DOME
USING A 3D FINITE ELEMENT MODEL**

Ionuț Radu RĂCĂNEL¹, Alexandru DIMA²

Abstract

The aim of this paper is to present some important results of the static and dynamic analyses of the “ROMEXPO” Pavilion Dome performed using a 3D-finite element model. The necessity of these calculations has been imposed because of the fact that the structure was designed and built between 1962-1964 and in that period of time the possibilities to compute complex structures were very limited. In the mean time, the norms and standards used for structures and also the computational possibilities have known till today a continuous and fast evolution.

The analysis of the project documentation, of the initial calculation methods and models underline some uncertainties of the obtained results, aspect which is mentioned in some successive expert’s reports made during the year 1963. The structure of the dome is a space structure made using circular hollow sections, welded at joints and at that period of time the norms and calculation possibilities concerning the check of tubular joints does not exists.

The 3D finite element model includes the concrete frames, radial disposed, having two circular floors and the steel dome consisting in a space structure, with truss arches and wind bracing system, all made from welded circular hollow sections.

The model has been established using the data from the initial design project, completed with those resulted from an inspection in situ. By considering this model a static analysis is performed, in order to obtain the maximum sectional stresses in the structural elements. The loads considered in this analysis were: self-weight of the structure, the effect of wind and snow combined in calculation hypotheses according to the actual norms and standards for limit state design. The model was also used for a dynamic analysis to establish the first nine eigenvalues of the structure and their corresponding periods. In the same time, according to the Romanian norm P100, the response of the structure under a seismic horizontal and vertical load is computed. In this paper only the results of the dynamic analysis are presented.

¹ Lecturer Ionuț Radu RĂCĂNEL, Ph. D, Technical University of Civil Engineering Bucharest, e-mail: ionut@cfdp.utcb.ro

² Assistant Professor Alexandru DIMA, Ph. D, Technical University of Civil Engineering Bucharest, e-mail: adima@cfdp.utcb.ro

1. Short historic

The central pavilion of the exhibition center of Bucharest has been opened for public in the 1961 and he had a single layer steel dome. The adopted solution was similar with the one used in Brno, the Czech Republic, but he had supplementary around the base of the dome a concrete flat roof inclined through the base of the dome. In the next winter, during a snow storm, a unsymmetrical snow load on one side of the dome, at her base is produced (the depth of the snow was about 5 m and the affected surface about 1000 m²), having as consequence the collapse of the steel dome.

Between 1963-1964 a new reconstruction solution for the steel dome has been adopted. This consist in a space structure with truss arches made from welded circular hollow sections, arches which are jointed together using steel rings and bracing system (Figure 1, 2).



Figure 1 – General view of the “ROMEXPO” pavilion

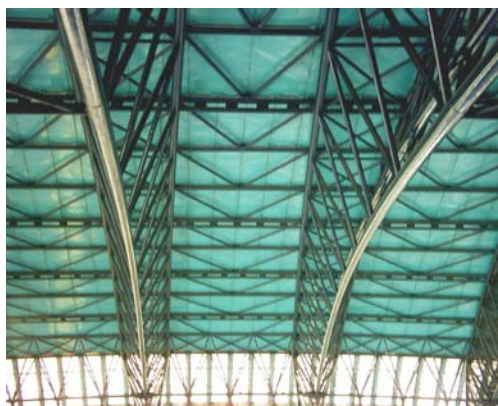


Figure 2 – View inside the dome. Truss semi-arches and bracing system

For the reconstruction of the dome structure, a number of tests on specimens on reduced scale are performed. This tests are carried out by loading the structure in different points of the structure at different load levels and till fracture. The behaviour of the dome under symmetrical and unsymmetrical snow loads has been also considered, by analyzing the effect of those on some reduced scale models (1:10). With this occasion some new welding and construction procedure are tested.

Even today, with the help of the new computational methods, the calculation of the steel structure still remain very complex and consume a lot of time.

2. Description of the structure

The concrete structure consist in concrete frames, radial disposed, starting from the base of the arches to the exterior and has at the upper part two concrete floors. The last floor is inclined through the interior of the pavilion and connected with a ring made from reinforced concrete. On this ring are disposed the supporting saddle which sustain the arches bearings and undertake a part from the reactions coming from arches.

The steel dome consist in 32 truss semi-arches having a triangular cross section (Figure 2). The elements of the arches are fabricated from circular hollow sections which are welded at joints. Each semi-arch has in the springing zone a bearing disposed on the reinforced concrete ring. At the semi-arches key stone region these are rigid fixed on a massive steel ring, consisting from riveted curved plate girders. On the top part of the truss arches are placed crossing diagonals and verticals. On the lateral faces of the semi-arches, the diagonals are executed in triangular system, without verticals. The upper and bottom flanges of the semi-arches are curved hollow sections and the distance between them varies. The dimensions of the circular hollow sections for the semi-arches flanges are: $\Phi 152 \times 18$ at the ends and $\Phi 146 \times 16$ in the span. The structural elements are fixed directly through welding at joints. Each semi-arch consist in two transoms welded at the site. All the joints disposed on the top part of the semi-arches follow a spherical cup with the dimensions:

- height, about 18.523 m
- diameter at the cup base (span of the dome) is 93.500 m.

Another component of the dome structure are “A”girders which make the connection between semi-arches in the springing zone. They are also truss girders with triangular cross section, having the upper flanges made from curved circular hollow sections and the bottom flange consist in a straight plate girder. The section of the bottom flange is rotated in order to simplify the connection with the cross section of the semi-arches (Figure 3).



Figure 3 – Detail with the semi-arches connection above the bearings

The “B” girders are truss girders having a triangular cross section and all structural elements made from curved circular hollow sections. They form a rigid ring above the skylight of the dome. Together, the “A” and “B” truss girders form frame panels in the zone of skylights, frames which can ensure the stability of the dome in absence of bracing system. In the initial project, the dome was equipped in the skylight zone with a bracing system consisting in tensioned steel cables Φ 35 mm, but at this moment these cables are not present.

The bracing system of the dome (Figure 2) is made from circular hollow sections and ensure the connection between semi-arches at the upper part on the zone starting from “B” girders and till the central ring at the key stone of the semi-arches. Supplementary, to increase the rigidity of each semi-arch, in some joints above the bracing system, another circular hollow section ring is disposed. This is connected with the bracing system through small welded plates like in figure 2.

In the semi-arches key stone region is placed the central steel ring (Figure 4). He has two walls connected with vertical diaphragms and horizontal webs at the connection with the semi-arches. The ring diameter between the walls axes is 5650 mm and the depth of the box cross section of the ring is about 2500 mm. All the elements forming the central ring have been assembled using rivets.

The bearings placed under each semi-arch enable only the rotation in a plane passing through the axis of each of them. They are fabricated from cast carbon steel OT 35 A and the bolt is made from steel OLC 35. Each bearing device is fixed with anchor bolts on the reinforced concrete ring forming the supporting saddle.

The desired curvature of the structural elements was obtained through cold or hot bending procedure taking into account the position of each element in structure.



Figure 4 – View with the connection between the bottom flanges of the semi-arches at the central ring

3. 3D Finite element model

The finite element model was build using one-dimensional straight frame elements to model the structural elements of the truss semi-arches, girder “A”, “B” and bracing system and shell elements to model the central ring of the dome. The total number of joints was 7536, the number of frame elements was 15360 and the number of shells was 32 (Figure 5).

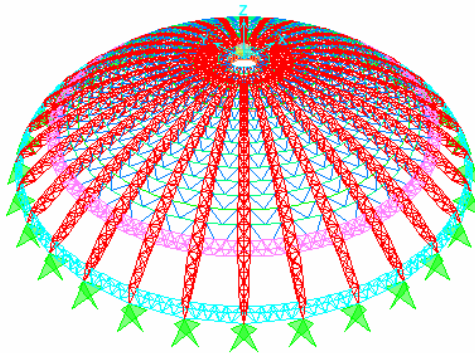


Figure 5 – 3D finite element model of the steel dome

The Frame element uses a general, three-dimensional, beam-column formulation which includes the effects of biaxial bending, torsion, axial deformation, and biaxial shear deformations.

The Shell element is a three- or four-node formulation that combines separate membrane and plate-bending behavior. The four-joint element does not have to be planar. The membrane behavior uses an isoparametric formulation that includes translational in-plane stiffness components and a rotational stiffness component in

the direction normal to the plane of the element. The plate bending behavior includes two-way, out-of-plane, plate rotational stiffness components and a translational stiffness component in the direction normal to the plane of the element. By default, a thin-plate (Kirchhoff) formulation is used that neglects transverse shearing deformation. A thick-plate (Mindlin/Reissner) formulation which includes the effects of transverse shearing deformation can be also chosen.

For the static analysis and for the checks of the structural elements in the limit states method only the finite element model of the steel dome was taken into account. For the dynamic analysis and further for the response of the structure under seismic load, the model of the dome was supplementary completed with the elements forming the concrete structure of the pavilion. This is made for the correct evaluation of the eigenmodes and periods of vibration of the whole structure.

The curved structural elements are modelled with a corresponding number of straight frame elements, so that the difference between the curve and the subtense of the circle has a minimum value, value established on optimization criteria.

The preliminary check of the meshed structure has been made for a load hypothesis consisting in vertical loads of 50 tf which were placed in all joints of the central ring. The comparison between the reactions values in the bearings and between the values of axial forces in the semi-arches flanges has shown that the geometry of the finite element model is correct and for this symmetrical load no asymmetry of sectional stresses or displacements occur.

The support conditions are modelled by restraining some d.o.f. (degrees of freedom), like the translations in all directions and rotations in two directions (with respect to the joint local coordinate system). Only the rotation about the local axis normal to the longitudinal mid plane of each semi-arch is free.

The material for the dome elements is the steel OL37, having an elasticity modulus of 210000N/mm^2 and a Poisson's coefficient of 0.3. The behaviour of the material was considered to be linear elastic.

4. Dynamic analysis of the structure

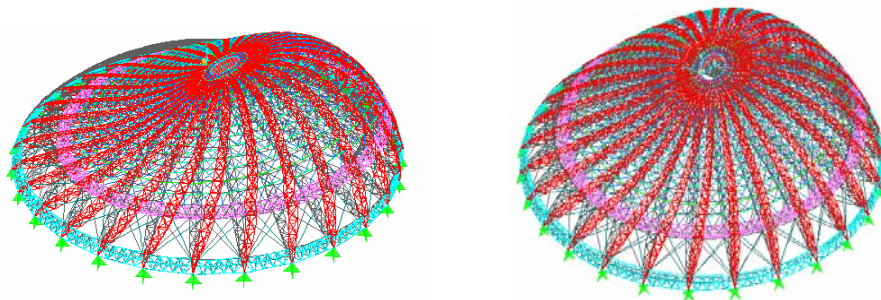
For the dynamic analysis, the whole model (concrete structure and steel dome) is considered. The software used to carry out this analysis is SAP 2000. There are two ways to perform dynamic analyses with SAP 2000:

- eigenvector analysis determines the undamped free-vibration mode shapes and frequencies of the system. These natural modes provide an excellent insight into the behaviour of the structure
- Ritz-vector analysis seeks to find modes that are excited by a particular loading. Ritz vectors can provide a better basis than do eigenvectors when used for response-spectrum or time-history analyses that are based on modal superposition.

Modal analysis is always linear. In the case presented in this paper the first method has been used.

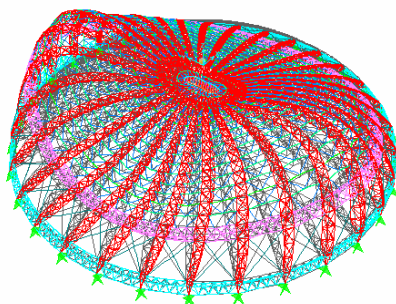
The masses applied to the structure coming from the self-weight of the structural elements, from snow weight tacked into account with an coefficient 0.4 (according to the loads combination) and a uniform distributed load acting on the concrete floors of the structure with a value of 0.2 tf/m (load corresponding to people action). The masses coming from the self-weight of the structure are determined from the geometry and mass density of the used materials and the other concentrated masses are applied to joints like translational and rotational masses.

In order to see the influence of the bracing system consisting in steel cables in the zone of skylights, the analysis has been carried out for the structure with and without these cables. A separate dynamic analysis, only for the steel dome has been carried out to find out the contribution of the concrete structure to the structure periods of vibration. The results of those kind of analyses are presented in the next chapter. The first three eigenmodes of the steel structure of the dome stiffened with cables in the skylight zone are presented in figure 6 (a. b. c).



a) First eigenmode of the dome

b) Second eigenmode of the dome



c) Third eigenmode of the dome

Figure 6 – Eigenmodes of the dome

6. Conclusions

The periods of vibration (for first three eigenmodes) resulted from the performed dynamic analyses are given in table 1 for the whole structure (concrete structure and steel dome) and in table 2 for the steel dome only.

Table 1: Periods of vibration for the whole structure

MODE NUMBER	Whole structure without cables - Period (sec.)	Whole structure with cables - Period (sec.)
1	1.172	1.167
2	1.167	1.162
3	1.154	1.152

Table 2: Periods of vibration for the steel dome

MODE NUMBER	Steel dome without cables - Period (sec.)	Steel dome with cables - Period (sec.)
1	0.520	0.415
2	0.519	0.414
3	0.281	0.244

From the above tables it can be concluded:

- the presence of the concrete structure cause the increase of the period of vibrations (for the relevant two eigenmodes) with 225% in the situation without cables and with 281% in the second case
- the third mode of the dome correspond to a torsion in the horizontal plane of the dome, which represent a disadvantageous situation for the arches in the skylights zone
- by introducing the Φ 35 mm steel cables in the skylight zone, the period of vibration for the steel dome decrease with about 20%
- the first two eigenmode are relevant and they can have a important contribution to the seismic response of the structure

7. References

1. Abedi, K., Parke, G.A.R. – *Pogressive collapse of single-layer braced dome*, International Journal of Space Structures, Vol. 11, No.3, 1996
2. A. Ivan, *Stabilitatea cupolelor metalice simplu strat*, Ed.Orizonturi Universitare, Timișoara, 2000
3. Computers ans Structures Inc., *SAP 2000 – Reference Manual*, 2003
4. S.C. Consis Proiect S.R.L., *Steel dome of the “ROMEXPO” pavilion – technical expert appraisalment*, 2003

ASPHALT MIXTURES CREEP SUSCEPTIBILITY

Carmen RĂCĂNEL¹

Abstract

To may estimate the permanent deformations of an asphalt mixture we need to know its creep susceptibility. This matter it is made in present paper by carrying out some static creep tests on asphalt mixture cylindrical samples, in our Laboratory of Roads from C.F.D.P. and by proper interpretation of results.

The asphalt mixtures were two: a classic asphalt mixture for wearing course, BA16 and an asphalt mixture with fiber, MASF16 (Stone Mastic Asphalt).

This paper gives emphasis to asphalt mixtures behavior at three test temperatures by drawing creep curves and creep compliance curves.

Finally, it was established the creep susceptibility of the two types of tested asphalt mixture using the "p" ratio and the coefficient of recovery.

1. Introduction

Under long period loads, the asphalt mixtures show the creep and relaxation phenomenon that is very important one by its consequences. The factors that play a decisive role in the analysis of this complex stress state are the deformation rate and the temperature.

In practice, this phenomenon may presents under the following respects:

- the creep phenomenon: the variation of strains according to time under a constant load;
- the relaxation phenomenon: the variation of stresses according to time under a constant deformation.

This paper is concerning to creep phenomenon and uses the uniaxial creep test. The creep acts like a plastic deformation. Because of creep, the deformations of pavement structures may increase several times than the instantaneous deformations. That is that at a high load levels or high surrounding temperatures, the creep can cause the premature failure of structure.

The complete rheological analysis of a certain body means the identification of aspect and measure of elastic, viscous and plastic behavior. This division of total deformations in differing components is difficult to make for some historic of load, because of plastic and viscous properties that lead in the same time at permanent

¹ Lecturer dr.eng., Tehcnical University of Civil Engineering, Bucharest, Romania, e-mail: carmen@cfdp.utcb.ro

deformations. In addition to this, the materials are ageing and their properties are time – temperature depending.

It is well known that, when it is studied the mechanical properties of asphalt mixtures, at low temperatures the elastic character is predominant and the materials are less affected by the loading time. If the temperature is high then the viscous character becomes predominant and the loading time will have an essential effect on mechanical properties.

In 1978, Van de Loo has achieved a detailed description for creep test at uniaxial compression. This test consists in a subsection of asphalt mixture cylindrical sample with plate and parallel faces, placed within two pans of steel, one of them fixed and the other mobile, at a constant loading on the mobile pan and measuring the sample deformation according to time. The test temperature is maintained constant during the test. The sample can be subjected at a single cycle or multiple cycles of loading / unloading, with the effort maintained constant during loading period. From this test, it can be calculated the parameters that determine the asphalt mixtures behavior at permanent deformations like creep compliance, recovery compliance, creep modulus, creep rate.

2. Laboratory test and materials

The used test in the study of this paper is the static uniaxial compression test.

The test was carried out on cylindrical samples with 70 mm in diameter and 140 mm in height, manufactured from BA16 (a classical asphalt mixture) and MASF16 (a stone mastic asphalt) type of asphalt mixture.

The test temperature was 23°C, 40°C and 60°C. The samples were subjected to a constant level of effort, 179 kPa, value that respects the recommendation of speciality literature.

During the test it was recorded the vertical deformations at loading and unloading period (60 min. and 60 min. respectively) at various time.

The asphalt mixtures were manufactured by Chileni crushed rock and sand, Basarabi filler, Viatop 80 plus fiber and ESSO 50/70 bitumen.

3. Results

Based on vertical deformations measured it was calculated the strains, ϵ and then it was plotted according to time. These are the creep curves, which are presented in figure 1 and 2, for three temperatures.

From these two figures it can be observed that the strain is temperature depending during the test. So, the higher the temperature the higher the strain.

These curves show that the total strain consists of an instantaneous part and a time dependent part and the deformation is partially recovered.

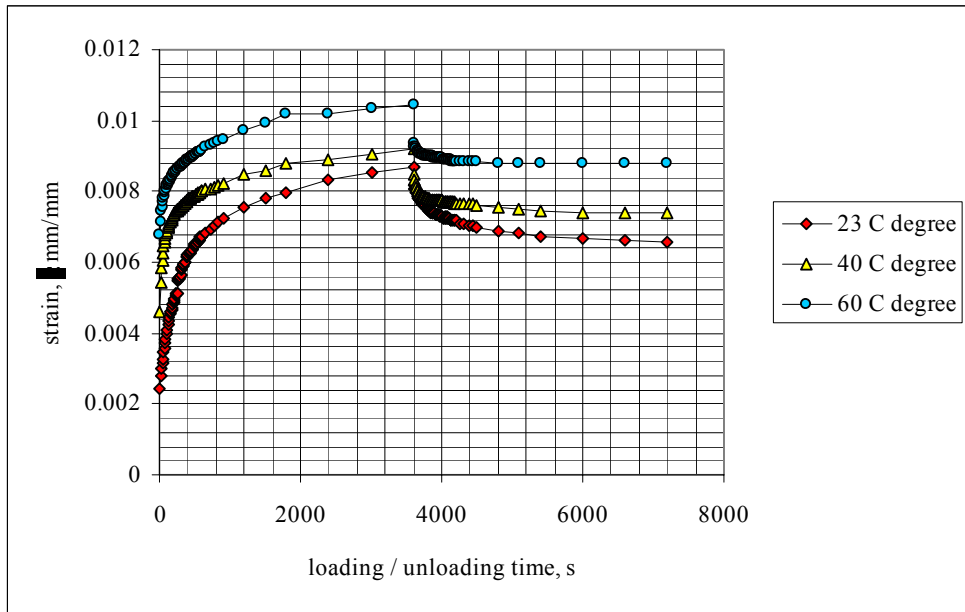


Figure 1 Creep curves for BA 16 asphalt mixture for three temperatures

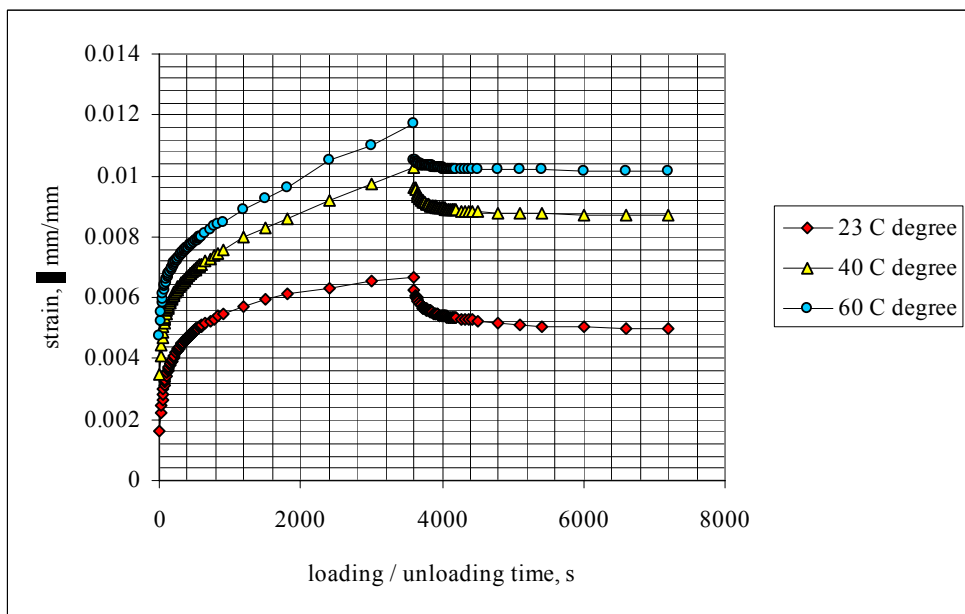


Figure 2 Creep curves for MASF 16 asphalt mixture for three temperatures

The plastic deformation can be obtained by subtracting from the deformation of loading moment the deformation of unloading moment.

Table 1 contains the strain for the three test temperature, in the case of BA 16 and MASF 16 asphalt mixture.

Table 1 The strains from creep curves for BA 16 and MASF asphalt mixture

Type of mixture	Temperature °C	Strain, mm/mm		
		total	elastic	plastic
BA16	23	0.002431	0.000537	0.001894
	40	0.00461	0.000745	0.003865
	60	0.00675	0.001108	0.005642
MASF16	23	0.00163	0.000443	0.001187
	40	0.003464	0.000621	0.002843
	60	0.00476	0.00121	0.00355

Based on creep curves the creep and recovery compliance, J_c and J_r , it were calculated and then plotted (figure 3, 4, 5, 6, 7, 8). We can conclude that the viscoelastic response of material cannot be interpreted as linear because the creep compliance curves are differing from the recovery compliance curves.

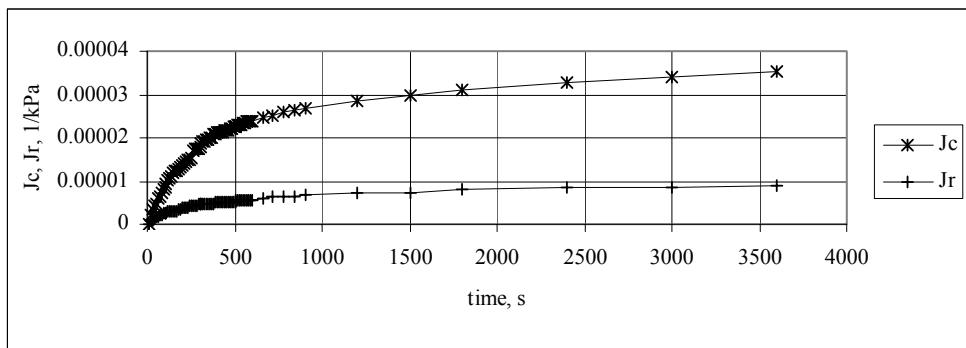


Figure 3 Creep and recovery compliance curves for BA 16 asphalt mixture at 23°C test temperature

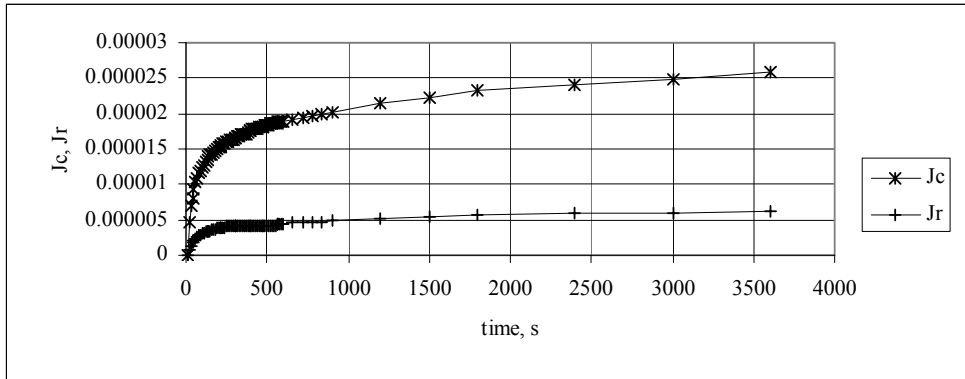


Figure 4 Creep and recovery compliance curves for BA 16 asphalt mixture at 40°C test temperature

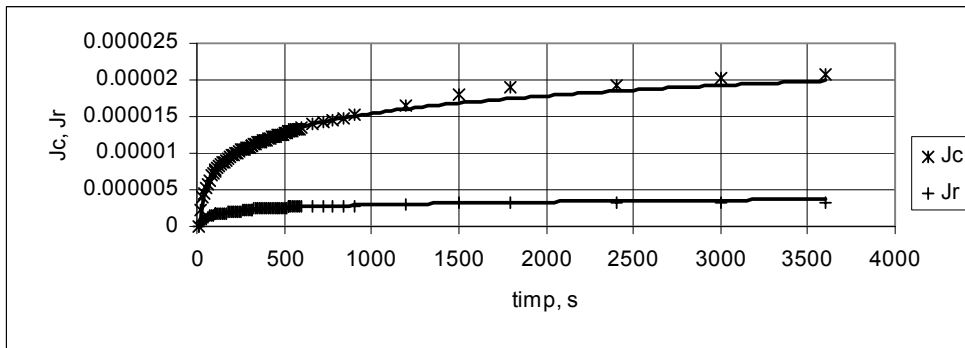


Figure 5 Creep and recovery compliance curves for BA 16 asphalt mixture at 60°C test temperature

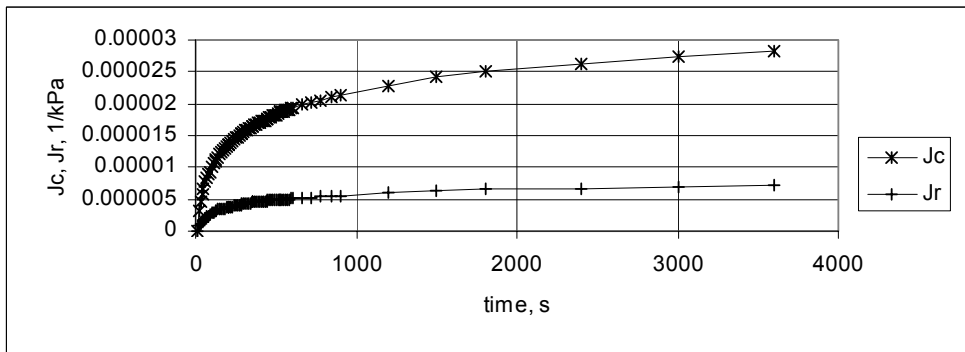


Figure 6 Creep and recovery compliance curves for MASF 16 asphalt mixture at 23°C test temperature

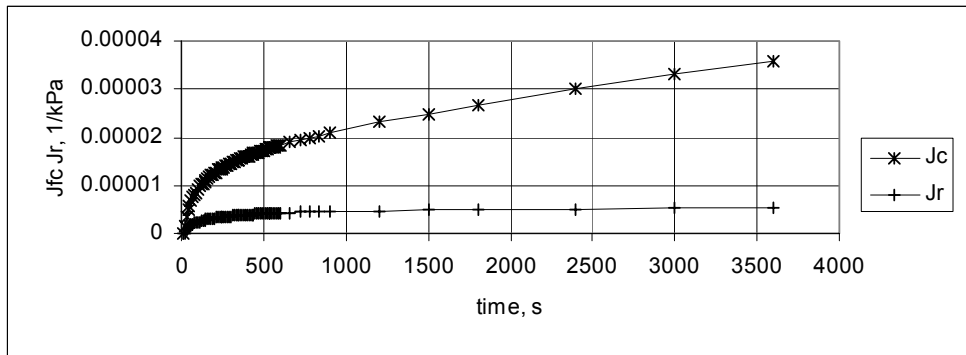


Figure 7 Creep and recovery compliance curves for MASF 16 asphalt mixture at 40°C test temperature

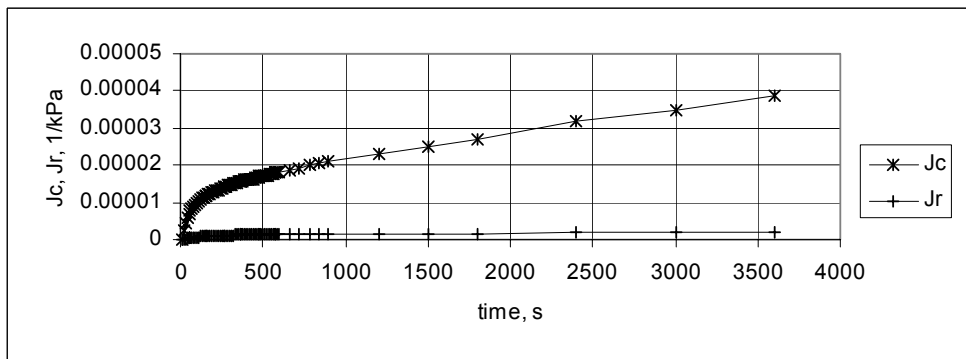


Figure 8 Creep and recovery compliance curves for MASF 16 asphalt mixture at 60°C test temperature

The "p" ratio and recovery coefficient calculus. The "p" ratio is the ratio between the slope of recovery curve (p_{Jr}) and the slope of creep curve (p_{Jc}). This ratio must be greater than 1 to have a good quality asphalt mixture, "p" indicating a high potential of recovery.

In table 2 we have the "p" values for the studied asphalt mixtures.

Table 2 The "p" values for BA 16 and MASF 16 asphalt mixtures

Type of asphalt mixture	Temperature °C	Slope of creep compliance curve, p_{Jc} , %	Slope of recovery compliance curve, p_{Jr} , %	"p" ratio, p_{Jr}/p_{Jc}
BA16	23	8.3	15.7	1.89
	40	9.6	9.47	0.99
	60	6.48	13.26	2.05

MASF16	23	9.6	21.05	2.19
	40	22.85	25	1.09
	60	22.12	22.92	1.04

From the above creep curves, we have the strain at the finish of the recovery period and at the finish of the creep period and it can be calculated the recovery coefficient. The values of recovery coefficient for each loading case are in the table 3.

Table 3 The values of recovery coefficient for BA 16 and MASF 16 asphalt mixtures

Type of asphalt mixture	Temperature °C	Strain, ϵ , at 3600 s mm/mm	Strain, ϵ , at 7200 s mm/mm	Recovery coefficient
BA16	23	0.008715	0.00659	24.38
	40	0.00922	0.007376	20.00
	60	0.010468	0.008786	16.07
MASF16	23	0.00668	0.004961	25.73
	40	0.010261	0.008689	15.32
	60	0.0117	0.010164	13.13

Another important parameter for mixture characterization is the creep modulus that was calculated by using the creep curves, too. The calculated values are in table 4.

Table 4 The values of creep modulus for BA 16 and MASF 16 asphalt mixtures

Type of asphalt mixture	Temperature °C	Strain, ϵ , at 3600 s microdef	Creep modulus, S, MPa
MASF16	23	6680	26.80
	40	10261	17.44
	60	11700	15.30
BA16	23	8715	20.54
	40	9220	19.41
	60	10468	17.10

4. Conclusions

From this research the following conclusions can be drawn:

- the value of strain from uniaxial compression test is time-temperature depending; the higher the temperature the higher the strain;
- the total strain consists of an instantaneous part and a time depending one;
- the strain is partially recovered;
- the form of creep and recovery compliance curves establish the viscoelastic response of material; in this case the both of mixture have a non-linear viscoelastic response;
- the "p" ratio must be greater than 1 for a very good asphalt mixture from permanent deformation point of view;
- the recovery coefficient indicates the recovery percent of material after a certain period of rest;
- all the specific parameters from uniaxial compression test of asphalt mixtures is temperature depending.

References

1. Drescher A., Kim J.R., Newcomb D.E., *Permanent Deformation in Asphalt Concrete*, Journal of Materials in Civil Engineering, vol.5, No 1, 1993.
2. Răcănel C., *Efectele din fluaj și oboseală asupra comportării mixturilor asfaltice*, teză de doctorat, U.T.C.B., 2002.

THE COMPACT METHOD FROM ANALYSIS OF WATER DISTRIBUTION SYSTEMS

Emanoil Bârsan¹, Călin IGNAT²

Abstract

The classical loop analysis of the water supply comprises two basically steps solved separately:

1 - selection of an initial distribution of flow rates (q) at the pipeline which satisfies conservation of flow rates at nodes ($\sum q = 0$), and

2 - correction of these flow rates till the satisfaction of energy conservation on the independent loops ($\sum h = 0$), (Lobatchev – Cross or Newton – Raphson procedures).

By convenient transformations referring to the node – pipeline incidence matrix (NPIM) there is established automatically an initial solution, a loop structure covering the network and the final flow on the pipelines, using a unitary method, without the help of the user.

Other hydraulic parameters of the water distribution network (velocity, piezometric heads, service pressure, etc) are obtained by additional procedure.

The important steps for realizing the network solver by Netwon – Raphson procedure are:

- The construction of node – pipeline incidence matrix (NPIM) of the network (with N -nodes, T - pipelines, M - loops) on the basis of the configuration of a given network.
- The application of a method of elimination (Gauss – Jordan) for unimodal matrix as NPIM, for obtaining an initial distribution of flow rates.
- The application of a procedure of a quasi-orthogonalization for the matrix part NPIM that corresponds to $T- N+ 1$ pipelines (that is M loops) to obtain a loop – pipeline incidence matrix (LPIM) that offers: a structure of independent loops that cover the network and the sparse matrix character that assures the increase of rapidity in for applying the Newton – Raphson procedure.

Other included facilities in network solver: the spatial graph consideration, the roughness of each pipeline, the water temperature, the extended period of simulation etc.

¹ Prof., Technical University “Gh.Asachi” of Iasi, Romania, e-mail: ebarsan@hidro.tuiasi.ro

² Prof., University “Al.I.Cuza” of Iasi, Romania, e-mail: ignat@uaic.ro

1 Introduction

For the study of water distribution network, there are generally used two procedures: the loop and the node analysis. The first procedure is used for the network calculus that considers as unknowns the discharges on pipelines.

The loop analysis principle of the water distribution network consists in the assurance of energy conservation on independent loops by successive corrections concerning the initial distribution of the discharges, complying this distribution with the continuity conditions at nodes and which serves, at the same time, at the pre-dimensioning of the network of the pipelines.

This correction of discharges may be done loop by loop (Lobatchev - Cross procedure) or simultaneously on all the loops (Newton – Raphson procedure [1]).

In the case of using the Newton–Raphson procedure, the correction at some step of iteration is realized by the values obtained solving the system of equations.

$$\mathbf{J}_{i-1} \Delta \mathbf{q}_i = \Delta \mathbf{h}_{i-1} \quad (1)$$

where: \mathbf{J}_{i-1} and $\Delta \mathbf{h}_{i-1}$ are Jacobian matrix and, respectively, the unbalanced vector obtained by applying the energy conservation equations on loops at step $i-1$; $\Delta \mathbf{q}_i$ – correction discharges vector on all the independent loops at step i .

The loop analysis of water distribution network using Newton–Raphson procedure requires the following steps: choosing of an initial discharges on loops (which may be subjected to a desired criterion); pre-dimensioning of the network pipelines; generation of the loop equation system; solving of the system of loop equations (by Newton – Raphson procedure); determining of the hydraulic parameters.

In the existing literature referring to the loop analysis the focus is on one or many from the mentioned steps. In the present paper the basis of a unitary procedure for the examining of water distribution system on the base of loop analysis and the practical possibility of application are presented.

2 Proposed Method

A water distribution system made up of M loops, N nodes and T pipelines ($T = M+N-1$), in steady-state, will be from hydraulic point of view balanced if the following conditions are satisfied.

1. Conservation of discharges at nodes (the algebraic sum of discharges in a node is zero):

$$\mathbf{f}_j = \sum_{\substack{i=1 \\ i \neq j}}^N \mathbf{q}_{ij} + \mathbf{C}_j = \mathbf{0}, \quad (\mathbf{j} = 1, \dots, N), \quad (2)$$

where: f_j represents the algebraic sum of the discharges in node j (unbalanced); q_{ij} – pipelines discharges ij with sign (+) for the discharges that enter in the node j and the sign (-) for the discharges that leaves from the node ($q_{ij} = 0$ if there is no connection ij); C_j - the node consumption discharge, with the same convention of signs.

2. Energy conservation; for the loop network the discharge on pipelines must also satisfy the condition that the algebraic sum of the head loss (h_{ij}) on the pipeline belonging to a m loop is zero:

$$f_m = \sum_{\substack{i,j \in m \\ i,j=1}}^T h_{ij} = 0, \quad (m = 1, \dots, M), \quad (3)$$

where h_{ij} is the head loss of the pipeline ij , positive if the sign of the pipeline discharge coincides with the loop sign, chosen arbitrarily.

The head loss is connected to the discharge by functional relation which, for the long pipelines, is calculated starting from the Darcy – Weisbach relation:

$$h_{ij} = \lambda_{ij} \frac{l_{ij}}{d_{ij}} \cdot \frac{v_{ij}^2}{2g}, \quad (4)$$

where l_{ij} , d_{ij} , v_{ij} represent, respectively, the length, the diameter and the average velocity of the water on the pipeline ij , [m; m; m/s]; g – gravity acceleration, [m/s²], λ_{ij} – Darcy hydraulic resistance coefficient, which is determined by the implicate relation Colebrook - White:

$$\frac{1}{\sqrt{\lambda}} = -2 \log \left(\frac{2.51}{Re \sqrt{\lambda}} + \frac{k}{3.71d} \right) \quad (5)$$

or by the explicite relation [2]:

$$\frac{1}{\sqrt{\lambda}} = 1.14 - \log \left(\frac{k}{d} + \frac{21.25}{Re^{0.9}} \right) \quad (6)$$

where: Re represents Reynolds' number; k and d - absolute roughness of the inner wall, respectively the diameter of same pipeline.

Depending on discharges, the relation (4) becomes:

$$h_{ij} = \frac{8\lambda_{ij}l_{ij}}{\pi^2 g d_{ij}^5} \quad (7)$$

In the case of loop analysis the application of Newton - Raphson procedure for (3) leads to solving of some linear systems of equations of type (1).

In the view of unitary treatment of loop analysis the loop definition is made so that the linear algebraic system have sparse matrix as calculus time to be short and the storage problems of this matrix can be solved in conditions of a given memory.

For realizing this objectives there is used a node – pipeline incidence matrix (NPIM) of the given network with the help of which there are obtained: a) the initial approximation for the problem solution (3) for the continuity conditions (2); b) a initial system of loops that cover the network. For thus purpose there is applied a method of Gauss - Jordan type adapted to the peculiarities of unimodal matrix of the NPIM, with there is obtained an initial distribution of discharges on the first $N - 1$ pipelines (the principal ones) which satisfies the condition (2) taking for the rest of $T - N + 1$ pipelines (the secondary ones), the discharge of zero value. In fact there is obtained an initial distribution on tree of the network graph.

Then to the matrix part corresponding for $T - N + 1$ pipelines (in an equal number with the loop number) is applied a procedure of quasiorthogonalisation in view of generating the incidence loop – pipeline matrix (LPIM) so that a pipeline to belong to no more than two loops. This last condition assures the sparse matrix character for Newton – Raphson system.

The matrix LPIM is at its turn unimodular, an element ij of this matrix being: 1 if the pipeline j belongs to the loop I and is crossed in positive sense; -1 if it is crossed in negative sense; 0 if the pipeline does not belongs to the loop.

In this way it not longer necessary to be established by the utilisator a loop structure and an initial solution, this being realized automatically.

At the same time on the basis of loop pipeline incidence matrix (LPIM) the matrix of Newton – Raphson system (1) have a determined structure, this calculus being summed up at the head loss determination for each pipeline in the given stage in respect of the determined discharges in anterior approximation.

At the end, based on these discharges, there are determined the head losses and the pipeline velocities, the piezometric heads at the network nodes starting from an imposed head in one of the nodes.

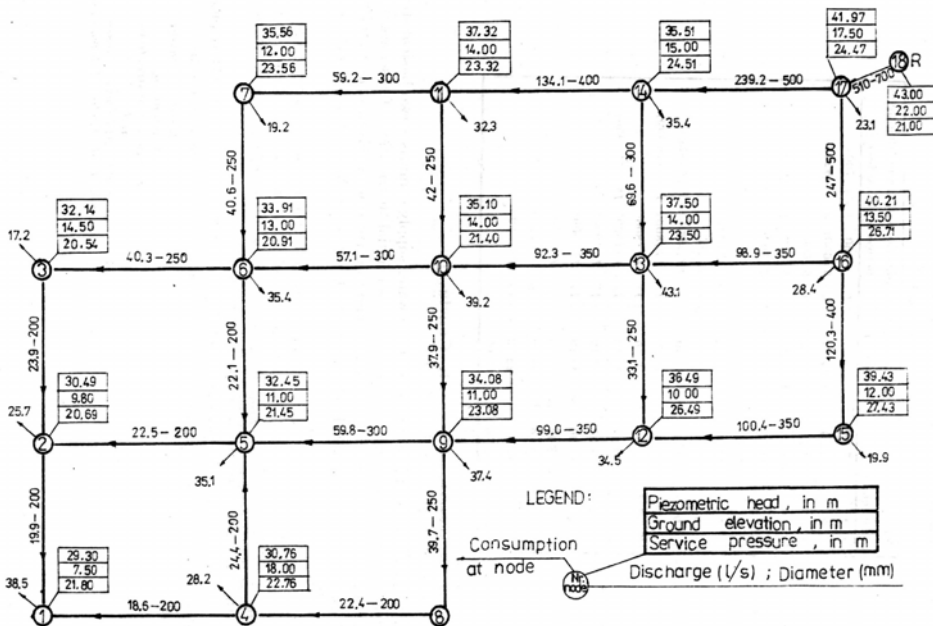
The may be obtained also further information, for instance, service pressures knowing the ground elevation at nodes, etc.

The calculus program consists in the following procedures: 1 – the incidence node – pipeline matrix construction (NPIM) and the solving of continuity equations (2);

2 – the minimal loop system determination which covers the network; 3 – the iterative Network – Raphson procedure for solving nonlinear system (3). In this stage, for every step there are up-dated the diameters after [3] and based on these are up – dated the head losses corresponding to the given discharge in the anterior step of the iteration using relation (6) together with (4) or (7); 4 – the calculus procedure of head losses and corresponding velocities of the established discharges in the anterior step; 5 – the procedure for the piezometric head determination at nodes starting from a node with an imposed head; 6 - other procedures introduced by necessities.

The program permits the following facilities: 1 – To take into account the pipeline material by k parameter (absolute roughness); 2 – To take into account the water temperature by ν (cinematic viscosity coefficient); 3 – The possibility of supplying the network to a node or to many nodes conveniently chosen (equivalent with the supply of one or more pump stations); 4 – The possibility of improving one or more piezometric heads at nodes (equivalent with introduction of one or more storage reservoirs)

For the casual combinations provided by the possibilities from points 3 and 4 there will be checked, previously, the condition or conditions of compatibility.



3 Application

We consider the water supply from fig.1 having a storage reservoir in node 18 and the characteristic elements given in Table 1. The water surface head in reservoir is $H_r = 43$ m WC. The network is made of precast concrete pipes ($k = 0,25 \cdot 10^{-3}$ m); the water temperature $t = 10^0$ C ($\nu = 1.31 \cdot 10^{-6}$ m²/s).

The obtained results are presented in Fig.1.

Table 1.

Nr. node	Ground elevation [m]	Consumption at node [L/s]	Connections of nodes (distances between the nodes), [m]
1	7.50	38.50	1 – 2 (500); 1 – 4 (700)
2	9.80	25.70	2 – 5 (650); 2 – 3 (520)
3	11.20	17.20	3 – 6 (600)
4	8.00	28.20	4 – 5 (480); 4 – 8 (650)
5	11.00	35.10	5 – 6 (500); 5 – 9 (650)
6	13.00	35.40	6 – 7 (500); 6 – 10 (650)
7	12.00	19.20	7 – 11 (700)
8	8.00	17.40	8 – 9 (480)
9	11.00	37.40	9 – 10 (500); 9 – 10 (800)
10	14.00	39.20	10 – 13 (800); 10 – 11 (600)
11	14.00	32.30	11 – 14 (800)
12	10.00	34.50	12 – 13 (500); 12 – 15 (950)
13	14.00	43.10	13 – 16 (900); 13 – 14 (600)
14	15.00	35.40	14 – 17 (900)
15	12.00	19.90	15 – 16 (350)
16	13.50	28.40	16 – 17 (600)
17	17.50	23.10	17 – 18 (500)
18	22.00	0.00	

4 Conclusions

1 – The classical loop analysis of the water supply comprises two basic steps solved separately: a) selection of an initial distribution of discharges at the pipeline which satisfies relation (2) and b) correction of this discharges till the satisfaction of relation (3) (Lobatchev – Cross or Newton – Raphson procedures)

2 – By convenient transformations referring to the incidence node – pipeline matrix there is established automatically an initial solution, a loop structure covering the network and the final discharges at the water supply pipelines, using an unitary method, without the help of the user.

3 – Other hydraulic parameters of the water network (velocity, piezometric heads, service pressure, etc) are obtained by additional procedure.

References

1. Barsan, Em., Ignat , C., *Water Distribution Systems*, Ed. Cermi, Iasi,2001 (in Romanian).
2. 2. Divenot, A., Une nouvelle methode de calcul des reseaux maillees. *La Houille Blanche*, 6 (1980).
3. 3. Jain, A., D., Accurate Explicit Equation for Friction Factor, *J. of the Hydr.Div.*, ASCE,102, HY5 (1976).
4. 4. Giurconiu, M., Mirel, I., Păcurariu, M., Popa, Gh., *Diagrams, nomograms and tables for urban public works calculus*, Ed. Facla, Timișoara, (1977) (in Romanian).

MONITORING OF WATER DISTRIBUTION SYSTEMS FOR MINIMIZATION OF ENERGETIC COSTS

Emanoil BÂRSAN¹, Călin IGNAT²

Abstract

The work presents the possibility of computer-assisted monitoring for the water distribution system working by pumping at which it is taking in to account consumption and pressure restrains in view of the energetic costs minimization.

The energetic costs represent the most expenses for water supply systems working by pumping from worldwide and can consume up to 65 % from the annual system budget.

The work presents a model for optimized control of water distribution systems operation. The proposed model establishes the working characteristics of a water distribution system (supplying flow rate and pumping head) in view of minimization of the pumping costs from a water distribution system with the satisfaction of imposed hydraulics requirements. Minimization of costs is realized by supplying the flow rate and pumping head control.

Supplying flow rate control is realized by the minimization of maximum supplying flow rate in the 24 hours of the day by rational utilization of tank storage capacity (which by it diameter and height significant influences this minimization). To this flow rate it may be introduced the supplementary conditions such as: the satisfaction of a minimum flow rate, a flow rate succession on hours which do not exceed as value a certain imposed size or the combination of these.

Pumping head control is realized by the minimization of the reference piezometric head (hydraulic grade line) of piezometric surface so that the pressure at nodes to be comprised between minimum and maximum allowable values.

The steps in flow rate and pumping head are: 1 – establishing of pumping flow rate by minimization of maximum supplying flow rate; 2 – hydraulic calculation of network using supplying flow rate from the point 1; 3 – establishing the pumping head by minimization of reference piezometric head.

The result model may be used to evaluate different schemes, tradeoffs between pumping and storage, improvement of operating efficiency and system reliability. The method may be used at any water distribution system which must optimize pumping operation and tank control and which proposes itself the integration of

¹Prof., Technical University “Gh.Asachi” of Iasi, Romania, e-mail: ebarsan@hidro.tuiasi.ro

² Prof., University “Al.I.Cuza” of Iasi, Romania, e-mail: ignat@uaic.ro

direct telemetric and optimal control systems with computer to reduce energetic costs and the realization of efficient operations

1. Introduction

Drinking and industrial water supply systems consume large quantities of electric energy that constitute, generally, the largest expenses for majority of these systems. Energetic costs are a function of consumed energy quantities and energy cost. Energetic costs are structured to promote the using of energy out of consuming peaks when the costs are less and penalization the energy using in peak periods when the costs are larger.

Measures for energy saving in water distribution systems may be realized in many kinds, beginning with field test and equipment maintenance up to using optimal control with computer. Energy utilization may be reduced by diminishing the water pumped volume (that is, adopting some limits for pressure zone), diminishing pumping head (that is, the optimization the of series of water levels in tank) or energy price reducing (that is, the avoid of pumping in peak hours and using the storage tanks so that their filling to be out the peak period and their draining in time of peak period) and increasing of pumps efficiency (that is, assuring as the pumps operate near by best efficiency point). Water supply systems may reduce further the costs by implementation of the direct telemetry and control systems (SCADA) and energy consumption control using optimization of pumping and storing operations in tank.

In recent years there was done different attempts to develop the optimal control algorithms with the view to help the operating of complex water supply systems. With that end in view the linear, nonlinear and dynamic programming and enumeration techniques (genetic algorithms) are used.

The grade and mode of application of these techniques was depended by the complexity of system.

Recently for optimal exploitation of pumps from a water supply system was applied the enumeration techniques – genetic algorithms [Boulos et al., 2000], that is, a program for hydraulic solving of a water supply system is combined with a enumeration algorithm of problem solutions realized on the genetic base (reproduction, mutation).

The paper presents a proper modality to realize the pumping in water supply systems consisting of separate optimization of pumped flow and pumping head for minimization of pumping energetic costs in system during of 24 hours.

2. Model formulation

Minimization of energetic costs in a distribution system made up from pumping station - distribution network – inflow/draining tank, it is proposed to be realized with a model unfolded in three steps:

The network supply flow (and therefore pumping flow) is determined to assure optimal use of tank in the sense to bring from source a strict necessary water quantity to assure the flows at nodes on hours, in 24 hours.

In this view it is added a auxiliary variable $debmax(z)$ for supplying flow in such way as $debit_t < debitmax$ in 24 hours ($t = 1, \dots, 24$). By minimization the $debmax$ it is established hour by hour from the 24 hours strict necessary supplying flow with optimal tank utilization

More concrete: being done the network configuration (lengths and diameters on pipe and ground level at nodes), consumptions in network at nodes in each hour from the 24 hours of day and the tank by diameter D and height H , the minimization of the largest value of network hour supplying flow that assures the consumption at nodes is followed.

Consider the variable x_1, \dots, x_{24} the network supplying flows hour by hour during a day; y_1, \dots, y_{24} tank supplying or draining flows in the same time interval; c_1, \dots, c_{24} network consumptions at nodes in 24 hours and z a variable that means network supplying maximum flow (on hour).

In this step it is solved the following problem:

$$\min z$$

with restrictions:

$$x_t = c_t + y_t$$

$$y_{t+1} - y_t \leq \text{tank volume}/3600$$

$$z - x_t \geq 0 \text{ with } t = 1, \dots, 24 \text{ hours}$$

In addition the supplying flow calculation may be done and setting the following conditions:

A – imposing of a minimum flow as a percent from the average consumption

$$x_t > \text{minimum flow (percent from average consumption)}$$

B - imposing of a maximum difference between two successive hour supplying flows.

$$x_{t+1} - x_t < \text{maximum difference}$$

$$x_t - x_{t+1} \text{ maximum difference}$$

C - combination of conditions (minimum of maximum flow, minimum flow, maximum difference)

The network is balanced with the supplying flows established in anterior step (1) with methodology from [Bârsan and Ignat, 2001]. It is determined the flows and head losses on pipes, the piezometric head at nodes etc.

At the 3rd step, the reference head H_{ref} needs for piezometric surface establishing is minimized. This must assure at nodes the pressure framing between a imposed minimum and maximum (current nodes i , adjacent ones j):

$$\min H_{ref}$$

$$H_i = H_j + h_{ij}$$

$$H_i \geq \text{ground level}_i + p_{min}$$

$$H_i \leq \text{ground level}_i + p_{max}$$

with p_{min} și p_{max} – minimum and maximum imposed pressure in node i

The calculation program establishes the pumping flow and height for a given distribution system.

3. Application example

Fig. 1 presents the distribution system considered for exemplification (pumping station (pipe 23 –1) – network (22 nodes) – inflow/draining tank (node 24)).

For the tank there exists a facility that permits the consideration of any type of tank. There are taken in consideration the following types of cylindrical tanks (D = diameter; H = height) I - $D = 27,5$ m and $H = 8$ m ; II – $D = 15$ m , $H = 6$ m ;

In fig. 2 is presented a screen for options that may be:

Tank position (by node), their dimensions (D and H)

Establishing of pumping flow and height by considering the minimization of maximum network hour supplying flow; taken in to consideration a minimum flow (in percents from average flow); imposing of a maximum difference between two successive hour flow or combination of the anterior considerations.

For a tank disposed in node 24, with $D = 15$ m and $H = 6$ m and options from fig. 2 (maximum flow, minimum flow, difference successive flows) the following graphs are presented:

Fig. 3. presents the supplying (by pumping) and consumption graph of network in 24 hours. In fig. 4 it is presented, on hours, the pumping height/head;

Figure 5 presents water level variation in tank but in fig. 6 it is presents the correlation between supplying flow and pumping height (necessary working point)

of a pumping system (in 24 hours) for choosing the type of pumps and running program.

Graphs from fig. 3, 4 and 6 serve for program establishing and pumping energy costs.

Authors have in view, for the near future, the realization of this stage with a computer program

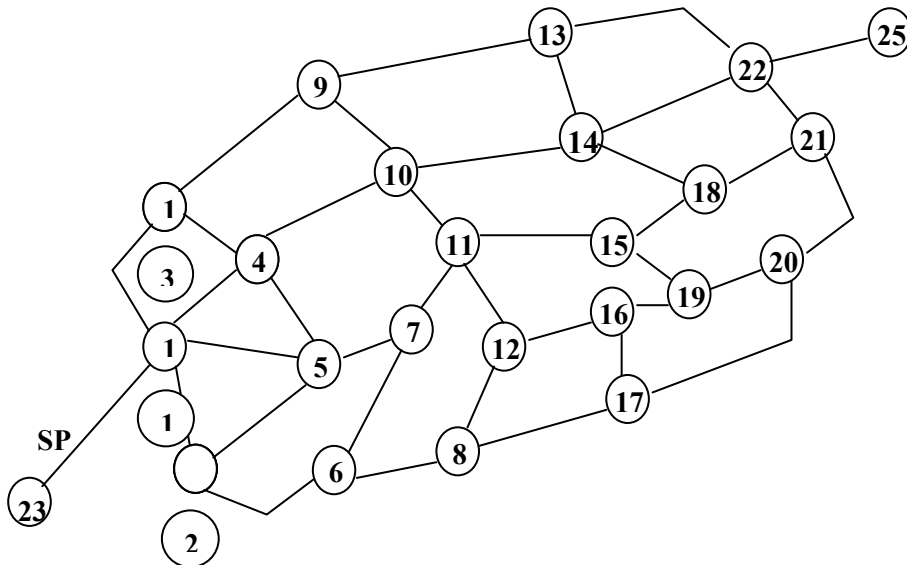


Fig. 1. Network graph.

Rezervoare

6

NOD: 24 1

Diametru: 15 000 Diametru: 15

Volum: 1060.290 Volum: 5000

H: 6 m

Accept Actualizare Exit

Parametri optimizare

Costuri debite

Debit Maxim 100

Debit minim 25

Diferente debite 10

Cancel Accept

Fig 2. Optimization options

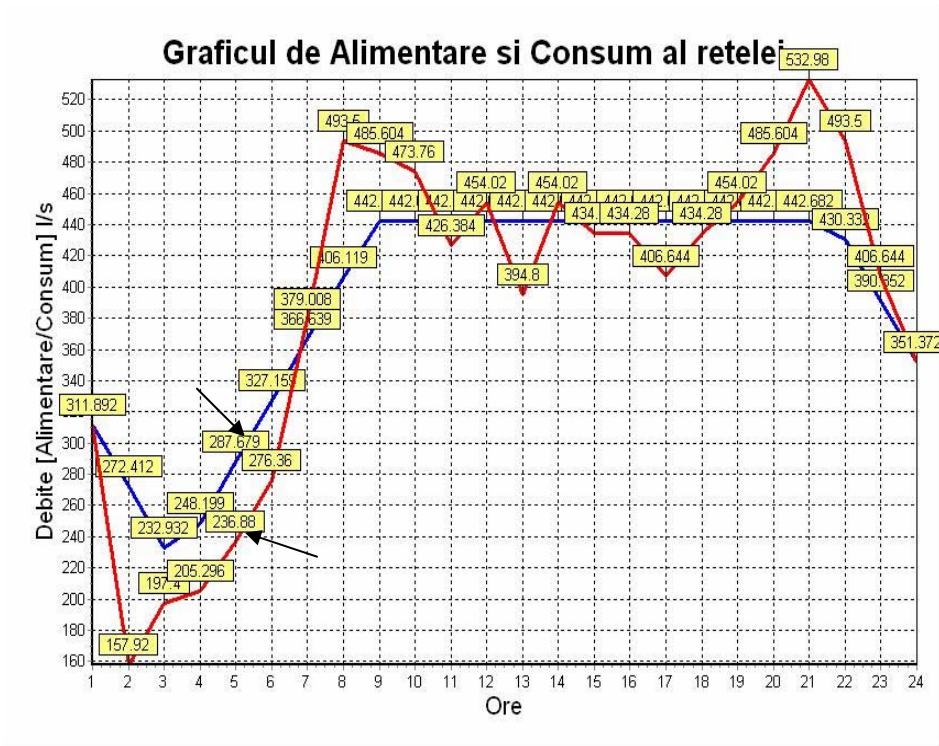


Fig. 3. Graph of network supply and consumption. (Debite = flow rates; ore = hours)

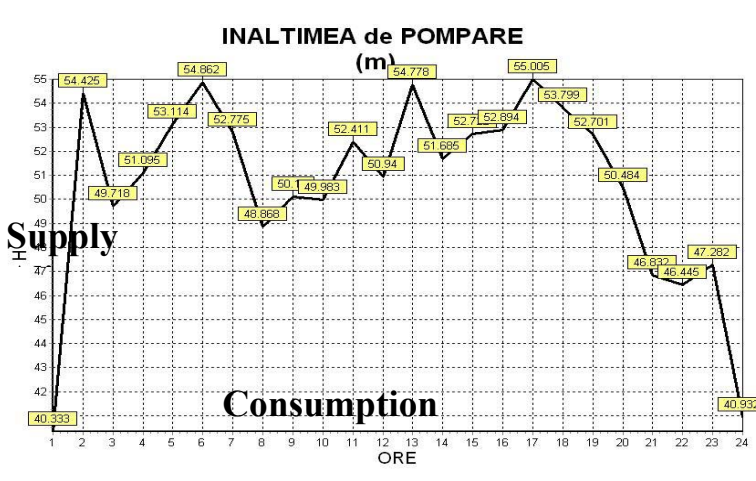


Fig. 4. Pumping head H (inaltime de pompare) vs hours (ore)

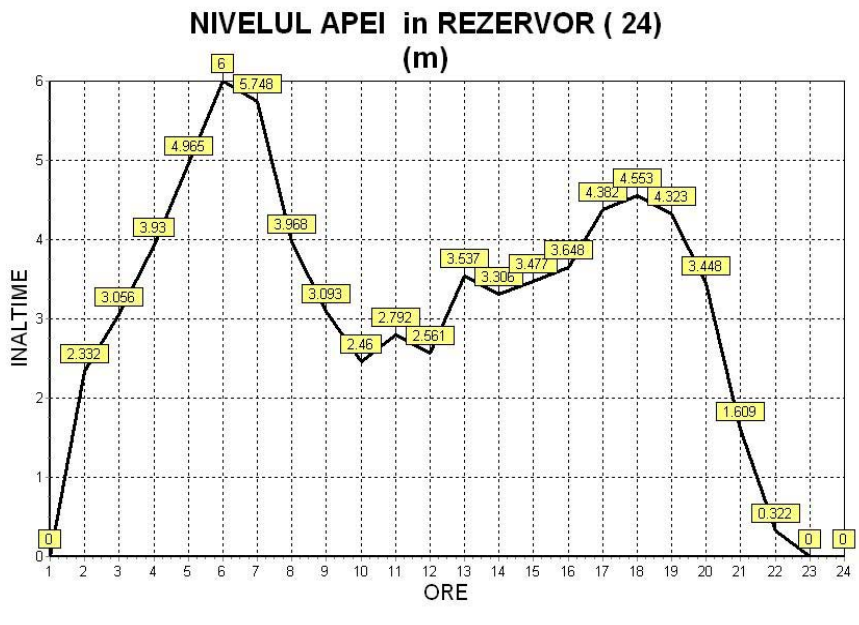


Fig. 5. Water level in tank (nivelul apei in rezervor). Height (inaltime) vs hours (ore)

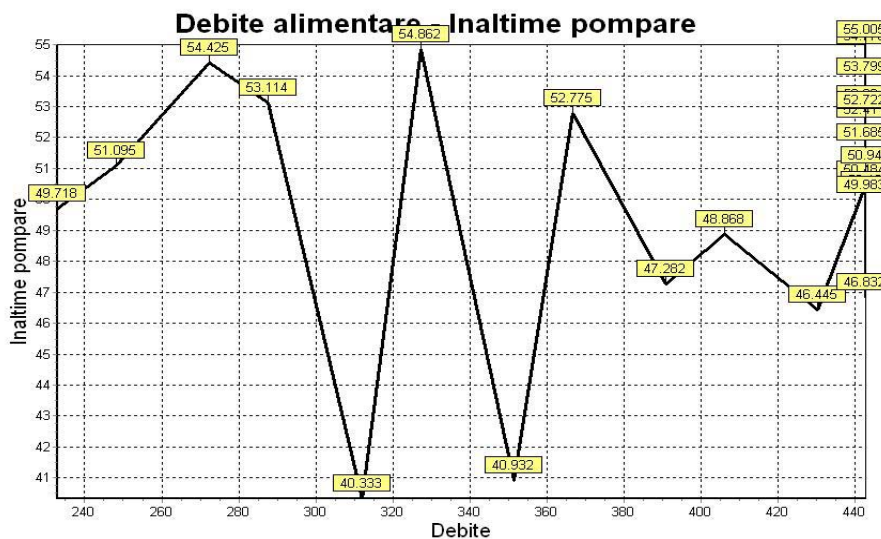


Fig. 6. Supplying flow rates (debite de alimentare) vs pumping head (inaltime de pompare). On abscissa – flow rates (debite); on ordinate – pumping head (inaltime de pompare)

4. Conclusions

The work presents a model for establishing the program and energetic costs in a supply system by pumping, unfolded in three stages:

- 1 – establishing of pumping flow by minimization of maximum supplying flow;
- 2 – network hydraulic calculus using the supplying flow from point 1 ;
- 3 – establishing of pumping height/head by minimization of referring piezometric head.

The proposed model contains the following facilities presented in fig. 2. – options for tank position (by nod) and their dimensions (D and H); options for minimization of maximum network hour supplying flow; taken in to consideration of a minimum flow (in percents from average flow); imposing of a maximum difference between two successive hour flows or combination of the anterior considerations.

The model was applied at the system presented in fig. 1. In fig. 3, 4, 5, 6, for a tank having $D = 15$ m and $H = 6$ m, are presented the supplying and consumption flows of network; pumping head; water level in tank and the correlation between supplying flow and pumping height of the considered system.

The model and program serve for realization the energetic analysis of a water supply system.

References

1. Bârsan, Em., Ignat, C., Technical-economic analysis of water distribution networks, *Water Science & Technology: Water Supply*, London, vol 1, no. 2, 2001, pp 201-210
2. Bârsan Em., Ignat C., *Sisteme de distributie apei*, Editura Cerme Iași, 2001.
3. Boulos, P.F., Wu, Z., Orr, Ch.H., Moore, M., Hsiung, P., Thomas, D., Optimal pump operation of water distribution system using genetic algorithm, *RBF Consulting*, 2002, 9pg.
4. IWSA *World Water Congress, 7 International Report*, State of the art regarding on-line control and optimization of water systems, vol.1 I.R., Buenos Aires, 1999, IR-1- 45.
5. Walski, Th., Chase, D.V., Savic, D.A., *Water Distribution Modeling*, Haestad Press, Waterbury, 2001, 333-372.

ANALYSIS OF WATER DISTRIBUTION NETWORKS BY A TECHNICAL-ECONOMIC METHOD

Emanoil BÂRSAN¹, Călin IGNAT²

Abstract

For the water distribution networks there are done the two type of analysis:

1. hydraulic analysis or the balancing of network and
2. technical – economic analysis or the network sizing. In technical – economic analysis at hydraulic condition (the continuity of flow rate at nodes and energy conservation on independent loops) is added and economic conditions (minimum annual expenses for construction and operation).

In these conditions, the technical-economic analysis represents a nonlinear programming problem with equality restrain which transform into a nonlinear system (Lagrange procedure) with which we determine flow rates and head losses on pipelines. This system has in its making up the hydraulic conditions (Kirchhoff's laws) and “economical” conditions, both being written in the same way. In case when the objective function (minimum annual expenses for construction and operation) is convex the establishing of flow rates and head losses is done directly, but in case when the same function is concave-convex it is necessary a intermediary step.

In this way it obtain the theoretically diameters what will be adjusted to meet commercial ones.

In the paper it is presented a model and a methodology for the application of the technical-economic analysis to the water distribution networks, and a mode of utilization for a practical example.

¹ Prof., Technical University “Gh Asachi” of Iasi ,Romania, e-mail: ebarsan@hidro.tuiasi.ro

² Prof., University “Al.I.Cuza” of Iasi, Romania, e-mail: ignat@uaic.ro

1. Introduction

The hydraulic calculus of water-distribution networks has for an object the determination of the flow rates on pipes (q_{ij}) and of the piezometric heads at nodes (H_i and H_j) using the continuity conditions of the flow rates and energy and a functional relation, proper on pipelines, between the head (h_{ij}) and flow (q_{ij}) starting from the previous knowledge of the pipeline diameters (d_{ij}), obtained by a pre-dimension calculus.

In case when along with the flow rates (q_{ij}) there are considered as unknown the pipeline diameters (d_{ij}), the number of equations provided by the hydraulic conditions are insufficient.

If the annual expenses (W) done for the construction and operation of the network are quantified and they are joined to the hydraulic conditions we shall reach to the technical-economic calculus formulated as follows:

To be minimized the annual expenses (W) that depend on the variable q_{ij} and d_{ij} knowing that the variables q_{ij} and d_{ij} are linked between them through the agency of h_{ij} and satisfy the flow rate continuity conditions at nodes and energy conservation on independent loops

In the present paper it is described a methodology for sizing of a water distribution system using a technical – economic model. For the formulation of model it is necessary to evaluate the annual expenses for construction and operation and adopting a model for hydraulic behavior of system.

2. Annual expenses for construction and operation of a water distribution network

For the annual expenses for construction and operation of a water-distribution network supplied with a pumping station it is adopted the following expression (Abramov, 1972; Paslarasu et al., 1991):

$$W = A \sum_1^T (a + b d_{ij}^c)_{ij} + P(H + \sum h_{ij})Q \quad (1)$$

The first term comprises the expenses for the pipeline distribution network realization (in number of T) and the second one, the exploitation expenses necessary for the water pumping on the line with maximum pumping head. In relation (1) a , b , c are the constants, statistically established (Paslarasu et al., 1991), d_{ij} and l_{ij} – diameter and length of pipelines; Q – flow supplied to the network; H – piezometric head necessary for the assured service pressure at the node with the most unfavorable position (long distance, high altitude etc); $\sum h_{ij}$ – head loss on the network pipelines on same line (usually the shortest) starting from the water entering into the network to the node with the piezometric head H . A and P from

relation 1 are specific factors of technical-economic nature which depend of concrete conditions of realization, redemption and operation of a water distribution system. Thus after (Paslarasu et al.,1991) A and P have the expression:

$$A = p_1 + \beta \tag{2}$$

$$P = \frac{9.81}{\eta} \left[f\sigma(p_2 + \beta) + 730 e \tau \sum_1^{12} \Phi_j \right] \tag{3}$$

where:

p_1, p_2 are the redemption, repair and maintenance quota for pipelines and pumping station, respectively

$\beta = 1/T_r$ – redemption quota for the time of recuperation T_r ;

η - overall efficiency of the pumping station;

f - cost of installation of a power unit for pumping ;

σ - supplementary factor for equipment of the pumping station;

e - tariff of electrical power ;

$\tau = T/8760$ coefficient which takes into account the effective number of pumping hours T during a year period ;

ϕ_j – the ratio between average monthly flow rate and pumping flow rate, with values from Paslarasu et al., (1991).

2. Mathematical model for hydraulic calculus of the water distribution networks

A water distribution system made up of M loops, N nodes and T pipelines ($T = M+N-1$), in steady - state, will be from hydraulic point of view balanced if the following conditions are satisfied.

Conservation of flow rates at nodes (the algebraic sum of flow rates in a node is zero):

$$f_j = \sum_{\substack{i=1 \\ i \neq j}}^N q_{ij} + C_j = 0, \quad (j = 1, \dots, N), \tag{4}$$

where: f_j represents the algebraic sum of the flow rates in node j (unbalanced); q_{ij} – pipelines flow rates ij with sign (+) for the flow rates that enter the node j and the sign (-) for the flow rates that leave from the node ($q_{ij} = 0$ if there is no connection ij); C_j - the node consumption flow rate, with the same convention of signs.

Energy conservation; for the loop network the flow rates on pipelines must also satisfy the condition that the algebraic sum of the head loss (h_{ij}) on the pipeline belonging to a m loop is zero:

$$f_m = \sum_{\substack{ij \in m \\ ij=1}}^T h_{ij} = 0, \quad (m = 1, \dots, M), \quad (5)$$

where h_{ij} is the head loss of the pipeline ij , positive if the sign of the pipeline flow rate coincides with the loop sign, chosen arbitrarily.

The head loss is connected to the flow rates by functional relation which, for the long pipelines, is calculated starting from the Darcy – Weisbach relation:

$$h_{ij} = \lambda_{ij} \frac{l_{ij}}{d_{ij}} \cdot \frac{v_{ij}^2}{2g}, \quad (6)$$

where l_{ij} , d_{ij} , v_{ij} represent, respectively, the length, the diameter and the average velocity of the water on the pipeline ij , [m; m; m/s]; g – gravity acceleration, [m/s²], λ_{ij} – Darcy hydraulic resistance coefficient, which is determined by the implicit relation Colebrook - White:

$$\frac{1}{\sqrt{\lambda}} = -2 \log \left(\frac{2.51}{Re \sqrt{\lambda}} + \frac{k}{3.71d} \right) \quad (7)$$

or by the explicit relation (Jain,1976):

$$\frac{1}{\sqrt{\lambda}} = 1.14 - \log \left(\frac{k}{d} + \frac{21.25}{Re^{0.9}} \right) \quad (8)$$

where: Re represents Reynolds' number; k and d - absolute roughness of the inner wall, respectively the diameter of same pipeline.

Depending on flow rate, the relation (6) becomes:

$$h_{ij} = \frac{8\lambda_{ij}q_{ij}^2 l_{ij}}{\pi^2 g d_{ij}^5} \quad (9)$$

or, by explicitness, it results the diameter expression d_{ij} in function of flow rate and head loss

$$d_{ij} = \left(\frac{8\lambda_{ij}}{\pi^2 g} \right)^{\frac{1}{5}} q_{ij}^{\frac{2}{5}} h_{ij}^{-\frac{1}{5}} l_{ij}^{\frac{1}{5}} \quad (10)$$

3. Mathematical model for technical - economic analysis of the distribution network

Having in view the annual expenses given by relation (1) and the diameter expression given by relation (10) as well as the continuity condition of flow rate and energy, the technical – economic analysis of the water distribution network can be done with model:

$$\min W = A \sum_T \left[a + b \left(\frac{8\lambda}{\pi^2 g} \right)^{\frac{c}{5}} q_{ij}^{\frac{2c}{5}} h_{ij}^{-\frac{c}{5}} l_{ij}^{\frac{c}{5}} \right] l_{ij} + P(H + \sum h_{ij})Q \quad (11)$$

$$\sum_{\substack{i \neq j \\ i=1}}^N q_{ij} + C_j = 0 \quad , \quad j = 1, \dots, N \quad (\text{no. of nodes}) \quad (12)$$

$$\sum_{\substack{ij \in m \\ ij=1}}^T h_{ij} = 0 \quad m = 1, \dots, M \quad (\text{no. of loops}) \quad (13)$$

Relations (11), (12) and (13) represent a nonlinear programming problem with equality restrains which transforms into a nonlinear system of equations with which we can determine q_{ij} și h_{ij} by following procedure:

Function F is formed (called lagrangean) having the form:

$$F = W + \sum_1^N \lambda_N \left(\sum_{\substack{i \neq j \\ i=1}}^N q_{ij} + C_j \right) + \sum_1^M \theta_M \sum_{\substack{ij \in m \\ ij=1}}^T h_{ij} \quad (14)$$

where λ_N and θ_M are Lagrange multipliers.

Optimal solution of the model given by relations (11), (12) and (13) is obtained by canceling the partial derivatives of first order of the function F in respect with $x_i \in \{q_{ij}, h_{ij}\}$ and the multipliers λ_N and θ_M

The system of nonlinear equations has the form:

$$\frac{\partial F}{\partial x_i} = \frac{\partial W}{\partial x_i} + \sum_{j=1}^N \lambda_N \frac{\partial(\sum q_{ij} + C_j)}{\partial x_i} + \sum_1^M \theta_M \frac{\partial(\sum h_{ij})}{\partial x_i} = 0 \quad (15)$$

$$\frac{\partial F}{\partial \lambda_N} = \sum_{\substack{i=1 \\ i \neq j}}^N q_{ij} + C_j = 0 \quad , \quad j = 1, \dots, N \quad (16)$$

$$\frac{\partial F}{\partial \theta_M} = \sum_{\substack{i=1 \\ ij \in m}}^T h_{ij} = 0 \quad , \quad m = 1, \dots, M \quad (17)$$

The derivatives of F in respect with h_{ij} (dF/dh_{ij}), have the following terms for one of the T equations:

a) a term having always the form:

$$-\frac{c}{5} A b \left(\frac{8\lambda}{\pi^2 g} \right)^{\frac{c}{5}} q_{ij}^{\frac{2c}{5}} h_{ij}^{-\frac{c+5}{5}} l_{ij}^{\frac{c+5}{5}}$$

b) a term of the form PQ present only if h_{ij} belongs to the route taken in consideration for the operation expenses calculus, and

c) a term made up of $\sum \theta_M$ for the loops that contain h_{ij} , considerate at item 5.

The derivative in respect with q_{ij} ($\frac{\partial F}{\partial q_{ij}}$), has the following terms for one of the T equations.

a) an existing term having always the form:

$$\frac{2c}{5} A b \left(\frac{8\lambda}{\pi^2 g} \right)^{\frac{c}{5}} q_{ij}^{\frac{2c-5}{5}} h_{ij}^{-\frac{c}{5}} l_{ij}^{\frac{c+5}{5}}$$

b) a term made up of $\sum \lambda_N$ for node equations that comprise q_{ij} in respect with the derivation is made.

The system of equations (15), (16), (17) has 3T equations with 3T unknowns (q_{ij} , h_{ij} , λ_N , θ_M). By eliminating Lagrange multipliers (λ_N , θ_M) the system is reduced to 2T equations with 2T unknown (q_{ij} , h_{ij}) made up of:

1. N nodal equations of type (16);
2. M loop equations of type (17);
3. N nodal “economical” equations of type

$$\sum_{\substack{i=1 \\ i \neq j}}^N Q_{ij} = \frac{PQ}{B} \quad j = 1 \quad (18-1)$$

(for the node supplied through pumping)

and

$$\sum_{\substack{i=1 \\ i \neq j}}^N Q_{ij} = 0 \quad , \quad j = 2 \dots N \quad (18-2)$$

(for other nodes)

where:

$$Q_{ij} = q_{ij}^{\frac{2c}{5}} h_{ij}^{\frac{c+5}{5}} l_{ij}^{\frac{c+5}{5}} \quad (19) \quad B = \frac{c}{5} A b \left(\frac{8\lambda}{\pi^2 g} \right)^{\frac{c}{5}} \quad (20)$$

These equations are written in the same way such as the continuity equations of flow rate at nodes, assigned to Q_{ij} the same sign as for q_{ij} .

4. M loop “economical” equations of form:

$$\sum_{\substack{ij \in m \\ ij=1}}^T H_{ij} = 0 \quad , \quad m = 1, \dots, M \quad (21)$$

where:

$$H_{ij} = q_{ij}^{\frac{2c-5}{5}} h_{ij}^{\frac{c}{5}} l_{ij}^{\frac{c+5}{5}} \quad (22)$$

These equations are written in the same way as the continuity equations of energy on loop assigned to H_{ij} the same sign as for h_{ij} .

As a rule the system of equations (16), (17), (18) and (21) determines the values of q_{ij} și h_{ij} .

It remains to search the character of the extremum of function W to which it corresponds the system of equations (16), (17), (18) and (21).

The derivative of second order of the function W with respect to variable h_{ij} and q_{ij} are:

$$\frac{\partial^2 W}{\partial h_{ij}^2} = \frac{c+5}{5} B q_{ij}^{\frac{2c}{5}} h_{ij}^{-\frac{c+10}{5}} l_{ij}^{\frac{c+5}{5}} \quad (23)$$

$$\frac{\partial^2 W}{\partial q_{ij}^2} = 2 B \frac{2c-5}{5} q_{ij}^{\frac{2c-10}{5}} h_{ij}^{-\frac{c}{5}} l_{ij}^{\frac{c+5}{5}} \quad (24)$$

Because the sizes q_{ij} and h_{ij} that enter the function of annual expenses (1) and relation (10) are positive, the derivative $\frac{\partial^2 W}{\partial h_{ij}^2}$ is always positive because

$\frac{c+5}{5} > 0$. The derivative $\frac{\partial^2 W}{\partial q_{ij}^2}$ is positive only for the condition: $\frac{2c-5}{5} > 0$ ($c > 2,5$)

When the two derivatives of second order are positive ($c > 2,5$) it exists a minimum of function W for which these are determined q_{ij} and h_{ij} and then the theoretical diameter with relation (10)

In case when $c < 2,5$ for establishing a minimum of function W it is necessary to impose or prescribe a set of variable q_{ij} by a desired criterion, accomplishing the conditions of continuity and the minimizing of the function W is done by h_{ij} , that is, solving the system of equations (17) and (18).

4. Calculus example

For exemplifying the application way of the technical-economic analysis it will be considered the network from Fig.1. made up of pressure cast iron pipes, with the absolute roughness $k = 0.25$ mm, supplied with a flow rate of $0,2 \text{ m}^3/\text{s}$

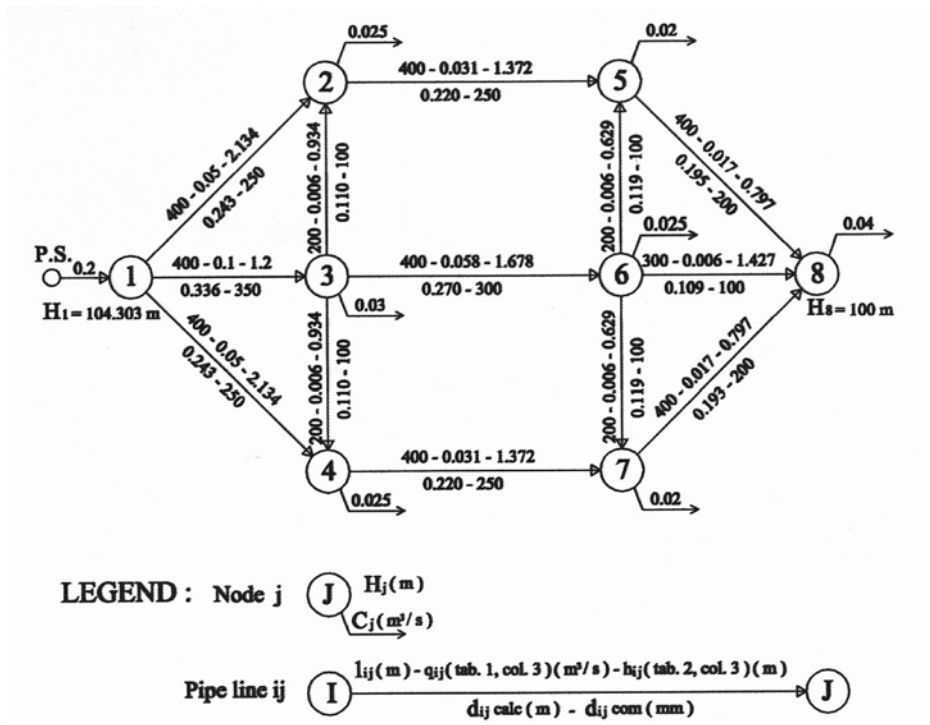


Fig.1. Water distribution network for the calculus example.

Because in the case of pressure cast iron pipes $\frac{\partial^2 W}{\partial q_{ij}^2} < 0$ ($c < 2.5$) (Paslarasu et al.,1991) (relation 24) it is necessary to establish an initial distribution of flows that can be optimized by a chosen criterion.

Starting from the model of water distribution analysis used in (Collins et al,1976; Barsan.and Ignat,1986) called the “content” model, the initial determination of optimized flow rates will be done having as a model:

$$\min \sum_{\substack{ij \in T \\ ij=1}}^T l_{ij} |q_{ij}^3| \quad (25-1)$$

$$\sum_{\substack{i \neq j \\ i=1}}^N q_{ij} + C_j = 0 \quad j = 1 \dots N \quad (25-2)$$

To this model we may also add the conditions:

$$q_{ij} \geq 0 \quad \text{or} \quad q_{ij} \geq b_{ij} \quad (25-3)$$

In the model given by relation (25) a term from relation (25-1) signifies the product between mechanical work (energy) of transit ($l_{ij} q_{ij}$) and the second power of flow rate of which depends the head loss recorded at the passing of a flow through a given pipe line

By the model (25) the network nodes are supplied on the shortest way and with a minimum transportation effort (minimum energetic content)

For determining the flow rates q_{ij} it is applied the conditioned gradients method (Pchenitchny and Daniline, 1977)

With the data from fig. 1, optimized distribution of flow rates results from the conditions:

$$\begin{aligned} \min \quad & (400q_{1-2}^3 + 400q_{2-5}^3 + 400q_{5-8}^3 + 200q_{2-3}^3 + 200q_{5-6}^3 + \\ & 300q_{1-3}^3 + 400q_{3-6}^3 + 300q_{6-8}^3 + 200q_{3-4}^3 + 200q_{6-7}^3 + 400q_{1-4}^3 + 400q_{4-7}^3 \\ & + 400q_{7-8}^3) \end{aligned}$$

with the restrains:

$$\begin{aligned} q_{1-2} + q_{1-3} + q_{1-4} - 0.2 &= 0; & q_{1-2} + q_{3-2} - q_{2-5} - 0.025 &= 0; \\ q_{1-3} - q_{3-2} - q_{3-4} - q_{3-6} - 0.03 &= 0; & q_{1-4} + q_{3-4} - q_{4-7} - 0.025 &= 0; \\ q_{2-5} + q_{6-5} - q_{5-8} - 0.02 &= 0; & q_{3-6} - q_{6-5} - q_{6-7} - q_{6-8} - 0.04 &= 0; \\ q_{4-7} + q_{6-7} - q_{7-8} - 0.02 &= 0; & (q_{ij} = -q_{ji}) & \end{aligned} \quad (26)$$

The optimized distribution of the flow rates is given by table 1. In column 2 there are shown the values of flow rates resulting from the optimization without the prescribing of a minimum flow rate of $q_{ij} = 0.006 \text{ m}^3/\text{s}$ (being possible to carry through a pipe of $D_n = 100 \text{ mm}$) and in the column 3 with the prescribing of this flow rate.

To note the fact that when it is not prescribed a minimum flow rate, the distribution network becomes in fact, partial branched out (vary small flow rates on the pipe lines 3-2; 6-5; 6-8; 3-4; 6-7).

For establishing the head losses on pipes it is necessary to make explicit the terms included in relations (17) and (18).utilizing the expenses assessment for network construction and water pumping. Thus, we consider by Paslarasu et al., (1991) a =

200; $b = 3060$ and $c = 1.52$, $p_1 = 0.035$; $p_2 = 0.09$; $\beta = 0.1$; $f = 5000$; $\sigma = 1.3$; $e = 0.4$; $\tau = 0.95$; $\sum_{j=1}^{12} \Phi_j = 10.44$; $\eta = 0.7$

Table 1. The optimized distribution of flow rates

Pipe line	q_{ij} (m ³ /s) without the prescribing for the minimum flow rate	q_{ij} (m ³ /s) with the prescribing of the minimum flow rate of 0.006 m ³ /s
1	2	3
1-2	0.06327	0.050
2-5	0.03868	0.031
5-8	0.01966	0.017
3-2	0.00041	0.006
6-5	0.00098	0.006
1-3	0.07345	0.100
3-6	0.04262	0.058
6-8	0.00129	0.006
3-4	0.00042	0.006
6-7	0.00033	0.006
1-4	0.06327	0.050
4-7	0.03869	0.031
7-8	0.01903	0.017

Using the above data with (2), (3) and (20) we obtain $A = 0.135$; $P = 57893.8$; $B = 17.289$; $PQ/B = 669.7$.

A term of relation (18) given by (19) has the form:

$$Q_{ij} = q_{ij}^{0.58368} h_{ij}^{-1.304} l_{ij}^{1.304} = a_{ij} h_{ij}^{-1.304}$$

where: $a_{ij} = q_{ij}^{0.58368} l_{ij}^{1.304}$

Using the obtained flow rates, from condition (26), the system of equations (17) and (18), for the example from fig.1, has the form:

$$\begin{aligned}
\mathbf{h}_{1-2} - \mathbf{h}_{3-2} - \mathbf{h}_{1-3} &= \mathbf{0}; & \mathbf{h}_{3-2} + \mathbf{h}_{2-5} - \mathbf{h}_{6-5} - \mathbf{h}_{3-6} &= \mathbf{0}; \\
\mathbf{h}_{6-5} + \mathbf{h}_{5-6} - \mathbf{h}_{6-8} &= \mathbf{0}; \\
\mathbf{h}_{1-3} + \mathbf{h}_{3-4} - \mathbf{h}_{1-4} &= \mathbf{0}; & \mathbf{h}_{3-6} + \mathbf{h}_{6-7} - \mathbf{h}_{4-7} - \mathbf{h}_{3-4} &= \mathbf{0}; \\
\mathbf{h}_{6-8} - \mathbf{h}_{7-8} - \mathbf{h}_{6-7} &= \mathbf{0}; \\
\mathbf{H}_1 - \mathbf{h}_{1-3} - \mathbf{h}_{3-6} - \mathbf{h}_{6-8} - 100 &= \mathbf{0}; \\
\mathbf{a}_{1-2}\mathbf{h}_{1-2}^{-x} + \mathbf{a}_{1-3}\mathbf{h}_{1-3}^{-x} + \mathbf{a}_{1-4}\mathbf{h}_{1-4}^{-x} + &= 669,7; \\
\mathbf{a}_{1-2}\mathbf{h}_{1-2}^{-x} + \mathbf{a}_{3-2}\mathbf{h}_{3-2}^{-x} - \mathbf{a}_{2-5}\mathbf{h}_{2-5}^{-x} &= \mathbf{0}; & \mathbf{a}_{1-3}\mathbf{h}_{1-3}^{-x} - \mathbf{a}_{3-2}\mathbf{h}_{3-2}^{-x} - \mathbf{a}_{3-4}\mathbf{h}_{3-4}^{-x} - \\
& & \mathbf{a}_{3-6}\mathbf{h}_{3-6}^{-x} &= \mathbf{0}; \\
\mathbf{a}_{1-4}\mathbf{h}_{1-4}^{-x} + \mathbf{a}_{3-4}\mathbf{h}_{3-4}^{-x} - \mathbf{a}_{4-7}\mathbf{h}_{4-7}^{-x} &= \mathbf{0}; & \mathbf{a}_{2-5}\mathbf{h}_{2-5}^{-x} + \mathbf{a}_{6-5}\mathbf{h}_{6-5}^{-x} - \mathbf{a}_{5-8}\mathbf{h}_{5-8}^{-x} &= \mathbf{0}; \\
\mathbf{a}_{3-6}\mathbf{h}_{3-6}^{-x} - \mathbf{a}_{6-5}\mathbf{h}_{6-5}^{-x} - \mathbf{a}_{6-7}\mathbf{h}_{6-7}^{-x} - \mathbf{a}_{6-8}\mathbf{h}_{6-8}^{-x} &= \mathbf{0}; & \mathbf{a}_{4-7}\mathbf{h}_{4-7}^{-x} + \mathbf{a}_{6-7}\mathbf{h}_{6-7}^{-x} - \\
& & \mathbf{a}_{7-8}\mathbf{h}_{7-8}^{-x} &= \mathbf{0}
\end{aligned} \tag{27}$$

where $x = 1304$.

The head loses of pipe lines corresponding to the flow rate from table 1 are given in table 2, column 2 (for q_{ij} from tab.1, col.2).and table 2, col. 3 (for q_{ij} from tab.1, col.3)

It is also established the piezometric head in the pumping-supply node (H_1) in respect to the imposed piezometric head of node 8 ($H_8 = 100$ m).

With the relation (10) there are determined the diameters.

In fig. 1 there are presented the flow rate values (tab.1, col. 3), the head losses (tab 2, col. 3), the diameters resulted from calculus and the chosen diameter from the ranges produced by industry (commercially).

With the commercially diameters we recalculated the head loses and piezometric heads of the supply node (tab.2, col.4) using the system (27)

The nonlinear system (27) needs an initial approximation in applying the Newton – Raphson method. We obtain this approximation considering the problem of

$$\text{minimum:} \quad \min \sum_1^N \left(\sum_{\substack{i=j \\ i=1}}^N \mathbf{a}_{ij} \mathbf{h}_{ij}^{-x} - \frac{PQ}{B} \right)^2 \tag{28-1}$$

with the linear constraint :

$$\sum_{\substack{ij \in m \\ ij=1}}^T h_{ij} = 0 \quad m = 1 \dots M \quad (28-2)$$

Table 2. The head loss on pipe lines (h_{ij})

Pipeline	q_{ij} (m) without prescribing of minimum flow rate	h_{ij} (m) with prescribing of the minimum flow rate of $q_{ij} = 0.006 \text{ m}^3/\text{s}$	h_{ij} (m) for trade (standard) diameters D_n specified in fig. 1
1	2	3	4
1-2	1.919	2.134	2.123
2-5	1.421	1.372	1.362
5-8	0.802	0.797	0.792
3-2	0.545	0.934	0.942
6-5	0.268	0.629	0.637
1-3	1.373	1.200	1.181
3-6	1.699	1.678	1.668
6-8	1.070	1.427	1.429
3-4	0.524	0.934	0.942
6-7	0.225	0.629	0.639
1-4	1.898	2.134	2.123
4-7	1.399	1.372	1.363
7-8	0.845	0.797	0.792
	$H_1=104.42 \text{ m}$	$H_1=104.303 \text{ m}$	$H_1=104.278 \text{ m}$
	$H_8 = 100 \text{ m}$	$H_8 = 100 \text{ m}$	$H_8 100 \text{ m}$

We notice that in the object function we have in fact $\sum_1^N \left(\frac{\partial W}{\partial h_{ij}} \right)^2$. For this problem we use again the conditioned gradients method (constraints being linear) (Pchenitchny and Daniline, 1977).

With the approximation thus obtained we initiate the iterative Newton - Raphson procedures applied to the system.(27).

The applying of intermediate step for determining the initial approximation has a special importance having in view the fact that convergence velocity and even the convergence of Newton-Raphson method depends essentially of the choosing of the first approximation.

In the case when it is necessary it may be reduced the calculus volume by diminishing the sizing of the system of equations using an equivalent network of smaller dimensions (Jeppson, 1982)

5. Conclusions

The sizing of a water distribution system (diameter determination) consists of optimized determination of flow rates and head losses in system by the technical – economic analysis. The optimized flow rates and head losses that are used for the determination of diameters on pipe lines (relation (10)) are established with equation systems (16),(17) (hydraulic conditions) and (18),(21) (“economic” conditions). The formulation of “economic” conditions is done in the same way as the hydraulic (technical ones) that is it results from the continuity writing, at nodes respectively on independent loops of the given sizes by the relations (19) respectively (22), “economic” network being supplied with PQ/B (relation (18 - 1)). (after case, in one or many nodes). In case when function W is concave-convex ($c < 2.5$) the problem is solved in two steps. In the first step it is established a distribution of flow rates q_{ij} with the objective function conveniently chosen after which in the second step it is solved the problem of minimum, only for the variable h_{ij} .

References

1. Abramov N. N., (1972) Theory and Method of Calculation of Water Transportation and Distribution Systems, Stroiizdat, Moscow (in Russian)
2. Bârsan Em.and Ignat C. (1986) Analysis of Water Distribution Networks Using “Content Model”, Hidrotehnica, **31**(8), 235-238, Bucharest, (in Rumanian)

3. Bârsan Em. and Ignat C. (1991), Aspects Concerning the Calculation of Water Distribution Networks Using Loop Analysis. Hidrotehnica, **36** (8-9), 233-235 (in Rumanian)
4. Bârsan Em. and Ignat C. (2000) An Analysis Method for Water Distribution. Bul.St.UP Timisoara, **46 (60)** (1,2), 174 -179
5. Jain A., K. (1976) Accurate Explicit Equation for Friction Factor, J. Hydr. Engrg. ASCE **102** (5),574-581
6. Paslarasu, I., Rotaru, N., Teodorescu, M., (1991) Water Supply, ET, Bucharest (in Rumanian)
7. Pchenitchny B. and Daniline Y. (1977), Numerical Methods for the Extremum Problems, Mir, Moscow (in French)

DEVELOPMENT OF A WATER SUPPLY NETWORK

Emanoil BÂRSAN¹, Călin IGNAT²

Abstract

The existed water supply networks are periodically subjected to some development that can be: extensions, flow rates increases at the consumers, supplies from new sources.

These evolutions influence the network behavior by the flow rate and pressure state modifications.

By an unitary method on an existed network, there are introduced the desired modifications using interactive procedures and by means of the loop analysis there is found out the network response in flow rates, the head loss and the velocities of the pipeline, the hydraulic heads and the pressure at nodes.

The paper presents the facilities offered by the programmer worked out by the authors for dimensioning, checking up, and development of the water supply network using the loop analysis.

The practical possibility of re-designing an existent network is shown by an example.

In case when there are imposed some hydraulic heads at the nodes or these hydraulic heads must be oscillated between a lower and upper values , the distribution system can have another hydraulic surface.

The artificial modification of hydraulic surface may be realized by increasing (with pump) or decreasing (with pressure reducing valves) of pressure.

In this case the devices location is done so that the energy of increasing / decreasing of pressure to be minimum. There is proposed a procedure that consists in combination of loop analysis for characterization of network state with simplex method for the minimization criterion.

¹ Prof., Technical University “Gh. Asachi” of Iasi, Romania, e-mail: ebarsan@hidro.tuiasi.ro

² Prof., University “Al.I.Cuza” of Iasi, Romania, e-mail: ignat@uaic.ro

Introduction

Romania possesses several centralized systems of water distribution, both in urban (263 systems) and rural settlements (2648 systems). These water supply networks have been designed in a certain moment for the required demand of water at a certain perspective period. After that, to the existed networks there were branched new consumers or there were joined new districts. The new demand of water was assured either by increasing the flow rate at the existed sources or by supplying the network from new water sources.

The mentioned evolutions before, influence the network behavior, modifying the distribution of flow rate and pressures in the network. Therefore, it is necessary that the existing networks be analyzed in the new created work conditions and if necessary to be re - designed in order to assure a proper functioning or to indicate the measures that should be taken for correcting the dysfunctions observed.

In the present paper it is shown an approach of this problem and the mode of using the loop analysis for carrying out these objectives.

The paper presents the facilities offered by the programme worked out by the authors for dimensioning, checking up, development and control of the water supply network using the loop analysis.

The introduction and the modification of the input data where there are included the restrains concerning piezometric heads at nodes are realized in the dialog way using Delphi components.

The facilities offered by the program and an example are presented

2. Proposed method.

The loop analysis principle of the water distribution network consists in the assurance of energy conservation on independent loops by successive corrections concerning the initial distribution of the flow rates, complying this distribution with the continuity conditions at nodes and which serves, at the same time, at the pre-dimensioning of the pipeline network.

This correction of discharges may be done loop by loop (Lobatchev - Cross procedure) or simultaneously on all the loops (Newton – Raphson procedure (Divenot, 1980; Barsan and Ignat, 1994).

In the case of using the Newton–Raphson procedure, the correction at some step of iteration is realized by the values obtained solving the system of equations.

$$\mathbf{J}_{i-1} \Delta \mathbf{q}_i = \Delta \mathbf{h}_{i-1} \quad (1)$$

where: J_{i-1} and Δh_{i-1} are Jacobian matrix and, respectively, the unbalanced vector obtained by applying the energy conservation equations on loops at step $i-1$; Δq_i – correction flow rates vector on all the independent loops at step i .

The loop analysis of water distribution network using Newton–Raphson procedure requires the following steps: choosing of an initial flowrate on loops (which may be subjected to a desired criterion); pre-dimensioning of the network pipelines; generation of the loop equation system; solving the system of loop equations (by Newton – Raphson procedure); determining the hydraulic parameters.

A water distribution system made up of M loops, N nodes and T pipelines ($T = M+N-1$), in steady-state, will be from hydraulic point of view balanced if the following conditions are satisfied.

1 conservation of flowrate at nodes (the algebraic sum of flow rates in a node is zero):

$$f_j = \sum_{\substack{i=1 \\ i \neq j}}^N q_{ij} + C_j = 0, \quad (j = 1, \dots, N), \quad (2)$$

where: f_j represents the algebraic sum of the flow rates in node j (unbalanced); q_{ij} – pipelines flow rates ij with sign (+) for the flow rates that enter the node j and the sign (-) for the flow rates that leaves from the node ($q_{ij} = 0$ if there is no connection ij); C_j - the node consumption flow rate, with the same convention of signs.

2. Energy conservation; for the loop network the flow rate on pipelines must also satisfy the condition that the algebraic sum of the head loss (h_{ij}) on the pipeline belonging to a m loop is zero:

$$f_m = \sum_{\substack{ij \in m \\ ij=1}}^T h_{ij} = 0, \quad (m = 1, \dots, M), \quad (3)$$

where h_{ij} is the head loss of the pipeline ij , positive if the sign of the pipeline flow rate coincides with the loop sign, chosen arbitrarily.

The head loss is connected to the flow rate by functional relation which, for the long pipelines, is calculated starting from the Darcy – Weisbach relation:

$$h_{ij} = \lambda_{ij} \frac{l_{ij}}{d_{ij}} \cdot \frac{v_{ij}^2}{2g}, \quad (4)$$

where l_{ij} , d_{ij} , v_{ij} represent, respectively, the length, the diameter and the average velocity of the water on the pipeline ij , [m; m; m/s]; g – gravity acceleration,

$[m/s^2]$, λ_{ij} – Darcy hydraulic resistance coefficient, which is determined by the implicate relation Colebrook - White:

$$\frac{1}{\sqrt{\lambda}} = -2 \log \left(\frac{2.51}{Re \sqrt{\lambda}} + \frac{k}{3.71d} \right) \quad (5)$$

or by the explicit relation (Jain, 1976):

$$\frac{1}{\sqrt{\lambda}} = 1.14 - \log \left(\frac{k}{d} + \frac{21.25}{Re^{0.9}} \right) \quad (6)$$

where: Re represents Reynolds’ number; k and d - absolute roughness of the inner wall, respectively the diameter of same pipeline.

Depending on flow rates, the relation (4) becomes:

$$h_{ij} = \frac{8\lambda_{ij}l_{ij}}{\pi^2 g d_{ij}^5} \quad (7)$$

In the case of loop analysis the application of Newton - Raphson procedure for (3) leads to solving some linear systems of equations of type (1).

In the view of unitary treatment of loop analysis the loop definition is made so that the linear algebraic system has sparse matrix as calculus time to be short and the storage problems of this matrix can be solved in conditions of a given memory.

For realizing these objectives there is used a node – pipeline incidence matrix (NPIM) of the given network with the help of which there are obtained: a) the initial approximation for the problem solution (3) for the continuity conditions (2); b) an initial system of loops that cover the network. For this purpose there is applied a method of Gauss - Jordan type adapted to the peculiarities of unimodal matrix of the NPIM, with there is obtained an initial distribution of flow rates on the first $N - 1$ pipelines (the principal ones) which satisfies the condition (2) taking for the rest of $T - N + 1$ pipelines (the secondary ones), the flow rate of zero value.

In fact there is obtained an initial distribution on tree of the network graph.

Then, to the matrix part corresponding for $T - N + 1$ pipelines (in an equal number with the loop number) is applied a procedure of quasiorthogonalisation in view of generating the incidence loop – pipeline matrix (LPIM) so that a pipeline to belong to no more than two loops. This last condition assures the sparse matrix character for Newton – Raphson system.

The matrix LPIM is at its turn unimodular, an element ij of this matrix being: 1 if the pipeline j belongs to the loop m and is crossed in positive sense; -1 if it is crossed in negative sense; 0 if the pipeline does not belong to the loop.

In this way it no longer necessary to be established by the user a loop structure and an initial solution, this being realized automatically.

At the same time on the basis of loop pipeline incidence matrix (LPIM) the matrix of Newton – Raphson system (1) has a determined structure, this calculus being summed up at the head loss determination for each pipeline in the given stage in respect of the determined flow rate in anterior approximation.

At last, based on this flow rate, there are determined the head losses and the pipeline velocities, the piezometric heads at the network nodes starting from an imposed head in one of the nodes.

There may be obtained also further information, for instance, service pressures knowing the ground elevation at nodes, etc.

The calculus program consists in the following procedures: 1 – the incidence node – pipeline matrix construction (NPIM) and the solving of continuity equations (2); 2 – the minimal loop system determination which covers the network; 3 – the iterative Network – Raphson procedure for solving nonlinear system (3). In this stage, for every step there are up-dated the diameters after [3] and based on these are up – dated the head losses corresponding to the given flow rate in the anterior step of the iteration using relation (6) together with (4) or (7); 4 – the calculus procedure of head losses and corresponding velocities of the established flow rate in the anterior step; 5 – the procedure for the piezometric head determination at nodes starting from a node with an imposed head; 6 - other procedures introduced by necessities.

3. The optimal location of devices for lifting / diminishing the pressure in order to maintain / carrying out of some ordered piezometric heads imposed / prescribed.

By the methodology presented (Barsan and Ignat,1994; Barsan and Ignat,1998) there may be established hydraulic parameters (flow rates, piezometric heads at nodes, head loss on pipelines etc) for dimensioning or checking up a water distribution network.

In the case when there are imposed certain piezometric heads at nodes, for example minimum – maximum, or a certain imposed head, the system of distribution must have another piezometric surface.

The artificial modification of the piezometric surface may be worked out either by pressure lifting devices (pumps) or by pressure reducing (valves)

In this case ,the location of devices is done in such a way that the pressure lifting and reducing energy to be minimum.

Because the location of devices is not known a priori, generally, for treating this problem it is considered that for every pipeline of distribution network ij a pump (or a pump station) and a valve is associated.

For actual cases pumps and valves are considered only on the pipelines where they really exist.

By introducing a pump and a valve on a pipeline ij between the piezometric heads from the ends of pipeline ij, it results the following relation:

$$H_i = H_j + h_{ij} + v_{ij} - h_p^{ij} \quad (8)$$

where:

H_i, H_j are the piezometric heads at nodes i and j imposed or necessary (calculated) for obtaining the new piezometric surface.

h_{ij} - the linear head loss on pipeline ij initially calculated;

v_{ij} - pressure reducing (in m CA) introduced by the valve on pipeline ij;

At the same time, there is imposed that at all nodes:

$$H_{\min} \leq H_i \leq H_{\max} \quad i = 1, \dots, N \quad (9)$$

Asking for :

$$\sum_{ij=1}^T v_{ij} + \sum_{ij=1}^T h_p^{ij} = \min \quad ij = 1, \dots, T \quad (10)$$

The criterion of introducing the pumps and valves on network pipelines is formulated as a linear programming problem where the objective function is relation (10) and the restrains (8) and (9).

The introducing of some pressure lifting and reducing devices at nodes is done in two stages:

1. On the existed network is calculated the hydraulic parameters (flow rate, piezometric heads, head losses etc)
2. For the imposed piezometric heads at nodes it is calculated the new piezometric surface and where there is necessary pumps and valves are introduced.

4. Facilities offered by the realized calculus program.

By using the graph DELPHI components for introducing and modifying the input data, inclusively restrains concerning pressures (piezometric heads at nodes) are

easily realized by dialogue way, dimensioning, development and the optimum position determination of the devices for lifting/ reducing pressure in order to maintain the ordered piezometric heads at some imposed nodes.

The program permits the following facilities:

1 – The program may consider a described network by a planar and spatial graph (by adjacent list) for the maximum hour consumption or for extended period of simulation (24 h)

2.- For the network pipelines there may be considered the unique absolute roughness or precisely stated for each pipeline from an initial specified list.

3- Taking into account the water temperature is done by cinematic viscosity coefficient ν (initial $\nu = 1,31 \cdot 10^{-6} \text{ m}^2/\text{s}$ for 10^0 C).

4.Accomplished calculus for a network subjected to dimensioning (diameter determination) for a given configuration and imposed consumption can be transformed automatically in the initial table for a given network (configuration, diameters, consumptions);

5.At the point 4 network there can be done the following operations specified in (Barsan and Ignat, 1994), that is:

a) increasing the supply flow rate of a given network (known diameters) with the network response calculus in flow rates, head losses and velocities on pipelines, piezometric heads and available pressures at nodes.;

b) increasing the local flow rate at nodes (fire or new consumers)

c) network behavior at damage coming out at some pipelines or zones (automatic elimination of pipelines and nodes);

d) the happened modifications at doubling, tripling etc. of some pipelines;

e) interior or exterior extension, supplementary nodes introduction on pipelines;

f) the network supply supplementation from other sources (reservoir or pump station);

g) problems a-f combination. The network response at points b-f are the ones specified at point a;

6. Imposing at nodes, if it is necessary, of a minimum or maximum limits for the piezometric heads or of an imposed piezometric heads that ask for the network equipping with pumps or valves that are located according to the procedure specified at paragraph 3

5. Example.

In what follows a distribution network extension was studied with water supply from two sources.

Table 1. Characteristic Elements for the Extended Network from fig. 1

Nr. node	Ground elevation (m)	Node consumption (l/s)	Node connections (distances between nodes, m; <i>Calculated diameters ,mm</i>)
1 - R	125	0	1-2 (600; <u>700</u>);
2	115	24,1	2-3 (650; <u>500</u>); 2-5 (750; <u>500</u>);
3	110,5	20,8	3-4 (350; 400); 3-6 (750; 350);
4	99,5	26,4	4-7 (900; 350);
5	114,3	20,5	5-6 (650; 350); 5-8 (800; 400);
6	108,5	34,2	6-7 (700; 250); 6-9 (800; 350);
7	96,2	42,2	7-10 (850; 350);
8	109,5	33,5	8-9 (650; 250); 8-12 (400; 300);
9	103,5	30,5	9-10 (700; 250); 9-13 (400; 300);
10	95,4	39,5	10-11 (400; 250); 10-14 (400; 250);
11	82,2	17,5	11-15 (400; 200);
12	103,2	20,2	12-13 (650; 250);
13	101,5	36,4	13-14 (700; 250); 13-16 (550; 250);
14	86,7	34,2	14-15 (400; 200); 14-17 (500; 200);
15	84,3	26,4	15-18 (500; 200);
16	83,2	16,5	16-17 (700; 200);
17	86	26,8	17-18 (400; 200)
18	85	35,2	

With the elements from table 1, and fig. 1, the hydraulic parameters may be calculated.

In comparison with an existent network (table 1 Fig 1 on-line graph) gravitationally supplied from reservoir R there are done the following modifications (fig. 1):

a - the demand of water at nodes is doubled;

5. Conclusions

1. The paper presents the offered facilities by the utilization of DELPHY graph components for design, development and control of water distribution networks by utilizing the loop analysis
2. The classical loop analysis of the water supply comprises two basically steps solved separately: a) selection of an initial distribution of flow rates at the pipeline which satisfies relation (2) and b) correction of this flow rates till the satisfaction of relation (3) (Lobatchev – Cross or Newton – Raphson procedures)
3. By convenient transformations referring to the incidence node – pipeline matrix there is established automatically an initial solution, a loop structure covering the network and the final flow rates at the water supply pipelines, using an unitary method, without the help of the user.
4. Other hydraulic parameters of the water network (velocity, piezometric heads, service pressure, etc) are obtained by additional procedure.
5. The water supply networks know developments in time – increased consumptions, doublings, tripling of pipelines, extensions, new supply sources – which modify the pipeline flow rate distribution and the pressure state at nodes.
6. By the loop analysis and interactive procedure there are introduced the new appeared modifications at an existed network and there are established the flow rate distribution and the pressure state in extended network.
7. The practical possibility of re-designing an existent network is shown by the example from Fig1.

References

1. Bârsan Em., Ignat C. (1994) The analysis of development of an extended water distribution network, *Hidrotehnica*, vol.39, nr. 2 ,1994, 7-13 (in Romanian)
2. Bârsan Em., Ignat C.,(1998). Facilities for the calculus of water distribution system using loop analysis, *Bul. Stiinț., U.P .Timișoara*, seria Hidrotehnica, tomul 43(57),vol.I, 324-333, (in Romanian)
3. Divenot, A.,(1980) Une nouvelle methode de calcul des reseaux maillees. *La Houille Blanche*,6 (1980).365-375.(in French)
4. Giurconiu, M., Mirel, I.,Păcurariu, M., Popa,Gh. (1977). *Diagrams, nomograms and tables for sanitary engeneering works calculus*, Ed.Facla, Timișoara (in Romanian).
5. Jain, A.D.,(1976) Accurate Explicit Equation for Friction Factor, *J. of the Hydr.Div., ASCE*,102, HY5 (1976), 674-677.
6. Pchenitchny, B.,Daniline, Y.(1977). Methodes numerique dans les problemes d’extremum, *Edition Mir*, Moscou, (in French).

METHODOLOGY FOR SIZING AND/OR REHABILITATION OF WATER DISTRIBUTION SYSTEMS

Emanoil BÂRSAN¹ Călin IGNAT²

Abstract

The paper presents a methodology for sizing and/or rehabilitation the water distribution networks in order to obtain a solution with minimum cost in a concrete situation. For designing and rehabilitation it is used a genetic algorithm on the basis of which there are realized two program variants with which it is chosen a rehabilitation strategy for a distribution network.

Designing and rehabilitation of a distribution network for a minimum cost leads to an optimization model with nonlinear relations. In the same time, an analytical solution of optimal problem solving is not justified because the diameters D from which it is realized the network belongs to a discrete multitude. Due to this fact it is considered that the optimization problem is more suitable to be done by a genetic algorithm specific to the problem of sizing and rehabilitation of distribution network.

The optimization method using a genetic algorithm consists in the generation of a solution with a genetic algorithm, its introduction in the network solver, the using of results from hydraulic calculation for verification of concordance / agreement or non concordance of conduit cost with the diameter, the application of a penalization in case of non concordance by increasing the objective function value, generation of a new solution and an iterative continuation of the presented steps until the optimum is obtained

For different optimization problems that appear in practice in the designing and rehabilitation of the networks it is modified the objective function according to the restrictions that are imposed..

In the present paper, for a studied case, it is exemplified the application of a genetic algorithm for two distinct ways.

In comparison with the existing programs, the presented methodology permits the automatic specification of modification / replacement that can be done and the evaluation of cost for the proposed solutions.

Another optimization requirements for designing and rehabilitation of networks (for example the k - absolute roughness - modification after a network washing or

¹ Prof., Technical University “Gh.Asachi” of Iasi, Romania, e-mail: ebarsan@hidro.tuiasi.ro

² Prof., University “Al.I.Cuza” of Iasi, Romania, e-mail: ignat@uaic.ro

taking in to the consideration pipe oldness) may be considered by the modification of the objective function corresponding to the objectives having in view.

1. Introduction

For designing, optimal exploitation and rehabilitation of water distribution systems the models and programs specialized for different objectives have been realized

In Barsan and Ignat (2001a) a proper, complex and flexible program for the calculation of water distribution network is presented. This program uses the loop and nodal analysis having multiple applications for various problems that appear in the modeling, monitoring and control networks of different dimensions as well as for their rehabilitation/upgrading.

The upgrading/ rehabilitation of water transmission and distribution systems (tanks, distribution network, pumping station) appears as necessary because of the effects that the corrosion and deposits upon the network; increased consumptions required in time; excessive water losses (reaching in some cases up to 50 - 60 %); complete reconstructing of a zone from distribution network; water quality problems

The problems that appear in rehabilitation are more difficult then the ones set in designing of a new system because: it is worked with a existed network; there are numerous difficulties due to other buried utilities; the problems are added due to the ground conditions; there are more alternative that may be taken in to consideration.

In realization a rehabilitation of a water distribution system, the designer is put again at some supplementary choosing. In place of simple option to size the pipes it may be taken in to consideration the replacement of existed pipes or their maintaining, doubling – tripling for additional capacities. In addition, the comparison with the system made up from new pipes, the designer may be take in to consideration one of the following options: washing with pressure water, lining with cement mortar or epoxy, introduction of coatings (tubing) by sliding or anterior pipe replacement burst with a special device. Each of these possibilities have the particularities in modeling..

The upgrading of water distribution systems may be done on basis of observation made by system monitoring, followed the actions for its remediation and improvement or with a system analysis made in this aim, by using of acalibrated model (Barsan and Ignat, 2001a; Walski, 2003)

Distribution system model have in its structure two elements:

- A program for network solving (solver) with which the flows, piezometric heads, head losses, velocities etc are determined.

- A data set (in form of file) that contain the necessary information for network configuration (making), network distributed water consumptions estimation and network operating (working) modality.

It is considered that a model is realized for a water distribution system when the calculating program with the set of initial data specified to system determine the unknowings of system (in principal the flow on pipes and pressure at nodes).

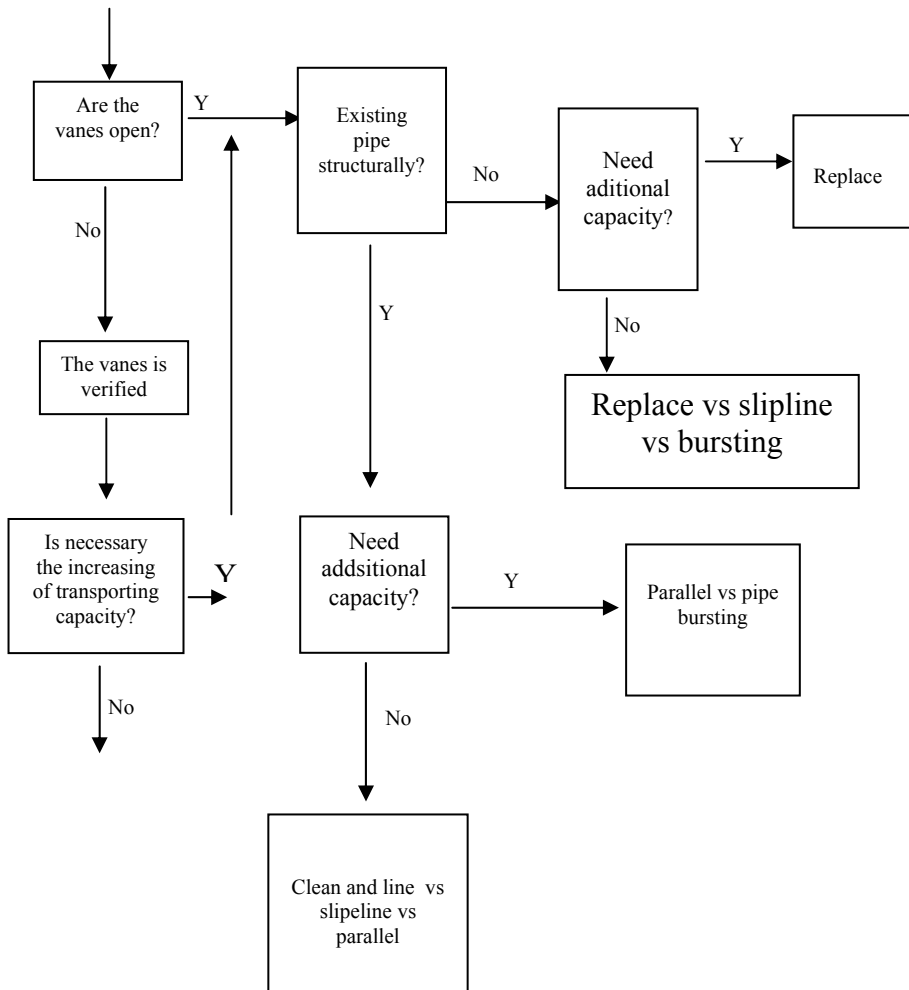


Fig. 1. Options for rehabilitation of distribution networks (after Walski, 2003)

To have the validity a model is calibrated. The calibration consists in bringing by a iterative adjustment process, realized manually or automatically, as the running data of model to be in acceptable limits with the field ones. Periodically, the model is recalibrated (e. g. yearly). With the calibrated model may be done different simulation

with regard to the system exploitation or development/upgrading. Thus may be discovered different troubles in working the network.

A synthetic sight on following strategies in rehabilitation of distributing network is presented in fig. 1.

2. Formulation for rehabilitation model.

The general model for rehabilitation has as the objective function the minimization of network rehabilitation cost (RC) that is a function of pipe rehabilitation action (R), diameter (D) and length (L):

$$\text{Min RC (R, D, L)} \quad (1)$$

This function is conditioned by three kinds of constraints:

1 – Conservation of mass and energy in system (hydraulic conditions)

The conservation of mass at nodes requires that in each node the algebraic sum of flow to be zero.

$$\sum Q_{in} - \sum Q_e = Q_{nod} \quad (2)$$

in which Q_{in} is the incoming flows, Q_e is the outgoing flow, and Q_{nod} is the nodal demand.

The conservation of energy requires that around each loop, the cumulated head loss (H_L) minus the head gain because of pumps (H_P) must be zero.

$$\sum H_L - \sum H_P = 0 \quad (3)$$

For networks with S source nodes, S-1 additional conservation of energy constraints are written between two source nodes. In this case, the algebraic sum of head losses must be equal to the difference in energy between the two source nodes (ΔE).

This can be expressed as:

$$\sum H_L - \sum H_P = \Delta E \quad (4)$$

in which the pipe head loss and pumping head are nonlinear expressions that are the function of the flow rate (relations Darcy-Weisbach or Manning)

2. Constrains for working conditions.

They refer to: pressure at nodes (P), water velocity (V) and hydraulic gradient (HG) for a given network loading conditions / consumptions. This can be expressed as:

$$P_{\min} \leq P \leq P_{\max} \quad (5)$$

$$V \leq V_{\max} \quad (6)$$

$$HG \leq HG_{\max} \quad (7)$$

in which P_{\min} is minimum allowable pressure, P_{\max} is the maximum allowable pressure, V_{\max} is the maximum allowable flow velocity and GH_{\max} is the permissible hydraulic gradient.

3. Restrains for diameter requirement

They are used to specify the minimum /maximum diameter and the discrete set of commercially available diameter values for the new pipes as:

$$D_{\min} \leq D \leq D_{\max} \quad (8)$$

$$D \in \{D\} \quad (9)$$

Equation (8) expresses the lower limit (D_{\min}) and upper limit (D_{\max}) of pipe diameters, whereas equation (9) asserts that the diameter of each new pipe must belong to a commercial set ($\{D\}$).

3. Methodology used to solve the problem

To solve the optimal pipe rehabilitation problem as it is formulated in eqs. 1 - 9 , a solving methodology is applied, in which a hydraulic network simulator is coupled with an optimization model. An initial feasible set of pipe rehabilitation parameters is introduced in network solver to establish the hydraulic parameters (i.e. flow rate, pressure, velocity etc). Network hydraulic solutions (i.e., pressure, velocity, hydraulic gradient) are introduced in optimization models to quantify the object function and checking the working restrains. When a hydraulic solution do not satisfy a working restrain, a penalty method is used to treat the non-fulfillment restrain. Penalty cost is added to the objective cost function to penalize an unfeasible solution (i.e., the moving-off from the space of solutions) and bringing in the zone of feasible solutions. Optimization model produces an improved set of pipe rehabilitation parameters that the restrains for diameters automatically satisfies and the objective function minimizes. This iterative process is repeated until the best solution is found. There are adopted as optimization model, a genetic algorithm and for the network solver, a performed network calculation model

It is remarked that in function of rehabilitation strategy, the costs for objective function are correspondingly chosen.

In application that follows it is considered that the rehabilitation is made by replacing, diameter modification or pipe doubling on a pipeline. For each objective function the costs on ml of pipe are known. (table 2).

For other rehabilitation strategies as the washing, washing and lining etc, that modify k absolute roughness coefficient or the satisfying of some working conditions is starting from rehabilitation unitary costs specified for respective type of operation

4. Application

It is considered the network from fig. 2 with 18 nodes gravitationally supplied from storage tank 1 - R ($H = 131$ m) . Table 1 presents the ground levels and consumptions at nodes (considered at peak demand hour), table of adjacencies for network graph definition and the determined diameters.

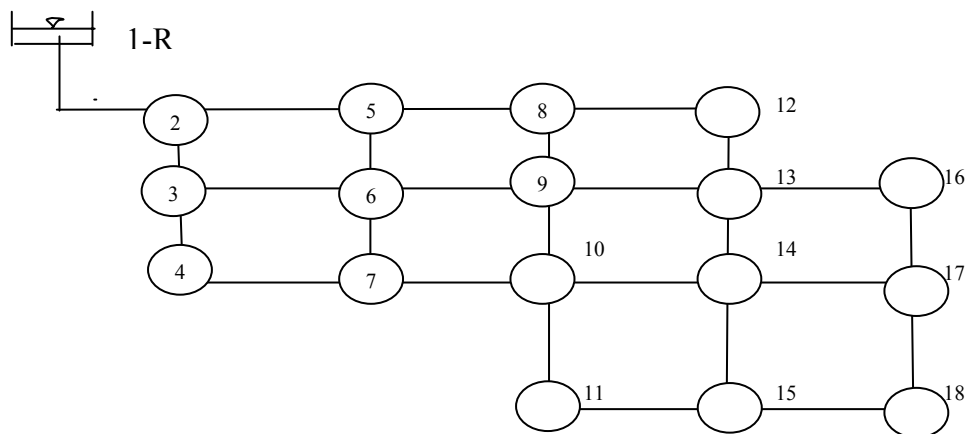


Figure 2

Table 1. Characteristic elements for network from fig. 2

No. of node	Ground level (m)	Node consumption (l/s)	Link of nodes (distance between nodes in m; calculated diameter, mm)
1 - R	125	0	1-2 (600; 700);
2	115	24,1	2-3 (650; 500); 2-5 (750; 500);
3	110,5	20,8	3-4 (350; 400); 3-6 (750; 350);
4	99,5	26,4	4-7 (900; 350);
5	114,3	20,5	5-6 (650; 350); 5-8 (800; 400);
6	108,5	34,2	6-7 (700; 250); 6-9 (800; 350);

7	96,2	42,2	7-10 (850; 350);
8	109,5	33,5	8-9 (650; 250); 8-12 (400; 300);
9	103,5	30,5	9-10 (700; 250); 9-13 (400; 300);
10	95,4	39,5	10-11 (400; 250); 10-14 (400; 250);
11	82,2	17,5	11-15 (400; 200);
12	103,2	20,2	12-13 (650; 250);
13	101,5	36,4	13-14 (700; 250); 13-16 (550; 250);
14	86,7	34,2	14-15 (400; 200); 14-17 (500; 200);
15	84,3	26,4	15-18 (500; 200);
16	83,2	16,5	16-17 (700; 200);
17	86	26,8	17-18 (400; 200)
18	85	35,2	

Table 2. Unit costs for the considered diameters

Dn (mm)	Cost /m		Dn (mm)	Cost /m
50	5		500	130
65	7		600	180
100	11		700	250
125	14		800	325
150	16		900	410
200	23		1000	500
250	32		1100	650
300	50		1200	825
350	60		1300	1000
400	90		1400	1250

Table 3. Network calculation with genetic algorithm, variant 1

Form1

Modificari Genetic Aduagari Exit

COST 460500.0

NrTron	Sursa	Dest	Diam	Diam2	Debit	Debit2	Cost	Penalizare
1	1	2	0.700	0.700	484.900	534.900	0.00	0.00
2	2	3	0.600	0.700	385.841	436.927	162500.00	0.00
3	2	5	0.300	0.300	74.959	73.873	0.00	0.00
4	3	4	0.500	0.600	246.390	297.265	63000.00	0.00
5	3	6	0.400	0.400	118.651	118.862	0.00	0.00
6	4	7	0.500	0.600	219.990	270.865	162000.00	0.00
7	5	6	0.050	0.050	0.250	-0.144	0.00	0.00
8	5	8	0.300	0.300	54.209	53.517	0.00	0.00
9	6	7	0.050	0.050	0.446	0.130	0.00	0.00
10	6	9	0.350	0.350	84.256	84.389	0.00	0.00
11	7	10	0.500	0.500	178.236	228.795	0.00	0.00
12	8	9	0.050	0.050	0.282	-0.040	0.00	0.00
13	8	12	0.200	0.200	20.427	20.056	0.00	0.00
14	9	10	0.050	0.050	0.359	0.245	0.00	0.00
15	9	13	0.300	0.300	53.679	53.604	0.00	0.00
16	10	11	0.300	0.350	77.422	102.886	24000.00	0.00
17	10	14	0.300	0.350	61.673	86.654	24000.00	0.00
18	11	15	0.300	0.300	59.922	60.386	0.00	0.00
19	12	13	0.050	0.050	0.227	-0.144	0.00	0.00
20	13	14	0.050	0.050	0.428	0.278	0.00	0.00
21	13	16	0.200	0.200	17.077	16.782	0.00	0.00
22	14	15	0.065	0.050	1.293	0.591	0.00	0.00
23	14	17	0.200	0.300	26.608	52.141	25000.00	0.00
24	15	18	0.250	0.250	34.815	34.577	0.00	0.00
25	16	17	0.050	0.050	0.577	0.282	0.00	0.00
26	17	18	0.050	0.050	0.385	0.623	0.00	0.00

Tronson 1 Label5

Parametri Algoritm Genetic

Cu dublari

20 Cromozomi

Table 4. Network calculation with genetic algorithm variant 2

Form1

File Modificari Genetic Aduagari Exit

COST 480950 - 0

NrTron	Sursa	Dest	Diam	Diam2	Debit	Debit2	Cost	Penalizare
1	1	2	0.700	0.700	484.900	534.900	0.00	0.00
2	2	3	0.600	0.700	385.841	434.442	162500.00	0.00
3	2	5	0.300	0.300	74.959	75.724	0.00	0.00
4	3	4	0.500	0.600	246.390	304.135	63000.00	0.00
5	3	6	0.400	0.350	118.651	108.901	0.00	0.00
6	4	7	0.500	0.600	219.990	277.735	162000.00	0.00
7	5	6	0.050	0.050	0.250	0.327	0.00	0.00
8	5	8	0.300	0.300	54.209	55.531	0.00	0.00
9	6	7	0.050	0.050	0.446	-0.333	0.00	0.00
10	6	9	0.350	0.300	84.256	75.967	0.00	0.00
11	7	10	0.500	0.500	178.236	235.202	0.00	0.00
12	8	9	0.050	0.050	0.282	0.585	0.00	0.00
13	8	12	0.200	0.200	20.427	20.861	0.00	0.00
14	9	10	0.050	0.050	0.359	-0.504	0.00	0.00
15	9	13	0.300	0.250	53.679	47.141	0.00	0.00
16	10	11	0.300	0.350	77.422	102.466	24000.00	0.00
17	10	14	0.300	0.350	61.673	92.732	24000.00	0.00
18	11	15	0.300	0.300	59.922	59.966	0.00	0.00
19	12	13	0.050	0.050	0.227	0.661	0.00	0.00
20	13	14	0.050	0.050	0.428	-0.581	0.00	0.00
21	13	16	0.200	0.150	17.077	11.982	0.00	0.00
22	14	15	0.065	0.050	1.293	0.555	0.00	0.00
23	14	17	0.200	0.300	26.608	57.397	25000.00	0.00
24	15	18	0.250	0.250	34.815	34.121	0.00	0.00
25	16	17	0.050	0.100	0.577	-4.518	7700.00	0.00
26	17	18	0.050	0.050	0.385	0.535	0.00	0.00

Tronson 1 Label5

Parametrii Algoritm Genetic

Cu dublari

30 Cromozomi

Table 4a. For added pipes the costs are given in situation presented below:

27	2	5		0.050		0.634	3750.00	0.00
28	3	6		0.050		0.606	3750.00	0.00
29	8	9		0.050		0.585	3250.00	0.00
30	17	18		0.050		0.544	2000.00	0.00

For the studied case, a genetic algorithm has been applied for two distinct ways.

- Variant 1, with the possibility of the pipes’ replacement.
- Variant 2, with the possibility of modification or doubling of pipes.

In variant 1, the objective function establishes, for replacement, the network cost with replaced pipes. At the disagreement between the cost and diameter, the penalization is of 10 times the pipe cost to force the change / replacement. The size of objective cost function is established on the basis of unitary costs on diameters from table 2.

In table 3 it is presented the network the calculation from fig. 2 in variant 1, in initial situation and modification of consumption flow rates from the nodes 11 and 17, each with a plus of 25 l/s.

In table 4 and 4a there are presented the calculation for the same network in variant 2, for the case of the modification and doubling some pipes at the increasing of consumption flow rates in nodes 11 and 17, each with a plus of 25 l/s.

For genetic algorithm 20 / 30 de chromosomes are used. A chromosome includes a vector of dimension equals with the pipe number. The values in a chromosome are: For variant 1, 0 – a pipe is not replaced, 1 – a pipe is replaced. For variant 2, 0 – initial pipe is kept, 1 – pipe is modified, 2 – pipe is doubled.

The used operators in the modification of chromosome populations are : mutation, crossover and sum mod 2 for variant 1 and mod 3 for variant 2, respectively.

From examining tables 3 and 4 it is found that variant 2 (modification and doubling of some network pipe) conducts at a cost more raised versus the variant 1 (replacement of pipes), for the same network.

5. Conclusions

1. The designing and rehabilitation of a distribution network for a minimum cost leads to an optimization model with nonlinear relations. In the same time, an analytical solution of optimal problem solving is not justified because the diameters D from which it is realized the network belongs to a discrete multitude. Due to this fact it is considered that the optimization problem is more suitable to be done by a genetic algorithm specific to the problem of sizing and rehabilitation of distribution network.

2. The optimization method using a genetic algorithm consists in the generation of a solution with a genetic algorithm, its introduction in the network solver, the using of results from hydraulic calculation for verification of concordance / agreement or non concordance of conduit cost with the diameter, the application of a penalization in case of non concordance by increasing the objective function value, generation of a new solution and an iterative continuation of the presented steps until the optimum is obtained.

3. For different optimization problems that appear in practice in the designing and rehabilitation of the networks it is modified the objective function according to the restrictions that are imposed.

4. In the present paper, for a studied case the application of a genetic algorithm for two distinct ways, is exemplified.

- Variant 1, with the possibility of the pipes' replacement.
- Variant 2, with possibility of modification or doubling pipes.

It is found from the examination of tables 3 and 4 that variant 2 (modification or doubling of some network pipelines) leads to a raised cost in comparison with variant 1 (replacement of pipelines), for the same network.

5. In comparison with the existing programs, the presented methodology permits the automatic specification of modification / replacement that can be done and the evaluation of cost for the proposed solutions.

6. Another optimization requirements for designing and rehabilitation of networks (for example the k- absolute roughness - modification after a network washing or taking in to consideration the conduit oldness) may be considered by the modification of the objective function corresponding to the objectives having in view.

References

1. ARA (2003), Conferinta: *Sisteme de monitorizare, concepte si realizari practice*, Editura Foton. ISBN 973-98547-6-1
2. ARA (2000), International Conference. *The Drinking Water Quality in the Distribution Network*, Bucuresti
3. Barsan, Em., Ignat,C., (2001a) *Sisteme de distributia apei*, Ed. Cerami-Iasi
4. Barsan, Em., Ignat,C., (2001b) Technical-economic analysis of water distribution networks, *Water Science & Technology: Water Supply*, London, vol 1, no. 2 pp 201-210
5. CNPDAR, (1997), Simpozion national, "*Reducerea pierderilor de apa si a consumurilor energetice in sistemele de alimentari cu apa*", Bucuresti, 10-11 aprilie;

6. Haestad Methods, Walski, Th., Chase, D.,Savic,D., Grayman W., Beckwith, S., Koelle, Ed., (2003) *Advanced Water Distribution Modeling and Management*, Haestad Pres, Waterbury, CT, USA, 348 - 354
7. Wu,Z.Y., Boulos, P.F., Orr,C.H. Ro,J.J. (2001) Using genetic algorithms to rehabilitate distribution systems, *Journal AWWA*, vol.93, no. 11, pg. 74 – 85

SIMULATION OF WATER DISTRIBUTION SYSTEMS ON EXTENDED PERIOD OF 24 HOURS

Emanoil BÂRSAN¹, Călin IGNAT²

Abstract.

Hydraulic calculus of water distribution system is done commonly at the maximum hour flow rates (STAS 1343). This calculation don't gives the sufficient information for the pump station sizing and the determining of volume of system tanks.

For taken into account the work of pumps and tanks in system at variation of demand in 24 hours, the authors realized a loop analysis – based program, with which it is realized the simulation of a water distribution system on the extended-period at 24 hours and which permits the following of hydraulic parameters in distribution network and the sections of tanks and pump stations

It is presented a practical application for a network supplied of two pump stations and one inflow/outflow tank, by visualization, with graphic components DELPHI, the evolution of hydraulic parameters in 24 hours for the sections with pump stations and tank which they forms the support for choice of pumps and tank capacity.

The simulation permits choosing of the pumps and with the concrete choosing characteristics of pumps is defined the hydraulic behavior (Q and H) of the system.

¹Prof., Technical University “Gh.Asachi” of Iasi, Romania, e-mail: ebarsan@hidro.tuiasi.ro

² Prof., University “Al.I.Cuza” of Iasi, Romania, e-mail: ignat@uaic.ro

1. Introduction

A water distribution system is composed of the distribution network, water storage tanks and / or pump stations which may be disposed in outer or inner of the network. The practical arrangement of components of water distribution system is of great diversity depending on source positions, terrain configuration, consumption values (quantities), building system etc.

The working way of water distribution system of several complexities may be followed by simulation with a model which comprises a network solution program, sometimes called network solver, and a data sets which define the network configuration (arrangement, lengths, diameters), water consumption (demand) at network nodes and scenarios after which the network will be operated [3], [4].

There are two ways for tackling the simulation in current practice.

Simulation considering a steady-state regime (modality of current practice in Romania - STAS 1343),

Simulation on the extended period (currently on 24 hours) [4]

In case of steady state simulation it is considered that the working conditions remain constant over a time period (e.g. one hour). In current way it is modeled only the maximum hour consumption and minimum hour consumption

The conditions of maximum hour consumption represent the time period in which the system will be most stressed and the minimum hour consumption verifies if the system assures the replenishment of tanks and if in replenishing period some pipelines are undersized.

The simulation on the extended period considers the system simulation for many consecutive time periods, e. g. 24 hourly time period in a single day. In this case the flow rates and the pressure are constantly on hourly time period.

This type of simulation establishes (on each hour from the day):

- inflow/outflow from tank, volume and water level in tank;
- flow rates and heights of pumping stations
- pipeline flow rates and node piezometric heads between maximum and minimum consumption level for every hour of the day.

The determination of these elements confers a more ample vision on the system behavior and assures a more correctly sizing of a pump station and of the storage tanks.

The required data for each type of simulation are essentially the same. However, greater amounts of data and some additional type of data are required for extended – period simulation (in fact, one set for each hour from period of simulation). At these are added the data concerning the initial state of system components and their

time modification, consumption fluctuation, simulation period and adopted step of time.

For taking in to account the pumps and tanks working in system at demand variation in 24 hours it was realized a simulation program for an extended-period simulation [3] based on loop analysis [1], [2] with which is may watch in 24 hours the hydraulic parameter evolutions (flow rate and pressure) in distribution network, tanks and pump stations.

The extended-period simulation program is applied to a network supplies by two pump stations and inflow/outflow tanks. The parameter evolution from pump stations and inflow/outflow tank are graphically presented using DELPHI components.

2. Program for a extended-period simulation

For the simulation of a water distribution system on an extended-period for 24 hours there were developed numerous programs having as base several computation methods. For example: loop, nodal and hybrid methods [3], [4], [6], [7][8],[9].

For the realized simulation at the application from this paper it was used loop analysis [1], [2], [3] with which it was developed a program for an extended period of 24 hours. In the program, the input and output data are done by DELPHI graphic components.

3. Analysis of water distribution system having 2 pump stations and an inflow/outflow tank

This system is frequently met in water distribution for urban settlements (fig. 1).

The water distribution configuration system is specified in fig 1 and table 1 and water demand multipliers in 24 hours from maximum demand day, in table 2.

The particularity of this system consists in the fact that at hour of maximum demand, the network supplies both pump station (s) and tank while at the hour of minimum demand the tank works as a consumer, storing the water over plus that is not consumed in the distribution system .

Table 1. Configuration of water distribution system (2 PS + network + inflow/outflow tank)

Node	Node flow rate (L/s) at maximum daily consumption	Elevation (m)	Connection (distances (m))
1	25,4	124,9	2 (300); 3 (1000); 4 (850);
2	22,4	123,8	5 (650); 6 (950);
3	67,3	125,5	4 (500); 9 (670);

Node	Node flow rate (L/s) at maximum daily consumption	Elevation (m)	Connection (distances (m))
4	29,8	123,8	5 (280); 10 (890);
5	13,4	123,6	7 (200);
6	24,6	120,5	7 (330); 8 (800);
7	17,5	122,8	11 (950);
8	25,2	120,5	12 (500); 17 (830);
9	19,3	126,6	10 (400); 13 (560);
10	28,6	126,1	11 (330); 14 (800);
11	29,9	124,8	12 (550); 15 (700);
12	16,9	123,2	16 (380);
13	20,9	127,6	14 (260); 22 (950);
14	25,5	127,0	18 (300); 22 (800);
15	14,4	126,0	18 (170); 19 (350);
16	14,4	125,7	17 (430); 19 (400);
17	27,3	124,0	20 (1050);
18	13,2	126,6	21 (650);
19	11,2	125,7	20 (200);
20	39,2	126,2	21 (900);
21	21,3	129,8	22 (250);
22	23,6	131,0	25 (200);
23	0	113,0	1 (3000);
24	0	113,0	2 (3000);
25	0	157,3	22 (200);

Table 2. Coefficients (multipliers) for hour consumption at the nodes in 24 hours in comparison with maximum daily consumption (table 1, col. 2)

Hour	0 – 1	1 – 2	2 – 3	3 – 4	4 – 5	5 – 6	6 – 7	7 – 8
Multipliers	0,79	0,40	0,50	0,52	0,60	0,70	0,96	1,25

8 – 9	9 – 10	10 – 11	11 – 12	12 – 13	13 – 14	14 – 15	15 – 16
1,23	1,20	1,08	1,15	1,00	1,15	1,10	1,10

16 – 17	17 – 18	18 – 19	19 – 20	20 – 21	21 – 22	22 – 23	23 – 24
1,03	1,10	1,15	1,23	1,35	1,25	1,03	0,89

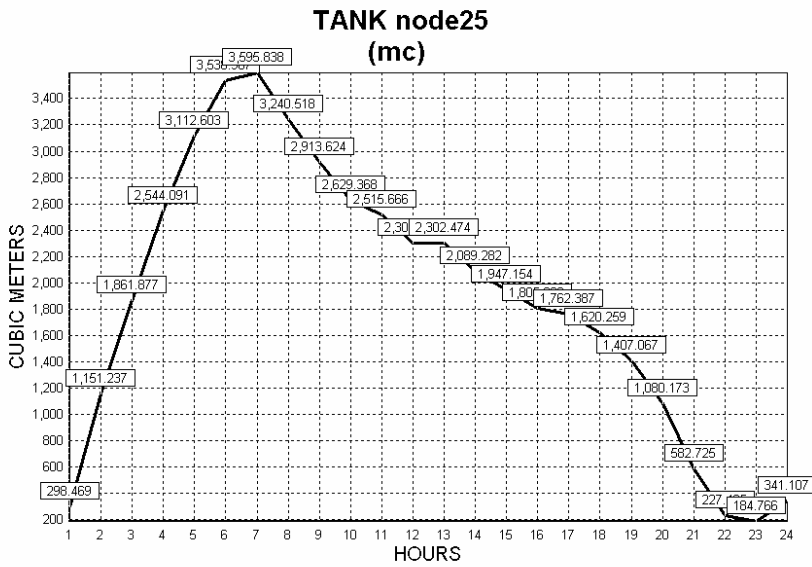
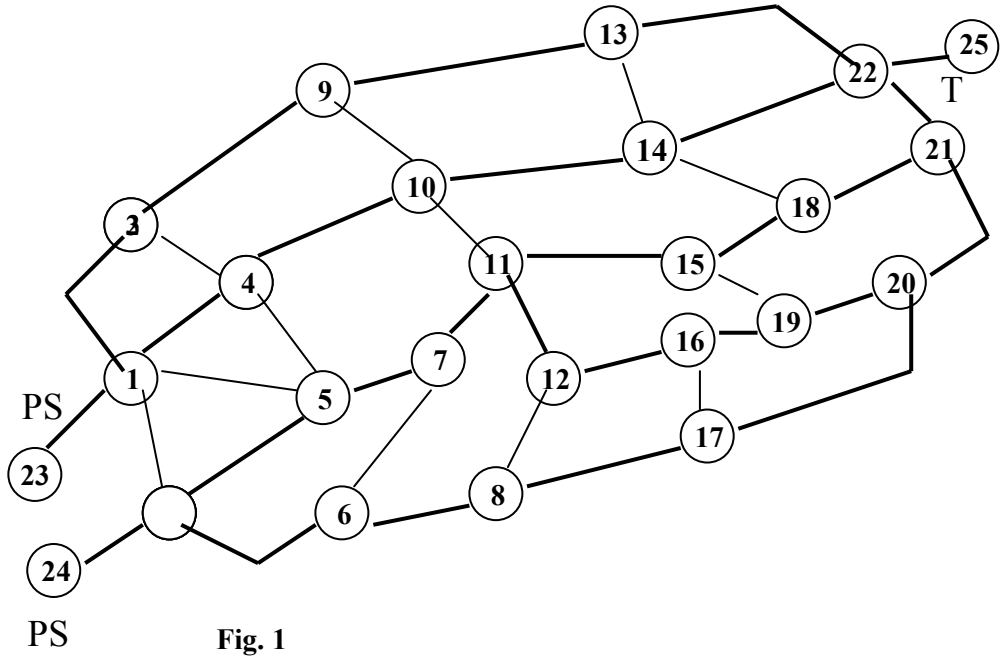


Fig. 2

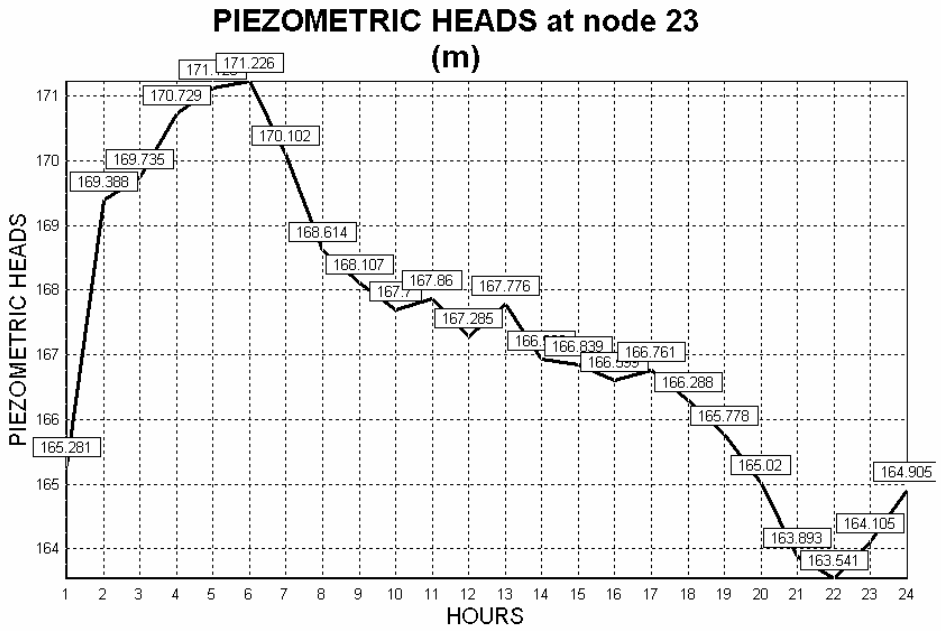


Fig. 3

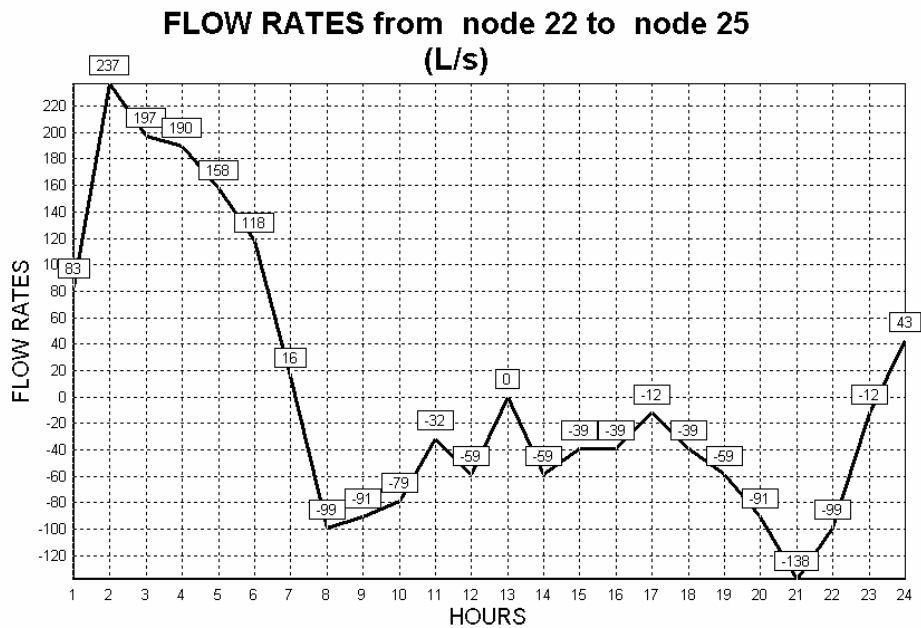


Fig. 4

With the program of loop analysis (on the extended period simulation of 24 hours) [3] in maxim demand day it is established, by dialogue, all hydraulic parameters of system

For exemplification there were extracted some hydraulic parameters of evolution concerning tanks and pump stations.

Thus in fig 2 there are presented the tank storage volumes in 24 hours.

In fig. 3 there are shown system piezometric heads at node 23 (pump station)

In fig. 4 there are shown flow rates from node 23 to node 25 (inflow/outflow tank in 24 hours)

With established hydraulic parameters at pump stations and storage tank sections there are chosen the pumps and is determined the tank volume. After the pump selection the simulation is taken again for establishing of effective system behavior

4. Conclusions

1. For pump station(s) and tanks sizing of a water distribution it is necessary to know the hydraulic parameters (flow rates and pressures) on 24 hours which is obtained over an extended period of time.
2. The system simulation is realized by a program realized by authors having at base the loop analysis of network and for the visualization of hydraulic parameters evolution in 24 hours there are used DELPHI graphic components.
3. A practical application for a network supplied of 2 pump stations and an inflow – outflow tank put in evidence the hydraulic parameters in pump stations and tank sections
4. The simulation at point 3 permits choosing of the pumps and with the concrete choosing characteristics of pumps is defined the hydraulic behavior (Q and H) of the system.

References

1. B â r s a n Em., I g n a t C., Aspecte privind calculul rețelelor de distribuția apei folosind analiza inelară, *Hidrotehnica*, **36**(8-9), 233-235, (1991).
2. B â r s a n Em., I g n a t C., Facilități pentru calculul sistemelor de distribuția apei folosind analiza inelară, *Bul. Științific al Univ. "Politehnica " Timișoara, secția Hidrotehnica*, tomul **43**, (57) vol.1, 324-333 (1998).
3. B â r s a n Em., I g n a t C., Sisteme de distribuția apei. Ed. Cermi Iași (2001).
4. C e s a r i o L. *Modeling, Analysis, and Design of Water Distribution System*, AWWA, Denver CO. (1995).
5. C h a n d r a s h e k a r M., Extented Set of Components in Pipe Network, *Journal of the Hydraulics Division*, ASCE, **106**, (HY1),133-149 (1980).

6. C i o c D., A n t o n A., Calculul automat în proiectarea și exploatarea rețelelor de distribuția apei. In: Simpozion național ARA “*Reducerea pierderilor de apă și a consumurilor energetice în sistemele de alimentări cu apă*”, București, 10-11 aprilie, 57-70 (1997).
7. Mays L.W., *Water Distribution Systems Network*, Mc Graw-Hill, New York, 2000, 12.1 – 12.21.
8. R o s m a n L. A., EPANET 2, US EPA, Cincinnati. (2000).
9. Haestad Methods , Walski, Th.M., Chase,V.D., Savic, A.D., Grayman,W., Beckwith, St., Koelle, E. *Advanced water Distribution Modeling and Management*, Haestad Press, Waterbury, CT, USA, 2003.

CONSIDERATIONS REGARDING THE REOLOGICAL ANALYSIS OF THE FAILURE MODE, SPECIFIC TO CLAYS

Ana Nicuță¹, Felicia Ursache²

Abstract:

The paper presents an analysis of clays failure phenomena by reological behavior. There are combined two general trends: on one hand we look for a mathematical expression of the physic phenomena and on the other hand it is introduced a structural mathematic model chosen to reproduce the essence of the physical phenomenon and to display the clay properties.

1. Introduction notions

A material system resistance (rock, clay etc.) depends of time. The clay resistance dependence to time can be defined as the maximal tension to which the clay resists, without failure no matter how much time the clay will be stressed. This type of resistance was named by Griggs (1936) „the fundamental resistance”; by Philips (1984) – „the real resistance”; by Potts (1964) „the tension state in time”; by Price (1966) „the long lasted time resistance”.

We have decided to accept the expression „**long lasted time resistance**”.

2. The theoretical aspects

The long lasted time resistance condition supposes that the clay failure produces when the plastic deformation value (creep strain), ε_f , gets to a certain constant limit ε_f^r , whom overtaking takes to destruction which means that $\varepsilon_f = \varepsilon_f^r = \text{constant}$. This is actually a constant for every clay type, independent of tension measure and time, till the failure. Considering the criteria of „constant multiplication” between the plastic deformation action speed and the failure time, we can write [2]

$$\dot{A} \cdot t_r = \text{constant} \quad (1)$$

where: \dot{A} = specific value of tension state determined by the relation [2,3]:

¹ Assoc.Prof., Ph.D., “Facultatea de Constructii”, Iasi, e-mail nicutaana@yahoo.com

² Ph.D., “Habitat Proiect”, Iasi;

$$\frac{\partial A}{\partial t} = \sigma_{ij} \cdot \dot{\epsilon}_{ij} \tag{2}$$

If \dot{A} is a the variable value in time, the relation(1) becomes:

$$\int_0^{t_r} \dot{A}(t)dt = \text{constant} \tag{3}$$

From the (1) - (3) expressions, we found out that the clay failure produces when the deformation gets to a certain limit value. **The long lasted time resistance** can be analytical expressed by a series of relations known in the technical literature. The most frequent types of equations are: logarithmical, exponential. The choice of one creep equation lead’s us to the fact that based on the experimental information it is determined the empirical formula which describes best the experimental curve. To solve this problem, the curve equality method will be used. This consists in using a graphical system of co-ordinates which allows the curve transformation in line.

Starting from a non-linear relation $y = f(x)$, by transformations [5] results the line equation:

$$y = Bx + D \tag{4}$$

where:

$$B = \frac{n \sum_{i=1}^n x_i y_i - \sum_{i=1}^n y_i \sum_{i=1}^n x_i}{n \sum_{i=1}^n x_i^2 - \left(\sum_{i=1}^n x_i \right)^2} \tag{5}$$

$$D = \frac{\sum_{i=1}^n y_i - B \sum_{i=1}^n x_i}{n}$$

n - number of selected experimental points.

3 The methodology of experimental data processing

This methodology is suggestively obtained by the use of an example. Considering this, there are going to be examined the data resulted from the long lasted time resistance determination in the case of different clay types.

The tests were done at a constant stress, for which it has been determined the time t_{∞} to failure.

To understand the principle, we will examine a logarithmical equation:

$$\sigma = \frac{\beta}{\ln \frac{t_r + t^*}{T}} \quad (6)$$

For the graphical display of the long lasted time resistance curves we transform the equation (4) [5], where $t^*=1$.

We will obtain:

$$\begin{aligned} x &= \ln(t_r + 1) \\ y &= \frac{1}{\sigma} \end{aligned} \quad (7)$$

The way in which the experimental points are situated in fig. 1 confirm the relation viability (6) – a line.

The line inclining angle, compared to OX axa, determines the $B = 1/\beta$ parameter, and the segment value which is determined by the line intersection with the OY axis represent the $D = -1/\beta \ln T$ parameter value. We can determine the B and D parameter with the help of relation (5) from where results the β and T parameter values.

The result is that the value of long lasted time resistance drops and for $t \rightarrow \infty$, $\sigma \rightarrow \infty$.

The limit of long lasted time resistance corresponds to a value of a certain limit moment of time, till failure t_∞ [2, 3].

$$t_\infty = \left(100T^{0,03}\right)^{\frac{1}{1,03}} \quad (8)$$

t_∞ represents the limit time for which the resistance decrease compared to failure resistance, at $t = 100$ years, means less of 3%:

$$\frac{\sigma_\infty - \sigma_{100}}{\sigma_{100}} = 0,03$$

where

σ_{100} - theoretical value of failure resistance at $t = 100$ years;

σ_∞ - long lasted time resistance conditional limit value.

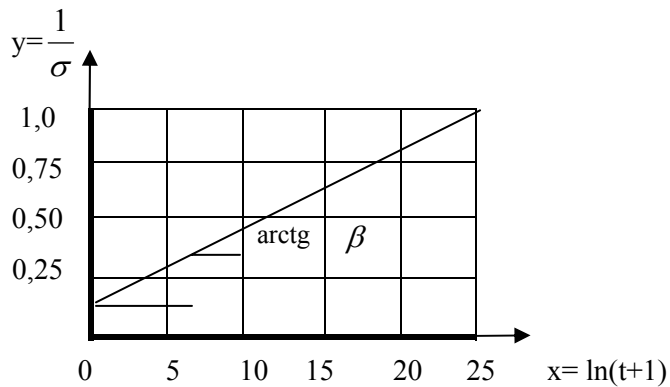


Fig.1: The curve adjustment using the logarithmical equation

4. Data results:

To a better understanding of the limit time variation t_{∞} , we'll consider different types of clays [5], for several variations of the initial times (6 months, 1 year).

t = 6 months

Table 1

	$E=12MPa$, $c=12KPa$, $\nu=0,3$			$E=15MPa$, $c=15KPa$, $\nu=0,25$			$E=18MPa$, $c=18KPa$, $\nu=0,3$		
	$\phi^{(0)}$			$\phi^{(0)}$			$\phi^{(0)}$		
	8	10	12	8	10	12	8	10	12
$\sigma_{[KPa]}$	22,31	22,63	22,92	27,88	28,28	28,64	33,45	33,94	34,38
t_{∞}	93,0226	93,0287	93,0331	93,0288	93,0348	93,0391	93,0337	93,0389	93,0439

$t = 1 \text{ year}$

Table 2

	$E=12MPa,$ $c=12KPa,$ $\nu=0,3$			$E=15MPa,$ $c=15KPa,$ $\nu=0,25$			$E=18MPa,$ $c=18KPa,$ $\nu=0,3$		
	$\phi(^{\circ})$			$\phi(^{\circ})$			$\phi(^{\circ})$		
	8	10	12	8	10	12	8	10	12
$\sigma_{[KPa]}$	22,31	22,63	22,92	27,88	28,28	28,64	33,45	33,94	34,38
t_{∞}	93,0255	93,0316	93,0398	93,0297	93,0364	93,0406	93,0348	93,0396	93,0449

5. Conclusions:

- Together with the long lasted time resistance growth, for the same friction angle, we will also grow the limit time till failure.
- For both cases ($t = 6$ months, $t = 1$ year), the t_{∞} time is around the value of 93 years.
- The bigger the initial time is, the bigger the t_{∞} value is, for the same (ϕ°) friction angle.
- Once the E (linear deformation module) and c (cohesion force) value grows, the σ and t_{∞} value will also grow (for the same ν - Poisson coefficient).

6. References:

1. Glusko V.T. „Strength Distribution in Hard Rock” Institute of Rock Mechanics and Mineral Science, 1973, p763 – 766;
2. Murayama S. „Reological Properties of Clays” The 5th Int. Conf. Soil Mechanics Found Eng., Paris, 1961;
3. Todorescu A. „Reologia rocilor cu aplicatii in minerit” Editura Tehnica, Bucuresti, 1986; (in Romanian)
4. Nicuta Ana „Contributii cu privire la comportamentul pamanturilor coezive, regim static si dinamic”, Teza de doctorat, Iasi 1994; (in Romanian)
5. Ursache F. „Studiu teoretic si experimental privind folosirea modelelor matematice in evaluarea deformatiilor, in terenul de fundare”, Teza de doctorat, Iasi, 2003; (in Romanian)

EXIGENCIES OF MODELLING THICK PLATES ON BI-MODULUS SUBGRADE

Ioana VLAD¹, Olimpia BLAGOI²

Abstract

The bending classical theory for elastic plates is based upon the assumption that the internal moments are proportional to the curvatures of the median deformed surface. This theory does not include the effects of shear and normal pressure in the plate. The model of a bi-modulus foundation is a realistic generalization of the Winkler’s classical one and is widely used to represent the subgrade of railroad systems, airport lanes [1], [2]. The derived equation of elastic thick plates on bi-modulus foundation considers the shear effect and the normal σ_z stress as linear variable across the plate thickness.

In the present paper numerical solutions, for the problem of thick plates resting on a bi-modulus Pasternak subgrade, which take into account the shear distortion, are compared to the solutions obtained by Finite Element Analysis and with the case of a plate resting on Winkler foundation. The paper presents the particular solutions for the rectangular plate of clamped boundary, for the hinged rectangular plate and for a semi-elliptical plate.

The numerical solutions consist of double power series and they were obtained based on the minimum of the total strain energy [1]. Parametric studies have been performed in order to emphasize the effects of the chosen foundation and that of the geometry.

1. Numerical Solutions of the Thick Plate on Bi-modulus Foundation

Elastic thick plates resting on bi-modulus foundation (Fig. 1) obey the fundamental system of differential equations:

$$\begin{aligned} (K + c_2)\Delta w - c_1 w + K\theta &= -p(x, y) \\ \frac{D}{2} \left[(1 - \nu)\Delta\varphi + \frac{\partial\theta}{\partial x} - \nu \frac{\partial}{\partial x} \Delta w \right] - K \left(\varphi + \frac{\partial w}{\partial x} \right) &= 0 \\ \frac{D}{2} \left[(1 - \nu)\Delta\psi + \frac{\partial\theta}{\partial y} - \nu \frac{\partial}{\partial y} \Delta w \right] - K \left(\psi + \frac{\partial w}{\partial y} \right) &= 0 \end{aligned} \quad (1)$$

¹ Prof., PhD, “Gh. Asachi” Technical University of Iasi, Romania, E-mail: vlad12000@yahoo.com

² Prof., PhD, “Gh. Asachi” Technical University of Iasi, Romania, E-mail: oblagoi@yahoo.com

In Eq. 1, $K = Gh = \frac{Eh}{2(1 + \nu)}$; $\theta = \frac{\partial\varphi}{\partial x} + \frac{\partial\psi}{\partial y}$; ν is Poisson's ratio of the plate (usually concrete), D is the plate bending stiffness, Δ is Laplace operator, c_1 and c_2 are the Pasternak (or bi-modulus) model elastic constants, φ, ψ are the complete rotations about x and y -axes due to the thin plate bending and due to shear (the thick-Mindlin) model. When φ and ψ were eliminated, it resulted [1]:

$$[D(2 - \nu)\Delta - 2K]\theta = (\nu D\Delta\Delta + 2K\Delta)w(x, y) \tag{2}$$

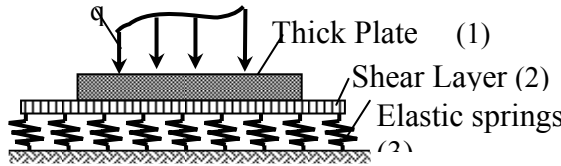


Fig. 1.
Elastic thick plate on bi-modulus foundation

Then:

$$D\Delta\Delta w(x, y) = \left(1 - D \frac{2 - \nu}{2K}\right)(p - q_s) \tag{3}$$

In Eq. 3, q_s is the response of the elastic bi-modulus foundation:

$$q_s(x, y) = c_1 w(x, y) - c_2 \Delta w(x, y) \tag{4}$$

From Eqs. 3 and 4 it yields finally:

$$D[2K + (2 - \nu)c_2]\Delta\Delta w(x, y) - [2Kc_2 + D(2 - \nu)c_1]\Delta w(x, y) + 2Kc_1 w = [2K - D(2 - \nu)\Delta]p(x, y) \tag{5}$$

The additional term of the right member, Eq. 5 takes into account the shear stress and the effect of inter-layer pressure, σ_z .

The approximate solution of the last Equation is taken as [1]:

$$w(x, y) = \sum_{m=0}^{\infty} \sum_{n=0}^{\infty} A_{mn} S_{mn}(x, y) \tag{6}$$

$$\varphi(x, y) = \sum_{m=0}^{\infty} \sum_{n=0}^{\infty} B_{mn} \frac{\partial}{\partial x} S_{mn}(x, y); \quad \psi(x, y) = \sum_{m=0}^{\infty} \sum_{n=0}^{\infty} C_{mn} \frac{\partial}{\partial y} S_{mn}(x, y) \tag{7}$$

in which $S_{mn}(x, y) = x^m y^n F(x, y)$ and $F(x, y)$ is a function depending on boundary conditions. If the principle of minimum strain energy were applied, it results a

system of linear equations of infinite degree, enabling to find the coefficients A_{mn} , B_{mn} , C_{mn} .

1.1. Rectangular Hinged Plate Acted by Uniform Load (Fig. 2a)

The load intensity $p(x,y)= p$, and the boundary function is chosen as:

$$F(x, y) = \prod_{i=1}^n [g_i(x, y)]^{p_i} \tag{8}$$

$g_i(x,y)$ is the boundary equation and $p_i=1$ for the simply supported edge. Finally S_{mn} will be:

$$S_{mn}(x, y) = x^m y^n F(x, y) = x^{m+1} y^{n+1} (x - a)(y - b) \tag{9}$$

The first approximation will be: $S_{00} = xy(x - a)(y - b)$

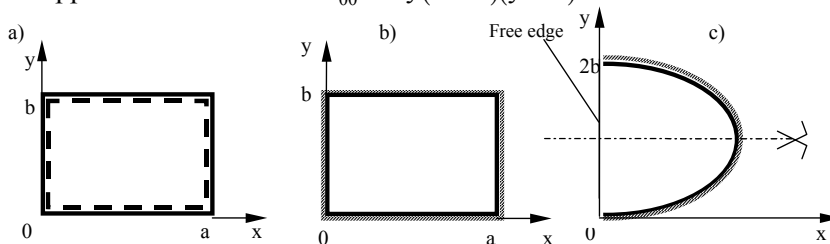


Fig. 2. Case Studies

- a) Rectangular hinged plate; b) Rectangular hinged plate; c) Elliptical plate clamped on the curved boundary and free on y-axis

The complete solution is given in [1].

1.2. Rectangular Clamped Plate Acted by Uniform Load (Fig. 2b)

In this case, the boundary function $F(x, y)$ was chosen as $F(x, y) = x^2(x - a)^2 y^2(y - b)^2$ and S_{mn} results from Eq. 9. The fully developed solutions are given in [1], and they require solving 3 x 3 or 6 x 6 algebraic systems of linear equation (for the first or the 2nd approximation of the solution).

The approximate functions $w(x,y)$, bending and twisting moments and shear forces depend on the mechanical properties of ground, i.e. c_1 which is the Winkler bed coefficient and c_2 is calculated as:

$$c_2 = G_0 H / 3 ; G_0 = E_0 / 2(1 + \nu_0) ,$$

E_0 and ν_0 are ground mechanical properties for the plane strain state; H is the depth of the ground interaction layer [1].

1.3 Semi-elliptical Plate (Fig. 2c)

In this case, the boundary function $F(x, y)$ was chosen as:

$$F(x, y) = \left(\frac{x^2}{a^2} + \frac{y^2}{b^2} - \frac{2y}{b} \right)^2 \quad (10)$$

$$S_{mn} \text{ results from Eq. 9: } S_{mn} = x^m y^n \left(\frac{x^2}{a^2} + \frac{y^2}{b^2} - \frac{2y}{b} \right)^2 \quad (11)$$

$$\text{The first approximation yields: } S_{00} = \left(\frac{x^2}{a^2} + \frac{y^2}{b^2} - \frac{2y}{b} \right)^2 \quad (12)$$

The vertical displacement $w(x, y)$ becomes:

$$w_{00}(x, y) = X_1 \left(\frac{x^2}{a^2} + \frac{y^2}{b^2} - \frac{2y}{b} \right)^2 \quad (13)$$

The rotation angles:

$$\varphi_{00}(x, y) = \frac{4x}{a^2} \left(\frac{x^2}{a^2} + \frac{y^2}{b^2} - \frac{2y}{b} \right) X_2$$

$$\psi_{00}(x, y) = \frac{4(y-b)}{a^2} \left(\frac{x^2}{a^2} + \frac{y^2}{b^2} - \frac{2y}{b} \right) X_3 \quad (14)$$

The bending and twisting moments are:

$$M_x(x, y) = -2D \left[\frac{A}{a^2} \cdot B(x, y) + \nu \frac{C}{b^2} \cdot R(x, y) \right]; \quad (15a)$$

$$M_y(x, y) = -2D \left[\frac{C}{a^2} \cdot R(x, y) + \nu \frac{A}{b^2} \cdot B(x, y) \right]$$

$$M_{xy}(x, y) = -2D(1-\nu) \frac{x(y-b)}{a^2 b^2} (X_1 + X_2) \quad (15b)$$

$$A = (2 - \nu)X_2 - \nu X_1; C = X_3 - X_1; B(x, y) = \frac{3x^2}{a^2} + \frac{y^2}{b^2} - \frac{2y}{b}; \quad (15c)$$

$$R(x, y) = \frac{x^2}{a^2} + \frac{3y^2}{b^2} - \frac{6y}{b} + 2$$

$$X_1 \dots X_3 \text{ are the solutions of the matrix equation: } \mathbf{A} \cdot \mathbf{X} = \boldsymbol{\delta} \quad (16)$$

The matrices \mathbf{A} and $\boldsymbol{\delta}$ are given below and depend on plate mechanical properties and geometry and also on bi-modulus subgrade mechanical properties.

$$\mathbf{A} = \begin{bmatrix} A_1 & b^2 A_2 & a^2 A_3 \\ A_2 & A_4 & a^2 A_5 \\ A_3 & b^2 A_5 & A_6 \end{bmatrix} \quad \boldsymbol{\delta} = \begin{Bmatrix} \delta_1 \\ \delta_2 \\ \delta_3 \end{Bmatrix} \quad (17)$$

$$A_1 = \frac{\nu^2}{1 + \nu} \cdot \frac{7}{6 \cdot 17} (45(a^4 + b^4) + 29a^2 b^2) + \alpha(a^2 + b^2) + \frac{c_1}{D} \cdot \frac{263a^4 b^4}{15 \cdot 16 \cdot 17} + \frac{c_2}{D} \cdot \frac{a^2 b^2 (23a^2 + 257b^2)}{12 \cdot 17} \quad (18a)$$

$$A_2 = -\frac{\nu(1 - \nu)}{1 + \nu} \cdot \frac{105}{4 \cdot 17} (29a^2 + 45b^2) + \alpha; \quad (18b)$$

$$A_3 = -\frac{\nu(1 - \nu)}{1 + \nu} \cdot \frac{105}{4 \cdot 17} (29b^2 + 45a^2) + \alpha$$

$$A_4 = \beta b^2 + \beta_1 a^2 + \alpha; A_5 = \frac{7}{6 \cdot 17} \frac{19\nu^2 + 10}{1 + \nu}; A_6 = \beta a^2 + \beta_1 b^2 + \alpha \quad (18c)$$

$$\alpha = \frac{6(1 - \nu)}{5h^2}; \beta = \frac{1 - \nu - \nu^2(1 + \nu^2)}{1 - \nu^2} \cdot \frac{105}{2 \cdot 17}; \beta_1 = 35 \frac{(1 - \nu)}{3 \cdot 17} \quad (18d)$$

$$\delta_1 = p \left(\frac{7a^4 b^4}{8 \cdot 24D} - \frac{105}{8 \cdot 17} \cdot \frac{\nu^2}{Eh} a^2 b^2 (a^2 + b^2) \right); \quad (18e)$$

$$\delta_2 = -p \frac{105}{8 \cdot 17} \cdot \frac{\nu^2}{Eh} a^2 b^2; \delta_3 = \delta_2$$

2. Models for Finite Element Analysis

Modeling is an art based on the ability to visualize physical interactions. All basic and applied knowledge of physical problems, finite elements and solution algorithms contribute to modeling expertise.

Sometimes, the user of a computer program does not understand the physical action and boundary conditions of the actual structure, and the limitations of applicable theory, well enough to prepare a satisfactory model.

Another difficulty occurs when the behavior of various elements, the program's limitations and options were not understood, well enough to make an intelligent choice among them. In this case the model fails to reflect important feature of the physical problem, fine detail irrelevant to the problem, a solution based on inappropriate loading or support conditions and an overflow of computed results which are not properly examined and questioned.

Choosing one element-type or mesh or others, is another problem. The analyst must understand how various elements behave in various situations. The practice of using Finite Element-based software showed that elements and meshes of intermediate complexity are better fitted to many problems.

A coarse mesh may not always depict the actual structure. Figures 3a and 3b show thick plates, clamped on the boundary, modeled by coarse meshes. The model surface is much smaller than the actual one, since only one internal node is not restrained, and the output results will be based only on nodal parameters of the non-restrained node.

Even the selection of the same number of elements but refined, with nodes at the mid-edge helps to a better approximation (Fig. 3c). Increasing the number of elements (Fig. 3d) leads to a similar result, since there are five free to move nodes in the last two cases.

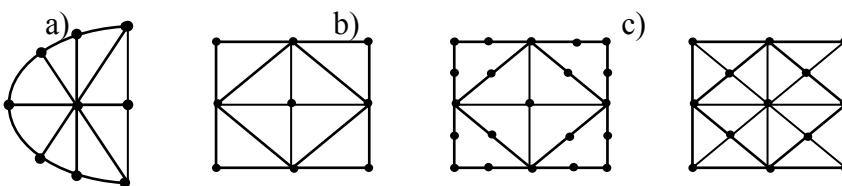


Fig. 3.

Coarse –mesh alternatives of modeling a plate clamped-on the boundary

The model should so include all structural parts, including those carrying little load or little stress. Most of commercial software may model curved boundary, but when this option is not available, the substituting polygon or polyhedron must preserve the actual volume of the structure. When the mesh is irregular, the recommended angles are from 45 to 135 (Fig. 4).

At least two layers of solid (brick) elements must be used, to include the effects from the median surface.

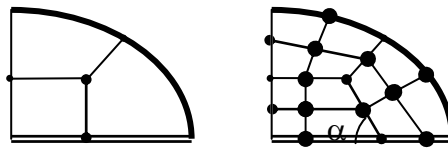


Fig. 4. Coarse and refined mesh for Finite Element Analysis of the semi-elliptical plate

Solid three-dimensional element [4] does not allow rotations, so that in this case the boundary conditions for simply supported and hinged edges are not accurately depicted. Additional elements like double hinged rigid rods may help to allow the edge rotation, if the software capabilities do not include thick plate elements. Do not forget considering the own weight, in all actual analyses.

3. Parametric studies

Parametric studies were performed in order to compare, for each type of previously presented plate, the numerical solution to other solutions and also to FEA results. Winkler classical case has been obtained, too, by setting $c_2=0$.

The clamped and hinged plates were quadratic, and the variable parameters were the ratio of Young moduli plate-subgrade, and the influence depth, H was also modified, for one case of analysis.

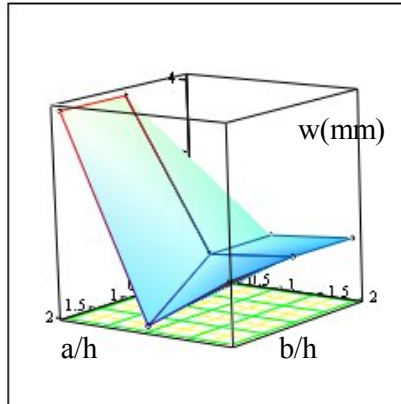
For elliptical plate, the ratio h/a and h/b was modified also, to state bounds of validity for the thick plate theory.

The results are presented in Table 1, and the next Section refers to them.

4. Conclusions

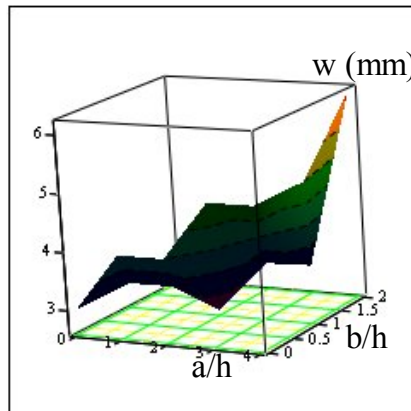
- **Influence of Ratio $E_{\text{plate}}/E_{\text{soil}}$:** It is obviously that the subgrade mechanical properties would influence the deflections, and then the reactive pressures, and the distribution of internal forces. This effect is more important for high ratios, for all analysed plates.
- **Influence of Aspect Ratio h/L_{max} :** Figure 5 shows that it is important to consider this ratio; otherwise, applying Kirchhoff theory instead of the thick plate theory would cause significant errors. As higher the aspect ratio, as flexible becomes the plate, so that further studies are required to state accurate bounds of using one or other theory (or one or other finite elements). The effect depends also on the general plate shape.
- **Influence Of Interaction Layer Depth, H :** The depth of the interaction layer has a little influence (1/10 mm) for almost all approximate solutions, including FEA.

- Winkler Model Versus Bi-modulus Model:** For all cases, Winkler model behaves much more elastically, but this feature is more obvious for $1 < n < 100$. The clay subgrade ($n=10^3$) is much more deformable than other cases. In this case, for rectangular plates the results were of the same order of magnitude, both for bi-modulus and for Winkler subgrade.



a)

M



b)

M2

Fig. 5

Plot of vertical deflection in terms of a/H and b/H ratios for an elliptical plate.

a) $a/h, b/h < 5$; b) $3 < a/h, b/h < 6$

- **FEA versus Polynomial Approximation:** Most of existing and available software considers the Kirchhoff plate behaviour [3], [4], or are cost-prohibitive (Lusas, Cosmos, Ansys, Elplae, etc). In this case, "brick" 8-node elements were chosen, but their weak point is related to the non-ability representing rotations. The FEA model is more rigid than those obtained using polynomial double series. Satisfactory and close results were obtained for small $E_{\text{plate}}/E_{\text{soil}}$ aspect ratios, especially for rectangular plates. A very coarse mesh has been used to model the semi-elliptical plate, where the results are of another order of magnitude. In this case, it is recommended to build up a SolidWorks or AutoCAD model and then use it for analysis.

References

1. Manole, O., *Plates on Elastic Foundation. Methods for Solving thick plates on Elastic Foundation* (in Romanian), PhD Thesis, Polytechnic Institute of Cluj Napoca, Romania, 1989.
2. Ungureanu, N., Vlad, I., Tibichi, V., *A Finite Element Approach for Beams Resting on Generalised Elastic Bed*, Proceedings of the 5th International Conference Finite and Boundary Elements, Oradea, Romania, May 2000
3. www.csiberkeley.com, *Safe Software User's Manual*
4. www.csiberkeley.com, *SAP 2000 Software User's Manual*
5. Chandrupatla, T, Belegundu, A, *Introduction to Finite Elements in Engineering*, Pearson Education Inc., 3rd Edition, 2002.

Table 1. A Synthesis of Parametric Studies

p=10 ⁷ N/m ² , Square plate, a=30 m, h=a/10		VERTICAL DEFLECTION (mm) AT THE PLATE CENTRE				
SIMPLE SUPPORTED PLATE						
n = E _{plate} /E _{soil}	10 ³	10 ²			10 ¹	10 ⁰
H (m)=12	H	H	2H	3H	H	H
Polynomial series, 1 term	142.412	65.887	63.683	61.6.23	38.019	11.857
Polynomial series, 2 terms	145.015	66.438	64.199	62.1.05	38.201	11.875
Winkler model, polynomial series 1 term	143.408	68.248			47.501	36.428
Winkler model, polynomial series 2 terms	146.048	68.843			47.708	36.596
FEA	65.45	65.22	60.797	60.522	47.8846	15.0136
CLAMPED PLATE						
Polynomial series 1 term	20.4128	17.546	17.201	16.87	13.683	5.2274
Winkler model, polynomial series 1 term	20.4572	17.906			16.22	14.824
SEMI ELLIPTICAL PLATE: a=12 m, B=9 m, h= 3m, H=12 m-MAXIMUM VERTICAL DEFLECTION						
Polynomial series 1 term	3.05627	3.15555	3.054985	2.96067	2.3228	0.68687
Winkler model, polynomial series 1 term	3.065358	3.26446			3.0653	2.599
FEA (coarse mesh)	10.703	10.391			8.099	3.093

THEORETICAL AND EXPERIMENTAL STUDIES OF A CLASS OF STEEL ROOF PROFILES

Mihai Budescu¹, Ioan P. Ciongradi¹, Octavian V. Roșca¹

Abstract

The main purpose of the tests is the checking of the stiffness characteristics of steel sheets at several load levels.

The tests were carried out in collaboration with INCERC, Iași Branch. The testing stand was built inside the Laboratory of the Structural Mechanics Department from the Faculty of Civil Engineering and Architecture, Technical University „Gh. Asachi” of Iași.

The testing of the elements was carried out according to EC3, chap.9, “Testing Procedure” because the elements are classified as cold-rolled thin-gauge profiles as stated in Romanian Norm NP 012-92 (EC 3 parts 1-3).

The testing procedure consisted of several repeated loading-unloading cycles. Finally, one specimen from each class was loaded until collapsed. The local buckling of the edge ribs caused the collapse of the profiles (in reality this is impossible because the steel sheets are coupled).

The ultimate deflections are limited according to several Norms between $L/100$ and $L/200$. The loading-unloading cycles pointed out the lack of permanent strains for maximum displacements below the $L/200$ limit. Out of this limit the permanent strains appear i.e. the rib folding in the support areas.

KEYWORDS: Thin-walled steel profiles, Local buckling, Quasi-static testing

¹ Structural Mechanics Department, TU “Gh. Asachi”, Iași, 700050, Romania

1. Introduction

The main purposes of the research (as stipulated in contract) are the study of the behavior under gravitational loads of the following types of NERGAL roof profiles: (a) 0.5mm, (b) 0.75mm and (c) 1.00mm. The strip of sheets is made of DX51DG steel according to the EN 10142 Euronorm and the EN 10027 parts 1 and 2. According to the EN 10142 this steel is denominated as 1.0226 and the ultimate strength is $R_m = 500 \text{ N/mm}^2$.

It was intended to establish the element behavior when are subjected to gravitational loads, according to EC3, chap.9, "Testing Procedure". This was because the elements are classified as cold-rolled thin-gauge profiles as stated in Romanian Norm NP 012-92 (EC 3 parts 1-3). Under these circumstances the elements behave different as the usual rolled profiles due to the fact that local buckling can occur, correlated with the profile shape and the sheet thickness.

The main purpose of the tests is the checking of the stiffness characteristics of the NERGAL steel sheets at several load levels.

2. The Testing Facilities

A special testing stand was designed in order to carry on the tests of the NERGAL steel sheets. The two KB600-5 profiles of the stand are assembled with four bolts, the span between the supports is 1500mm. The supporting elements of the displacement inductive transducers are attached to the KB profiles. In the figure No. 1 it is presented the testing stand built inside the Laboratory of the Structural Mechanics Department from the Faculty of Civil Engineering and Architecture, Technical University „Gh. Asachi” of Iaşi. The tests were carried out in collaboration with INCERC, Iaşi Branch.

The load transfer is performed according to the EC3 provisions, Chap.9, "Testing Procedure", by the means of an air mattress that assures the uniform load repartition and the keeping unaltered the stiffness characteristics of the specimen. The direct placement of the ballast on the steel sheet may alter the stiffness characteristics by friction and vault effect.

The displacements were measured in three points, at the midspan and the quarter of span in every space between the ribs. Inductive transducers were used to measure the transverse deflections; their positions are presented in Fig No. 2.

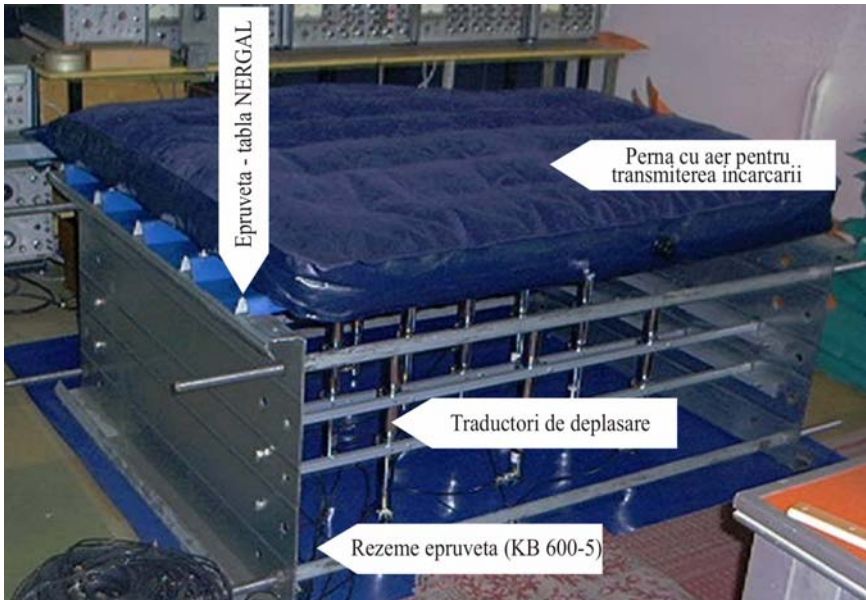


Fig. 1 View of the testing stand



Fig.2. The testing stand with the inductive transducers

The displacements were recorded by the means of inductive transducers in the format of analogical electric signal. The loading was performed by ballast with successive layers with 50N gravel filled sacks.

In the case of the 0.75 and 1mm NERGAL steel sheets the air mattress couldn't be used because the load capacity was lower then the loading level corresponding to collapse. In this case it was performed the direct ballasting with sacks only on the sheet ribs.

3. The Testing Procedure

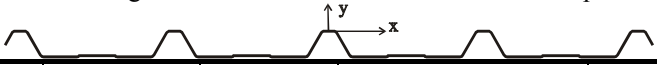
The testing procedure consisted of two steps:

- (i) The ballasting was performed in loading-unloading cycles for checking the stiffness characteristics;
- (ii) The ballasting was performed up to a level corresponding to the specimen's collapse by local buckling.

In the Table No. 1 there are presented the theoretical values of the geometrical characteristics and the tested sections, in order to be compared to the experimental stiffness characteristics of the NERGAL profiles.

The length of the specimen is 1600mm and the span between the supports (bolted connections were used) is 1500mm.

Table 1 The geometric characteristics of the NER GAL profiles



Pos. No.	Thickness (mm)	Area (cm ²)	Weight (kg/m ²)	Position of centroid		Moment of inertia (cm ⁴)
				X _G (cm)	Y _G (cm)	
0	1	2	3	4	5	6
1	0.40	4.327	3.397	-0.291	-0.146	0.126
2	0.45	4.868	3.821	-0.291	-0.148	0.142
3	0.50	5.409	4.246	-0.291	-0.151	0.158
4	0.60	6.491	5.095	-0.291	-0.156	0.191
5	0.75	8.114	6.369	-0.291	-0.163	0.240
6	1.00	10.818	8.492	-0.291	-0.176	0.324
7	1.25	13.523	10.616	-0.291	-0.188	0.411

4. The 0.5mm Profile Test

The tests for all three specimens were carried out in increasing loading-unloading cycles. The maximum loading level for every cycle was of 100, 150 and 200 daN/mp.

The force-displacement relationship for all the three specimens is sinuous, the steel sheet acting relatively unstable. For example, in the Figure No. 3 there is presented the average displacement of the T1, T4, T7 and T10 transducers, mounted at the midspan of the E2-0.50 specimen.

The displacements measured at midspan are greater in average by 30% up to 40% than the computed values. These increases are explained by the sheet deformation in the support areas. Because of that, the stiffness characteristic is determined by taking into account the relative displacement at the middle and quarter of span.

By analyzing the results one notice the fact that stiffness differs as a function of the loading level, i.e. it decreases as the load increases. Thus, in the case of 100 daN/mp loading step the stiffness reduction is only 10.2% while in case of 200 daN/mp loading step the reduction reaches 22.75%. The explanation of this phenomenon is given by the sheet folding when subjected to load. Folding diminishes the rib height, thus the stiffness characteristic is significantly decreased (the moment of inertia).

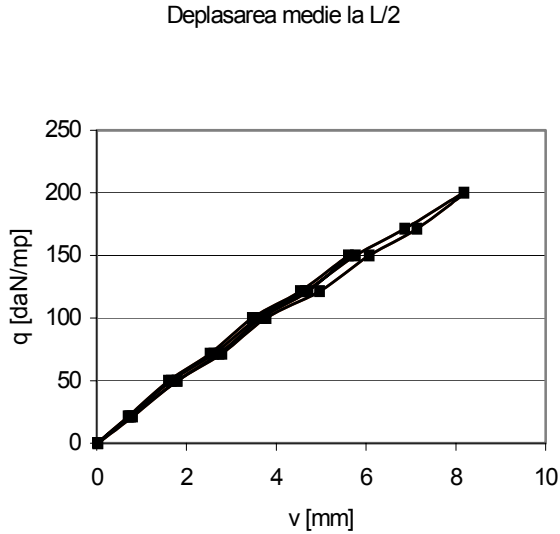


Fig. 3 The measured displacement at the midspan of the E2-05 specimen

The E3-050 specimen was loaded up to the occurrence of the local buckling phenomenon. The collapse occurred suddenly at a loading level of 270 daN/mp. The buckling was local and occurred simultaneously at the midspan of the two edge ribs. In the Figure No. 4 it is presented the collapse of the specimen.

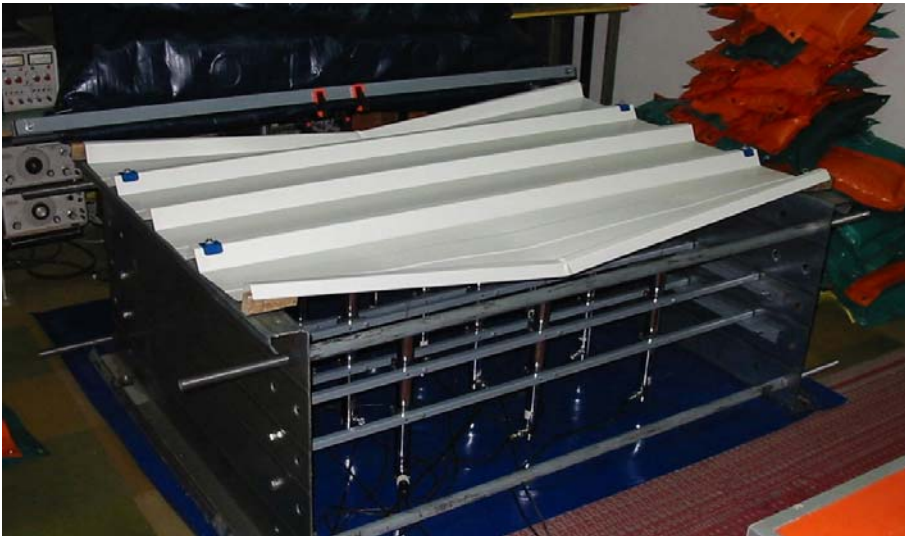


Fig. 4 The collapse of the E3-050 specimen (buckling)

4. The 0.75mm Profile Test

In the same way that in case of the NERGAL 0.5mm profile the tests for all three 0.75mm specimens were carried out in increasing loading-unloading cycles. The maximum loading level for every cycle was: 100, 150, 200, 250, 300, 350 and 400 daN/mp.

For all kinds of specimens the loading-unloading cycles were carried out in order to obtain the residual strains. The results prove that no residual strains occur at low levels of loads, the residual effects being nothing else but re-arrangements in the support areas (these elements are very sensitive). At high levels of loading the residual effects may be caused by the change of the profile cross-section.

In the Figure No. 5 there is presented the load-average displacement relationship (transducers T1, T4, T7 and T10, mounted at the midspan) during a loading-unloading cycle up to 100 daN/mp. One can notice a linear shape of this variation, straighter than in case of 0.5mm profiles. Some non-linearities are caused by the different stiffness of the edge ribs.

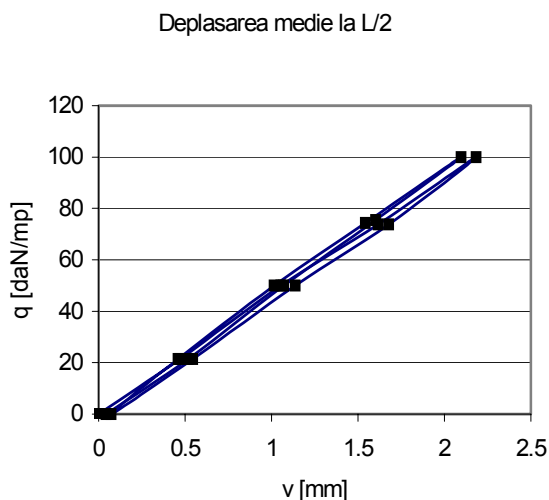


Fig. 5 The behavior of E1-075 specimen during two consecutive cycles

After reloading of the specimen for next cycle one notice a path almost identical to the last curve, thus meaning the residual deflections were consumed after the first loading cycle.

By analyzing the stiffness characteristics on the basis of the recorded deflections at midspans there are noticed differences up to 20-30% when compared to the theoretical values. Under these circumstances it is noticed a better behavior of the 0.75mm NERGAL sheet than the 0.5mm profile. Even though, the stiffness characteristics were also obtained from relative deflections, to avoid distortions.

In the same way like 0.5mm NER GAL sheet, the 0.75mm profile provides a stiffness depending on the loading step. In the Figure No. 6 it is presented this correspondence after processing the results from the three specimens.

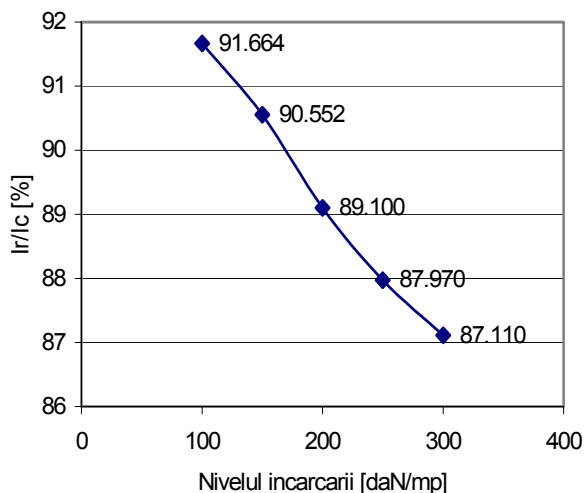


Fig. 6 The variation of stiffness characteristic vs. load level (0.75mm steel sheet)

Thus, at the 100daN/mp loading step, the stiffness decay is only of 8.336%, at the 200daN/mp loading step it attains 10.900% and when the 300daN/mp step is applied, the reduction is of 12.890%.

The folding effect that leads to the reduction of the moment of inertia is less significant that in case of 0.50mm steel sheet. Moreover, during a significant increase of the load it is not observed an important stiffness decrease, as it was expected, thus the shape of the graph from Fig. No. 6 is approximately linear.

In the end the E3-075 specimen was ballasted in order to obtain the ultimate load. Thus it was attained a 500daN/mp load, when the first signals of damage occurred, i.e. noises that forecast the stability loss. In order to avoid the damage of the equipment, the experiment was interrupted because the specimen loading was very large.

The maximum average displacement recorded at this loading level was of 11.391mm. The load applied directly changes dramatically the specimen behavior, i.e. the loading-unloading relationship. Thus, in the Figure No. 7 it is presented the situation of the last two loading steps of the E3-075 specimen, first with air mattress, and the second without. In the first loading step without air bed one notice a stiffness increase, after that the slope becomes similar to the situation when the load is transmitted though the airbed.

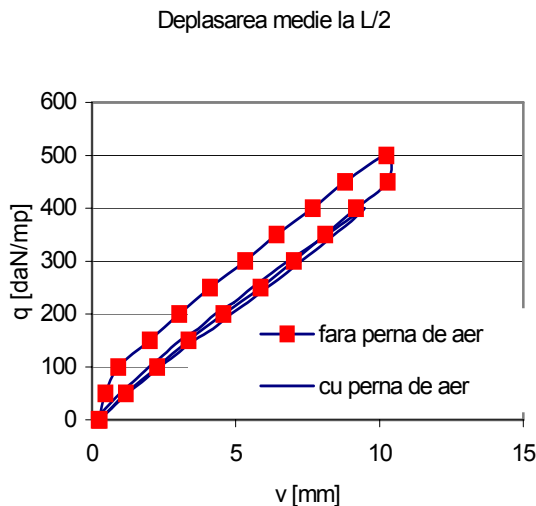


Fig. 7 The behavior of the E3-075 specimen (with / without airbed)

5. The 1.0 Mm Profile Test

The tests of the 1.0mm NERGAL profile were carried out in the same way like the previous two profiles, i.e. the loading and measurements. The behavior of these specimens looks more stable than those of the 0.5 and 0.75.

The shape of the $F-\delta$ relationship is almost linear, the sinuosity is due to the averaging, the measured stiffness characteristic is computed from the relative deflections at $L/2$ and $L/4$ and for the first two cycles it represents 95.186% from the theoretical value.

In the case of the 1mm NERGAL profile the folding effect that leads to the reduction of the moment of inertia is less significant than in the other cases, see Fig. No. 8.

Finally, the E3-1 specimen was ballasted in order to find out the ultimate load. The first signs of collapse were similar to those of the 0.75mm sheet, i.e. specific noises. The maximum loading level was of 700daN/mp, which corresponds to a maximum mean deflection at the midspan of 11.049mm.

In the case of this test it was noticed the lack of the stiffness difference caused by the direct placement of the load, thus meaning that for bigger thickness the stiffness increase due to the loading fashion (independent poliplan sacks) is insignificant.

The Fig. No. 9 presents the force-deflection relationship in case of the E3-1 specimen at the last test with the airbed and with direct placement of load over the sheet.

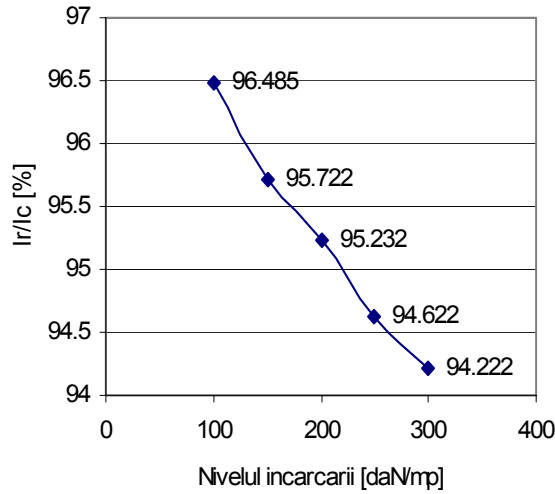


Fig. 8 The stiffness characteristic-load level relationship (1mm thickness sheet)

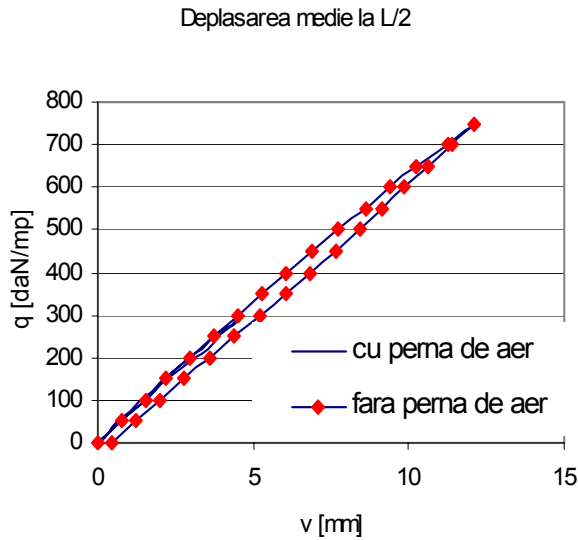


Fig. 9 The behavior of the E3-1 specimen (with / without airbed)

6. Conclusions

This paperwork deals with the results of the experimental analysis of the 0.50, 0.75 and 1.00mm NERGAL profiles when subjected to gravitational loads. The purpose of the tests was the checking of stiffness characteristics for the NERGAL sheets at several loading steps.

The NERGal profile is made of DX51DG steel sheet according to the EN 10142 and EN 10027 parts 1 and 2 (Euronorms), the steel is denominated as 1.0226 according to EN10142; the ultimate strength is $R_m = 500 \text{ N/mm}^2$.

The testing of the elements was carried out according to EC3, chap.9, “Testing Procedure” because the elements are classified as cold-rolled thin-gauge profiles as stated in Romanian Norm NP 012-92 (EC 3 parts 1-3). The tests were performed on a special stand. The loading was performed by ballasting with 50N sacks, distributed over an air mattress that provides the uniform load distribution and doesn't affect the stiffness characteristics of the specimen.

The deflections were measured at every three points at midspan and quarter span, on every space between the ribs, thus using 12 measurement points.

The testing procedure consisted of several repeated loading-unloading cycles. Finally, one specimen from each class was loaded until collapsed.

The loading-unloading cycles pointed out the lack of permanent strains for maximum displacements below the $L/200$ limit. Out of this limit the permanent strains appear i.e. the rib folding in the support areas.

The local buckling of the edge ribs caused the collapse of the NERGal profiles (in reality this is impossible because the steel sheets are coupled). As a consequence, the assembly technique of the steel sheet edges becomes very important.

The stiffness reduction of the NERGal tested profiles in case of a limited displacement ($L/200$):

- For the 0.50mm profiles it reaches about 20%;
- For the 0.75mm profiles it reaches about 10%;
- For the 1.00mm profiles it reaches about 5%.

One may notice that the ultimate deflections are limited according to several Norms between $L/100$ and $L/200$.

References

1. Budescu, M., and all. *Incercari experimentale – Panouri de tabla tip NERGal*, Contract: K2603/2003.
2. Wei-Wen Yu *Cold-formed steel design*, 3rd Ed., Wiley & Sons, Inc., NY, 2000.
3. American Iron and Steel Institute, *Cold-formed steel design manual*, 50th Commemorative Issue, 1996.
4. American Iron and Steel Institute, *Load and Resistance Factor Design Specification for Cold-formed steel Structural Members*, 1991.
5. European Committee for Standardisation, *Eurocode 3: Design of Steel Structures*, ENV 1993.
6. STAS 10108/2-83, *Romanian Specification for Calculation of Thin-Walled Cold-Formed Steel Members*.
7. CEN/TC250 – *EUROCODE 1: Basis of design and actions on structures*, ENV1991-1.
8. NP 012-1997, *Normativ pentru calculul elementelor din oțel cu pereți subțiri formate la rece*.
9. STAS 10101-0A/77, *Acțiuni în construcții*.
10. STAS 10108/0-78, *Calculul elementelor din oțel*.

METODOLOGIA DE INVESTIGARE ANALITICO- EXPERIMENTALĂ ȘI DE IDENTIFICARE ÎN CONCEPT DINAMIC A TABLIERELOR DE PODURI.

STUDII DE CAZ

Cristian Claudiu COMISU¹, Constantin IONESCU²

Abstract

Primul obiectiv în administrarea optimizată a podurilor, ca un factor strategic al procesului de reabilitare și dezvoltare a infrastructurii rutiere, îl constituie elaborarea unor metode moderne de investigare și diagnosticare a stării tehnice a podurilor aflate în exploatare. Datorită avantajelor tehnico-economice pe care le asigură, tablierele cu structură compusă (mixtă) reprezintă o soluție constructiv modernă care, în ultimii ani, atât în țară cât și în străinătate, cunoaște o aplicabilitate din ce în ce mai mare.

Metodologia este caracterizată de exploatarea interactivă a două procedurii de analiză. În procedura de analiză analitică, sunt calculate caracteristicile dinamice ale modelului de calcul construit prin discretizarea în elemente finite a suprastructurii mixte reale. În procedura de analiză experimentală sunt identificate prin investigații in situ, caracteristicile dinamice ale tablierului mixt. Compararea caracteristicilor dinamice determinate experimental, pentru sistemului real, cu cele calculate în procedura analitică, utilizând tehnica de simulare cu ajutorul calculatorului electronic, asigură validarea modelului de calcul și implicit identificarea dinamică a suprastructurii mixte reale. Exploatarea interactivă a celor două proceduri oferă avantajul cunoașterii prealabile a caracteristicilor dinamice ce trebuie determinate experimental, asigurându-se astfel posibilitatea de identificare și izolare a tuturor modurilor proprii de vibrație, chiar și a celor foarte apropiate.

Această metodologie se aplică cu ocazia determinării stărilor tehnice la recepția podurilor noi, periodic - la un interval de 5 ani, la podurile aflate în exploatare și în mod obligatoriu după evenimente deosebite (seisme, inundații, accidente prin lovirea elementelor constructive, convoaie excepționale, etc.), sau în cazul apariției unor procese de degradare suplimentare față de cele constatate la ultima clasificare a stării tehnice, care sunt semnalate cu ocazia reviziilor curente.

Aplicarea metodologiei de identificare dinamică a stărilor tehnice, are drept scop stabilirea tipului de proces de degradare, debutul și consecințele produse de manifestarea lui asupra comportării în exploatare a tablierului mixt.

¹ Conf., Facultatea de Construcții Iași, e-mail: comisucc@ce.tuiasi.ro

² Prof., Facultatea de Construcții Iași, e-mail: cionescu@ce.tuiasi.ro

1. Introducere

Primul obiectiv în administrarea optimizată a podurilor, ca un factor strategic al procesului de reabilitare și dezvoltare a infrastructurii rutiere, îl constituie elaborarea unor metode moderne de investigare și diagnosticare a stării tehnice a podurilor aflate în exploatare. De altfel, la al XXII-lea Congres al Asociației Mondiale a Drumurilor, care a avut loc în anul 2004 la Durban, Republica Sud Africană, strategia cercetării în domeniul podurilor prevede ameliorarea tehnicilor de investigare și de diagnosticare, în scopul stabilirii cu mai mare precizie a unei relații între modul de degradare și reducerea funcționalității structurale.

Datorită avantajelor tehnico-economice pe care le asigură, tablierele cu structură compusă (mixtă) reprezintă o soluție constructiv modernă care, în ultimii ani, atât în țară cât și în străinătate, cunoaște o aplicabilitate din ce în ce mai mare.

Metodologia de investigare analitico-experimentală a tablierelor de poduri cu structură compusă oțel-beton este caracterizată de exploatarea interactivă a două procedurii de analiză: analitică și experimentală.

2. Tabliere fără degradări

Pentru *suprastructura mixtă fără degradări, având schema statică de grindă simplă rezemată și deschiderea de 50,00 m*, au fost determinate, în cadrul procedurii de investigare analitică, caracteristicile dinamice pentru primele 30 de moduri proprii de vibrație. În scopul identificării dinamice a stării tehnice a tablierului mixt, cu ocazia recepției preliminare, dintre modurile proprii care pot caracteriza comportarea dinamică a structurii, în cadrul procedurii de investigare analitică, a fost selectat modul propriu fundamental de vibrație (fig. 1).

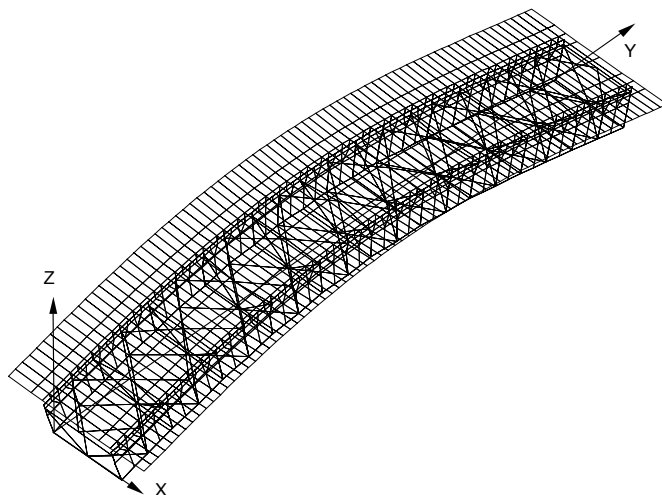


Fig. 1. Modul propriu 1. Tablier compus oțel-beton fără degradări

Criteriul de selecție constă în alegerea unei forme simple de vibrație, caracteristică modului propriu 1 (încovoiere în plan vertical), care are drept consecință adoptarea unei scheme de excitație într-un singur punct, cu un singur vibrator, dispus în secțiunea centrală a tablierului. Principalul parametru ce va fi extras din această diagramă este frecvența proprie fundamentală, care este identificată pe baza criteriului amplitudinii maxime (fig. 2).

Pentru diferite valori ale intensității forței de excitație (se recomandă mai întâi, o tatonare grosieră - din 100 în 100 daN, până la încadrarea valorii de referință a deplasării modale în punctul 347, urmată de o variație mai fină - de ordinul zecilor de daN), se obține valoarea de $F_0 = 218$ daN, care produce o deplasare $\delta_{347} = 0,04676$ cm, care coincide cu deplasarea în același punct caracteristic pentru modul propriu fundamental.

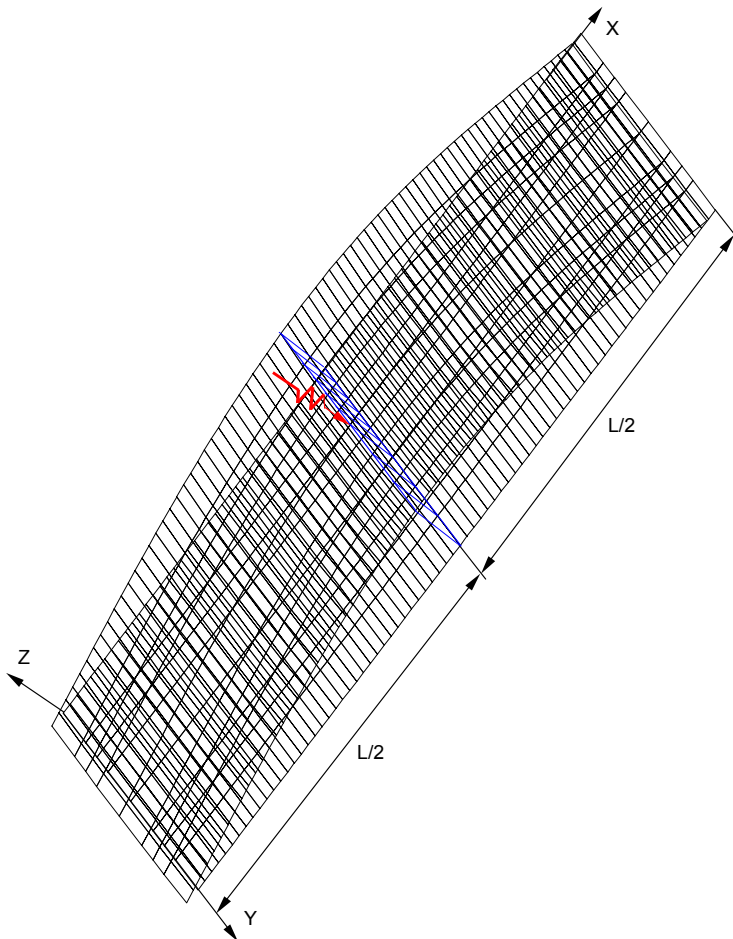


Fig. 2. Modul propriu fundamental pentru tablierul mixt fără degradări. Deplasări modale de referință ale platelajului de beton.

Procedura de investigare analitică este oprită atunci când:

- în *diagrama defazajelor*, calculată pentru modul propriu fundamental, defazajul între forță și deplasare prezintă valoarea caracteristică $\varphi_c = 90^{\circ}$, ceea ce indică prezența rezonanței de fază;

- în *diagrama amplitudinii totale a răspunsului* (figura 3), calculată pentru modul propriu prestabilit de vibrație (modul propriu fundamental) și în punctul caracteristic (punctul 347 din secțiunea centrală a tablierului), între valoarea de amplitudine a deplasării modale induse prin excitație și cea calculată, se înregistrează o diferență minimă.

Diagrama defazajelor indică faptul că primele moduri proprii de vibrație ale tablierului mixt fără degradări prezintă pulsații proprii relativ depărtate. Prin identificarea pulsației fundamentale, ca abscisă a punctului de inflexiune a diagramei defazajului, conform *metodei răspunsului în cvadratură*, se consideră că în vecinătatea rezonanței vibrația are loc exclusiv în modul de vibrație rezonat, iar componenta “în fază” a răspunsului este nulă. În acest caz, revenind în diagrama amplitudinii totale, porțiunile corespunzătoare ale diagramei se asimilează cu curba de răspuns a unui sistem dinamic cu un singur grad de libertate, ceea ce permite identificarea parametrilor modali.

3. Studiu de caz - Diagnosticarea tablierelor mixte având aparatele de reazem degradate

În etapa I-a de aplicare a metodologiei, în cadrul unei proceduri de investigare analitică, utilizând tehnica de simulare cu ajutorul calculatorului electronic, a fost selectat modul propriu care va fi identificat in situ, în cadrul unei proceduri de investigare experimentală, prin identificarea caracteristicile dinamice ale tablierului mixt fără degradări.

Exploatarea interactivă a procedurilor de investigare analitică și experimentală, utilizând bucle feed-back de evaluare și corecție, permite validare modelului analitic utilizat în analiză și implicit a caracteristicilor dinamice calculate pentru tablierul mixt fără degradări. Dintre primele 30 de moduri proprii de vibrație calculate în studiul de caz pentru tablierul mixt fără degradări, sunt selectate acele moduri de vibrație care prin caracteristicile lor dinamice bine individualizate - atât la nivelul valorilor cât și a vectorilor proprii - pot fi identificate și izolate in situ, printr-o procedură experimentală cât mai simplă și precisă.

În faza a II-a de aplicare a metodologiei, în cadrul unei proceduri de investigare analitică, utilizând tehnica de simulare cu ajutorul calculatorului electronic, sunt stabilite scheme de excitare și poziționare a vibratoarelor pe tablierul mixt fără degradări, care să permită izolare modurilor proprii de vibrație preselectate în faza I-a de aplicare a metodologiei.

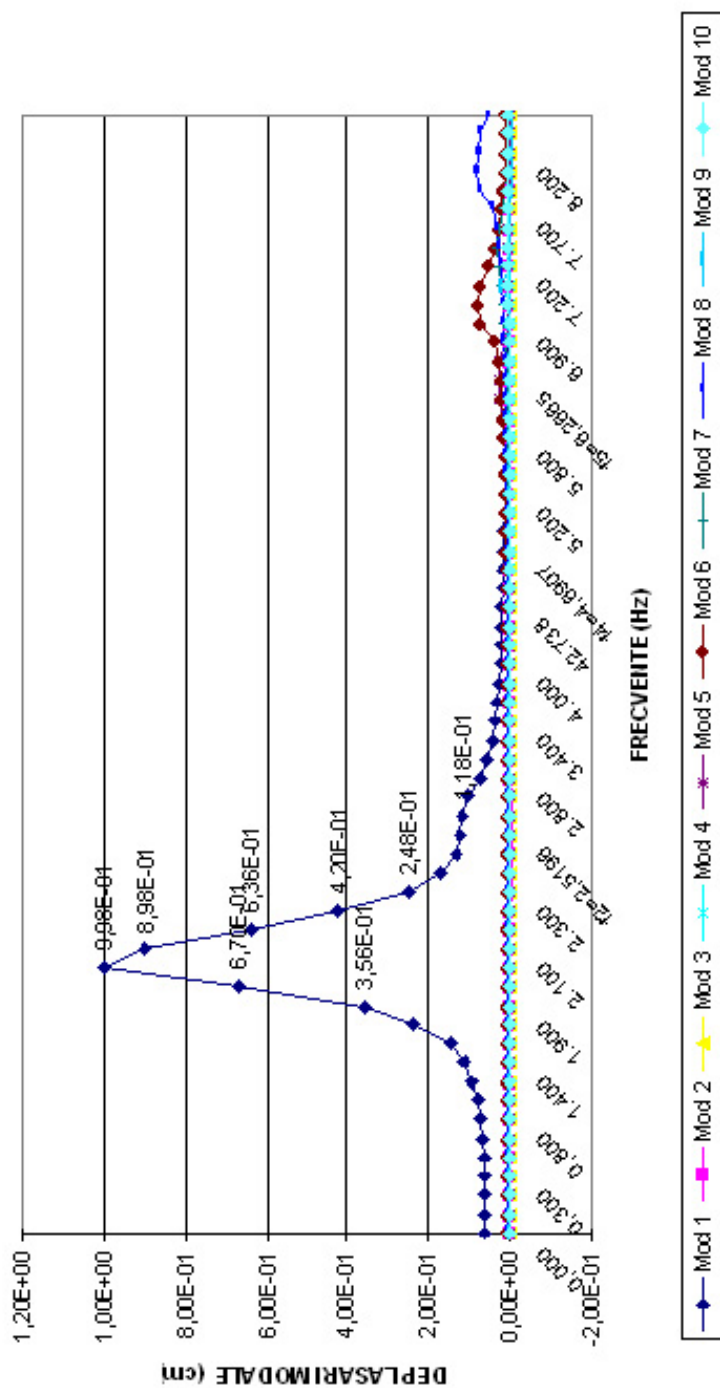


Fig.3. Diagrama amplitudine - frecvență calculată pentru modul fundamental de vibrație

Validarea schemelor de excitare se realizează în cadrul unei proceduri de investigare experimentală, în care, la o valoare proprie prestabilită, se obține o “coincidență” între starea de deplasări modale calculată și cea determinată experimental, prin măsurători efectuate in situ. Începând cu darea în exploatare a tablierului mixt, această schemă de excitare se aplică cu ocazia fiecărei etape în care se stabilește starea tehnică a podului.

Procesul de exploatare a tablierului mixt conduce la manifestarea pe structură a unor procese specifice de degradare. Momentul în care procesul începe să se manifeste este marcat prin determinarea in situ a unei stări de deplasări modale diferite de cea prestabilită prin aplicarea schemei de excitare validate. Tipul procesului de degradare care se manifestă pe structura mixtă se stabilește experimental, prin aplicarea pe structura investigată a unor scheme de investigare prestabilite analitic, utilizând tehnica de simulare pe calculator, pentru fiecare proces de degradare specific tablierelor mixte. Schemele de excitare trebuie să permită identificarea și izolarea modurilor proprii (la nivelul valorilor și vectorilor proprii) preselectate, prin aplicarea unei proceduri de investigare analitică, pentru fiecare din cele patru tipuri de degradare analizate. Unul dintre procesele de degradare posibile a se manifesta pe structura mixtă, care poate conduce la modificarea caracteristicilor dinamice ale tablierului, constă în degradarea aparatelor de reazem din neopren fretat.

Aplicarea metodologiei de diagnosticare în concept dinamic a tablierului mixt având aparate de reazem degradate se va concentra asupra modului propriu prestabilit în procedura de investigare analitică - modul propriu 14 de vibrație. Procedura de diagnosticare constă în aplicare unei scheme de excitare prestabilite a tablierului mixt având aparatele de reazem degradate, care să permită identificare și izolarea modului propriu 14 de vibrație, pentru care, caracteristicile dinamice - frecvența proprie $f_{14} = 11,04$ Hz și deplasarea modală maxim negativă $\delta_{14} = -2,00$ cm - au fost stabilite în cadrul unei proceduri de investigare analitică. Disponerea excitatoarelor sinusoidale la nivelul panoului de contravântuire orizontală superioară presupune dificultăți tehnologice de realizare, iar rigiditatea redusă a acestora în raport cu rigiditatea întregii suprastructuri mixte nu permite excitarea la rezonanță a tablierului mixt. Cea mai simplă schemă de excitare constă în dispunerea unui singur excitator în secțiunea centrală (punct 338) a tablierului mixt având aparatele de reazem degradate.

Alcătuirea schemei de excitare (poziția vibratorului pe structură, valoarea de amplitudine și defazajul forței de excitare) se stabilește pe baza metodelor de identificare folosind excitația armonică într-un punct. Conform metodologiei propuse, scopul pentru care se determină analitic această schemă de excitare este de a permite diagnosticarea în concept dinamic a stării tehnice a tablierului mixt având aparatele de reazem degradate.

Experimental, tablîerul mixt este solicitat de o forță armonică $f_{338} = \hat{f}_{338} \cdot e^{i\omega_{14}t}$ aplicată în punctul caracteristic 338 (corespunzător coordonatei generalizate q_{338}) și se măsoară răspunsul atât în punctul în care se aplică excitația $q_{338} = \tilde{q}_{338} \cdot e^{i\omega_{14}t}$ cât și în toate punctele caracteristice de pe structură $q_j = \tilde{q}_j \cdot e^{i\omega_{14}t}$ astfel încât să se poată trasa deformată dinamică modală.

În acest studiu de caz, răspunsul structurii este reprezentat grafic, în următoarele două forme:

a) ca diagrame amplitudine - pulsație ($q_{338} - \omega_{14}$, respectiv $q_j - \omega_{14}$) și fază - pulsație ($\phi_{338}^{14} - \omega_{14}$, respectiv $\phi_j^{14} - \omega_{14}$);

b) ca diagrame de variație cu pulsația a componentei în fază cu forța ($q_{338,R} - \omega_{14}$) și a componentei răspunsului în cvadratură cu forța ($q_{338,I} - \omega_{14}$).

Atunci când tablîerul mixt investigat in situ (considerat în analiză ca un sistem dinamic disipativ), este excitat la frecvența prestabilită f_{14} a modului propriu 14 de vibrație, modul real forțat de vibrație (modul de distorsiune) va lua forma modului propriu de vibrație a sistemului dinamic conservativ asociat, $\{\Phi^{(14)}\} = \{\Psi^{(14)}\}$. În cazul acestui tip particular de excitație, deplasările tuturor nodurilor structurii sunt în fază una față de alta și defazate cu același unghi caracteristic ($\phi_{338}^{14} = 90^\circ$) în raport cu forțele de excitație. Pentru ca, prin aplicarea schemei de excitație care utilizează un singur vibrator (excitația armonică aplicată într-un singur punct), să se obțină in situ, aceeași valoare de amplitudine a deplasărilor modale în raport cu cea de referință ($\delta_{338}^{14} = -0,01035\text{cm}$), se pune problema determinării valorii de amplitudine a forței de excitație.

Procedura de investigare analitică, utilizând tehnica de simulare cu ajutorul calculatorului electronic și un soft specializat pentru analize în frecvență, permite ca prin cicluri iterative (bucle feed-back de evaluare și corecție), să se identifice valoarea exactă a amplitudinii forței de excitație.

Procedura de investigare analitică parcurge următoarele etape:

1. Se efectuează mai întâi, o variație grosieră a amplitudinii forței de excitație (din 1000 în 1000 daN) până la încadrarea valorii de referință;
2. Se realizează o variație din ce în ce mai fină a amplitudinii forței de excitație - din 100 în 100 daN, urmată de o variație a amplitudinii de ordinul zecilor de daN, care trebuie să încadreze valoarea de referință;
3. Procedura de investigare analitică pentru determinarea amplitudinii forței de excitație, se oprește atunci când valoarea de amplitudine a deplasării modale calculată în punctul caracteristic 338, se apropie, la o diferență mai mică de 10%, de valoarea de referință.

În studiul de caz efectuat, în 4 cicluri iterative, procedura de investigare analitică a permis calcularea unei valori de amplitudine a forței de excitație $F_{0,338} = 1180$ daN, care determină o deplasare în punctul 338.

Dacă se compară valorile în cvadratură (defazate cu 90^0) ale deplasărilor modale calculate în punctul 338 ($\delta_{14}^a = -0,01030$ cm), cu valorile de referință ($\delta_{14}^r = -0,01035$ cm), remarcăm o diferență foarte mică (de ordinul 0,00005 cm).

Pentru o schemă de excitație în care sunt utilizate numai un singur vibrator sinusoidal, această “coincidență” între deplasarea modală calculată și cea de referință, în punctele caracteristice secțiunii centrale a tablierului mixt, se consideră ca fiind foarte bună (mai mică decât marja de eroare de 10%).

În acest studiu de caz, efectuarea unui baleiaj de frecvență a permis identificarea primelor 30 de moduri proprii studiate, prin calcularea diagramei defazajelor și a diagramei amplitudine-frecvență. Atunci când, în timpul baleiajului de frecvență, pulsația excitatoare se apropie de valoarea proprie prestabilită

$$\omega_{14} = \sqrt{\frac{k_{14}}{m_{14}}} = 69,37 \frac{rad}{sec}$$

contribuția modului propriu 14 de vibrație, la răspunsul total al structurii mixte, devine predominantă, iar variația acestui parametru cu pulsația, ar trebui în vecinătatea rezonanței, ca în mod teoretic, să corespundă comportării a unui sistem dinamic echivalent, cu un singur grad de libertate, având parametrii dinamici m_{14} , k_{14} și c_{14} .

Din procedura de investigare analitică aplicată pentru modul propriu 14 de vibrație, se remarcă faptul că, pentru frecvența proprie $f_{14} = 11,04$ Hz, defazajul caracteristic este $\varphi_{338}^{14} = 89,20^0$, ceea ce indică contribuția la răspunsul total al structurii mixte a modurilor proprii apropiate și nerezonate (fig. 4).

Efectuarea baleiajului de frecvență permite evidențierea contribuțiilor modurilor proprii apropiate și nerezonate, atât la nivelul defazajului, cât și a amplitudinilor deplasărilor modale, calculate în ipoteza de excitație caracteristica modului propriu 14 de vibrație.

Necesitatea eliminării acestor contribuții care parazitează răspunsul total al structurii mixte excitate în modul forțat de vibrație 14, introduse de modurile apropiate și nerezonate, a impus aprofundarea studiului de caz.

A fost efectuată o analiză în frecvență, pentru aceeași schemă de excitație (un singur vibrator montat în secțiunea centrală a tablierului mixt - punct 338), pentru care s-a calculat diagrama de variație cu pulsația a componentei răspunsului în fază, a componentei răspunsului în cvadratură cu forța și a răspunsul total (fig. 5).

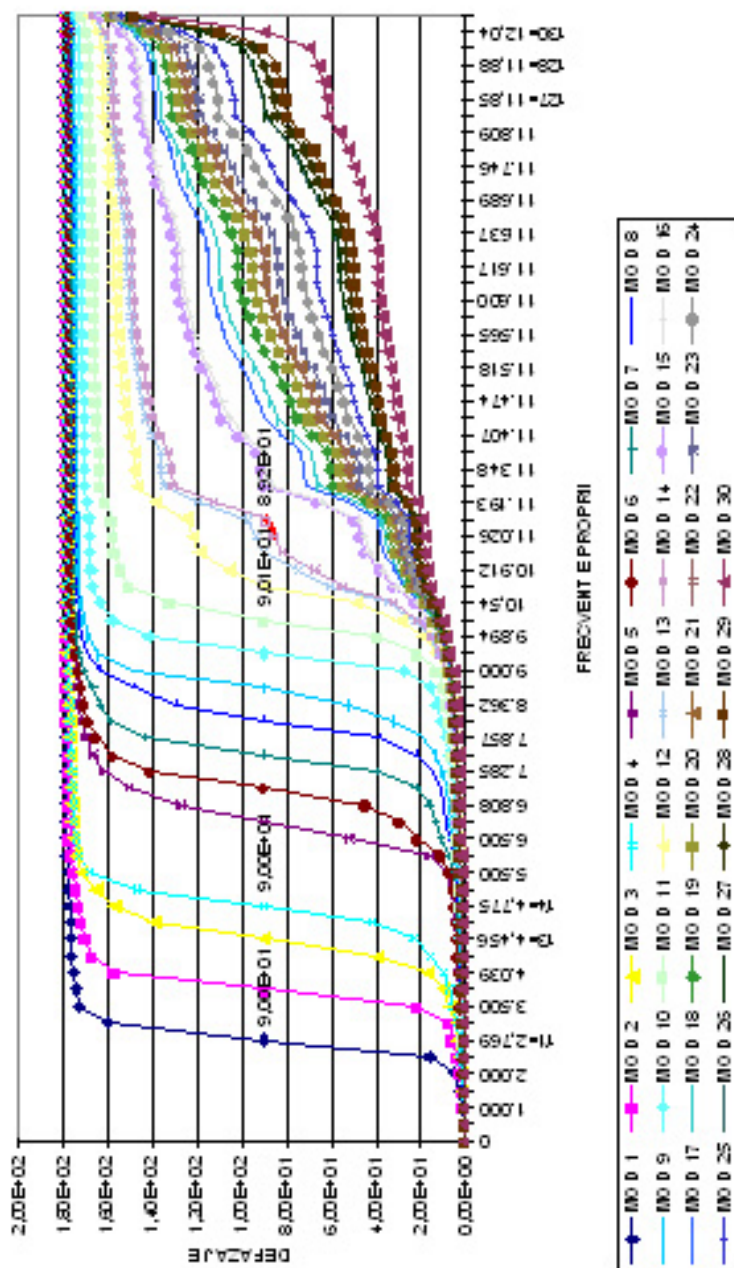


Fig. 4. Diagrama defazajelor calculată pentru primele 30 de moduri proprii stud

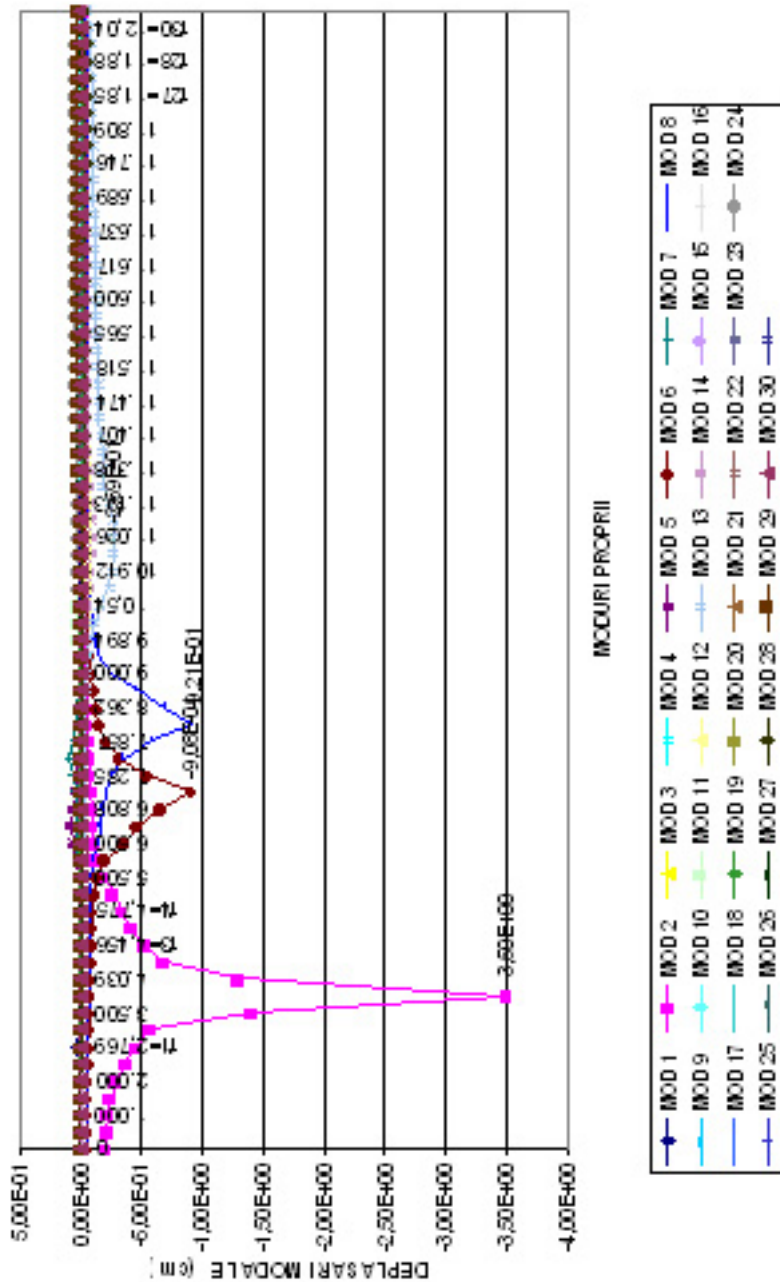


Fig. 5. Diagrama amplitudine - frecvență calculată pentru primele 30 de moduri proprii studiate

4. Concluzii

Metodologia actuală, aplicată conform “Instrucțiuni pentru clasificarea stării tehnice a unui pod”, prevede stabilirea stării tehnice ca un proces de analiză având drept scop, ca pe baza unui indice global de calitate al stării tehnice, stabilirea unui ansamblu de lucrări, începând de la cele de reparații curente sau capitale și ajungând până la lucrări de înlocuire sau consolidare a unor elemente sau chiar a structurii în ansamblului său.

În cazul tablierelor de poduri cu structură compusă, datorită alcătuirii constructive specifice, aprecierea unui “*început de degradare cu defecte vizibile*”, care impune lucrări de reparații curente, sau “*prezența unei degradări vizibile pe zone întinse*”, care necesită lucrări de reparații capitale, constituie în acest caz un proces de decizie relativ și subiectiv, în măsura în care el nu este susținut de un mijloc corespunzător de investigare și diagnosticare.

Metodologia de investigare analitico-experimentală și de diagnosticare în concept dinamic propusă în cadrul acestei teze, are drept scop principal, ca prin studiul caracteristicilor dinamice, să definească parametrii obiectivi necesari identificării stării tehnice a tablierelor de poduri cu structură compusă. Această metodologie completează metodologia actuală de stabilire a stării tehnice a podurilor, conferindu-i un caracter obiectiv și precis de aplicare.

În cazul podurilor noi, aplicarea metodologiei are drept scop stabilirea momentului în care pe tablierul compus se manifestă un proces de degradare acestor tipuri de structuri. Atât pentru tablierele mixte fără degradări (aflate în faza de recepție), cât și pentru cele afectate de procesele de degradare specifice, construirea modelelor analitice de calcul, în cadrul unei proceduri de investigare analitică, se realizează pe baza datelor primare, cuprinse în procesele verbale de recepție pe faze, din cartea tehnică a construcției, cu ocazia recepției preliminare. Pentru podurile noi, precizia de aplicare a procedurii de identificare a stării tehnice a suprastructurii mixte este maximă, pentru că procedura experimentală, de comparație a răspunsurilor și de validare a modelului matematic, se realizează prin raportare la o structură a cărei stare tehnică a putut fi stabilită și înregistrată în baza de date, încă de la darea ei în exploatare.

În cazul podurilor aflate în exploatare, aplicarea metodologiei de investigare analitico-experimentală și de diagnosticare în concept dinamic parcurge aceleași etape, cu deosebirea că procedura de comparație se realizează pentru un caz de bază a cărui stare tehnică este stabilită corespunzător fazei respective de exploatare a tablierului mixt. În acest caz, precizia de aplicare a metodologiei de identificare a stării tehnice este direct proporțională cu precizia cu care este stabilită starea tehnică a suprastructurii mixte din momentul inițierii procedurii de investigație analitico-experimentală.

Cunoașterea prealabilă, din procedura analitică, a caracteristicilor dinamice ale modului propriu ce urmează a fi excitat in situ, permite reducerea duratei de aplicare a procedurii de analiză experimentală, prin eliminarea procesului de baleiere manuală a domeniului de frecvențe, până la realizarea fenomenului de rezonanță (atingerea vârfului de amplitudine).

Cunoașterea prealabilă a schemelor de excitare, a căror distribuții de forțe este optimizată prin aplicarea tehnicii de simulare cu ajutorul calculatorului electronic în cadrul procedurii de analiză analitică, permite simplificarea procedurii experimentale, asigură izolarea precisă a modului propriu analizat și permite diagnosticarea în concept dinamic (analiza efectuându-se la nivelul caracteristicilor dinamice) a tablierului mixt. În acest scop, exploatarea interactivă a procedurii de investigare analitico-experimentală a suprastructurilor mixte cu procedura de diagnosticare în concept dinamic a acestora, corelate prin bucle feed-back de corectare/reevaluare, permit stabilirea unei metodologii moderne de identificare a stării tehnice a tablierelor de poduri cu structură compusă, care să permită optimizarea stabilirii stării tehnice și implicit a întreținerii infrastructurii rutiere din țara noastră.

Diagnosticul diferențial realizat prin identificarea în timp real, dintre scenariile posibile, a procesului de degradare care se manifestă pe tablierul mixt, permite focalizarea analizei experimentale asupra subsistemului constructiv (placa de beton, conectori, structura metalică, aparate de reazem) cel mai afectat și adoptarea în consecință a soluțiilor specifice de remediere.

Aplicarea în procedura de analiză experimentală, a unei scheme prestabilite (din analiza analitică) de poziționare și funcționare a excitatoarelor sinusoidale sincrone pe tablierul mixt (numărul minim necesar, poziția lor, amplitudinea forțelor și defazajul dintre ele) permite:

a) Aplicarea procedurii de comparație a răspunsului structurii reale, obținut experimental pentru un sistem dinamic disipativ, cu răspunsul modelului matematic, determinat analitic pentru un sistem dinamic conservativ. Procedura de comparație, aplicată în aceste condiții, devine posibilă numai dacă vibratoarele excită structura sincron și echifazic (sau defazate cu 180°), caz în care deplasările tuturor punctelor sunt toate în fază una față de alta și defazate cu același unghi caracteristic față de forțe.

b) Aplicarea procedurii de analiză experimentală, folosind excitația armonică simultană în mai multe puncte caracteristice ale tablierului mixt, conform unei scheme prestabilite, asigură o precizie corespunzătoare de izolare (cu o marjă de eroare acceptată de maxim 10%) a unui modului propriu prestabilit în cadrul procedurii analitice.

Cunoașterea prealabilă a schemelor de poziționare și funcționare a excitatoarelor pe structura mixtă, permite dimensionarea optimă a lanțului de aparatură necesar

captării și prelucrării răspunsului. Această metodologie va permite utilizarea cu maximă eficiență a datelor obținute din identificarea stărilor tehnice ale acestor tipuri de poduri, contribuind astfel la realizarea și implementarea unui nou sistem de management al podurilor, obiectiv prioritar și de strictă actualitate în cadrul unui nou sistem decizional privind planificarea optimizată a lucrărilor de întreținere și reparații la poduri.

Programele de eficientizare a activităților operaționale și de modernizare a Administrației Naționale a Drumurilor fac parte din strategia globală de restructurare și dezvoltare a AND și au drept scop fundamental reabilitare și dezvoltare a infrastructurii rutiere, alături de realizarea și susținerea unei piețe deschise a lucrărilor de construcții prin promovarea inițiativei private și antreprenoriale în domeniu.

Bibliografie

1. Badoux, J.C., *L'évolution des ponts mixtes en Suisse ces vingt-cinq dernières années*, Annales de l'Institut Technique du Batiment et des Travaux Publics, nr. 431, Janvier 1985.
2. Clough, R. W., Penzien, J., *Dynamics of Structures*, Mc. Graw - Hill 1989.
3. Comisu, C.C., *Metode de calcul ale tablierelor compuse (mixte) pentru poduri deșosea*, Referat 1 la teza de doctorat 30.06.1991.
4. Comisu, C.C., *Studiul caracteristicilor dinamice ale structurilor liniare ale podurilor*, Referat 2 la teza de doctorat 30.01.1992.
5. Comisu, C.C., *Contribuții la studiul caracteristicilor dinamice ale tablierelor de poduri cu structură compusă (mixtă)*, Teza de doctorat, 1997.
6. Comisu, C.C., *Determinarea experimentală a caracteristicilor dinamice structurale ale podurilor. Valorificarea rezultatelor*, Referat 3 la teza de doctorat 30.06.1992.
7. Ionescu, C., *Analiza dinamică și seismică a podurilor*, U.T. "Gh. Asachi", 1996.
8. Ionescu, C., *Poduri. Caracteristici dinamice*, U.T. "Gh. Asachi", 1995.
9. Ionescu, C., *Asigurarea viabilității și fiabilității podurilor. Studii de caz*. U.T. "Gh. Asachi", 1996.

ANALYSIS OF A MULTILAYERED WALL TO FIRE ACTION BASED ON THERMAL INSULATION CRITERION

Dan Diaconu¹, Mihaela Ibanescu¹

Abstract

The paper presents the analysis of a multilayered wall by performing a numerical simulation, in order to check the results obtained by the producers during the experimental tests.

This analysis has in view the thermal insulation criterion that must be accomplished by a non-structural multilayered wall belonging to the fire compartment. The wall is subjected on one of its faces to a temperature change according to the standard curve presented in ISO 834, and on the opposite face, to a constant temperature that equals the environmental medium temperature, in normal conditions.

The numerical simulation of the phenomenon is performed by using the Finite Element Method (FEM), the non-stationary analysis of the conductive heat transfer being carried out with the help of step by step direct integration technique.

This procedure appeals to the performances of a computer program with special toolboxes for non-stationary analysis of conductive heat transfer.

1. Justification of Structural Element Analysis from Fire Safety Point of View

The design and execution of constructions and equipments must be performed so that, in case of a fire, the following requirements to be accomplished:

- protection and evacuation possibilities for the users, according to their age and physical condition;
- limitation of goods lost;
- avoiding the fire propagation;
- protection for firemen and other forces that contribute to persons rescue and evacuation, to goods protection, to fire limitation and extinction, to elimination of fire consequences.

In order to accomplish and maintain along the whole building or equipments life the quality requirement referring to fire safety, the following performances criteria must be satisfied:

¹ Technical University “Gh. Asachi” Iasi

- fire risk;
- fire resistance;
- avoiding fire propagation;
- behavior under fire action;
- stability under fire action;
- access, evacuation and intervention paths.

The fire resistance is the property of a structural element or structure to maintain along a certain period of time its stability, tightness and/or the thermal insulation, and/or other required function, when it is submitted to a standard fire test.

The fire resistance of a structural element which separates or delimitates the fire compartments from other spaces represents the time interval in which the element loses its carrying capacity due to standard fire action.

The structural elements fire resistance levels are expressed in time units of measuring (hours and minutes), It is necessary to mention the kind of resistance, referring to stability or tightness.

The fire resistance of a structural element is defined by adopting the strength to fire action that represents the time needed by the element to lose its capacity to respond to the action of a standard fire, which is represented by the temperature – time logarithmic curve.

This strength is determined based on the following criteria:

- carrying capacity (or stability);
- thermal insulation;
- tightness.

It is evaluated for each element, by testing it into a furnace, according to a thermal program that follows a curve defined by ISO 834.

According to thermal insulation criterion, the strength to fire action is considered to be the time needed to attain one of the following limit states:

- the average temperature on the element face that is not exposed to fire action exceeds the initial temperature with more than 140°C ;
- the maximum temperature attained at any point of the element face that is not exposed to fire action exceeds with more than 180°C the initial temperature or, the maximum temperature reaches 220°C , no matter the value of the initial temperature.

2. Analysis of the Element to Fire Action

2.1. Analysis Purpose

The present analysis of a non-structural multilayered wall belonging to a fire compartment is performed according to thermal insulation criterion. The element heating program is given by a curve defined in ISO 834.

To solve the problem means to approach a non-stationary analysis of conductive heat transfer.

The evaluation of temperature distribution in the characteristic sections of the wall, at certain moments is performed by using the Finite Element Method (FEM) The non-stationary problem is solved by appealing to the step by step direct integration technique.

2.2. Element Modeling

The non-structural wall consists of two layers of glass fibre reinforced plaster, 0.036 m in thickness and between them, a mineral wool layer, 0.092m in thickness. The element function is to separate two fire compartments where, before fire breaking out, the environmental medium temperature is 15⁰C. It can be presumed that the temperature over the wall thickness is 15⁰C, too.

The fire breaks out in one of the compartments and leads to environmental medium temperature increasing according to the standard curve given by ISO 834. The temperature in the other compartment is still 15⁰C.

In order to study the conductive heat transfer, a parallelepiped is imaginarily cut from wall thickness. The two end faces are in direct contact with the fired and unfired medium, respectively. This is the way of obtaining the virtual model presented in Fig.1.

The thermal characteristics of the component materials are:

- for the glass fibre reinforced plaster
 - the coefficient of thermal conductivity $\lambda=0,41\text{W}/(\text{m}\cdot^{\circ}\text{C})$;
 - the specific heat under constant pressure $c_p =840\text{J}/(\text{kg}\cdot^{\circ}\text{C})$;
 - the density $1100\text{ kg}/\text{m}^3$;
- for mineral wool
 - the coefficient of thermal conductivity $\lambda=0,041\text{W}/(\text{m}\cdot^{\circ}\text{C})$;
 - the specific heat under constant pressure $c_p =750\text{J}/(\text{kg}\cdot^{\circ}\text{C})$;
 - the density $115\text{ kg}/\text{m}^3$.

The design model adopted in the finite element method is obtained by dividing the virtual model in adequate finite elements for simulating the conductive heat transfer.

The discretized model consists of 176 three-dimensional finite elements (SOLID).

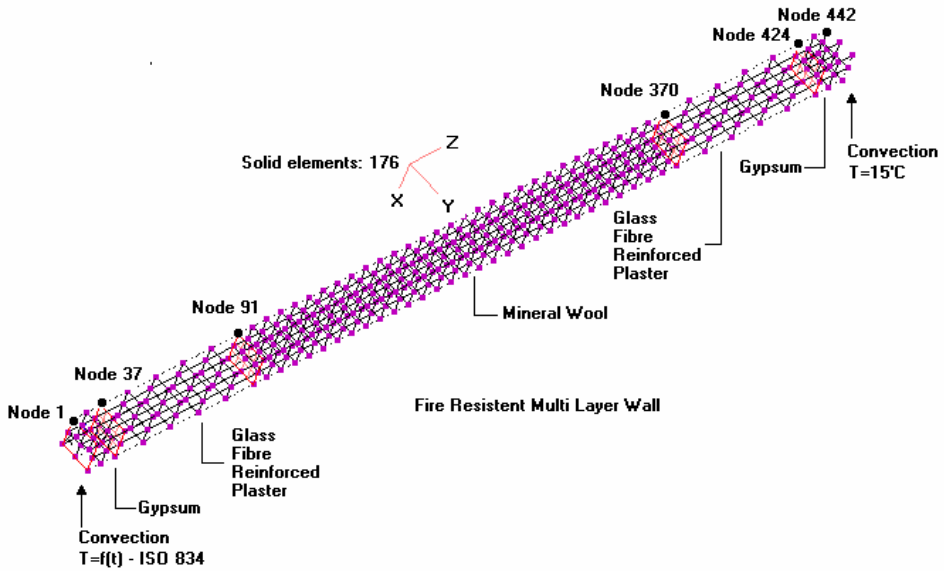


Figure 1. The multilayered wall virtual model

2.3. Boundary and Initial Conditions

The modeling of thermal loads on the two faces of the wall appeals to boundary conditions of Cauchy type, that is, convective heat change variable in time on one face and constant on the opposite one. The convection factors are:

- on the fired surface (average value, according to European codes)
 $\alpha=25\text{W}/(\text{m}^2\cdot^{\circ}\text{C})$;
- on the opposite surface $\alpha=8\text{W}/(\text{m}^2\cdot^{\circ}\text{C})$.

In order to study the temperature time history, that is a non-stationary analysis of conductive heat transfer, a design soft based on FEM is used.

The variation curve for the temperature in the fire compartment is given in relation (1) and shown in Fig.2.

$$T=T_0 + 345\cdot\log_{10}(8\cdot t+1) \quad (1)$$

where: T is the temperature near the tested element;

T_0 – the initial temperature in the compartment where the test is performed.

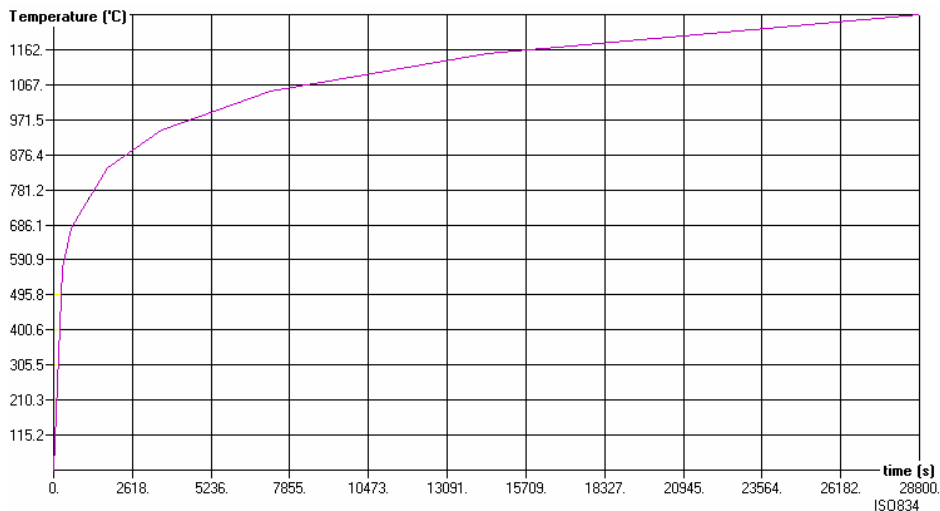


Figure 2. Temperature – time curve according to ISO 834

The heat transfer analysis is performed during 28800 seconds (480 minutes or 8 hours). The time mesh is automatically checked by the program, in order to assure the algorithm stability and the convergence to the exact solution (relation 2):

$$\Delta t < \delta^2 / (10 \cdot \alpha) \tag{2}$$

where: Δt is the integration mesh;
 δ – conductivity length;
 α – thermal diffusibility.

The initial temperatures result from the thermal equilibrium attainment when the boundary conditions prior to fire breaking out are expressed. In this case, the initial temperature is 15°C at all model nodes.

3. Analysis Results

The temperature time history at different characteristic sections (defined by the corresponding nodes) of the multilayered wall can be noticed on the graphs presented in Fig.3.

In figure 4, the time history of the temperature on the unfired side of the wall is presented. It can be noticed that after 240 minutes (14400 seconds) the temperature of this side reaches 48°C.

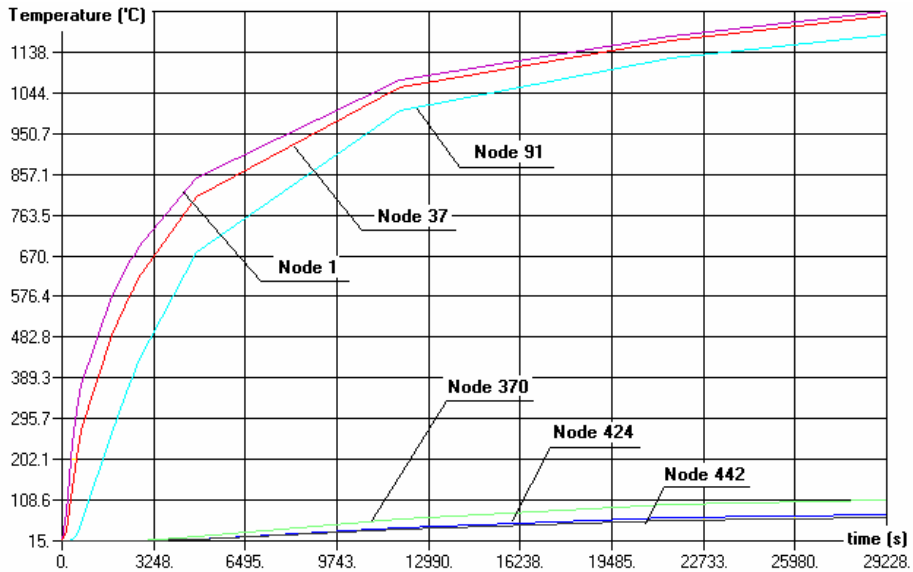


Figure 3. Temperature variation on the characteristic model sections

4. Comparative Analysis and Conclusions

The design model submitted to a conductive heat transfer analysis is the virtual representation of a multilayered wall of Glasroc FireWall type, produced by BPB RIGIPS, which consider that:

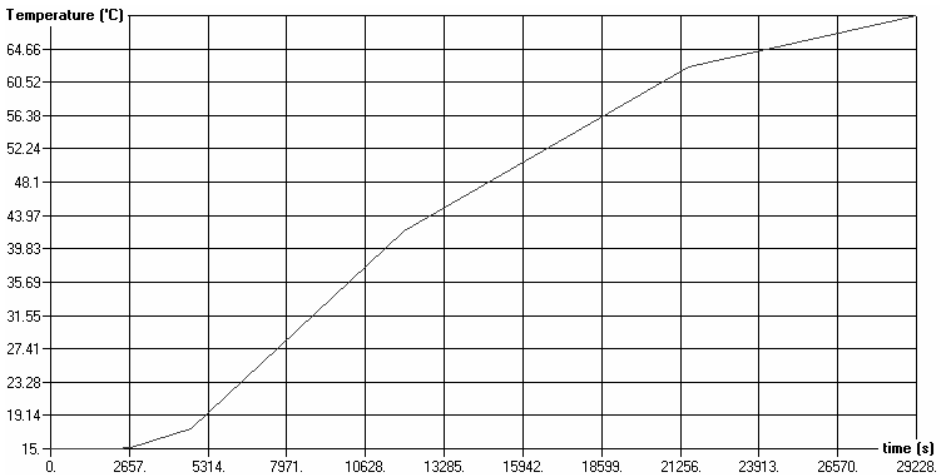


Figure 4. Temperature variation on the unfired wall side

“Glasroc FireWall is a non-structural wall that assures the fire resistance up to 240 minutes. It can be used for shops and industrial warehouses located at the basement

or first floor of buildings, in specific service conditions, as they are requested by assurance companies...The wall contains a frame made of steel rolled shapes I, 92 mm in height. The distance between their axes is 600 mm. Between these shapes the mineral wool is introduced. The frame is covered by Riflex plates, in order to assure the required strength....”

It can be noticed that the temperature increasing on the unfired side of the wall is approximately 33⁰C (from 15⁰C to 48⁰C), so that it has an important safety reserve up to 140⁰C.

The conclusion of the analysis is that the resistance of this wall to fire action is not based on thermal insulation criterion, but on stability or tightness ones.

5. References

1. D. Diaconu, V. Hobjilă, I. Ciongradi, Principii și aplicații în calculul automat al structurilor termodeformabile, Ed. “Gh. Asachi”, Iași, 2000.
2. BPB RIGIPS, Ridurit-Sisteme de protecție la foc, Rigips, București, 2002
3. MLPTL-CNATC, Agreement Tehnic 020-02-021-2002, București, 2002.
4. MLPTL-CNATC, Agreement Tehnic 020-03-021-2002, București, 2002.

ISSUES REGARDING THE EFFECT OF THE SUPPORTING MEDIUM ON THE BENDING VIBRATIONS OF BEAMS

Mihai VRABIE¹

Abstract

The bending vibrations of the straight beam laying on an elastic medium are significantly influenced by a series of characteristics of the supporting medium. From the classic theory of beams laying on a Winkler elastic support (medium), these characteristics are included in the stiffness coefficient k of the elastic support (coefficient of soil reaction), coefficient that is usually taken constant.

Actually, the factors on which the structure's response depends (the diversity of natural placement conditions, use of soil improvement techniques, different loads along the beams, etc.), are more or less variable. This implies also the variability of the k coefficient, and subsequently the differential equation that rules the oscillating phenomenon has variable coefficients, which calls for finding an “accurate” (“exactly”) analytical solution. The use of solving approximation calculus becomes mandatory (the finite differences method, the finite elements method, the line element method). This paper considers the elastic medium (support) as having variable coefficient of subgrade reaction along the beam and uses the finite element method, in the Galerkin approach, for solving the differential equation.

This technique allow to separe the effects of rigidity of beam and of elastic medium in answer of the beam.

It is distinguish a stiffness matrix in wich the effect of the supporting medium is separate from the effect of the geometric and elastic characteristics of the proper beam. This fact allows a better evaluation of the supporting medium induced effect on the bending vibrations of the beam.

¹ Assoc. Prof., PhD., Technical University of Iasi, Romania, Faculty of Civil Engineering,
e-mail: mihai_vrabie@yahoo.com

1. The Differential Equation of the Deformed Axis

One takes straight beams with constant section, laying on an elastic Winkler support (fig. 1). The connection between the beam’s deflections w and the intensity of the support’s reactions p , in the Winkler model hypothesis, is linear [1]:

$$p = kw \tag{1}$$

where, the k stiffness coefficient of the elastic support that may vary along the beam, so:

$$k(x) = k_0(x) \cdot b \tag{2}$$

b - the beam’s width on the face that lays on the elastic support;

k_0 - the bed modulus or coefficient of soil reaction, for which this paper considers a linear variation along the beam.

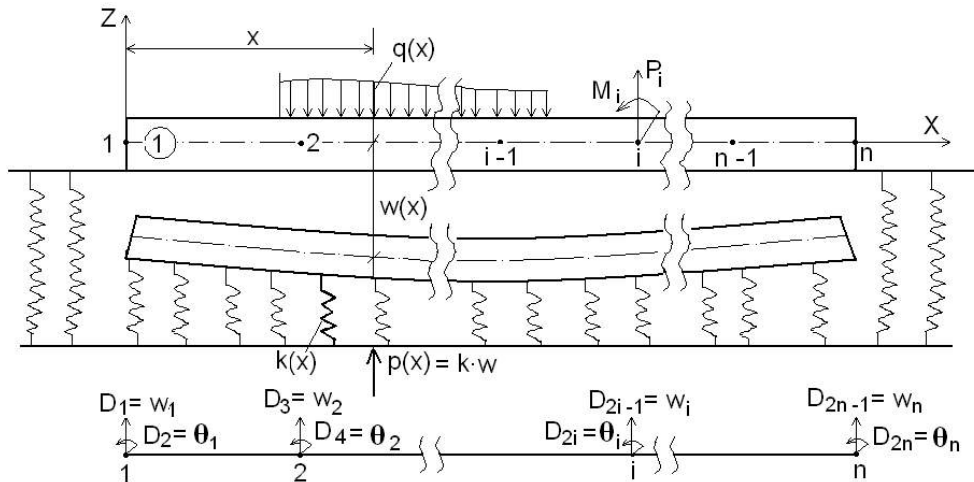


Fig.1. The finite element model of the beam

According to the relations (1) and (2), the differential equation of the average deformed axis of the beam on elastic support (medium) can also be written in a dynamic situation:

$$EI \frac{\partial^4 w(x,t)}{\partial x^4} + k(x) \cdot w(x,t) = q(x,t) \tag{3}$$

where, E - the elasticity modulus of the material of which the beam is made, $I=I_y$ - the moment of inertia of the section versus the bending axis y - y of the beam, $q(x,t)$ - the intensity of the exterior load distributed on the length.

In the issue of free bending oscillations, $q(x,t)$ is the intensity of the inertial forces and, according to Newton’s law, it will be:

$$q(x,t) = -m \frac{\partial^2 w}{\partial x^2} \tag{4}$$

m - the mass per length unit of the beam; t - the time.

Using the equation (4), the equation (3) becomes:

$$EI \frac{\partial^4 w(x,t)}{\partial x^4} + k(x) \cdot w(x,t) + m \frac{\partial^2 w(x,t)}{\partial t^2} = 0 \tag{5}$$

2. Finite Element Modeling and Shape Functions

Next, we use the finite element method for solving the equation (5). It is for this purpose that the beam on elastic medium, related to the general referential system XOZ, is discretized in $n-1$ finite elements, connected in n nodal points (fig 1).

Each node is assigned two degrees of freedom, the displacement w and the rotation θ (at bending oscillations the beam has bending displacements-deformations).

One analyzes a current finite element „ e ” to establish the linking relation between the forces and the pertaining nodal displacements (fig 2).

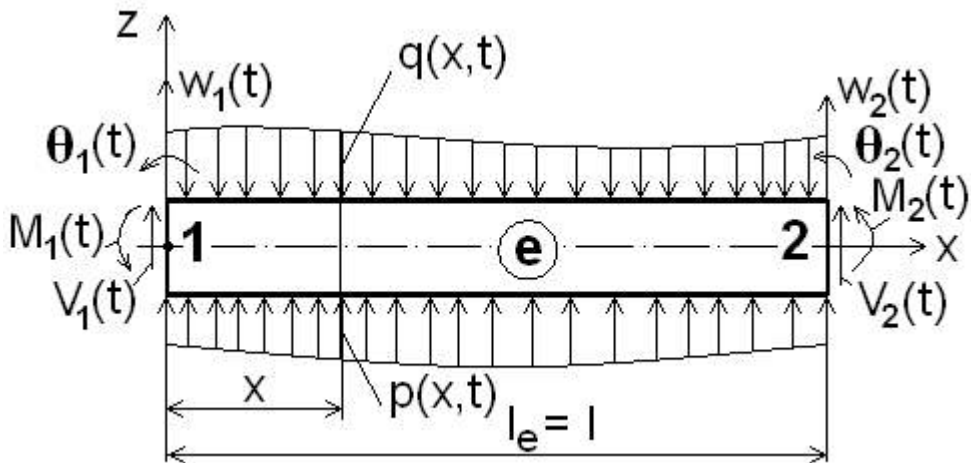


Fig. 2. A current finite element „ e ”

One approximates the finite element displacement function with a 3rd degree polynomial with separate variables [3]:

$$w_e(x,t) = \alpha_1(t) + \alpha_2(t) \cdot x + \alpha_3(t) \cdot x^2 + \alpha_4(t) \cdot x^3 \tag{6}$$

The boundary conditions lead to the expression of the coefficient vector $\{\alpha(t)\}$, by means of the elementary nodal displacement vector $\{d_e(t)\}$:

$$w_e(x,t) = [N_i(x)]^T \{d_e(t)\} \tag{7}$$

where, $[N_i(x)]$ - the matrix of the shape functions, which are L'Hermite polynomials,

$$[N_i(x)] = \begin{bmatrix} N_1(x) \\ N_2(x) \\ N_3(x) \\ N_4(x) \end{bmatrix} = \begin{bmatrix} 1 - \frac{3x^2}{l^2} + \frac{2x^3}{l^3} \\ x - \frac{2x^2}{l} + \frac{x^3}{l^2} \\ \frac{3x^2}{l^2} - \frac{2x^3}{l^3} \\ -\frac{x^2}{l} + \frac{x^3}{l^2} \end{bmatrix} \quad (8)$$

3. The Galerkin Approach

If one inputs the approximate solution (7) in equation (5), one gets a residuum:

$$\varepsilon(x,t) = EI \frac{\partial^4 w_e}{\partial x^4} + k(x)w_e(x,t) + m \frac{\partial^2 w_e}{\partial t^2} \neq 0 \quad (9)$$

The residuum (9) must be minimum and for that one builds the weighed minimum functional type Galerkin, which is annulled to minimize the residuum:

$$\begin{aligned} \Pi_e = \int_0^l N_i(x)\varepsilon(x,t)dx = EI \int_0^l N_i(x) \frac{\partial^4 w_e}{\partial x^4} dx + \\ + \int_0^l N_i(x)k(x)w_e(x,t)dx + m \int_0^l N_i(x) \frac{\partial^2 w_e}{\partial t^2} dx \end{aligned} \quad (10)$$

The first integral from (10) results [2], [3], [5]:

$$\begin{aligned} EI \int_0^l N_i(x) \frac{\partial^4 w_e}{\partial x^4} dx = - \begin{Bmatrix} V_1 \\ M_1 \\ V_2 \\ M_2 \end{Bmatrix} + EI \int_0^l \begin{bmatrix} (N_1'')^2 & N_1''N_2'' & N_1''N_3'' & N_1''N_4'' \\ N_2''N_1'' & (N_2'')^2 & N_2''N_3'' & N_2''N_4'' \\ N_3''N_1'' & N_3''N_2'' & (N_3'')^2 & N_3''N_4'' \\ N_4''N_1'' & N_4''N_2'' & N_4''N_3'' & (N_4'')^2 \end{bmatrix} dx \begin{Bmatrix} w_1 \\ \theta_1 \\ w_2 \\ \theta_2 \end{Bmatrix} = \\ = - \begin{Bmatrix} V_1(t) \\ M_1(t) \\ V_2(t) \\ M_2(t) \end{Bmatrix} + \frac{EI}{l^3} \begin{bmatrix} 12 & 6l & -12 & 6l \\ 6l & 4l^2 & -6l & 2l^2 \\ -12 & -6l & 12 & -6l \\ 6l & 2l^2 & -6l & 4l^2 \end{bmatrix} \begin{Bmatrix} w_1 \\ \theta_1 \\ w_2 \\ \theta_2 \end{Bmatrix} = -\{S_e\} + [k_e]\{d_e\} \end{aligned} \quad (11)$$

where, $\{S_e\}$ - the vector of nodal internal forces, $\{d_e\}$ - the nodal displacements vector, $[k_e]$ - the elastic stiffness matrix of the beam.

Assuming a linear variation of the stiffness coefficient:

$$k(x) = k_1 \left(1 - \frac{x}{l} \right) + k_2 \frac{x}{l} \quad (12)$$

the second integral from (10) is written as [4]:

$$\int_0^l N_i(x)k(x)w_e(x,t)dx = \left(\int_0^l \left[k_1 \left(1 - \frac{x}{l} \right) + k_2 \frac{x}{l} \right] N_i(x) [N_1 \ N_2 \ N_3 \ N_4] dx \right) \{d_e\} =$$

$$\frac{l}{840} \begin{bmatrix} 24(10k_1 + 3k_2) & 2l(15k_1 + 7k_2) & 54(k_1 + k_2) & -2l(7k_1 + 6k_2) \\ 2l(15k_1 + 7k_2) & l^2(5k_1 + 3k_2) & 2l(6k_1 + 7k_2) & -3l^2(k_1 + k_2) \\ 54(k_1 + k_2) & 2l(6k_1 + 7k_2) & 24(3k_1 + 10k_2) & -2l(7k_1 + 15k_2) \\ -2l(7k_1 + 6k_2) & -3l^2(k_1 + k_2) & -2l(7k_1 + 15k_2) & l^2(3k_1 + 5k_2) \end{bmatrix} \begin{Bmatrix} w_1 \\ \theta_1 \\ w_2 \\ \theta_2 \end{Bmatrix}$$

$$= [k_e^m] \{d_e\} \tag{13}$$

where, $[k_e^m]$ - the stiffness matrix of the medium (the soil below the beam).

The last integral from (10), has as a result [2], [3], [5]:

$$m \int_0^l N_i(x) \frac{\partial^2 w_e}{\partial t^2} dx = m \int_0^l \begin{bmatrix} N_1^2 & N_1 N_2 & N_1 N_3 & N_1 N_4 \\ N_2 N_1 & N_2^2 & N_2 N_3 & N_2 N_4 \\ N_3 N_1 & N_3 N_2 & N_3^2 & N_3 N_4 \\ N_4 N_1 & N_4 N_2 & N_4 N_3 & N_4^2 \end{bmatrix} dx \begin{Bmatrix} \ddot{w}_1 \\ \ddot{\theta}_1 \\ \ddot{w}_2 \\ \ddot{\theta}_2 \end{Bmatrix} =$$

$$= \frac{ml}{420} \begin{bmatrix} 156 & 22l & 54 & -13l \\ 22l & 4l^2 & 13l & -3l^2 \\ 54 & 13l & 156 & -22l \\ -13l & -3l^2 & -22l & 4l^2 \end{bmatrix} \begin{Bmatrix} \ddot{w}_1 \\ \ddot{\theta}_1 \\ \ddot{w}_2 \\ \ddot{\theta}_2 \end{Bmatrix} = [m_e] \{\ddot{d}_e\} \tag{14}$$

where, $[m_e]$ - the inertial matrix of the finite element (the mass matrix), $\{\ddot{d}_e\}$ - the vector of nodal accelerations.

Gathering the three integrals from (10), results the elemental physical relationship:

$$([k_e] + [k_e^m]) \{d_e\} + [m_e] \{\ddot{d}_e\} = \{S_e\} \tag{15}$$

4. Assembly of the Global Matrix and Solution of the Finite Element Equations

In view of assembling the finite elements, the relation (15) is expanded (one adds null lines and columns to the element matrices, zeroes respectively in the element vectors to bring the to the dimensions of the structure).

The expanded (15) can be written function of the expanded vectors:

$$([\bar{k}_e] + [\bar{k}_e^m]) \{D_e\} + [\bar{m}_e] \{\ddot{D}_e\} = \{\bar{S}_e\} \tag{16}$$

where the expanded vectors $\{d_e\}$, $\{\ddot{d}_e\}$ are noted by $\{D_e\}$ and $\{\ddot{D}_e\}$.

Next, it adds the expanded relations and results the structural physical relation that depends on the global stiffness:

$$([K] + [K^m])\{D\} + [M]\{\ddot{D}\} = 0 \quad (17)$$

where, $[K] = \sum_{e=1}^m [\bar{k}_e]$ – the global (assembled) stiffness matrix of the beam;

$[K^m] = \sum_{e=1}^m [\bar{k}_e^m]$ - the assembled stiffness matrix of the support medium;

$[M] = \sum_{e=1}^m [\bar{m}_e]$ - the assembled inertial matrix of the beam.

If the beam also has punctual bearings, then the relation (17) shall split, and get rearranged, outlining the constrained displacement on these supports (bearings):

$$\left(\begin{bmatrix} K_{nn} & K_{nr} \\ K_{rn} & K_{rr} \end{bmatrix} + \begin{bmatrix} K_{nn}^m & K_{nr}^m \\ K_{rn}^m & K_{rr}^m \end{bmatrix} \right) \begin{Bmatrix} D_n \\ D_r \end{Bmatrix} + \begin{bmatrix} M_{nn} & M_{nr} \\ M_{rn} & M_{rr} \end{bmatrix} \begin{Bmatrix} \ddot{D}_n \\ \ddot{D}_r \end{Bmatrix} = \begin{Bmatrix} 0 \\ 0 \end{Bmatrix} \quad (18)$$

where, $\{D_n\}$ - the sub-vector of displacements of free nodes (unknowns), $\{D_r\}$ - the constrained displacements sub-vector (knows).

In the case of punctual fixed supports, $\{D_r\} = \{0\}$ and from (18) results:

$$([K_{nn}] + [K_{nn}^m])\{D_n\} + [M_{nn}]\{\ddot{D}_n\} = 0 \quad (19)$$

which, is a quadratic differential equations system with constant coefficients, to which initial conditions need to be added (the $\{D_0\}$ displacements and the $\{\dot{D}_e\}$ velocity vector at $t = 0$ time).

The solving of the dynamic equation system is performed through [3]:

- specific integration methods for linear differential equation systems (Runge-Kutta, Adams, Milne etc.);
- specific methods for a quadratic differential equations system (finite differences, Newmark, Wilson);
- modal analysis method that is used hereon.

For the nodal displacement vector one assumes a harmonic variation in time:

$$\{D_n\} = \{D_n^0\} \sin(\omega t + \varphi) \quad (20)$$

where, $\{D_n^0\}$ - the vector of vibration amplitudes, ω - own circular frequency, φ - phase difference.

The nodal accelerations vector will be:

$$\{\ddot{D}_n\} = -\omega^2 \{D_n^0\} \sin(\omega t + \varphi) \quad (21)$$

By replacing the equations (20) and (21) in (19) results:

$$([K_{nn}] + [K_{nn}^m] - \omega^2 [M_{nn}])\{D_n^0\} = 0 \quad (22)$$

The (22) relation shall be multiplied by $1^3/EI$, and it marks the matrices without common factor with $\bar{\quad}$, getting:

$$\left(\left[\overline{K}_{nn} \right] + \frac{l^4}{840EI} \left[\overline{K}_{nn}^m \right] - \frac{ml^4 \omega^2}{420EI} \left[\overline{M}_{nn} \right] \right) \{ D_n^0 \} = 0 \quad (23)$$

It notes:

$$\left[\overline{K}_{nn} \right] + \frac{l^4}{840EI} \left[\overline{K}_{nn}^m \right] = \left[K_{nn}^* \right], \quad \frac{ml^4 \omega^2}{420EI} = \lambda \quad (24)$$

and (23) equation can be written more compact:

$$\left(\left[K_{nn}^* \right] - \lambda \left[M_{nn}^* \right] \right) \{ D_n^0 \} = 0 \quad (25)$$

and that is a general problem of eigenvalues and eigenvectors:

$$\left([A] - \lambda [B] \right) \{ X \} = 0 \quad (26)$$

in which $[A]$, $[B]$ - the symmetrical square matrix, λ - a scalar named eigenvalue, $\{X\}$ - eigenvector.

By solving the system (25) it gets the eigenvalues λ_i , and the corresponding eigenvectors $\{X_i\}$. From λ_i results the own circular frequencys

$$\omega_i = \sqrt{\frac{420EI\lambda_i}{ml^4}} \quad (27)$$

and than the other dynamic characteristics of the structure.

The eigenvectors $\{X_i\}$ represents the vector of vibration amplitudes of the beam.

5. Conclusions

- 1) The bending vibrations of beams layed on elastic medium Winkler are significantly influenced by a series of characteristics of the support-medium. These characteristics are included in the stiffness modulus of the support-medium k , wich is constant usually considered.
- 2) In fact, the characteristics of the support-medium are variable and this fact lead to a differential equation of the deformed axis with variable coefficients. Consequently, is difficult to obtain analytic „accurate „ solutions.
- 3) The Galerkin approach of the finite element method allows to obtain a stiffness matrix of the support-medium, by wich we can to estimate the influence of the support-medium on the bending vibrations of the beam settled on the elastic medium Winkler.
- 4) With help of FEM may be obtained a numerical solution which approximate the exact solution with an acceptable degree of precision in engineering practice. The precision of the method can be improved using a more refined discretization, the approximation of the displacements field with high degree polynoms or with transcendent functions simultaneously with additional degree of freedom adjusted on node.
- 5) The obtained results may be also extended to vertical members of foundations (piles, columns, pilings etc.) where, taking into account the layers of the ground, the coefficient of subgrade reaction is variable on depth.

References

1. Păunescu, M., Pop, V., Sillion, T., *Geotehnică și fundații*, Ed. Didactică și Pedagogică, București, 1982.
2. Pascariu, I. *Elemente Finite. Concepte – Aplicații*, Editura Militară, București, 1985.
3. Jerca, St., Ungureanu, N., Diaconu, D., *Metode numerice în calculul construcțiilor*, U. T. “Gh. Asachi” Iași, 1997.
4. Jerca, Șt., Vrabie, M., Răileanu, P., Mușat, V., Răileanu, L., *Static Analysis of Beams on Elastic Foundations with Variable Coefficient of Soil Reaction Using the Finite Element Method*, Bul. IPI, Tomul XLVI (L), Fasc. 1-2, 2000.
5. Chandrupatla, T.R., Belegundu, A.D., *Introduction to Finite Elements in Engineering*, Prentice-Hall International Editions, 3-rd Edition, 2002.

FAULT TREES

Danuț BABOR¹, Ancuța ROTARU²

Abstract

The concept of a fault tree is used rather widely in the reliability analysis of industrial processes, and to a lesser extent in the reliability analysis of structural systems.

In the context of Building Pathology, a fault tree can be described as a cognitive model or diagram, which represents an outline of the possible errors affecting the performance of a building system or a building component. The tree can indicate correlated phenomena and chains of events leading from error to failure.

A fault tree is basically cause-oriented. Given some defect or failure normally called an “undesired top event” - all possible events causing that top event or intermediate events are analyzed and ordered in a logical way. Intermediate events are placed in rectangular boxes. Basic events, meaning those events which cannot be, or which do not need to be analyzed further, are placed in circles. An event that might be caused by one or more 'lower' events is indicated by a so-called 'OR-gate' at the connection. An 'AND-gate' is used if the considered event only produces when two or more events occur simultaneously.

The main advantage of such a qualitative fault tree is that it forces the investigator to a logical and complete analysis of a given problem and that it helps in not overlooking possible causes.

A fault tree does not contain all necessary information related to the given problem. But the combination of fault tree and other relevant information may be very useful as guidance through the diagnostic process, for instance by determining which efforts are likely to be most effective, or by eliminating less probable events.

The use of a fault tree is most powerful if the basic events can be quantified in terms of probability of occurrence. Then, by combining these probabilities, and taking into account the mathematical logic of OR-and AND-gates, the probability of occurrence of the top event can be determined. This kind of assessments is rather unusual in building pathology and it needs an understanding of probabilistic techniques.

In practice, the 'erection' of a fault tree may be rather complicated. It takes more time than originally thought, and the first attempt is mostly a faulty fault tree. It is helpful to distinguish certain main components of the considered system, or to recognize levels of importance.

¹ Lecturer, „Gh.Asachi” Technical University of Iași, Romania, danbabor@yahoo.com

² Phd. „Gh.Asachi” Technical University of Iași, Romania, arotaru@ce.tuiasi.ro

1. Introduction

A fault tree is basically cause-oriented. Given some defect or failure -normally called an “*undesired top event*” - all possible events causing that top event or intermediate events are analyzed and ordered in a logical way. An example of a fault tree called “*Inadequate functioning of facade element*” is given in Figure 1. Intermediate events are placed in rectangular boxes. Basic events, meaning those events which cannot be, or which do not need to be analyzed further, are placed in circles. An event that might be caused by one or more “*lower*” events is indicated by a so-called “*OR-gate*” at the connection. An “*AND-gate*” is used if the considered event only occurs when two or more events occur simultaneously.

The main advantage of such a qualitative fault tree is that it forces the investigator to a logical and complete analysis of a given problem and that it helps in not overlooking possible causes.

A fault tree does not contain all necessary information related to the given problem, but the combination of fault tree and other relevant information may be very useful as guidance through the diagnostic process, for instance, by determining which efforts are likely to be most effective, or by eliminating less probable events. The use of a fault tree is most powerful if the basic events can be quantified in terms of probability of occurrence. Then, by combining these probabilities, and taking into account the mathematical logic of OR- and AND-gates, the probability of occurrence of the top event can be determined. This kind of assessments is rather unusual in building pathology and it needs an understanding of probabilistic techniques.

In practice, the 'erection' of a fault tree may be rather complicated. It takes more time than originally thought, and the first attempt is mostly a faulty fault tree. It is helpful to distinguish certain main components of the considered system, or to recognize levels of importance. The fault tree 'hierarchy' as presented in Figure 2 might be useful for the analysis of building defects.

Another example, though not consistent with usual way of fault tree representation, is given in figure 3. This condensed tree might be helpful in analyzing detachment and rising of ceramic floor covering.

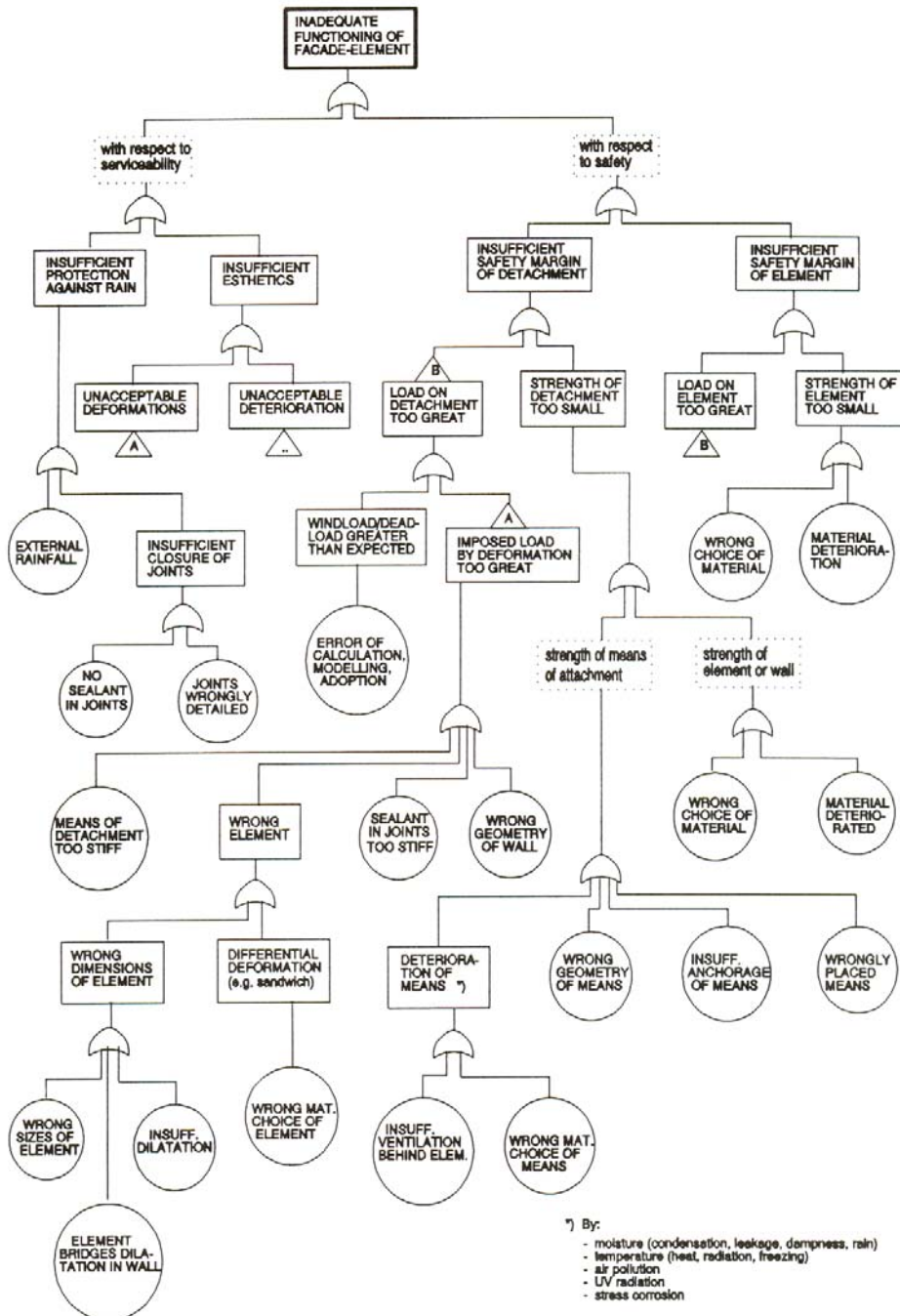
A. Failure level - Is the final decay event (a structural and/or a performance failure).

B. Defect level - Represents the hypercritical condition which caused the failure.

Actions/reactions level - The level where an exceeding of a limit state is inquired.

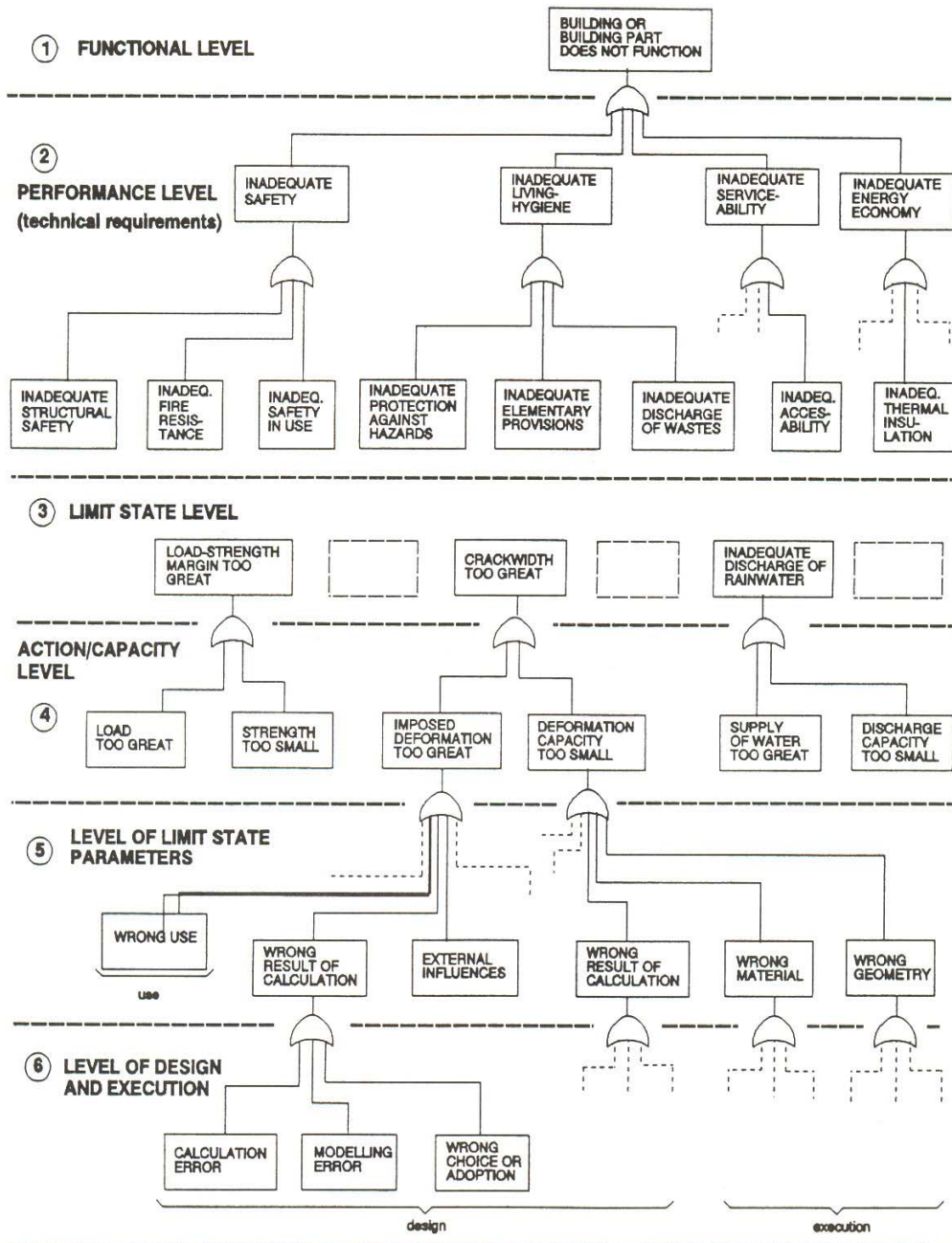
D. Error level - This is the basic level that represents the possible errors (technical as well as human errors) that lead to failure.

Despite different wording, these levels correspond reasonably well with the levels 2 through 5 of Figure 2.



*) By:
 - moisture (condensation, leakage, dampness, rain)
 - temperature (heat, radiation, freezing)
 - air pollution
 - UV radiation
 - stress corrosion

Fig.1. Example of a fault tree: Inadequate functioning of façade element.



REMARK 1. This diagram is not a fault tree, but a schematic subdivision of events into different levels.

REMARK 2. Any event in the limit state level (3) always splits up into two events in the action/capacity level (4).

Fig.2. Fault tree hierarchy.

2. The diagnostic tree

A fault tree is helpful in understanding the relations between a given undesired event and all its possible causes. But it does not give an answer on the actual cause(s) of a certain event. For this purpose, the instrument of a 'diagnostic tree' might be useful. The diagnostic tree is a procedural guide for the diagnostic inquiry. It is used for a specific situation where the actual 'branches' of the fault tree have already been determined.

The necessary elements to form a diagnostic tree are:

- the given failure;
- questions which need an answer in order to proceed along the diagnostic tree branches;
- decision instruments for answering those questions; the primary defects and the conjectural diagnosis.

The two most meaningful advantages of the diagnostic tree are:

- It makes it possible to order and to systemize the development of the diagnostic.
- It guards against neglecting some of the possible failure mechanisms.

As an example, Figure 3 shows a part of the diagnostic tree concerning ceramics floor coverings.

3. Expert systems

The application of expert systems to the construction industry is of special interest to building pathology. Informatics technologies may have significant advantages for the diagnostic process operator during different phases of this process:

- filing of information concerning surveyed buildings, in order to have it always at one's disposal;
- filing of information necessary to describe a particular pathologic phenomenon (description of defects, agents which start defects, consequent anomalies, failures, etc.);
- formulation of algorithms used to identify relations between surveyed data (for example: thermo hygrometric relations can be analyzed by the Glaser algorithm so as to give information about the presence of surface or cavity condensation; cracked concrete elements can be analyzed by finite element methods to identify the tension active systems which are responsible for cracking, etc.).

These are just some of the operations, which can be done profitably by using a computer and adequate software. But, as indicated in previous sections, the survey process is complex. It is based on the integrated analysis of non-homogeneous data (for instance: numeric, verbal-descriptive, qualitative, quantitative, certain,

uncertain,). Sometimes the necessary data are completely lacking, or are hard to establish, or they cannot easily be modeled.

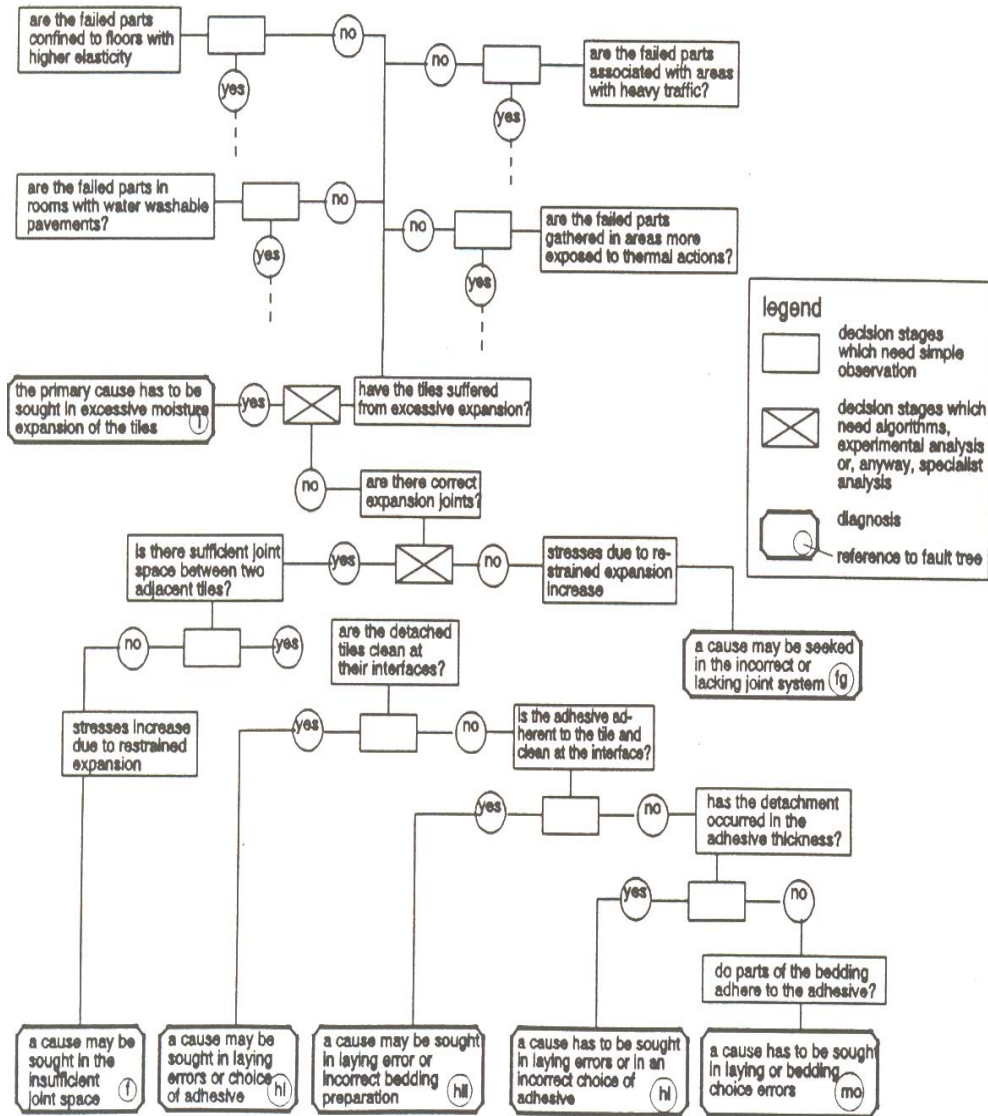


Fig.3 The Diagnostic Tree.

The whole set of data must be managed, taking into account all the relations between these data. If we decide to execute an integrated analysis by computer, we arrive

at the limits of traditional informatics: its inadequacy to manage non-deterministic data cannot be overcome.

A further limitation of traditional informatics is its inadequacy to simulate human reasoning, for instance, to give acceptable formulations despite missing or ambiguous data, or to handle non-algorithmic deductions.

The science of artificial intelligence, which started to develop around the fifties and is now more or less consolidated, tries to overcome these limits. This is done by introducing structures based on formulation processes.

4. Expert systems structure and logic

Among the several products of artificial intelligence, the expert system is certainly the most suitable one for use in diagnostics. An expert system is a programmed system aimed at giving adequate answers to questions of the user in the concerned knowledge sector by analyzing a great amount of data concerning the problem.

The expert system is a 'sector specialist' which 'knows everything' about the delimited field. It can produce - in that field - information, and may arrive at satisfactory conclusions even when the available data are incomplete and uncertain.

As the presence of much knowledge is crucial for the success of an expert system, the problem of knowledge representation is crucial for the system planning. This knowledge outlines the statements (truths about the object) and rules (deductive or inductive mechanisms) to produce new knowledge from the statements. These rules are known as *if - then rules*, or *antecedent - consequent rules*.

An expert system, able to manage typical diagnostic problems (in the building sector like in many others) is based on the following components (Figure 4):

- **knowledge base** containing facts, statements, relations between data, deductive/inductive rules related to the surveyed field; an **inference engine** — the expert 'brain' — which is the mechanism able to analyze and to interpret the knowledge contained in the knowledge base so as to give answers to the user about a specific problem;

- a **fuzzy logic manager** or an **uncertainty handling mechanism**, which is a mechanism that allows the system to elaborate uncertain information, or to proceed despite lack of information by the user

- an **explanation mechanism** which can present the reasoning of how the *F* system came to its conclusions. The explanation mechanism generally answers questions about answers questions about "why" and "how"; the same kind of questions which a human expert might be asked by the user. This is an important component for diagnosis in the expert system, because it offers additional

certainty to the more or less uncertain diagnosis itself;

➤ a **user/computer interface (UCI)** which allows the user to communicate with the system, even when the user is not an expert on informatics.

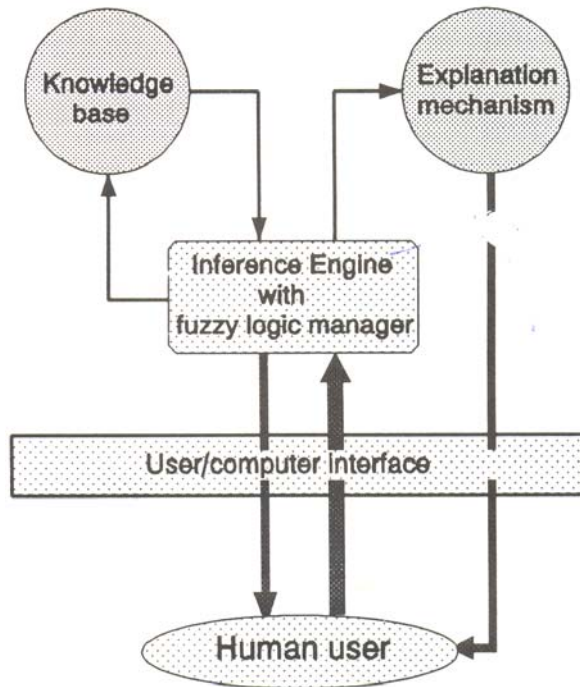


Fig.4. The system of human user - expert system.

References

1. ADDLESON. L., Building Failures: A Guide to Diagnosis, Remedy and Prevention, 2nd Ed., The Architectural Press, Ltd., London, England, 1989.
2. American Society of Civil Engineers, Performance of Constructed Facilities, Vol. 1, No. 1, February 1987; Vol. 2, No. 2, May 1988, ISSN 0887-3828 CODEN: JPCFEV.
3. American Society of Civil Engineers, Research Council on Performance of Structures, Structural Failures: Modes, Causes, Responsibilities, ASCE, New York, NY, 1973.
4. American Society of Civil Engineers, Research Council on Performance of Structures, Guide to Investigation of Structural Failures, ASCE, New York, NY, 1979.

UNITARY METHODOLOGY OF INVESTIGATION

Danuț BABOR¹, Ancuța ROTARU²

Abstract

Because there are many defect investigators as well as many types of defects, it is quite understandable that there exist a variety of investigation procedures and methods. It is obvious that an investigation method is highly dependent on the expertise and viewpoint of the investigator, and on the nature of the defect. Moreover, for given identical defects, different investigators may chose different approaches and may sometimes even reach different conclusions. The latter aspect of different conclusions - for given symptoms of a defect - must, if possible, be avoided. It emphasizes the need for a science like building pathology, and for its use by experts. From this point of view it makes sense to present a more or less basic investigation process, which gives the essentials of a systematic approach for dealing with defect.

The investigation process is thought to be a synthesis of all logic elements, which play distinct roles in the diagnosis and analysis of defects. This process flow does not pretend to give something new. It is just an attempt to indicate logic steps in the investigation process.

The diagnostic process starts from the observation of an occurred failure or from the acknowledgment of anomalies that indicate the presence of either a defect or a condition of incipient failure. The diagnostic process develops so as to deal with and to methodically analyse all the diagnostic possibilities, which may somehow be related to the failure itself. The analysis of the anomalies that may be found in the building is a strategic stage in the diagnostic activity. In fact if they are interpreted as symptoms, this will allow for a pre-acknowledgment of the defects, which have caused the failure. Subsequent confirmation of the pre-diagnostic conjectures based on a more accurate instrumental/analytical survey, and on repeated elimination of conjectures that do not fit obtained data, will finally lead to a sub-group of definitive diagnoses characterized by some degree of certainty. The presence of different possible diagnoses must be considered at the prequalification stage. Diagnostics, if correctly applied and supported by adequate tools (operative and methodological) can optimise the prequalification procedures.

Where the survey stage has to be completed in only one visit, it may be necessary to collect information, which later proves to be redundant, because of the difficulty of establishing what is truly relevant to the failure before all the data has been analysed. It is therefore preferable wherever possible, to iterate the survey stage, so that later examinations ca be used to test the developing diagnosis.

¹ Lecturer, „Gh.Asachi” Technical University of Iași, Romania, danbabor@yahoo.com

² Phd. „Gh.Asachi” Technical University of Iași, Romania, arotaru@ce.tuiasi.ro

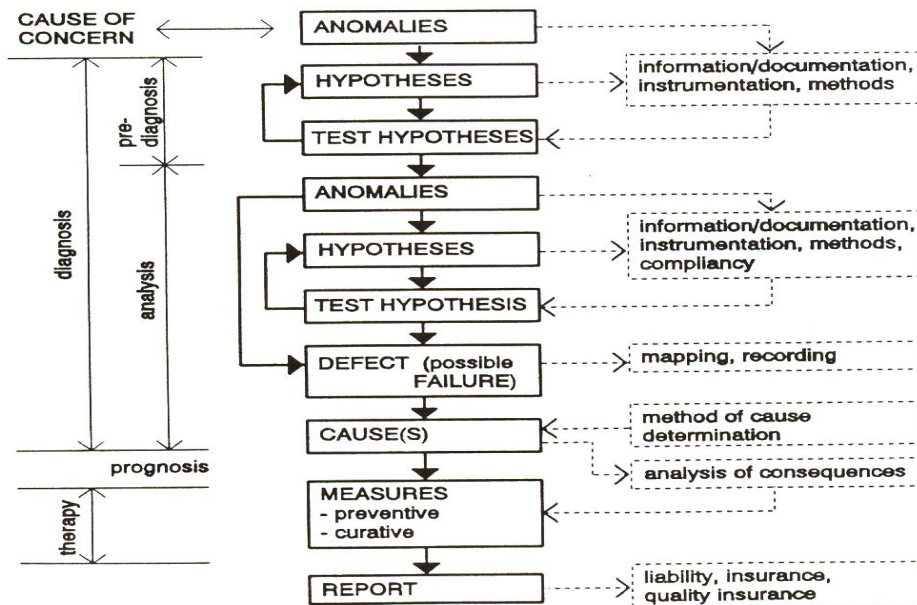


Fig.1. The investigation process.

1. Introduction

The investigation process is presented in Figure 1. The solid boxes and arrows represent the main process flow. Additional notions and 'tools' are indicated alongside. The notion 'anomalies' indicates that signs or symptoms first observed may not always be reliable indicators and should be checked.

It is evident that many variations of this diagram can be made, depending on scope and details of the investigation concerned. An example of a slightly different representation, called 'the diagnostic process' is given in Figure 2. The diagnostic process starts from the observation of an occurred failure or from the acknowledgment of anomalies that indicate the presence of a defect or a condition of incipient failure. The diagnostic process develops so as to methodically analyze all the diagnostic possibilities, which may somehow be related to the failure itself.

The analysis of the anomalies that may be found in the building is a strategic stage in the diagnostic activity. In fact, if they are interpreted as symptoms, this will allow for a pre-acknowledgment of the defects, which have caused the failure. Subsequent confirmation of the prediagnostic conjectures based on a more accurate instrumental/analytical survey, and on repeated elimination of conjectures that do not fit obtained data, will finally lead to a sub-group of definitive diagnoses. These are characterized by some degree of certainty. The presence of different possible diagnoses must be considered at the prequalification stage. Diagnostics, if correctly

applied and supported by adequate tools (operative and methodological) can carry out the function of optimizing the prequalification procedures.

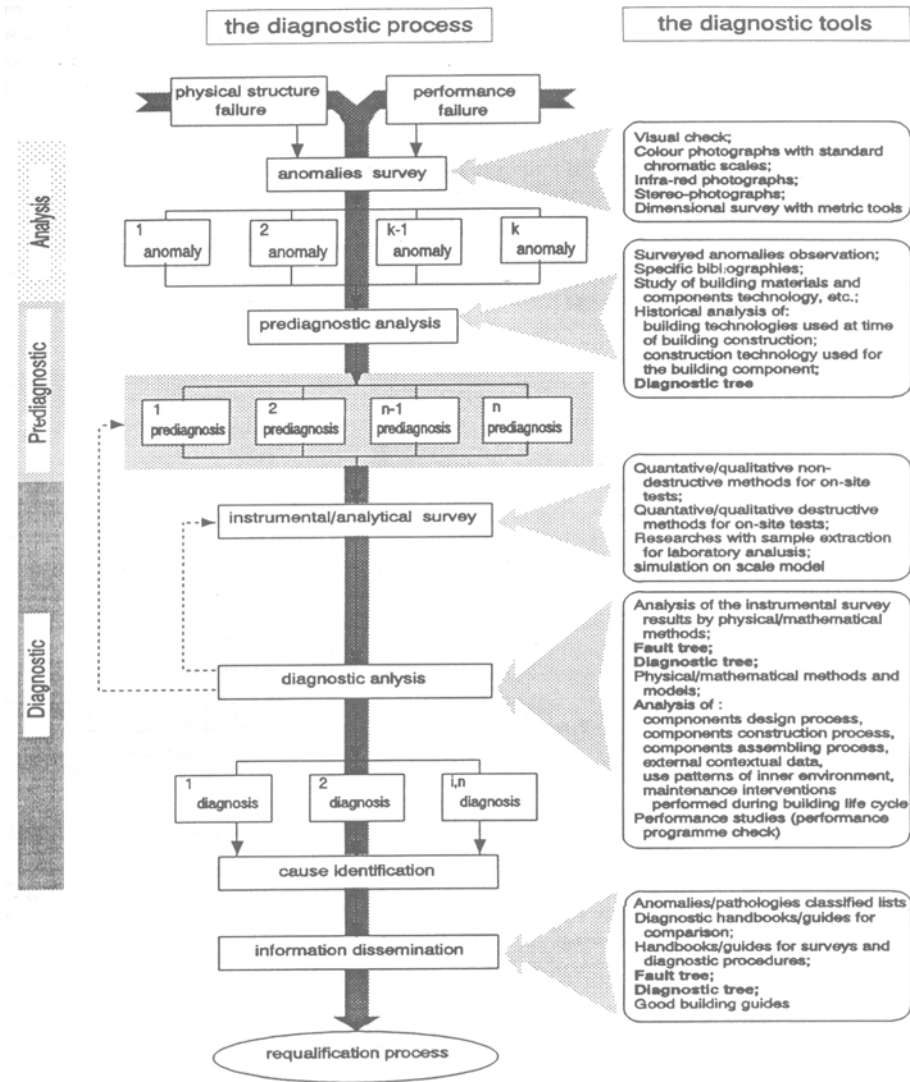


Fig.2: The diagnostic process and its tools.

When dealing a specific defect – or better: an anomaly indicating a possible defect – checking the list can play an important role. This may concern the different aspects, which call attention, or a list of possible symptoms to be checked, or a list of instruments or measuring devices.

A defect might be structural or non-structural, or combined. This distinction should be made, because a structural defect means insufficient safety. And 'safety' cannot be observed or measured directly. It must be assessed by calculations based on material properties, strength parameters, loads, dimensions and other properties. Safety should preferably be expressed in terms of 'probability of failure'. Also, such a probability of failure must be related to some acceptable risk. This belongs to the domain of a structural engineer, acquainted with probabilistic approaches.

In reality, the investigation is a decision-making process that might also be influenced by disturbing factors like time-pressures, missing or unrecoverable information and irrationalities. This implies that the investigator has to face uncertainties and to handle them in some probabilistic way.

2. Cause determination

It is evident that the cause of a defect should be known in order to take the necessary effective measures. But where does the 'tracing back' stop? In general, any event or situation is the consequence of some foregoing event. This leads inevitably to a conclusion about imperfect human behavior or knowledge, but does not imply that humans are always to blame. Assuming that the analysis of cause(s) is determined by what use is made of the results, three types of cause descriptions are recognized, thus delimiting the in-depth search:

- technique -oriented descriptions (what caused the defect?)
- liability-oriented descriptions (who caused the defect?)
- system-oriented descriptions (how did the defect originate?).

A *technique-oriented description* of causes is needed to allow for the formulation of technical measures, which will cure or prevent an identical defect. Apart from the direct interests of involved parties, this type of information may well be of interest to building participants and building 'educators'. In fact, this output of building pathology is generally given in forms like publications, seminars, defect information sheets, etc.

A *liability-oriented description* may be imposed by reasons of liability and insurance. Such descriptions point to 'faults' of persons or parties. The investigator should pay careful attention to objective evidence, and keeping also in mind those technical descriptions must be well understood and unambiguous.

An illustrative but surely not complete example is given in Figure 3.

A *system-oriented description* is required when causes of defects need to be 'input' for quality assurance (QA) in the building process. It is believed that QA - being a tool for managing a process efficiently and effectively - is most powerful in preventing defects. But QA is basically system-oriented: it deals in a managerial way with systems that aim at controlling matters like organization, resources, communication, information, means, human resources, motivation, and systematic

feedback. This implies that the output of building pathology – i.e. causes of defects - should be described in terms of system failures in order to be useful as input to QA. This way of looking at causes of defects is to a great extent analogous to the statement "building defects result from procedural inadequacies". This way of looking at causes of defects is little practiced by building pathologists.

	AIR HUMIDITY	RISING	RAIN WATER
SOURCES	<ul style="list-style-type: none"> -people -cooking -space under ground floor -gas water-heater -building moisture 	<ul style="list-style-type: none"> -ground water -rain water 	<ul style="list-style-type: none"> -rain water (direct) -rain water (indirect) -leakage -snow
INDICATIONS & ANOMALIES	<ul style="list-style-type: none"> -mould on furniture -condensation (frequently showing) on double glazing -mould or wet spots on structure -mould in cupboards 	<ul style="list-style-type: none"> -distinct moisture front from below -timber rot (floor joists) also at (founded) interior wall is efflorescence at moisture 	<ul style="list-style-type: none"> -distinct relation with rain (especially driving rain)
CAUSES OR STIMULATING CONDITIONS	<ul style="list-style-type: none"> -poor functioning or poor design of ventilation system -filthy ventilation system -wrong use of ventilation system -gas water-heater without external outlet -wash-drier without external outlet -wet space under ground floor with open connection to dwelling thermal bridges (design execution) 	<ul style="list-style-type: none"> -high ground water level -poor drainage -presence of salts -masonry foundation without moisture barrier (damp proof course) -lime mortar, used in masonry 	<ul style="list-style-type: none"> solid walls (masonry) poor pointing wrongly placed cavity anchors poorly executed or designed details cavity walls (fully filled) with imperfections of insulation material cavity walls filled with insulation slabs (open joints)

Figure 3. Check list 'Moisture problems'.

The way of getting to the 'sources' of a defect very much depends on its nature. But in general the determination process will follow some strategy of assessing possible causes, setting hypotheses and rejecting or adopting these hypotheses on

the basis of facts. Such a process is quite close to the more or less formalized method of the so-called *fault tree analysis*, which is known from (industrial) processes and reliability analysis of structures.

3. Origins of causes

It might be interesting to know where building defects originate during the building process. Some findings are given in the following Figure 4. It should be noticed that the manifestation of the defects does not necessarily coincide with the time of origin.

COUNTRY	design	execution	material	use	un know
Finland	50	30	10	10	5
France	30	60	10		
Germany (Fed.Rep.Germ.)	50	25	25		
Germany (Germ.Dem.Rep.)	40	40	20		
Great Britain	40	50	10		
Netherlands	40	35	10	10	
Norway	45	40	15		
USA	50	25	15	10	
average	43	38	14		
Czechoslovakia	5	70	25		
Hungary	20	38	42		
Poland	15	63	22		
average	13	57	30		

Figure 4. Building defects in % of main origins

These data, abstracted from data presented at the 'ECE Consultation on Building Pathology and Prevention of Disorders' (19/20 March 1987, Bonn), are believed to be reasonably indicative. But they are of limited value because the types of errors are not specified. It emphasizes once more that preventive measures at the level of improved quality management of the building process are needed. This aspect is also illustrated by the observation that 'material' (in Figure 4) is considered as an origin of possible defects. But material is as it is, and can never be blamed. There must be other causes leading to 'wrong material'.

In this report it is mainly technical aspects of building defects that are considered. But one should not overlook the fact that the real origins of defects are mainly lack of knowledge; know—how, information and communication.

4. The decay process and maintenance

Diagnosis, which is the basic part of the building pathology discipline, requires knowledge of the decay process suffered by the building components. This process is defined as the evolution from a performance to a non-performance condition. The pathological decay is always started by one or more *errors* (Figure 5), which might have been committed during different stages of the building process. But, errors committed during design or construction cause *defects*. These defects can either remain in a latent form, or manifest themselves by the action of *external agents*. Interaction between external agents and defects is the necessary condition for the manifestation of the decay as a failure.

The failure in building components can be structural, i.e. loss of certain physical, chemical and technological characteristics. Or it can be a performance failure, i.e. the drop of the initial performance level below an established acceptable limit. Or - finally and most commonly - it may concern both aspects. Under these terms, the manifestation (called the anomaly) by which the building user becomes aware of a failure may concern both the structural and performance aspects.

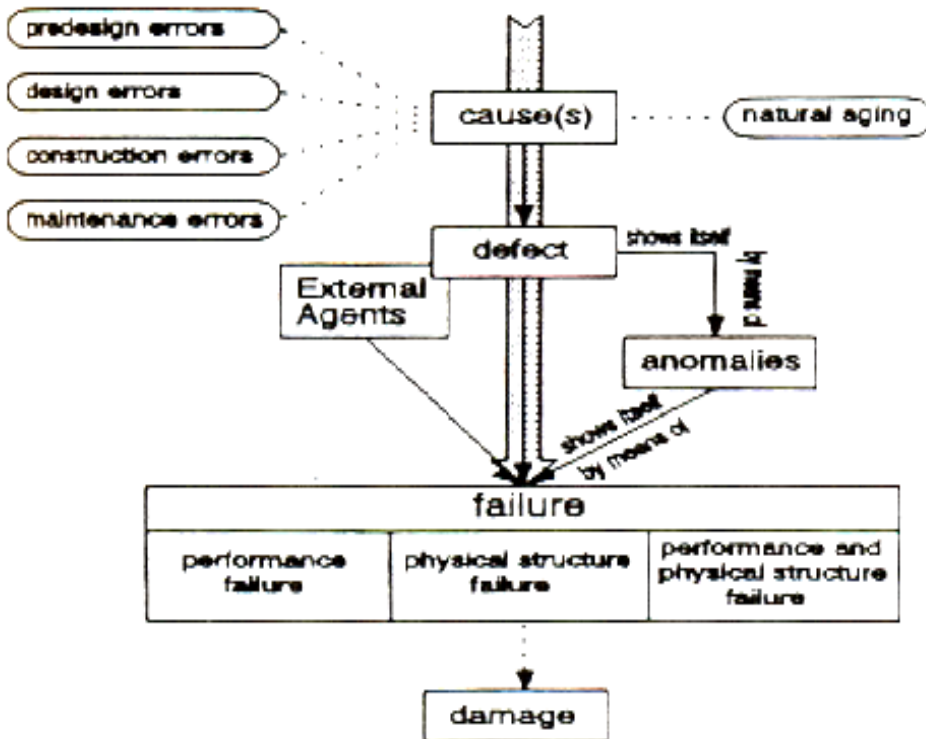


Figure 5. The decay process

The decay process needs time to develop and it does not immediately cause components to pass from a performance to a failure condition. This is highly relevant to the possibility of planning maintenance strategies with a preventive purpose. Anomalies mostly manifest themselves before the final failure occurs. Then the anomaly becomes a sort of symptom, which points at one or more (possible) defects. Therefore, to study anomalies seems to be an easier way to set up a maintenance programme than to base it on the knowledge of time-dependent parameters of reliability, duration of service life, 'mean time between failure', etc. which is harder to obtain.

5. Conclusions

So, if on one hand the correct diagnosis of an occurred failure is an important condition to carry out an effective emergency maintenance strategy, the possibility of a correct acknowledgement of anomalies - when the failure has not yet occurred - is fundamental to preventive maintenance planning. Finally, as a consequence of the failure, the (economic) damage appears at the end of the process.

References

1. ADDLESON. L., **Building Failures: A Guide to Diagnosis, Remedy and Prevention**, '2nd Ed., The Architectural Press, Ltd., London, England, 1989
2. American Society of Civil Engineers, **Performance of Constructed Facilities**, Vol. 1, No. 1, February 1987; Vol. 2, No. 2, May 1988, ISSN 0887-3828 CODEN: JPCFEV
3. American Society of Civil Engineers, Research Council on Performance of Structures, **Structural Failures: Modes, Causes, Responsibilities**, ASCE, New York, NY, 1973
4. American Society of Civil Engineers, Research Council on Performance of Structures, **Guide to Investigation of Structural Failures**, ASCE, New York, NY, 1979
5. DIB, A., J.K. GRANT, **1985 Legal Handbook for Architects, Engineers & Contractors**, Clark Boardman Co., Ltd., 1985
6. DiPASQUALE, R., **Building Failures Forum**, Vol. 1, No. 1, October 1980, Vol. 1, No. 6, June 1981
7. DiPASQUALE, R., **Building Failures Briefs**, Vol. 1, No. 1, September 1983, Vol. 1, No. 6, February 1984.

ON THE SOLUTION OF THE STIFF SYSTEMS OF EQUATIONS

Octavian V. Roșca¹,

Abstract

The Structural Dynamics involve a large amount of computational effort. Most dynamic structural models require the solution of a set of 2nd order differential equations. The solution methods are divided into the modal superposition (this requires the modal analysis; thus the method becomes unusable in case of the nonlinear systems – the K – stiffness matrix is a variant in time coordinate) and the direct integration techniques.

There are developed integration techniques for the 1st order and 2nd order differential equations. The 2nd order set of equations is submitted to a transformation [12] in order to obtain the first order system.

This paperwork deals with the "stiff" systems of (1st order) differential equations. From the physical point of view the stiff system consists of two components – one with a fast dynamic behavior and the other one, slow. By ignoring the high frequency component may lead to wrong results.

There are presented some advanced solution methods, criteria for choosing the appropriate techniques and a case study.

KEYWORDS: Numerical Methods, Dynamic Analysis

¹ Structural Mechanics Department, TU “Gh. Asachi”, Iași, 700050, Romania

1. Introduction

From the physical point of view the stiff system consists of two components – one with a fast dynamic behavior and the other one, slow. By ignoring the high frequency component may lead to wrong results.

Let us consider the following system of equations [2] where x_1 and x_2 are time (t) variables:

$$\begin{cases} x_1' = 998 \cdot x_1 + 1998 \cdot x_2 \\ x_2' = -999 \cdot x_1 - 1999 \cdot x_2 \end{cases} \quad (1)$$

and the initial conditions:

$$x_1(0) = 1 \quad x_2(0) = 0 \quad (2).$$

By changing the variables

$$x_1 = 2y - z \quad x_2 = -y + z \quad (3)$$

the solution is obtained

$$\begin{cases} x_1 = 2 \cdot e^{-t} - e^{-1000 \cdot t} \\ x_2 = -e^{-t} + e^{-1000 \cdot t} \end{cases} \quad (4).$$

In [12] there are extensively presented many methods for the solution (i.e. single step techniques, like Euler, 2nd and 4th order Runge-Kutta, Fehlberg, the Richardson extrapolation and the Bulirsch-Stoer method; also multistep methods: Adams-Bashford, Rosenbrock and Shampine) of the system (4).

If one uses un-avoided the previously mentioned methods to integrate the system (1), the term that contains the $e^{-1000 \cdot t}$ needs an integration time step with a length of $h \ll 1/1000$ to obtain the stability. This phenomenon occurs even the value of $e^{-1000 \cdot t}$ can be completely neglected for the computation of x_1 and x_2 immediately near the 0 point, as is depicted in the Fig. No. 1.

This is the disadvantage of the stiff systems of equations – we are obliged to follow the solution path by taking into account the smallest step in order to achieve the stability – although the final solution can be obtained by an algorithm with a bigger time step.

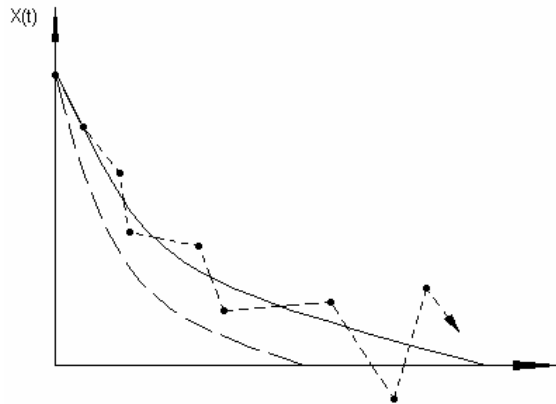


Figure No. 1. The instability phenomenon that occurs during the integration of stiff equations.

In the Fig. No. 1 it is depicted the solution of such a differential equation, consisting of two components, one marked with solid line and the other with a dotted line. The solution stability depends on the dotted line, that converges faster to 0.

2. The Solution Techniques

In the Fig. No. 2 it is presented the Simulink model of this problem (1) with the solution provided by (4), by the means of the Matlab programming environment. Although on the entire domain the solution behaves well, in the vicinity of the start point some numerical problems occur, as it can be noticed in the zoom window of the 0... 0,1sec.

In order to find out the solution there is considered the case of a single equation

$$x' = -p \cdot x \quad (5)$$

where $p > 0$ is a constant coefficient. The explicit Euler integration scheme for (5) – with constant time step h is:

$$x_{n+1} = x_n + h \cdot x'_n = (1 - p \cdot h) x_n \quad (6).$$

The method becomes unstable if $h > 2 / p$, because in this case $|x_n| \rightarrow \infty$ as $n \rightarrow \infty$.

The simplest method for the solution in this case is the implicit integration, in which the right-hand side is evaluated at the new location, x . We apply the backwards Euler scheme:

$$x_{n+1} = x_n + h \cdot x'_{n+1} \tag{7}$$

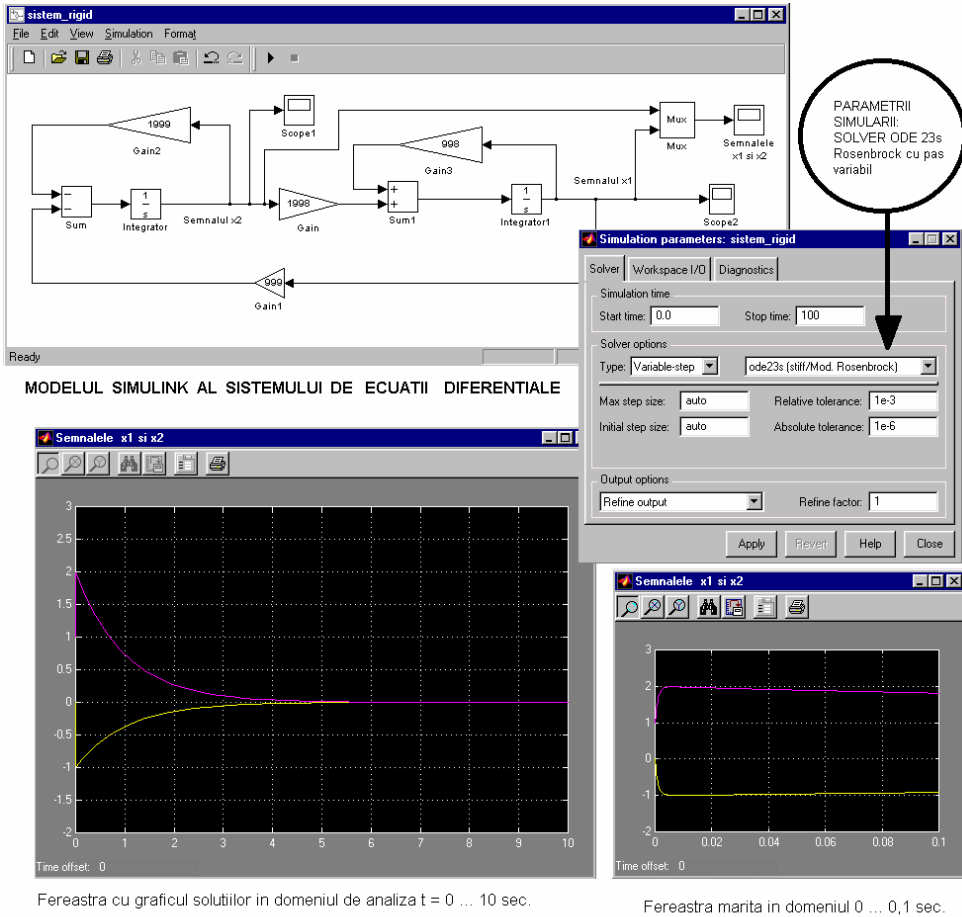


Figure No. 2

or:

$$x_{n+1} = \frac{x_n}{1 + p \cdot h} \tag{8}$$

The method is unconditionally stable even $h \rightarrow \infty$, $x_{n+1} \rightarrow 0$ and this is the correct solution of the differential equation; if we analyze the physical/ mechanical phenomenon the implicit method converges to the real solution – the equilibrium. This important feature of the implicit methods is applicable only to the linear systems, but also in the general case the implicit methods offer a better stability.

This is the case of the implicit methods with the 1st order of precision. To solve the stiff systems of equations one may use some methods provided with higher orders of precision. There are 3 major classes of higher order integration techniques for the stiff systems:

- Generalizations of the Runge-Kutta method, from which the best is the Rosenbrock method. The first implementations were carried out by Kaps and Rentrop;
- generalizations of the Bulirsch-Stoer method, particularly the semi-implicit Bader and Deuffhard extrapolation method;
- The predictor-corrector methods, most of them derived from the Gear differentiation method.

There will be discussed the implementations of the first two classes. The systems of equations are depending explicitly of time t on the right-hand side $f(X, t)$; they are transformed by adding t to the variable vector

$$\begin{pmatrix} X \\ t \end{pmatrix}' = \begin{pmatrix} f \\ 1 \end{pmatrix} \quad (9).$$

It is very important to scale correctly the variables from the stiff systems. Like the case of the common systems, it has to be taken a vector X_{scal} in order to scale the errors. For instance, to obtain constant errors in a fraction format, X_{scal} is scaled by $|X|$. In rigid problems often appear components of the solution that decay fast so can be eliminated. It is advisable to control the relative error from P , a possible way is to apply a limit value such as:

$$X_{scal} = \max(P, |X|) \quad (10).$$

The Rosenbrock methods are easily implemented. They are recommended for the systems that need a medium precision for the solution ($\varepsilon \leq E-4 \dots E-5$ in the error criterion) and for small sizes (10 equations). In case of large systems the semi-implicit extrapolation methods are recommended.

The Rosenbrock method proposes a solution of the following form:

$$X(t_0 + h) = t_0 + \sum_{i=1}^s c_i \cdot k_i \quad (11)$$

where the correction factors k_i are found by solving of "s" linear equations that generate:

$$(1 - \gamma h f') \cdot k_i = h f \left(X_o + \sum_{j=1}^{i-1} \alpha_{ij} k_j \right) + h f' \sum_{j=1}^{i-1} \gamma_{ij} k_j, \quad i = 1, \dots, s \tag{12}$$

By f' was denominated above the Jacobi matrix. The γ , c_i , α_{ij} and γ_{ij} coefficients are independently constants having fixed values for a given problem. If $\gamma = \gamma_{ij} = 0$, then the method becomes a classical Runge-Kutta. The equations (12) can be successively solved for k_1, k_2, \dots .

The main element that leads to the good result is the algorithm for the automatic adjustment of the step size. Kaps and Rentrop [17] proposed an optimized Runge-Kutta-Fehlberg method that lies on the computation of two estimators for (11), a “real” X and one of a smaller order \hat{X} , that have the coefficients $\hat{c}_i, i = 1, \dots, \hat{s}$ with different values, where $\hat{s} < s$ and the k_i coefficients are the same. The difference between X and \hat{X} leads to the estimation of a round off error, that can be used as control parameter for the length of the time step. Kaps and Rentrop showed that the smallest value for s that improves the solution is $s = 4$ and $\hat{s} = 3$. These values lead to a IVth order numerical method. In order to reduce to minimum the number of matrix products between the matrices and vectors of the right side of (12), the equations are re-write in terms of

$$g_i = \sum_{j=1}^{i-1} \gamma_{ij} k_j + \gamma k_i \tag{13}$$

The equations are now:

$$\begin{aligned} (1/\gamma h - f') \cdot g_1 &= f(X_o) \\ (1/\gamma h - f') \cdot g_2 &= f(X_o + a_{21} \cdot g_1) + c_{21} \cdot g_1 / h \\ (1/\gamma h - f') \cdot g_3 &= f(X_o + a_{31} \cdot g_1 + a_{32} \cdot g_2) + (c_{31} \cdot g_1 + c_{32} \cdot g_2) / h \\ (1/\gamma h - f') \cdot g_4 &= f(X_o + a_{41} \cdot g_1 + a_{42} \cdot g_2 + a_{43} \cdot g_3) + (c_{41} \cdot g_1 + c_{42} \cdot g_2 + c_{43} \cdot g_3) / h \end{aligned} \tag{14}$$

Kaps and Rentrop offered two sets of parameters which provide different stability characteristics. There are provided also other sets, which a very used one is that of Shampine [18] and is implemented in the MATLAB / SIMULINK Software; the coefficients are presented in Table No. 1.

The semi-implicit extrapolation method is applied instead of the Bulirsch-Stoer method (that partitions the differential equation by the modified midpoint rule) that doesn't work for stiff problems. Bader and Deuflhard [19] discovered a semi-implicit partition that works very well and leads to an extrapolation just like in the case of the Bulirsch-Stoer method.

Table No. 1

The coefficients implemented by Shampine for the Rosenbrock method	
γ	0.5
a_{21}	2.0
a_{31}	48.0 / 25.0
a_{32}	6.0 / 25.0
c_{21}	-8.0
c_{31}	372.0 / 25.0
c_{32}	12.0 / 5.0
c_{41}	-112.0 / 125.0
c_{42}	-54.0 / 125.0
c_{43}	-2.0 / 5.0
b_1	19.0 / 9.0
b_2	1.0 / 2.0
b_3	25.0 / 108.0
b_4	125.0 / 108.0
e_1	17.0 / 54.0
e_2	7.0 / 36.0
e_3	0.0
e_4	125.0 / 108.0
C_{1x}	1.0 / 2.0
c_{2x}	-3.0 / 2.0
c_{3x}	121.0 / 50.0
c_{4x}	29.0 / 250.0
a_{2x}	1.0
a_{3x}	3.0 / 5.0

The start point is represented by an implicit formula of the midpoint rule:

$$X_{n+1} - X_{n-1} = 2h f\left(\frac{X_{n+1} + X_{n-1}}{2}\right) \quad (15)$$

The eq. (15) is converted in the semi-implicit form by the linearization of the right side around of $f(X_n)$. The result is the semi-implicit rule of the midpoint:

$$\left[1 - h \frac{\partial f}{\partial X}\right] \cdot X_{n+1} = \left[1 + h \frac{\partial f}{\partial X}\right] \cdot X_{n-1} + 2h \left[f(X_n) - \frac{\partial f}{\partial X} \cdot X_n\right] \quad (16)$$

In this method a special value is used for the first step size, which is the value from the semi-implicit Euler method and a step with a re-calculated step size where the last X_n is replaced by:

$$\bar{X}_n = \frac{1}{2}(X_{n+1} + X_{n-1}) \quad (17).$$

Bader and Deuffhard demonstrated that the error series involve only even powers of h . For the simplification of the programming process it is recommended the re-

writing of the above eqs. using $\Delta_k \equiv X_{k+1} - X_k$. Considering $h = H / m$, the integration process starts with:

$$\Delta_0 = \left[1 - h \frac{\partial f}{\partial X} \right]^{-1} \cdot h \cdot f(X_0) \tag{18}$$

$$X_1 = X_0 + \Delta_0$$

Then, for $k = 1, \dots, m-1$ one calculates:

$$\Delta_k = \Delta_{k-1} + 2 \left[1 - h \frac{\partial f}{\partial X} \right]^{-1} \cdot [h \cdot f(X_k) - \Delta_{k-1}] \tag{19}$$

$$X_{k+1} = X_k + \Delta_k$$

Finally:

$$\Delta_m = \left[1 - h \frac{\partial f}{\partial X} \right]^{-1} \cdot [h \cdot f(X_m) - \Delta_{m-1}] \tag{20}$$

$$\bar{X}_m = X_m + \Delta_m$$

The sequence for the computation of the time step lengths:

$$n = 2, 6, 10, 14, 22, 34, 50, \dots \tag{21}$$

where each member differs from its predecessor by the smallest multiple of 4 that makes the ratio of the successive terms be $\leq 5/7$.

3. Case-study

We consider a simple case of a SDOF dynamic system in free damped motion, with the following law of motion:

$$\ddot{x} + 100 \dot{x} + 0.9999 x = 0 \tag{22}$$

and initial conditions $x(0) = 1, \dot{x}(0) = 0$. For the system with the governing eq. (22) the SIMULINK model is shown in Fig. no. 3. The above equation is transformed from the t-space into s-space by the means of the Laplace transform, where by $X(s)$ was denoted the Laplace transform of $x(t)$, $X(s) = L \{ x(t) \}$:

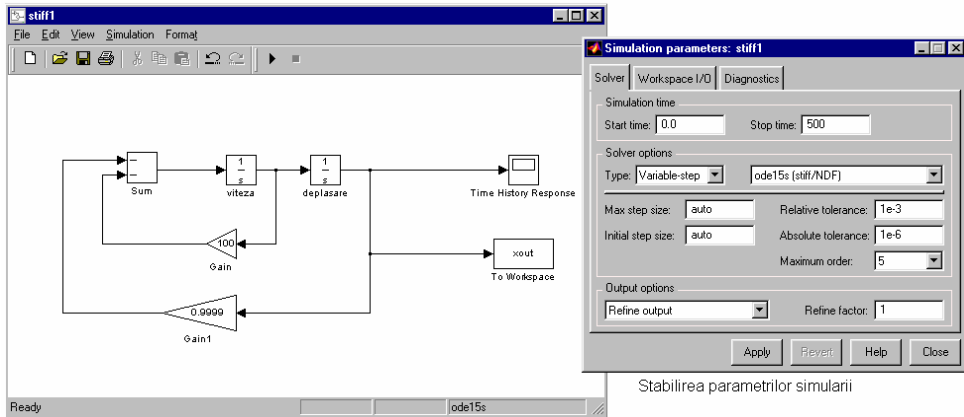
$$s^2 X(s) - s x(0) - \dot{x}(0) + 100 s X(s) - 100 x(0) + 0.9999 X(s) = 0 \tag{23}$$

The transfer function of the system becomes:

$$H(s) = \frac{1}{s^2 + 100s + 0.9999} \tag{24}$$

and the output in the s-space is

$$X(s) = H(s) \cdot (s + 100) \tag{25}$$

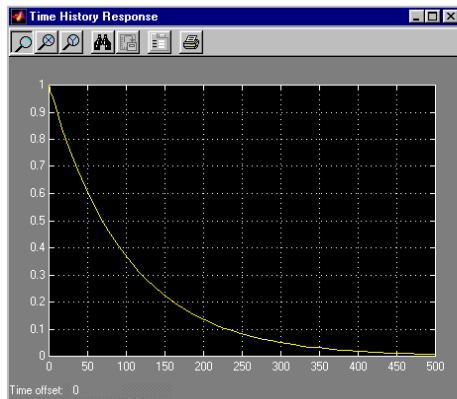


Modelul SIMULINK al unui sistem rigid de ordinul al II - lea

Stabilirea parametrilor simulării

Fixarea condițiilor inițiale

Răspunsul în timp al deplasărilor - algoritmul de integrare ODE 15 S



Oscilația soluției rezultată în urma utilizării algoritmului ODE 45

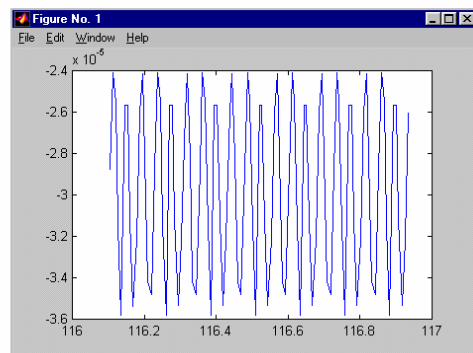


Figure No. 2 The oscillation of the “stiff” system solution.

After applying the inverse Laplace transform one obtains the solution:

$$x(t) = +1.0001e^{-0.01t} - 0.0001e^{-99.99t} \tag{26}$$

The system response has two components. The first component has a magnitude of 4 orders greater than the second one but also decays 10000 times slower. The second member has a much smaller magnitude (0.0001) and decays fast. Thus, the slower response has the predominant role.

Let us focus on the Simulink model from Figure No. 3, in which are depicted the model and the initial conditions. The Integrator block has the Initial condition set on 0 and the Integrator block for displacement has the Initial condition value of 1 set on the Dialog box. In the Simulation Parameters block the start time is set to 0 and stop time is set to 500. It was used an “xout” transfer block of the output parameters to the Matlab workspace. The simulation has the goal the analysis of several integration algorithms for the 1st order differential equations, implemented for the solution of these "stiff" systems.

4. Results. Conclusions

Initially, the simulation was performed with the ODE 15S routine. The result is very quickly obtained, in few hundredths of seconds (CPU time). The output vectors to Matlab contain approximately 150 elements, computed at the automatically fixed time steps. If the model is run by using an ODE 23S integrator, designed on the basis of the Rosenbrock method, the runtime is reduced to 0,002 sec. The results are presented in the Table No. 2.

Table No. 2

The runtimes of several Matlab routines involved in the model analysis		
Routine (solver)	Time step Size	Run Time CPU Time (seconds)
ODE 23 S (Rosenbrock method)	variable, automatically adaptive	0.002
15 S	variable, automatically adaptive	0.06
23 S (stiff systems – trapezoidal)	variable, automatically adaptive	0.06
ODE 45 (Dormand – Prince)	variable, automatically adaptive	3.30
ODE 113 (Adams-Bashford)	variable, automatically adaptive	4.29
ODE 4 (Runge-Kutta of IV th order)	4 sec., fixed	Error – Divergent Analysis
ODE 4 (idem)	0,01 sec., fixed	5.38

The Simulink software uses the ODE 45 routine as the implicit integrator (based on the Dormand – Prince algorithm). After the computation with this routine one may notice the same output window (in the complete time domain 0, ..., 500 sec) like in the case of ODE 23 S. Unlike in the other case, the run is performed in 3,30 sec. and the automatically adjusted time step produces the output vectors with 15,000 elements.

A zooming window of 1 sec. length was selected, depicted in the bottom-right corner of the Figure No. 3. In comparison to the bottom-left frame, that shows the global response, one may notice a high frequency component (with a fast dynamic) in the response trajectory, of a 10^{-5} order magnitude. This proves the fact that the performances of such a kind of analysis are highly dependent on an adequate solution algorithm.

Finally, a mention regarding the inappropriate choice of an ODE 4 solver with a fixed time step (which is the 4th order Runge-Kutta algorithm with fixed step) leads to the collapse. For this model, the setting of a 4s time step which is equivalent to 125 time steps for analysis (equal to the number of the used time steps by the Rosenbrock ODE 23 S algorithm) produces the divergence. The simulation is stopped and an error message is produced (caused by the singularity). The numerical experiments evidenced that the Runge-Kutta routine needs a time step of 0,01s to attain the convergence.

References

1. L. Collatz, *The Numerical Treatment of Differential Equations*, Springer-Verlag, N.Y., 1966.
2. S. H. Crandall, *Engineering Analysis*, Mc-Graw-Hill Book Company, New York, 1956.
3. C. E. Fröberg, *Introduction to Numerical Analysis*, Addison-Westley Publishing Company, Inc., Reading, Mass., 1969.
4. B. C. Kuo, *Automatic Control Systems*, Englewood Cliffs, N.J., Prentice Hall, 1995.
5. J. Dabney, *The Student Edition of SIMULINK – Dynamic System Simulation for Matlab*, Prentice-Hall, 1998.
6. Gh. Dodescu, M. Toma, *Metode de Calcul Numeric*, EDP, București, 1976.
7. Ion Nistor, *Analiză Numerică*, UT “Gh. Asachi” Iași, 1997.
8. M. Abramowitz, I. A. Stegun, *Handbook of Mathematical Functions*, Appl. Math. Series, Vol. 55, 1964.
9. W. Gear, *Numerical Initial Value Problems in Ordinary Differential Equations*, Englewood Cliffs, NJ, 1971.
10. L. Shampine, H.A. Watts, *Mathematical Software III*, Appl. Math. and Comp., vol. 5, pp. 257-275, 1979.
11. J.R. Rice, *Numerical Methods, Software and Analysis*, McGraw-Hill, NY, 1983.
12. O. Roșca, *Optimizarea programelor de calcul al structurilor supuse acțiunilor dinamice și seismice*, teză de doctorat, UT “Gh. Asachi”, Iași, 2002.
13. J. Stoer, R. Bulirsch, *Introduction to Numerical Analysis*, Springer-Verlag, NY, 1980.
14. G. E. Forsythe, M. Malcolm, C. Moler, *Computer Methods for Mathematical Computations* (Englewood Cliffs, NJ, Prentice-Hall, 1977).
15. J. R. Cash, A. Karp, *ACM Transactions on Mathematical Software*, vol. 16, pp. 201-222, 1990.
16. P. Deuffhard, *SIAM Review*, vol. 27, pp. 505-535.
17. P. Kaps, P. Rentrop, *Numerische Mathematik*, vol. 33, pp. 55-68.
18. L. F. Shampine, *ACM Transactions on Mathematical Software*, vol. 8, pp. 93-113.
19. G. Bader, P. Deuffhard, *Numerische Mathematik*, vol. 41, pp. 373-398, 1983.
20. L. F. Shampine, M.W. Reichelt, *The MATLAB ODE Suite*, The Mathworks, Inc., Natick, Massachusetts, 1996, www.mathworks.com

INELASTIC TIME–HISTORY ANALYSIS OF ONE DEGREE OF FREEDOM SYSTEM UNDER SEISMIC MOTIONS

Violeta–Elena CHIȚAN¹, Doina ȘTEFAN²

Abstract

A research program intended to investigate the dynamic and seismic nonlinear inelastic behaviour, useful for reinforced concrete structures acted beyond the elastic limits has been started since 1968 in the Building Research Centre from Iasi. A special attention has been devoted to the hysteretic behaviour, to the evolution of energy dissipation in different steps of the time-history. Experimental investigations have been undertaken by means of a set of shaking tables of small, average and large capacities and other actuators. In the present paper, based on the experimental tests and earthquake–like simulations, some results of a study concerning the influence of the main parameters on the inelastic response—especially of the energy dissipation factors are discussed. The analysis has been made taking into account the model configuration, the slope ratios of loading and unloading branches of the hysteretic loops, the combined viscous and the hysteretic Penzien type damping factors, different seismic actions, and other parameters. The analysis has been carried out on an equivalent inelastic one–degree–of–freedom system with variable characteristics (as natural period, stiffness ratios, ductility factors, type of yielding hysteretic loop model, a.s.o.). The present paper is restricted only to some aspects concerning the damping force variation and spectral values response.

1. Introduction

In order to select the main parameters which are relevant in the time–history response of a structure subjected to a set of eight earthquake–like motions and harmonic actions, the authors have considered an equivalent yielding one degree of freedom system provided both with viscous Voigt damping and also with a proportional with displacement Penzien type of dissipation. In this way, a combined damping force, proportional with the velocity and with the displacement, in different rates, could be taken into account. In an attempt to estimate the major factors interfering in the inelastic response of the mono–massic structure and their influence on the peak values of the dynamic and seismic inelastic response, the study has been restricted to a few number of natural periods and damping values, slope ratios of the loading and unloading branches, inelastic configurations of the hysteresis loops, coefficient of post-elastic solicitation, and other relevant

¹ Lecturer, Ph.D., Technical University of Iasi, Romania

² Assoc. Prof., Technical University of Iasi, Romania

parameters. Nevertheless, the range of the considered parameters proved to be in good agreement with the most frequently encountered reinforced concrete buildings subjected to seismic excitations stressed beyond the elastic limits. The simulated excitations comprise accelerograms of some major earthquakes recorded in our country and abroad, which are specific for areas revealing strong tectonic activity. For comparison, a sinusoidal excitation with a reference $2c/s$ frequency, which was modelled in order to obtain other values of the circular frequency by changing the time scale, has been also included.

2. Research Programme

In order to investigate the influence of the type of seismic motion, natural period, damping of the one degree of freedom system, also the influence of shape and other characteristic elements of the hysteretic loop, a number of 400 runs have been undertaken trying to draw some conclusions about the inelastic response of the single degree of freedom equivalent system throughout the time-history of the dynamic action. The seismic motions with their main characteristics are listed in Table No.1, inclusively the harmonic sinusoidal action. The duration, the time step, the number of discrete points and the peak accelerations of the earthquake motions are also presented in that table.

Tabel. 1. The seismic motions

No. crt.	Naming	Description of Earthquake	Duration (s)	No. of points	Δt (s)	$\left \ddot{x}_0^{max} \right $ (cm/s^2)
0	1	2	3	4	5	6
1	BucNS	Bucharest, March 4, 1977, component NS	40.1	4010	0.01	194.927
2	BucEW	Bucharest, March 4, 1977, component EW	7.8	780	0.01	163.087
3	El Centro	El Centro, May 18, 1940, S00E	53.76	2688	0.02	341.7
4	Mexico	Mexico City, Sept. 19, 1985, SCT Station, S60E	120	9006	0.02	167.918
5	Sin	Harmonic Action with 2 Hz frequency	10	1000	0.01	200
6	BNS	Bârlad, Aug. 30, 1986, component NS	7.8	780	0.01	165
7	El Centro	El Centro, California, May 18, 1940, S90W	53.48	2674	0.02	210.1
8	Mexico S60E	Mexico City, Sept. 19, 1985, SCT Station, S60E	120	9006	0.02	97.965

The runs have been undertaken with a program elaborated especially for this purpose. This program succeeded to simulate the seismic and non-seismic response of the response spectra in elastic and inelastic range considering a number of three hysteretic models: bilinear elastic-perfectly plastic behaviour, bilinear hysteretic Clough (Qhyst) model with degrading behaviour $\alpha \neq 0$, bilinear non-degrading hysteretic Clough model $\alpha = 0$, and elastic model without plastic deformations. Since the number of parameters defining the inelastic structural

response in the time history of the motion is rather large, in the present analysis only a restricted number of parameters, which are relevant in the study, have been considered /2, 3/.

The hysteretic models are shown in Figs 1 and 2.

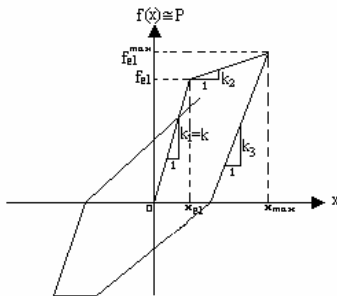


Figure 1– The bilinear Q_{hyst} model with degradation

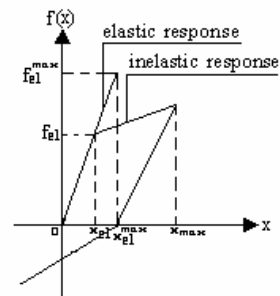


Figure 2 – The bilinear non-degrading inelastic Clough model

Most part of the tested structures have been cast-in-place and prefabricated reinforced concrete structures, scaled to 1/2 and 1/5 sizes, but also some of them have been constructed full-scale. Incidentally, metal structural models have been also investigated, finally concluding that results are in good agreement with the analytic response in displacements, velocities and accelerations. We mention that, in the last case, the use of Ramberg–Osgood two parametric curves lead to a close coincidence.

The selected variable parameters adopted in the study are the following:

- A number of four natural periods of the one degree of freedom oscillator in the $(0.5 \div 2.0)s$ range
- A number of two types of damping ratios: the "classical" equivalent viscous damping fraction proportional with velocity (Voigt damping component) and another damping component, proportional with the displacement of Penzien type, which have been considered in different proportion
- The slope or stiffness of the post-elastic loading (ascending) branch of the hysteretic relation
- The slope of the unloading or descending branch at load reversal
- The configuration of the elastic-plastic model, of Clough and Q_{hyst} type. In such a way, the inelastic models simulate the non-degrading and also the degrading behavior
- The harmonic SIN excitation in the range from 0.10 up to 2.0 sec.

In most of the undertaken runs, for every type of model and earthquake, some constant parameters have been maintained constant, such as: the mass value, the design seismic peak acceleration, the time increment, the limit elastic force (which

must be smaller than the reference elastic force, the initial velocity $v_0 = 0$ and the elastic solicitation factor:

$$\mu_0 = \frac{f_{el}}{m \cdot a_0^{\max}} \quad (1)$$

For the same seismic or harmonic action, the value of parameter μ_0 expressing the ratio between the limit elastic force and the maximum elastic seismic force is constant. The resulting variable response elements are following: the Fourier spectrum, the maximum velocity, the natural period T , the maximum elastic force, the post-elastic excursion factor $\mu_1 < 1$, the maximum spectral values of displacement, velocity, acceleration, the variation of damping force and of the restoring force during the time-history of the motion. The limit elastic force has been arbitrarily adopted, as a study case, equal to 1000 daN. As a rule, the smaller is the ratio μ_0 , the greater will result the degree of degradation of the structure, the more advanced will be the level of damage. On the contrary, if this parameter is greater, we are situated in the neighbourhood of the elastic behaviour, corresponding to purely viscous damping, without the damping component, which is proportional with the displacement. The values of linear spectral response are not depending upon the slope of the ascending branch k_2 . The incremental time is:

$$\Delta t \leq \frac{T}{50} \quad (2)$$

The numerical analysis is made for 1000 points. The sine force has been simulated in the program by a sinusoidal reference frequency of $2c/s$ which can be converted also to other input frequencies. For this purpose, different values of the incremental time Δt are taken in the analysis, according to discretization goals in order to reach a good accuracy of the numerical analysis.

As it is known, applying the d'Alembert principle, the dynamic equilibrium for the one degree of freedom system with viscous damping is given by:

$$m\ddot{x}(t) + c\dot{x}(t) + kx(t) = -ma_0 \quad (3)$$

In the case of the system featuring inelastic behavior, after reaching the elasticity limits, the function $f(x)$ becomes a variable complex non-linear parameter along the time-history of the motion; as a consequence hysteretic loops are changing their loading and unloading curves. This type of behavior is usually called in the case of seismic actions, low cycle fatigue. Equation (3) can be written under the form:

$$m(\ddot{x} + a_0) + fa + f(x) = 0 \quad (4)$$

where: f_a is the damping force, which can be, as in our case, a combination between the Voigt viscous component and the Penzien type damping proportional with the displacement, taking into account inelastic hysteretic characteristics.

The expression adequate for the present study, in the case of the one degree of freedom system has the form:

$$ma + \frac{v_1 kt}{\pi} v + \pi v_2 k |x| \operatorname{sgn} v + f(x) = 0 \quad (5)$$

Therefore we obtain:

$$\operatorname{sgn} v = \frac{v}{|v|} = \frac{\dot{x}(t)}{|\dot{x}|} \quad (6)$$

The previous relations characterize the inelastic system having combined damping namely:

- viscous Voigt damping;
- damping force of the second type, which is proportional with displacement and in phase with the velocity.

In the solution of the equation system, interferes the *amplitude Fourier spectrum*. If the seismic motion has duration from $\tau = 0$ up to $\tau = t_n$, the amplitude Fourier spectrum is given by the relationship:

$$|F(\omega)| = \sqrt{\frac{2E(t_n, \omega)}{m}} \quad (7)$$

The ductility factor associated to an oscillation cycle is:

$$\mu_i = \frac{x_{\max}}{x_{el}} \quad (8)$$

As for the stiffness decrease, Clough and other authors have assumed for the slope k_3 at load reversal the relationship, where, $\alpha = (0.4 \div 0.5)$:

$$k_3 = k_1 \left(\frac{x_{el}}{x_{\max}} \right)^\alpha \quad (9)$$

In the present analysis, this index has been considered equal to 0.4, valid for usual concrete grade. If $\alpha = 0$ we reach to the bilinear elastic–perfectly plastic model, where $k_3 = k_1$. In that case, load reversal takes place after a line parallel with the linear ascending (loading) line, according to Gerstner assumption.

3. Some Results of the Parametric Analysis

In case of the Bârlad Seismic Motion and in parallel to the period extension (Table No. 2) $T = (0.5 \div 2.0) s$, that is during the interval when the speed controls the intensity of the earthquake (in the areas of medium periods where the intensity of the ground movement is measured through speed) significant lowering of the speed spectrum is ascertained (Fourier Spectrum), irrespective of the value brought by the two absorption parameters ν_1 and ν_2 . The values of the pseudo spectrum speed PSv are close to the values of the spectrum speed Sv , less the case of the equivalent viscous absorption case ($\nu_1 = 15.9\%$), these values remaining the same for $T = 1.0 s$, but smaller then those for $T = 2.0 s$.

The slope of the post elastic branch k_2 and the absorption percentage do not influence the spectral values. These statements have implications in the operating mean of the earthquake intensity as a measure of the seismic movement capacity to damage the structures having an average period. The relative movements present a time history with one way evolution, cumulating significant non elastic deformations with maximum values of $4.16 cm$. This is a characteristic of *low cycle fatigue* process for a reduced number of cycles in one direction.

The force vs. movement diagrams ($F-x$), present an aspect with linear segments and a hysteretic one with curvy lines curves. There are preserved the characteristic aspects with of the time history diagrams according to the share of the viscous absorption ν_1 and Penzien ν_2 (fig. 3). When $\nu_1 = 5\%$ and $\nu_2 = 0\%$ the force vs. movement diagram $F-x$ is of the curvilinear histerezis type and the diagram absorption force vs. movement $P_{dm}-x$ is type of irregular ball with two movement centers.

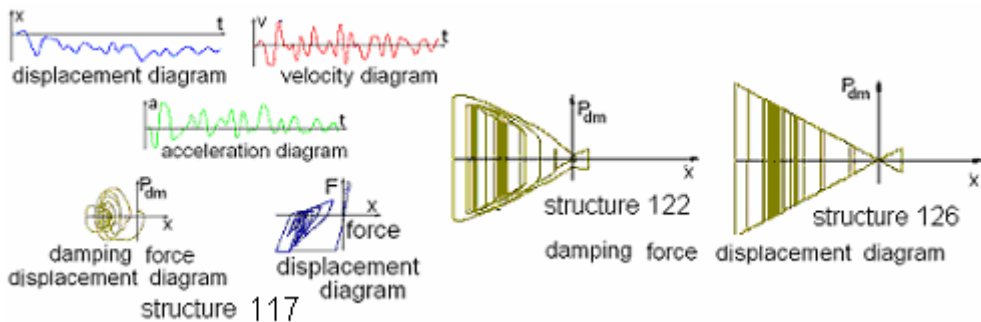


Fig. 3 Inelastic time history for different damping rates Bârlad seismic motion

When $\nu_1 = 5\%$ and $\nu_2 = 0\%$ the force vs. movement diagram $F-x$ is of the curvilinear histerezis type and the diagram absorption force vs. movement $P_{dm}-x$ is type of irregular ball with two movement centers. When $\nu_1 = 0\%$ and $\nu_2 = 5\%$ the hysteretic curves have linear branches.

Nr. crt.	$\sqrt{2E(t)}/m$ (cm/s)	SF	T (s)	k (daN)	V_1 (%)	V_2 (%)	C_1 (daN*s/cm)	C_2 (daN/cm)	k_2 (%)	x_{el}^{max} (cm)	f_{el}^{max} (daN)	μ_1	Sd(T) (cm)	Sv(T) (cm/s)	F_{lim}^{max} (daN)	a_{max} (cm/s ²)	Pd_m (daN)
0	1	2	3	4	5	6	7	8	9	10	11	12	13	14	15	16	17
117	103.15	100.35	0.5	7895.7	5	0	62.832	0	0	2.911	22986.9	0.087	-4.156	12.76	801.97	59.45	-2365.3
118	41.62	38.108	1.0	1973.9	5	0	31.416	0	0	-3.288	-6489.7	0.308	-4.763	-15.86	-498.18	51.93	-2137.5
119	26.61	14.136	1.5	877.3	5	0	20.944	0	0	-3.886	-3408.9	0.587	-3.667	-17.62	-369.08	49.52	-2122.6
120	19.41	14.378	2	493.5	5	0	15.708	0	0	-4.191	-2068.2	0.967	-4.194	-17.83	-280.06	41.01	-2010.8
121	41.62	38.108	1	7895.7	15.9	0	99.903	0	0	-2.599	-5129.4	0.390	-3.332	13.32	1330.64	68.86	2263.7
122	103.15	100.35	0.5	7895.7	2.5	2.5	31.416	620.126	0	2.839	22415.9	0.089	-2.719	12.14	-1779.95	83.97	-2418.6
123	41.62	38.108	1.0	1973.9	2.5	2.5	15.708	155.031	0	-3.325	-6562.7	0.305	-4.297	-16.0	-735.74	58.49	-2204.5
124	26.61	14.136	1.5	877.3	2.5	2.5	10.472	68.903	0	-3.933	-3450.3	0.58	-3.724	-17.97	-356.06	50.10	-2149.1
125	19.41	14.378	2	493.5	2.5	2.5	7.854	38.758	0	-4.09	-2018.4	0.991	-4.09	-18.11	-222.25	43.36	-2000.7
126	103.15	100.35	0.5	7895.7	0	5	0	1240.25	0	2.793	22054.3	0.091	-2.357	-11.65	2923.72	106.14	-2388.9
127	41.62	38.108	1.0	1973.9	0	5	0	310.063	0	-3.367	-6647.0	0.301	-4.03	-16.16	-1249.59	68.78	-2189.4
128	26.61	14.136	1.5	877.3	0	5	0	137.806	0	-3.982	-3493.8	0.572	-3.812	-18.32	525.35	50.88	-2019.0
129	19.41	14.378	2	493.5	0	5	0	77.516	0	-3.964	-1956.2	1.022	-3.964	-18.4	-307.28	45.27	-1956.2
130	103.15	100.35	0.5	7895.7	5	0	62.832	0	15	2.911	22986.9	0.087	-2.434	19.55	1228.17	98.47	-4751.9
131	41.62	38.108	1.0	1973.9	5	0	31.416	0	15	-3.288	-6489.7	0.308	-3.855	-15.52	-487.51	62.98	-2925.2
132	26.61	14.136	1.5	877.3	5	0	20.944	0	15	-3.886	-3408.9	0.587	-3.654	-17.62	-369.08	49.72	-2285
133	19.41	14.378	2	493.5	5	0	15.708	0	15	-4.191	-2068.2	0.967	-4.193	-17.83	-280.06	41.01	-2019.6
134	103.15	100.35	0.5	7895.7	2.5	2.5	31.416	620.126	15	2.839	22415.9	0.089	-2.139	18.35	1421.31	115.02	-4395
135	41.62	38.108	1.0	1973.9	2.5	2.5	15.708	155.031	15	-3.325	-6562.7	0.305	-3.854	-15.69	-708.8	72.13	-2962.3
136	26.61	14.136	1.5	877.3	2.5	2.5	10.472	68.903	15	-3.933	-3450.3	0.58	-3.71	-17.97	-355.84	52.28	-2315
137	19.41	14.378	2	493.5	2.5	2.5	7.854	38.758	15	-4.09	-2018.4	0.991	-4.09	-18.11	-222.25	43.36	-2003.4
138	103.15	100.35	0.5	7895.7	0	5	0	1240.25	15	2.793	22054.3	0.091	1.931	17.26	2395.49	-140.35	4621.8
139	41.62	38.108	1.0	1973.9	0	5	0	310.063	15	-3.367	-6647.0	0.301	-3.855	-15.88	-1195.32	83.95	-3002.4
140	26.61	14.136	1.5	877.3	0	5	0	137.806	15	-3.982	-3493.8	0.572	-3.792	-18.32	522.58	54.75	-2215.1
141	19.41	14.378	2	493.5	0	5	0	77.516	15	-3.964	-1956.2	1.022	-3.964	-18.4	-307.28	45.27	-1956.2
142	103.15	100.35	0.5	7895.7	5	0	62.832	0	30	2.911	22986.9	0.087	2.705	-22.23	-1396.89	-177.93	8692.4
143	41.62	38.108	1.0	1973.9	5	0	31.416	0	30	-3.288	-6489.7	0.308	-3.694	18.57	583.42	75.86	-3656.2
144	26.61	14.136	1.5	877.3	5	0	20.944	0	30	-3.886	-3408.9	0.587	-3.641	-17.62	-369.08	51.4	-2444.1
145	19.41	14.378	2	493.5	5	0	15.708	0	30	-4.191	-2068.2	0.967	-4.193	-17.83	-280.06	41.01	-2028.3

Table 3. Seismic Motion Barlad– Q_{hyst} Model, August, 1986

When $v_1 = v_2 = 2.5\%$ the force vs. movement curve $F-x$ is the non linear hysteresis type and the absorption force vs. movement curve $P_{dm}-x$ is a bow with non linear branches. According to the value of non elastic stress degree μ_1 the value of the limit elastic force, must be recalculated, where from the hysteretic cycles of the cycle begin. In this case the value of the limit elastic force shall be: $f_{el}^{lim} = 2000$ daN.

4. Conclusive Remarks

- The undertaken study has revealed some aspects of the influence of the major parameters interfering in the inelastic timehistory response using an equivalent one degree of freedom system subjected to a set of seismic motions and to a sine excitation with circular frequencies in the usual range of the actual structures.
- Restricting to the configuration of the damping force versus displacement relationship, the influence of the damping is obvious and defines the shape of the obtained diagrams. The butterfly or the bow versus tie shape is visible in all diagrams excepting the case when only classical viscous damping is considered. If the slope of the bilinear inelastic curve changes, the damping force representation is independent of this parameter and also of the natural period, when using Q_{hyst} model.
- In the case when damping rates of the two types are equal, the functions of the damping force display a curvilinear symmetric shape; in the case of pure Penzien type of damping, the outlines of the diagrams are straight lines.

References

1. Șesan, A., D'Albon G., Ciongradi, I., Strat, L., *A New Shaking Table Used to Test Structures at Seismic Actions*, B. I. P. Iași, tom XV(XIX), 1–2, Constr & Arh., pp. 14–22, 1969.
2. Strat, L., Budescu, M., Olaru, D., *A Simple Bilinear Hysteretic Model Featuring Post-elastic Structural Behaviour*. B. I. P. Iași, XXXIII(XXXVII), 1–4, Constr & Arh., pp. 15–20, 1987.
3. Chițan, Violeta–Elena, Strat, L., Murarasu, V., *A Comprehensive Study of Equivalent Hysteretic Viscous Damping in the Post-elastic Range*, B. I. P. Iași, XLVI(L), (3–4), Constr. & Archit., pp. 7–17, 2000.
4. Strat, L., Chițan, Violeta– B. I. P. Iași, XLVII(LI), 1–2, Constr. & Arch., pp. 13–23, 2001.
5. Chițan, Violeta–Elena, Contribuții privind studiul parametrilor unor modele de calcul neliniar și de tip histeretic asupra răspunsului unor structuri supuse la acțiuni statice și dinamice, Ph. D. Diss, Tech. Univ. "Gh. Asachi", Jassy, 2003. (in Romanian)

DEFORMABILITY ANALYSIS OF ROCK FOR HOMOGENIOUS AND DISCONTINUOUS MULTI-CRACK MASSES

Ancuța ROTARU¹, Traian – Dănuț BABOR²

Abstract

The deformation and failure of a rock mass is largely dependent on the presence of geological discontinuities such as cracks or faults. Akira Sato from Kumamoto University, Kurokami, Japan, proposed a Homogenized Multi-Crack Model, in order to estimate the deformability of a rock mass with high crack density. In his model, all cracks are parallel and infinitely arranged at equal intervals in all directions, and the crack pattern around a crack is always the same at any part of the model.

In the case of high crack density the mechanical properties of the rock mass, such as compliance or Young’s modulus, are strongly affected by the mechanical interaction between the cracks, and therefore an evaluation of this interaction is necessary. There are few studies about these problems, especially in the compressive stress field or mixed mode-loading problem. Consequently, all cracks behave the same, and the mechanical properties and fracture process of the model can be estimated from the analysis of a region containing one crack.

Discontinuous Deformation Analysis (DDA) is a method used by Zhou Weiyuan from Tsinghua University, Beijing, China, to analyze the motional law for discontinuous, jointed rock masses. This method has been widely used in engineering practice, but there are still some limitations in both its theory and practical application. Some good results were obtained and played a significant role in designing the systems of support stabilization and the sequence of work.

Joints, faults and other discontinuities, which control the failure and sliding of the masses, always dissect rock masses. The discontinuous deformation model provides the most rational way to analyze such geotechnical problems. The commonly used discontinuous numerical methods include: Discrete Element Method, Rigid-Block Spring Method, Fast Lagrangian Analysis of Continua, Contact-Spring Model and Discontinuous Deformation Analysis (DDA).

The DDA method provides the theoretical basis for a numerical model of rock block systems, and a more convenient approach in numerical analyses. This method was developed to compute stress, strain, sliding and opening of rock blocks; rigid body movement and deformation occurred simultaneously. Input data

¹ Ph.eng, „Gh.Asachi” Technical University of Iași, Romania, arotaru@ce.tuiasi.ro

² Lecturer, „Gh.Asachi” Technical University of Iași, Romania, babor@ce.tuiasi.ro

consist of block geometry, loading forces, the deformability constants Young's modulus E and Poisson ratio ν , and the restraint or boundary conditions of the block system. The output of such analyses includes the movements, deformations, stresses and strains of each block, and the sliding and detachment, or rejoining of blocks.

1. Introduction

The Homogenized Multi-Crack Model is proposed in order to estimate the deformability of a rock mass, which has a high crack density. The effective compliance of this model is estimated by applying the 2-Dimensional Displacement Discontinuity Method (2D-DDM) (Crouch, 1983) and linear fracture mechanics. The influence of the mechanical interaction of each crack towards the effective compliance is also discussed. It was found that the deformability of the model in the direction normal to the cracks is strongly affected by crack length, crack intervals in the normal direction of cracks and crack patterns.

2. Homogenized Multi-crack Model

The homogenized multi-crack model is shown in Figure 1. In this model all cracks are parallel and present in an isotropic and linear elastic medium. Each crack has a length of $2a$, an interval of $2w$ in the x -axis direction, an interval of $2h$ in the direction normal to each crack, and all cracks are inclined at an angle θ to the y -

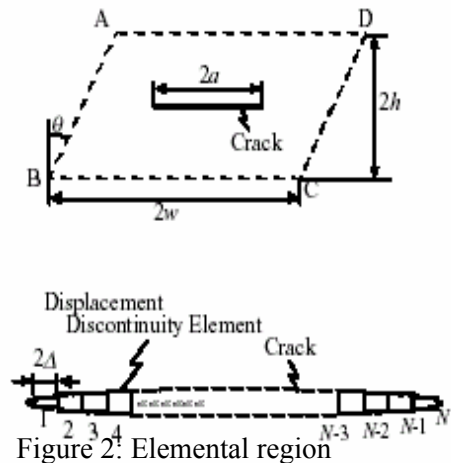
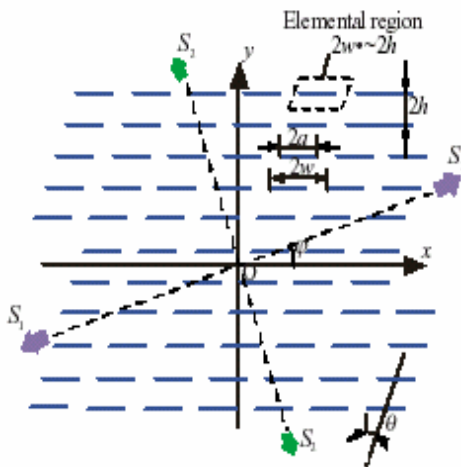


Figure 1: Homogenized multi-crack model

Figure 3: Displacement discontinuity elements on the crack line.

axis.

The characteristic of this model is that the cracks are arranged in a uniform pattern. Consequently, the displacement of each crack and the stress distribution around each crack are the same. An evaluation of the macroscopic strain field is possible by estimating the displacement distribution of a representative crack in the elemental region (Figure 2).

In the model, the relationship between far field stress state $(\sigma_{xx}^0, \sigma_{yy}^0, \tau_{xy}^0)$ and macroscopic strain $(\epsilon_{xx}^0, \epsilon_{yy}^0, \gamma_{xy}^0)$ is given by using effective compliance $\beta_{xx\ xx}, \beta_{xx\ yy}, \dots, \beta_{xy\ xy}$.

$$\epsilon_{xx}^0 = \beta_{xx\ xx} \sigma_{xx}^0 + \beta_{xx\ yy} \sigma_{yy}^0 + \beta_{xx\ xy} \tau_{xy}^0 \tag{1}$$

$$\epsilon_{yy}^0 = \beta_{yy\ xx} \sigma_{xx}^0 + \beta_{yy\ yy} \sigma_{yy}^0 + \beta_{yy\ xy} \tau_{xy}^0 \tag{2}$$

$$\gamma_{xy}^0 = \beta_{xy\ xx} \sigma_{xx}^0 + \beta_{xy\ yy} \sigma_{yy}^0 + \beta_{xy\ xy} \tau_{xy}^0 \tag{3}$$

3. Application of 2D-DDM and Homogenization

HMCM consists of groups of displacement discontinuity elements. Each element has a length of 2Δ and uniform shear and normal displacements (D_s, D_n). Each crack, with length $2a$, is expressed by N number of elements (Figure 3), which approximate smooth crack surface displacement. Therefore, it is necessary to have as many elements as possible on the crack line to obtain accurate crack surface displacement.

Let us denote the displacement discontinuity of the j -th element on the i -th crack as $(D_{s\ ij}, D_{n\ ij})$. The vector $\{D_i\}$, which consists of displacement discontinuity components of the i -th crack is defined as

$$\{D_i\}^T = \{D_{s\ i1}, D_{n\ i1}, D_{s\ i2}, D_{n\ i2}, \dots, D_{s\ iN}, D_{n\ iN}\} \tag{4}$$

As stated above, all cracks deform uniformly and the stress distribution around each crack is the same. Therefore, the vectors of displacement discontinuities $\{D_i\}$ are equal and the number of displacement discontinuities, as unknown quantities become $2N$. Stress components acting on each element can be expressed as the displacement discontinuities. Let us denote the shear stress and normal stress acting on the j -th discontinuity element on the i -th crack as $(\tau_{sij}, \sigma_{nij})$. The stress vector, which consists of stress components of the i -th crack, is defined as

$$\{\sigma_i\}^T = \{\tau_{s\ i1}, \sigma_{n\ i1}, \tau_{s\ i2}, \sigma_{n\ i2}, \dots, \tau_{s\ ij}, \sigma_{n\ ij}, \dots, \tau_{s\ iN}, \sigma_{n\ iN}\} \tag{5}$$

The stress vectors $\{\sigma_i\}$ are equal to each other, as are the vectors of displacement discontinuities.

Applying the principle of superposition to the crack problem, a solution is obtained from the superposition of the following two answers: (a) the answer when a uniform stress ($\sigma_{xx}^0, \sigma_{yy}^0, \tau_{xy}^0$) is acting on an elastic body without cracks, and (b) the answer when the normal and shear stresses (σ_n, τ_s) are acting on the inner surface of cracks and the far field stress is zero. Here, stresses (σ_n, τ_s) have to satisfy the boundary condition on the crack surface by superposition. We denote the stress which corresponds to the uniform stress ($\sigma_{xx}^0, \sigma_{yy}^0, \tau_{xy}^0$) on the crack line as (σ_n^0, τ_s^0). In the case of the open crack problem, the stress on the crack surface is given by ($-\sigma_n^0, -\tau_s^0$).

Since the far field strain is zero in the analysis of 2D-DDM, constraint stress ($\sigma_{xx}^*, \sigma_{yy}^*, \tau_{xy}^*$), which corresponds to the constraint of the displacement at far field, is acting in the model. Therefore, in this answer (we call it answer (c)), inner stress and constraint stress are simultaneously acting on the model when 2D-DDM is applied to the problem. In order to obtain the correct solution, it is necessary to eliminate the constraint stress from the answer of (a) + (c).

This elimination is achieved by loading the constraint stress ($-\sigma_{xx}^*, -\sigma_{yy}^*, -\tau_{xy}^*$) acting at the far field while the stress on the crack surface is zero. If we denote this answer as answer (d), the final solution is obtained by (a)+(c)+(d). The relation between answer (d) and the solution has to be discussed. In the original problem, no stresses act on the crack surface and uniform stress ($\sigma_{xx}^0, \sigma_{yy}^0, \tau_{xy}^0$) is acting at the far field. In the case of answer (d), no stresses act on the crack surface and constraint stress ($-\sigma_{xx}^*, -\sigma_{yy}^*, -\tau_{xy}^*$), which corresponds to the constraint of displacement, is acting at the far field. Therefore, the difference of the correct solution and answer (d) is the magnitude of the stress acting at the far field. In the following section, the method to estimate the effective compliance from the constraint stress ($\sigma_{xx}^*, \sigma_{yy}^*, \tau_{xy}^*$) is discussed by focusing on the relation stated above.

4. Estimation of Constraint Stress and of Effective Compliance

It is necessary to analyze the stress distribution in the model in order to estimate the constraint stress from displacement discontinuity analysis. As stated before, the stress distribution is the same around each crack in any part of the model. Therefore, the constraint stress can be evaluated as the mean value of the stress distribution around the representative crack.

As the boundary of elemental regions coincide, it is necessary to determine the stresses acting on the boundary. In this study, imaginary elements are arranged on the boundaries of the elemental region (ABCD) with zero displacement, and the stress distribution acting on each boundary (AB, BC, CD and DA) is calculated. The constraint stress components are given as the mean values of the stress distribution acting on these boundaries.

By considering the macroscopic strain of HMCM, the effective compliance of the model can be obtained. The correct solution of strain components is obtained using Equations (1) to (3). On the other hand, since the macroscopic strain in answer (c) is zero, summation of the strain components of answers (a) and (d) represents the correct strain components.

The relations between compliance and constraint stress are given by

$$\beta_{xx\ xx}(\sigma_{xx}^0 + \sigma_{xx}^*) + \beta_{xx\ yy}(\sigma_{yy}^0 + \sigma_{yy}^*) + \beta_{xx\ xy}(\tau_{xy}^0 + \tau_{xy}^*) = (1 - \nu^2)\sigma_{xx}^0/E + \nu(1 + \nu)\sigma_{yy}^0/E \quad (6)$$

$$\beta_{yy\ xx}(\sigma_{xx}^0 + \sigma_{xx}^*) + \beta_{yy\ yy}(\sigma_{yy}^0 + \sigma_{yy}^*) + \beta_{yy\ xy}(\tau_{xy}^0 + \tau_{xy}^*) = -\nu(1 + \nu)\sigma_{xx}^0/E + (1 - \nu^2)\sigma_{yy}^0/E \quad (7)$$

$$\beta_{xy\ xx}(\sigma_{xx}^0 + \sigma_{xx}^*) + \beta_{xy\ yy}(\sigma_{yy}^0 + \sigma_{yy}^*) + \beta_{xy\ xy}(\tau_{xy}^0 + \tau_{xy}^*) = 2(1 + \nu)\tau_{xy}^0/E \quad (8)$$

In order to obtain nine components of compliance, it is necessary to estimate the components of the constraint stress. When displacement discontinuity analysis is applied to the following independent three loadings: first loading ($\sigma_{xx}^0 = \sigma$, $\sigma_{yy}^0 = 0$, $\tau_{xy}^0 = 0$), second loading ($\sigma_{xx}^0 = 0$, $\sigma_{yy}^0 = \sigma$, $\tau_{xy}^0 = 0$) and third loading ($\sigma_{xx}^0 = 0$, $\sigma_{yy}^0 = 0$, $\tau_{xy}^0 = \sigma$), the components of the constraint stress for each loading are obtained.

The components of the constraint stress are taken to be the mean values of the stress distribution. From the components of the constraint stress for the three loadings and equation (6), $\beta_{xx\ xx}$, $\beta_{xx\ yy}$ and $\beta_{xx\ xy}$ can be estimated. The other components of the compliance are also estimated from the constraint stress for the three loadings, and equations (7) and (8) respectively.

The displacement discontinuity analysis is applied to this model and the compliance of the model is estimated when the uniaxial stress is loaded from an arbitrary direction.

The compliance of the alternative stacking model is greater than that of the latticed model for all crack lengths and densities, and these results show the same tendency as the numerical analyses by Kaneko (1990) and Hirakawa (1999). Therefore, the crack pattern is also an important factor in the deformability of the model.

5. Theoretical Background of the Failure Simulation of Rock Masses by Discontinuous Deformation

The displacement u, v of any point x, y of a block can be represented by six displacement variables ($u_0, v_0, r_0, \epsilon_x, \epsilon_y, \gamma_{xy}$).

For a system of N blocks, with the total potential energy as π , minimizing the total potential energy derives the equilibrium equations.

$$\partial \Pi / \partial d_{ri} = 0 \quad r = 1, \dots, 6 \quad (9)$$

where: d_{ri} denotes the displacement component of the i -th block.

After minimization of potential energy π ,

$$F_{ri}^j = - \partial \Pi (0) / \partial d_{ri}, \quad r = 1, \dots, 6 \quad (10)$$

$$[\kappa_{ij}] = \partial^2 \Pi / \partial d_{ri} \partial d_{sj}, \quad r = 1, \dots, 6 \quad (11)$$

According to DDA, the slope is in an original stable state under the given mechanical parameters. From the initial stable state of the slope, diminishing geomechanical parameters pursues a DDA computation process, so that the slope becomes collapsed. By diminishing values of the strength in rock and joints, the rock in the slope will start crack in blocks and will progressively mobilize.

6. Conclusions

In order to evaluate the deformability of a rock mass containing many cracks, the Homogenized Multi-Crack Model (HMCM) was proposed. In addition, a method to estimate the compliance of the model was introduced by applying 2-Dimensional Displacement Discontinuity Method (2D-DDM). It was found that the distribution of the compliance to the arbitrary loading direction shows complicated shape when crack length increases.

When the interval of cracks in the normal direction decrease, the compliance shows complicated distribution. The alternative stacking model deforms more than the latticed model for a given crack length and crack density. These results indicate that both the mechanical interaction in the crack line direction and in the normal direction of cracks are crucial to the compliance of the model. These effects also depend on the pattern of the cracks in the model.

DDA is a very promising numerical computing method, but DDA method still needs more improvements to fulfill more engineering requirements, especially in three-dimensional problems and its numerical computation method.

References

1. Anderson, D. L., Minister, B. and Cole, D. (1974). "The Effect of Oriented Cracks on Seismic Velocities" *J.Geophys., Res.*, Vol.79, pp. 4011-4015.
2. Hirakawa, Y., Sato, A., Sugawara, K. (1999). "Evaluation of Deformation and Fracture Characteristics of Rock Mass by Applying Homogenized Multi-crack Model" *ISRM*, Vol.2, pp.909-912.
3. Sato, A., Hirakawa, Y., Sugawara, K. (2000) – „Homogenized Multi-crack Model for Deformability Analysis of Rock Mass” - *Proceedings of International Conference of Geotechnics and Foundations* – Melbourne, Australia.

4. Shi, G., Goodman, R.E. (1989). “Generalization of Two-dimensional Discontinuous Deformation Analysis for Forward Modelling” *Int. J. for Num. and Analy. Methods in Geomech*, Vol.13, pp.359-380
5. Shi G., Goodman, R.E. (1989) “The Key Blocks of Unrolled Joint Faces in Developed Maps of Tunnel Walls” *Int. J. for Num. & Analy. Methods in Geomech*, Vol.13, pp.131-159.
6. Shi, G., Goodman, R.E.. (1987) “Two-dimensional Discontinuous Deformation Analysis” *Int.J. Num.and Analy.Methods in Geomech.*, Vol.9, pp.541-556
7. Shi, G. (1997) “Numerical Manifold Method” *Proc. Of ICADD-2, The Second International Conference on Analysis of Discontinuous Deformation*. Kyoto, November, Yuzo Ohnishi Eds., pp.1-35
8. Walsh, I. B. (1974). “The Effect of Cracks on the Compressibility of Rock”. *J.Geophys. Res.*, Vol.70, pp.381-389.
9. Weiyuan, Z, Tianchi, Q, Ruoqiong, Y. (2000) “The Failure Simulation of Rock Masses by Discontinuous Deformation Analysis” – *Proceedings of International Conference of Geotechnics and Foundations* – Melbourne, Australia.

STABILITY COEFFICIENTS VERSUS STABILITY EVALUATION USING FINITE ELEMENT-NEURAL NETWORK HYBRID ALGORITHMS FOR EARTH SLOPES ANALYSIS

Ancuța ROTARU¹, Traian – Dănuț BABOR²

Abstract

The application of the effective stress analysis to earth slopes has suffered through lack of a general solution such as that presented by Taylor (1937) for the total stress analysis. Developments in computing technique have been applied to the slip circle method and have made it possible to present the results of the effective stress analysis in terms of stability coefficients from which the factor of safety can be rapidly obtained (Bishop, 1960).

Recent developments, based on structural tests of soil specimens, have applied a neural network (NN) soil model incorporated into the finite element method (FEM), and the stability of an excavated soil slope is evaluated by means of finite element-neural network (FE-NN) hybrid algorithms.

The practising engineer frequently requires a rapid means of estimating the factor of safety of a cutting, an embankment, or a natural slope. A detailed analysis was often impracticable in the preliminary stage when a number of alternative schemes are under consideration. Current methods of stability analysis used for the long-term stability of slopes and for most earth-dam problems include the observed or predicted pore-pressure distribution as a major factor in the calculation. These problems call for a general solution but expressed in terms of effective stress rather than of total stress.

An important recent interest in neural networks (NNs) within soil mechanics and geotechnics is the question of its coupling with other numerical methods. In the majority of reported cases, the application of NNs leads to a stand-alone system. In some cases it is difficult to establish exactly how these new tools fit together with the existing tools (numerical methods). The key to maximizing the benefits of this new NN technology is in its integration into our existing tools, for example FEM, thereby endowing the later with increased capability. This paper targets this issue specifically, evaluating stability for an excavated soil slope employing FE-NN hybrid model, and the numerical results are quite good. The training data for the new NN computation containing the knowledge of the nonlinear mapping to be modeled must include a sufficient number of stress paths, acquired by the network.

¹ Ph.eng. „Gh.Asachi” Technical University of Iași, Romania, arotaru@ce.tuiasi.ro

² Lecturer, „Gh.Asachi” Technical University of Iași, Romania, danbabor@ce.tuiasi.ro

The paper presents both methods: the classical one, using the stability coefficients with the distribution of pore pressure encountered in typical earth dams and cuts and the use of neural networks, a new technology for earth slopes analysis.

1. Introduction

The factor of safety is defined as the factor by which the shear strength parameters in the terms of effective stress, c' and $\tan \Phi'$, can be reduced before the slope is brought into a state of limiting equilibrium.

For simple slopes having homogeneous distribution of pore pressure it appears that the factor of safety is given by the circular arc method to a degree of accuracy adequate for all practical proposes. Taylor presented his results in terms of the value of stability number $c/F \cdot \gamma \cdot H$ required, for a given value of friction angle, Φ , to maintain the equilibrium. This enabled the general solution to be presented in a very compact form but also meant that a step-by-step numerical method had then to be used to evaluate the factor of safety of any actual slope not in limiting equilibrium. In Taylor's solution the stability coefficients lead directly to the factor of safety. This presentation occupies rather more space, but permits the results in any particular case to be obtained by simple interpolations. Taylor's solution can be considered a solution in terms of effective stress with no pore pressures. The derivation of the numerical slices method was gave by Bishop (1955).

An important recent interest in neural networks (NNs) within soil mechanics and geotechnics is the question of its coupling with other numerical methods. In the majority of reported cases, the application of NNs leads to a stand-alone system. In some cases it is difficult to establish exactly how these new tools fit together with the existing tools (numerical methods). The key to maximizing the benefits of this new NN technology is in its integration into our existing tools, for example FEM, thereby endowing the later with increased capability. This paper targets this issue specifically, evaluating stability for an excavated soil slope employing FE-NN hybrid model, and the numerical results are quite good.

2. Constitutive Modelling

Modeling is a fundamental method in research of engineering problems. Modeling of the observed phenomena, such as the constitutive behavior of material, enables the understanding of phenomena and makes most engineering analysis possible. NNs (Fig.1) offer a new and fundamentally different method of approaching the task of constitutive modeling. First, the material behavior, as represented in the experimental data, is examined in order to identify the major features of material behavior. Once the material behavior is sufficiently well understood, and its main features identified, then a mathematical model is developed to simulate this behavior. The artificial neurons in the input layer may represent the state of

stresses, the state of strains and the stress increments. The units in the output layer may represent the strain increments. In the new constitutive modeling method, the constitutive behavior is directly captured from structural test results by means of the learning capabilities of NNs and is encoded within the connection strengths of a self-organizing feed-forward NN. During the training, the activation values of both the input and the output layers are specified and the learning rules are applied to modify the strengths of the connections. After a NN has been trained with a sufficient amount of test data, along different stress paths, it will be capable of giving the correct strain for any set of stress increments, at any state of stress.

The new constitutive modeling model provides the mapping from stress increments to strain increments (stress controlled model). However, in computational mechanics and finite element analysis, the inverse mapping from the strain increments to the stress increments (strain controlled model) is needed. One of the important features of the NN computational models is that the inverse mapping can be developed as easily as the direct mappings.

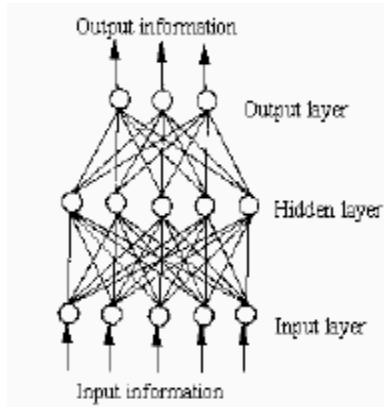


Fig.1: A three-layer NN constitutive model for soil.

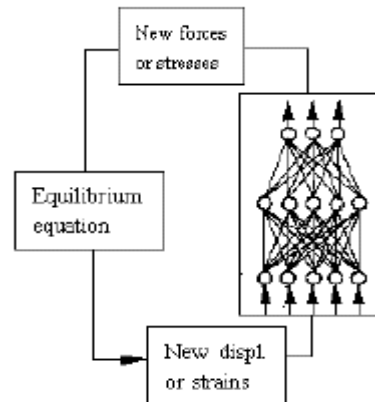


Fig.2: Incorporation of a NN constitutive model within the FE.

The training data for the new NN computation containing the knowledge of the nonlinear mapping to be modeled must include a sufficient number of stress paths, acquired by the network. A data set, which includes the relevant knowledge, is called a comprehensive data set. A NN trained with a comprehensive data set on the constitutive behavior will be able to use the generalization capability of the NN and respond appropriately when queried about the stress paths not included in the training data set.

3. Incorporation of a NN Constitutive Model within the FE

Fig.2 shows the concept of incorporation of a NN constitutive model within the FE. The purpose of a NN constitutive model employed within the FE is to use the measured boundary forces and displacements to train a NN soil model, where the NN exactly replaces the role of the more conventional constitutive laws in the FE. The FE-NN hybrid approach allows the training of the NN soil model in a FE analysis of the structural test (Fig.3). The FE-NN hybrid algorithm is based on applying one set of the measured boundary conditions in the FE analysis and iteratively modifying the connection weights of the NN material model so that the FE results match the second set of the measured boundary conditions.

The algorithm steps in which force boundary conditions are applied and displacement boundary conditions are enforced through training of the NN material model are (apply the measured load increment ΔP_v and analyze the structure):

$$P_n = P_{n-1} + \Delta P_n \quad (1)$$

$$K_t^{j-k} = \delta U_n^j = p_n - I_{n-1} - \delta I_{n-1}^{j-1} \quad (2)$$

n=load increment number ; j=iteration number

$$\delta \varepsilon_n^j = B \delta U_n^j \quad (3)$$

$$\Delta U_n^j = \Delta U_n^{j-1} + \delta U_n^j \quad (4)$$

$$\Delta \varepsilon_n^j = \Delta \varepsilon_n^{j-1} + \delta \varepsilon_n^j \quad (5)$$

$$\Delta \sigma_n^j = \Delta \sigma_n^{j-1} + \delta \sigma_n^j \quad (6)$$

Compute the boundary displacement errors $\delta \Delta \bar{U}_n^j$, as the difference between the measured boundary displacements and the computed boundary displacements:

$$\delta \Delta \bar{U}_n^j = \Delta \bar{U}_n^m - \Delta \bar{U}_n^j \quad (7)$$

If the boundary displacement errors are less than a prescribed tolerance, then update the displacements, strains and stresses

$$U_n = U_{n-1} + \Delta U_n^j \quad (8)$$

$$\varepsilon_n = \varepsilon_{n-1} + \Delta \varepsilon_n^j \quad (9)$$

$$\sigma_n = \sigma_{n-1} + \Delta \sigma_n^j \quad (10)$$

and go to the first step and apply the next load increment. Otherwise, continue. Apply the boundary displacement errors as displacement boundary conditions.

The strain increments, $\delta \Delta \varepsilon_n^j$, at the integration points are computed and they are propagated through the NN soil model to determine the corresponding stress increments, $\delta \Delta \sigma_n^j$. These stress increments are the errors at the output of the NN soil models, corresponding to the errors at the measured boundary displacements.

The error at the output of the NNs, $\delta\Delta\sigma_n^j$, is back-propagated through the NN soil model and the connection weights are modified.

These steps are repeated until the NN soil model learns the material behavior. With the trained NN, the FE analysis will be able to produce the correct measured boundary displacements, when subjected to the measured boundary forces.

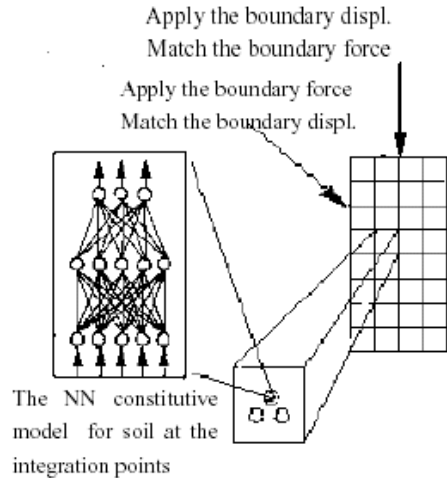


Fig.3: Training of the NN soil model within the FE.

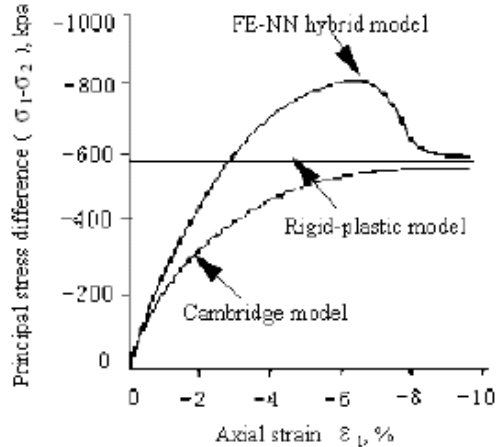


Fig.4: FE-NN hybrid model for soil.

4. The FE-NN Hybrid Model for Soil

The studied results show that FE-NN hybrid model for soil has a nonlinear stress-strain relation and the asymptote of the relation curve is the horizontal straight line of rigid-plastic model for soil (Fig.4). Cambridge model, which was developed in the early days of the 1960s, represents a nonlinear elastoplastic stress-strain relationship for soil mass.

5. Stability Evaluation for Excavated Slope by the FE-NN Hybrid Algorithms

Fig.5 shows the analytical model of a 10m high-excavated soil slope. Movement on the vertical boundaries is constrained horizontally only, while movement on the bottom boundary is constrained in both horizontal and vertical directions. A mesh consisting of 250 nodes and 216 rectangular elements is utilized in the analysis. The deformed geometries of the soil slope, after excavation, are presented with solid lines in Fig.6.

The ground surface behind the crest settles approximately 0.88m (In-situ measurement: 0.88m; Limit analysis: 0.94m) and the bulging extends 0.16m (Site measurement: 0.15m; Limit analysis: 0.21m) from the originally vertical slope line. It seems clear from the analysis that for the FE-NN hybrid model case the loss of ground, which is usually evaluated by the largest horizontal displacement along the vertical slope line, would occur at the nodal point immediately above the toe.

We can conclude that the results of the FE-NN hybrid model are quite good.

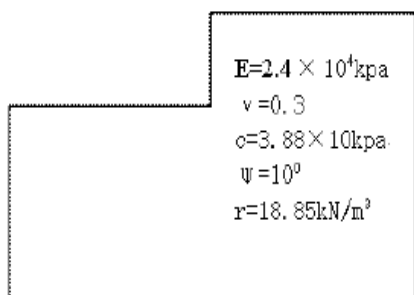


Fig.5: The analytical model of an excavated soil slope.

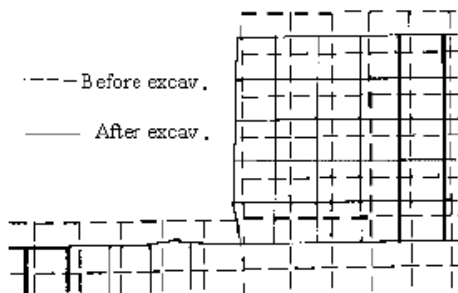


Fig.6: Geometry of slope after excavation.

6. Conclusions

1. The research shows that after excavation of the soil slope, the ground surface behind the crest settles approximately 0.88m and the bulging extends 0.16m from the originally vertical slope line. The results are in agreement with the site material.
2. The FE-NN hybrid model for soil has a nonlinear stress-strain relation and the asymptote of the relation curve is the horizontal straight line of rigid-plastic model for soil.
3. The FE-NN hybrid model for soil is able to use the generalization capability of the NN and is capable of giving the correct strain increments for any set of stress increments, at any stress paths not included in the training data set.

References

1. Bishop, A.W., Morgenstern, N. (1960) “Stability coefficients for earth slopes” *Geotechnique*, Vol.10, No.4, pp.129-151.
2. Chen, W.F., Mizuno, E. (1990). “Nonlinear analysis in soil mechanics ” *Elsevier Publishers B.V.*, pp.661.
3. Hertz, J. (1991) “Introduction in the theory of neural computation” Redwood City, California *Addison-Wesley Publishing Company*, pp.228.

4. Henkel, D.J.(1959) "The relationships between the strength, pore-water pressure, and volume change characteristics of saturated clays" *Geotechnique*, Vol.9, pp.28.
5. Wu, H. (1996) "Roof controlling in longwall face using neural networks" *Ground Pressure and Strata Control*, Vol.15, pp.6-9.
7. Wu, H.(1998). "Constitutive model simulation for soil by using finite element-neural network hybrid algorithms" *J.of Guizhou Univ. of Tech.*, Vol.28, pp. 95-99.
8. Wu, H., Martens, H.L., Al-jibouri, S., Bao, T., Chang, X.B. (2000) "Stability Evaluation for Excavated Slope Using F. E. Neural Network Hybrid Algorithms – *Proceedings of the Geotechnics and Foundation Conference*, Melbourne.

DESIGN CRITERIA OF TUNED MASS DAMPER FOR VIBRATION CONTROL OF MULTI-DEGREE OF FREEDOM STRUCTURES

Septimiu LUCA¹, Cristian PASTIA², Vitalie FLOREA³

Abstract

Building structures designed according to the current building code are expected to deform into the inelastic range thereby dissipate seismic energy induced from strong ground motions. Physically, it represents energy dissipated through nonlinear behaviour of the structural members after yielding, and the more hysteretic energy dissipated, the higher the structural damage. The displacements and the accelerations can become very large especially if the dynamic load frequency matches the structure's natural frequency, resulting in resonance.

One of the approaches to reduce excessive oscillation on buildings due to dynamic forces is by installing a passive mechanical device called tuned mass damper (TMD). Although active vibration control nowadays has received significant attention from many researchers, a passive control technique is still considered. One of the reasons for the acceptance of such devices is that they are very reliable since external power sources are not required for their operation. During the earthquake, the TMD will move against the direction of main structures reducing the response of structure.

This paper presents a study on the effectiveness of TMD in reducing the response of structures that are subjected to seismic excitation. The effectiveness of a TMD is dependent on the mass ratio (of the TMD to the structure itself), the ratio of the frequency of the TMD to the frequency of the structure (which is ideally equal to one), and the damping ratio of the TMD (how well the damping device dissipates energy). The earthquake accelerograms of El Centro 1940 and Northridge 1994 are considered, and two-dimensional linear-elastic model with TMD on the top is used in performing dynamic analysis. Frequency domain responses and time domain responses are computed using a Matlab program that relies on the state space formalism which is widely used in control system theory. The effectiveness of the TMD is evaluated by comparing the response: displacement and acceleration, with and without TMD. The results of the study show that the responses are generally decreased. However, in some cases the responses could be larger, thus using of TMD for reducing seismic response should be reconsidered.

¹ Ph.D Student, Technical University of Iasi, Romania, e-mail: septigeo@yahoo.com

² Ph.D Student, Technical University of Iasi, Romania, e-mail: pastiacristian@yahoo.com

³ Assistant, PhD, Technical University of Iasi, Romania, e-mail: vflorea@ce.tuiasi.ro

1. Introduction

The tuned mass damper (TMD) is such an energy absorber consisting of a mass, a spring, and a viscous damper. The motion of its mass is activated when the natural frequency of the TMD is tuned to be in or near resonance with the predominant frequency of the main structure. Because the energy dissipated on the TMD does not depend on the relative motion of parts of the structure, it can be implemented and installed in both new and retrofitted structures.

According to Ormondroyd and Den Hartog [1], the use of TMDs was first suggested in 1909. Since then, much research has been carried out to investigate their effectiveness for different dynamic loading applications. Tuned mass damped was found effective in reducing the response of structures to harmonic [2] or wind [3, 4] excitation. For seismic applications, however, there has not been a general agreement on the efficiency of TMD systems to reduce the structural response.

2. Analytical Formulation of a Tuned Mass Damper for MDOF Systems

We will consider a Multiple Degree of Freedom-MDOF system with TMD on each storey (Figure 2.1). For reason of practicality, the equations of motion will be written only for three degree of freedom.

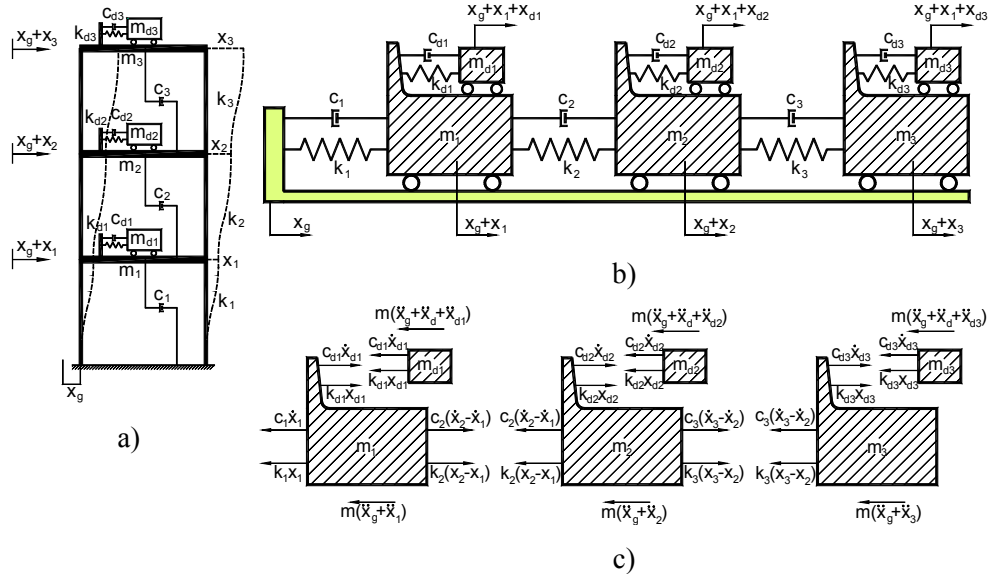


Figure 2.1: Mathematical model of TMD

According to d'Alembert principle, the differential equations of motion for each mass from figure 2.1 take the form

$$\begin{cases} m_1\ddot{x}_1 + c_1\dot{x}_1 + k_1x_1 - c_2(\dot{x}_2 - \dot{x}_1) - k_2(x_2 - x_1) - c_{d1}\dot{x}_{d1} - k_{d1}x_{d1} = -m_1\ddot{x}_g \\ m_2\ddot{x}_2 + c_2(\dot{x}_2 - \dot{x}_1) + k_2(x_2 - x_1) - c_3(\dot{x}_3 - \dot{x}_2) - k_3(x_3 - x_2) - c_{d2}\dot{x}_{d2} - k_{d2}x_{d2} = -m_2\ddot{x}_g \\ m_3\ddot{x}_3 + c_3(\dot{x}_3 - \dot{x}_2) + k_3(x_3 - x_2) - c_{d3}\dot{x}_{d3} - k_{d3}x_{d3} = -m_3\ddot{x}_g \\ m_{d1}\ddot{x}_{d1} + c_{d1}\dot{x}_{d1} + k_{d1}x_{d1} + m_{d1}\ddot{x}_1 = -m_{d1}\ddot{x}_g \\ m_{d2}\ddot{x}_{d2} + c_{d2}\dot{x}_{d2} + k_{d2}x_{d2} + m_{d2}\ddot{x}_2 = -m_{d2}\ddot{x}_g \\ m_{d3}\ddot{x}_{d3} + c_{d3}\dot{x}_{d3} + k_{d3}x_{d3} + m_{d3}\ddot{x}_3 = -m_{d3}\ddot{x}_g \end{cases} \quad (2.1)$$

or in matrix form

$$\begin{cases} M\ddot{x} + C\dot{x} + Kx - C_d\dot{x}_d - K_dx_d = -M\ddot{x}_g \\ M_d\ddot{x}_d + C_d\dot{x}_d + K_dx_d + M_d\ddot{x} = -M_d\ddot{x}_g \end{cases} \quad (2.2)$$

It's convenient to represent the vibrating structural system response by a state space model in order to apply passive, semi-active or active techniques. The second order differential equation of Equation (2.2) can be written as a first order linear time-invariant system with state vector $z = [x^T \quad \dot{x}^T]^T$ as

$$\dot{z}(t) = Az(t) + B\ddot{x}_g(t) \quad (2.3)$$

where

$$A = \begin{bmatrix} O & I & O & O \\ -M^{-1}K & -M^{-1}C & M^{-1}K_d & M^{-1}C_d \\ O & O & O & I \\ M^{-1}K & M^{-1}C & -M^{-1}K_d - M_d^{-1}K_d & -M^{-1}C_d - M_d^{-1}C_d \end{bmatrix} \quad B = \begin{bmatrix} O \\ -I \\ O \\ O \end{bmatrix}$$

The evaluation responses are the displacement and the velocity relative to the ground, and absolute acceleration of masses, given by

$$y(t) = Cz(t) + D\ddot{x}_g(t) \quad (2.4)$$

where

$$C = \begin{bmatrix} I & O & O & O \\ O & I & O & O \\ -M^{-1}K & -M^{-1}C & M^{-1}K_d & M^{-1}C_d \end{bmatrix} \quad D = [0]$$

The solution of the state vector for the first order linear Equation (2.3) is

$$z(t) = \Phi(t,0)z(0) + \int_0^t \Phi(t,\tau)B\ddot{x}_g(\tau)d\tau \quad (2.5)$$

where the state transition (or principal) matrix for time invariant systems is $\Phi(t,\tau) = e^{A(t-\tau)}$ and the initial conditions are given by $z(0)$.

Besides a time domain approach, which is a good way for evaluating the response, a transfer function analysis can provide further insight into the response of structure as the parameters of TMD are varied. The transfer function $H(s)$ is given by

$$H(s) = C(sI - A)^{-1}B + D \quad (2.6)$$

where I is the identity matrix.

3. Response of the 3DOF system using Tuned Mass Damper (TMD)

We will consider a Three Degree of Freedom-3DOF system. The mass, stiffness and damping matrices will be used in the analytical model as follow:

$$M = \begin{bmatrix} 20000 & 0 & 0 \\ 0 & 20000 & 0 \\ 0 & 0 & 20000 \end{bmatrix} \text{ (Kg)} \quad C = \begin{bmatrix} 21272 & -10636 & 0 \\ -10636 & 21272 & -10636 \\ 0 & -10636 & 10636 \end{bmatrix} \text{ (N/m)}$$

$$K = \begin{bmatrix} 70972000 & -48147000 & 0 \\ -48147000 & 135558000 & -87413000 \\ 0 & -87413000 & 87412000 \end{bmatrix} \text{ (N*s/m)}$$

With the above matrices, it is easy to calculate the natural periods of the structure and corresponding eigenvectors, where each mode is normalized to 1.

$$\Omega = \begin{bmatrix} 17.33 & 0 & 0 \\ 0 & 61.28 & 0 \\ 0 & 0 & 103.16 \end{bmatrix} \text{ rad/s} \quad \Phi = \begin{bmatrix} 1 & -0.61 & -0.697 \\ 0.931 & -0.086 & 1 \\ 0.69 & 1 & -0.339 \end{bmatrix} \quad \begin{matrix} T_1 = 0.363(s) \\ T_2 = 0.103(s) \\ T_3 = 0.061(s) \end{matrix}$$

Figure 3.1 shows the comparison of the frequency domain responses between the excitation and displacement at the 3rd level with uncontrolled structure and structure controlled with a TMD. In the case of controlled structure has been considered four situations for TMD implementation. In the first situation, one TMD tuned to the first natural frequency of the structure has been attached on top of it. The ratio μ between the mass of the TMD and the system was chosen typically to be 1/100 and the damping ratio of TMD $\xi_d=6\%$. The TMD stiffness (k_d) and TMD damping (c_d) can be calculated as following:

$$\begin{aligned} - k_d &= (2\pi f_d)^2 m_d = (2\pi \rho f) \mu m ; \text{ (N/m)} \\ - c_d &= 2\xi_d (2\pi f_d) m_d = 4\pi \xi_d \rho f \mu m ; \text{ (N*s/m)} \end{aligned}$$

where f is the structure nature frequency, and ρ is the ratio between frequency of the structure and the TMD, which is chosen typically 1.

In the second case, three TMDs have been placed in the analytical model, one per storey. The masses of the TMDs were assumed to be equal and they were tuned to first natural frequency of the structure. The mass of TMDs was chosen, as in the

first cases, to be 1% of the mass of the structure. The response of the structure is higher then in the first situation so that for the 3rd case will remove the TMD from the first storey. The mass ratios of the other two TMDs are assumed to be equal to 0.5% of the mass of the structures.

In the last case one TMD is placed on each floor and is tuned to one mode of vibrations. Ideally, each TMD should be placed at the floor where the maximum value of the corresponding mode occurs. According to the mode shapes the locations of the TMD’s are: 1st storey (second mode), 2nd storey (third mode), 3rd storey (first mode);

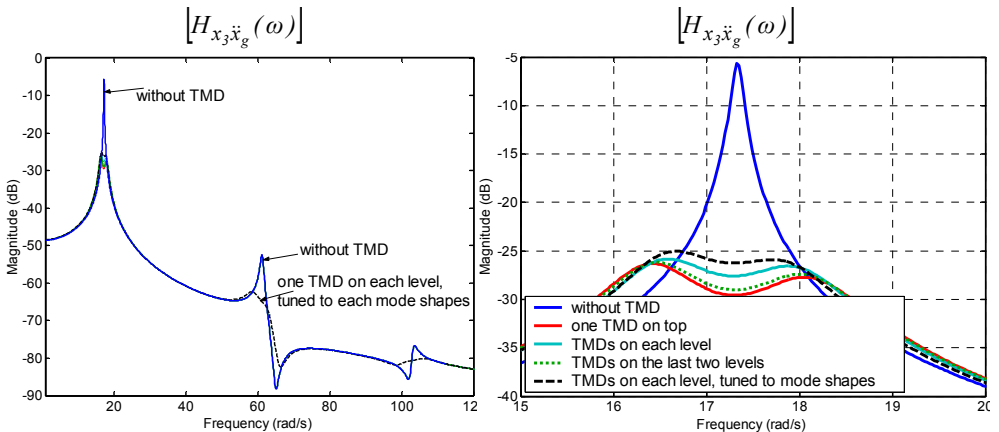


Figure 3.1: Comparison in the frequency domain responses of the structural model without and with TMD

As we can see in Figure 3.1 the response of the structures is reduced for all mode shapes when the frequencies of the TMDs are properly tuned. In our case the first mode of vibration is the most imported so that the effectiveness of TMD is maxim when is placed on top of the structures and is tuned to first mode of vibration.

The study of the system response only under harmonic excitation can't provide enough information about its real behaviour. For this reason, it will be analysed the time history response of SDOF model with TMD under earthquake acceleration. Two earthquake signals, depicted in figure 3.2 are considered:

- El Centro earthquake signal: North-South component recorded at Imperial Valley Irrigation District substation in El Centro, California, during the Imperial Valley, California earthquake of May 18, 1940. The magnitude is 7.1 and the maximum ground acceleration is 0.3495 g.

- Northridge earthquake signal: North-south component recorded at Sylmar County Hospital parking lot in Sylmar, California, during the Northridge, California earthquake of Jan. 17, 1994. The magnitude is 6.8 and the maximum ground acceleration is 0.8428 g.

The response of the structure is highly dependent on the frequency content of earthquake accelerations. Figure 3.3 shows the Fourier spectrum for the two signals, scaled at the same peak of maximum ground acceleration, 3 m/s². The spectrum it was elaborated using a Matlab function (fft) that returns the discrete Fourier transform, computed with a fast Fourier transform (FFT) algorithm [5].

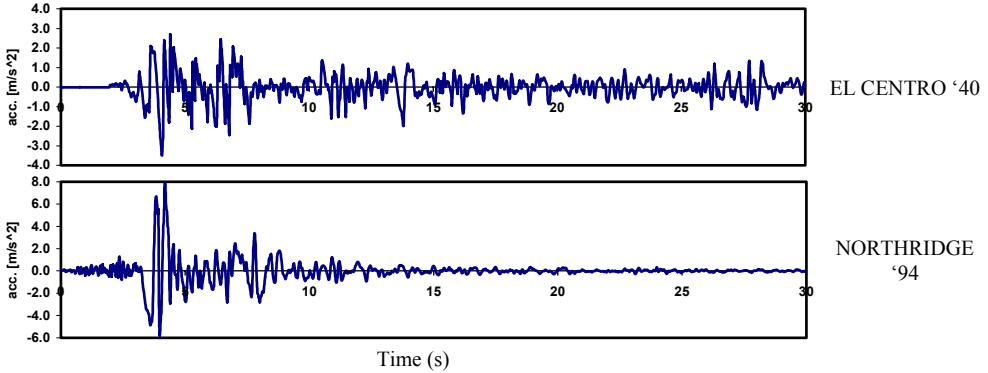


Figure 3.2: Earthquake signals

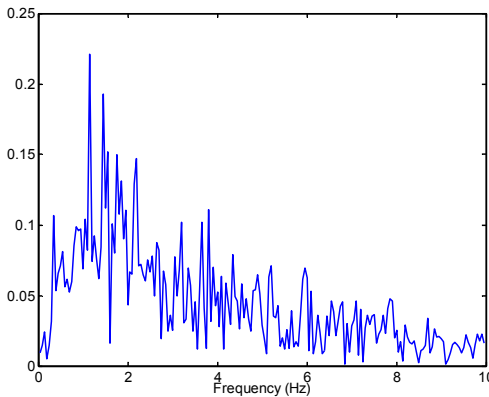


Figure 3.3a: Fourier spectrum of the El Centro '40 ground acceleration

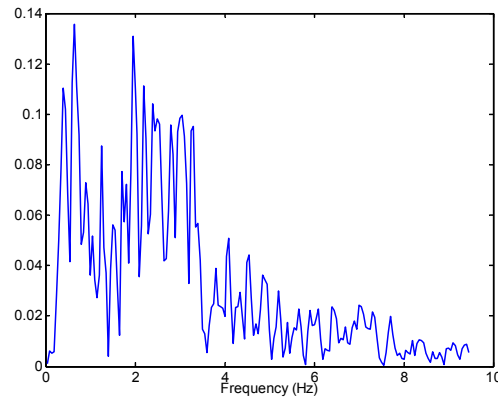


Figure 3.3b: Fourier spectrum of the Northridge '94 ground acceleration

The effectiveness of a TMD is dependent on the mass ratio μ , the ratio of the frequency of the TMD to the frequency of the structure (which is ideally equal to one), and the damping ratio of the TMD, ζ_d . Figures 3.4, 3.5 depict the maximum response of the structural model at 3rd level when the damping ratio of the TMD is varied from 0% up to 10%, for different mass ratio, under El Centro and Northridge earthquake accelerations.

Figures 3.6 and 3.7 shows the comparison of the time domain responses at 3rd level with uncontrolled structure and structure controlled with TMD for the two earthquake signals.

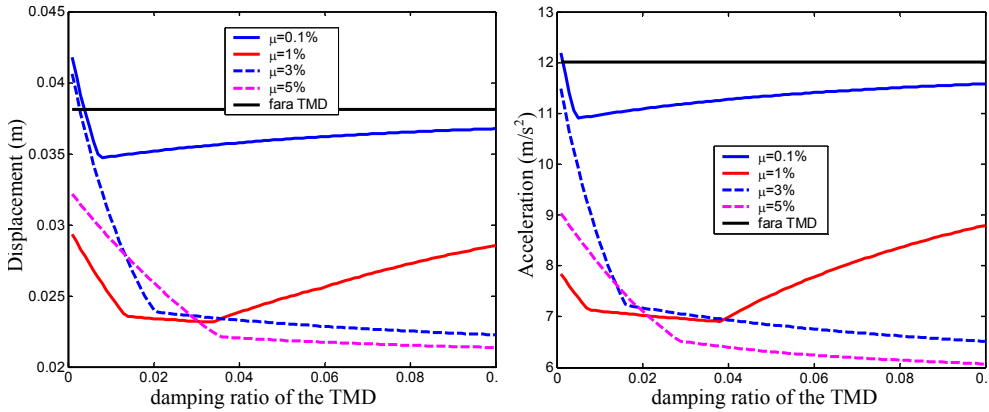


Figure 3.4: The maximum structural response under El Centro earthquake acceleration for different mass ratio μ and for different damping ratio of the TMD, ξ_d

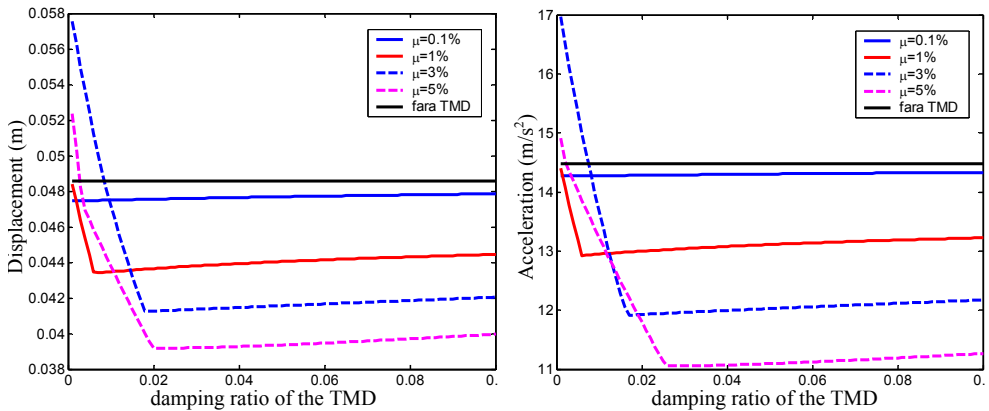


Figure 3.5: The maximum structural response under Northridge earthquake acceleration for different mass ratio μ and for different damping ratio of the TMD, ξ_d

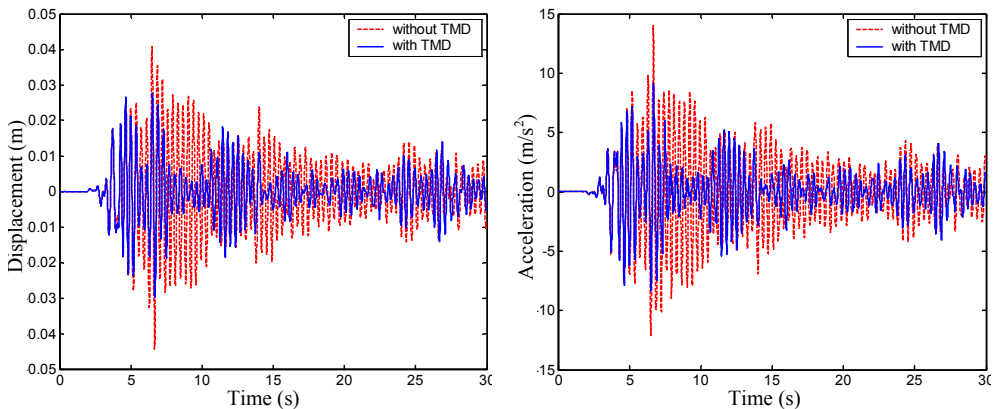


Figure 3.6: Numerical simulations of the structural model under El Centro earthquake acceleration, $\mu=1\%$

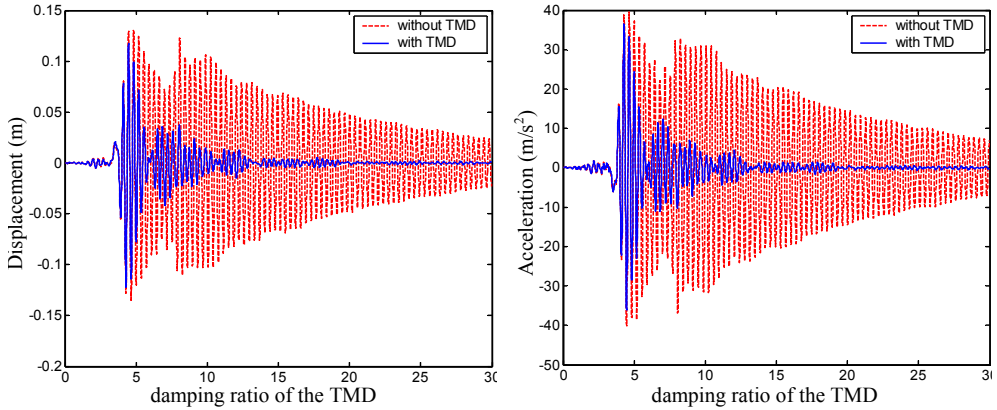


Figure 3.7: Numerical simulations of the structural model under Northridge earthquake acceleration, $\mu=1\%$

4. Conclusions

Tuned mass damper (TMD) systems have been incorporated into many structures and dynamic systems throughout the world to effectively reduce undesirable oscillations. In this study, the effectiveness of the TMD using the proposed tuned parameters has been investigated through numerical example. A properly tuning leads to excellent reductions in displacement and acceleration for loads applied at the resonant frequency but is less effective for loads of different frequencies. The results of the study show that the responses are generally decreased. However, in some cases as we can see in figures 3.4, 3.5 the responses could be equal or even larger, thus using of TMD for reducing seismic response should be reconsidered.

References

1. J. Ormondroyd and J. P. Den Hartog, *The theory of dynamic vibration absorber*, Trans. ASME APM-50-7, 1928, pp. 9-22.
2. J. P. Den Hartog, *Mechanical Vibrations*, 4th ed., McGraw-Hill, New York, 1956.
3. R. W. Luft, *Optimum tuned mass dampers for buildings*, J. struct. div. ASCE 105, 2766-2772 (1979).
4. R. J. McNamara, *Tuned mass dampers for buildings*, J. struct. div. ASCE 103, 1785-1798 (1977).
5. Cooley, J. W. and J. W. Tukey, *An Algorithm for the Machine Computation of the Complex Fourier Series*, Mathematics of Computation, Vol. 19, April 1965, pp. 297-301.

DESIGN DECISIONS OF A CONTROL SYSTEM FOR A SINGLE-DEGREE-OF-FREEDOM STRUCTURE FROM ENERGY BALANCE POINT OF VIEW

Cristian PASTIA¹, Dan COVATARIU², Setimiu George LUCA³

Abstract

This paper presents design criterions of a passive, active or semi-active control strategies taking into account the balance energy for the whole system (control mechanism and structure). If passive control systems are used for enhancing the structural damping, stiffness or strength, the other control techniques employ controllable forces to add or to dissipate energy in a structure, or both, due to the specific devices integrated with sensors, controllers and real-time processes to operate. For analytical results, there was considered the shear-type model of a single-degree-of freedom structure under the NS component recorded at El Centro.

The phenomenon by which the mechanical energy is dissipated in dynamic systems is called damping. Usually the input energy is converted into internal thermal energy or structural damage. It's well known that the *energy dissipation* or *damping* is related by a hysteresis loop in the force-displacement path. It is important to characterize the damping of the dynamic system because in this way we can understand the major mechanisms associated with mechanical-energy dissipation in the system. Two damping models (hysteretic damping of SDOF model and passive hysteretic damping device) have been performed to represent the associated energy dissipation for the case study in this paper.

The traditional approach to mitigate vibrations due to the earthquake and wind loads is to design some members of a structure with sufficient strength and deformation capacity in a ductile manner. This method is based on the non-linear behaviour of certain elements of the structure, which are considered as passive systems to dissipate the input energy.

The analytical studies with respect to the energy balance of the model are carried out to mitigate the energy dissipation demand for the primary structural elements in the following three cases: 1) the non-linear behaviour of the primary structural system; 2) a passive hysteretic damper attached at the primary structural system; 3) an active system that applied control forces on the structural mass.

Design decisions in order to choose a right control strategy regarding the reduction of energy requirement and the decreasing of the displacement response for a SDOF structure will be discussed.

¹ Phd student, Technical University of Iași, pastiacristian@yahoo.com

² Phd student, Technical University of Iași, cosoftco@xnet.ro

³ Phd student, Technical University of Iași, septigeo@yahoo.com

1. Introduction

During the past decades many techniques have been proven to develop successful physical, analytical, numerical and experimental models in predicting the dynamic behaviour of the civil engineering systems that are subjected to excitations. Therefore, in recent years, it has been paid a considerable attention to new concepts of structural control including passive, active and semi-active techniques. Passive, semi-active or stable active control reduces the energy demand for a structure. It's well to know that the effect of a lower energy demand through the use of active or semi-active control can be met by a passive control [3].

2. Energy balance

Generally, the work done by the external forces acting on a system is equal to the sum of the mechanical energy stored temporarily in the structure (kinetic and potential energy) and the energy transformed to another form, through either energy dissipation or absorption mechanisms. The energy balance equation takes the following form:

$$E_{input} = E_k + E_{el} + E_{pl} + E_{da} + E_{sup} \quad (1)$$

where,

E_{input} - energy inputted in structure by ground excitation.

$$E_{input} = \int_0^t f_{input}(\tau) dx(\tau) = \int_0^t -m a_g(\tau) \frac{dx(\tau)}{d\tau} d\tau = -m \int_0^t a_g(\tau) v(\tau) d\tau \quad (2)$$

E_k - kinetic energy stored in the mass that is equal to the work done by the force f_m on the mass. Considering the Newton's second law given by

$$f(\tau) = ma(\tau) \quad (3)$$

the relationship becomes:

$$E_k = \int_0^t f_m(\tau) dx(\tau) = \int_0^t f_m(\tau) \frac{dx(\tau)}{d\tau} d\tau = \int_0^t f_m(\tau) v(\tau) d\tau \quad (4a)$$

$$E_k = m \int_0^t a(\tau) v(\tau) d\tau = \frac{m}{2} v(t)^2 \quad (5b)$$

E_{pl} - potential energy stored in the spring that is equal to the work done by the force f_p on the spring.

$$E_p = E_{el} + E_{pl} = \int_0^t f_p(\tau) dx(\tau) = \int_0^t f_p(\tau) v(\tau) d\tau \quad (6)$$

E_{el} - energy due to elastic deformations.

$$E_{el} = \int_0^t kx(\tau)v(\tau)d\tau = \frac{k}{2}x(t)^2 \quad (7)$$

E_{pl} - energy due to plastic deformations.

E_{da} - energy dissipated due to the viscous damping of the structure.

$$E_{da} = \int_0^t f_c(\tau)dx(\tau) = \int_0^t cv(\tau)v(\tau)d\tau = c \int_0^t v(\tau)^2 d\tau \quad (8)$$

E_{sup} - energy dissipated or added by the supplemental passive, semi-active or active system.

The passive and semi-active control provide energy storage and energy dissipation. The magnitude of active control force adds the energy in structure. The actuator force is selected to oppose the motion and does negative work on the mass. Considering an active force f_{active} proportional to the displacement and the velocity, the relationship is given by

$$f_{active} = -k_{act}x(\tau) - c_{act}v(\tau) \quad (9)$$

The active control based on the equation can be interpreted as introducing virtual stiffness and damping. In case of linear SDOF the energy balance equation becomes:

$$-m \int_0^t a_g(\tau)v(\tau)d\tau + \int_0^t f_{active}v(\tau)d\tau = \frac{m}{2}v(\tau)^2 + \frac{k}{2}x(\tau)^2 + c \int_0^t v(\tau)^2 d\tau \quad (10)$$

When f_{active} is taken to have the same sign as v , active control decreases the energy input to the system since the integral is always negative.

3. Case study of a SDOF structural model

Let's consider a SDOF model in order to make energy comparisons among passive and active control strategies. The corresponding dynamic characteristics are as follow: $m = 10000$ Kg; $k = 2000000$ N/m; $c = 2815$ Ns/m; $\omega = 14.14$ rad/s; $T = 0.44$ s; $f = 2.25$ Hz; $\zeta = 0.01$. The system is subjected to El Centro seismic record.

It's known that damping reduces the strain energy and the system response, especially in the vicinity of the resonance. Figures 1(a) and 1(b) illustrate the influence of viscous damping for energy balance response in two cases, when the system is under El Centro's earthquake. For low viscous damping case ($\zeta = 0.005$), the energy dissipated per cycle is small. For a greater damping value ($\zeta = 0.01$) the dissipated energy increases, and the stored energy is reduced.

The approach using energy dissipation mechanisms is to transfer as much energy as possible from the primary structural members to secondary damping or ductile

elements. Let's consider now that the stiffness element of structure is designed as energy dissipation device. In this case, a hysteresis loop corresponds to energy dissipation and is formed by the cyclic inelastic deformation path (Figure 2(b)).

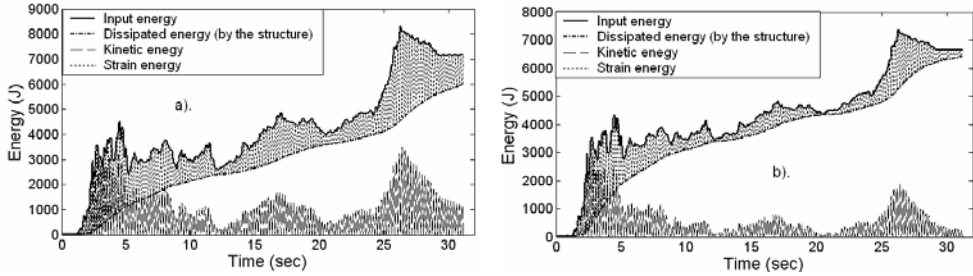


Figure 1: Energy Balance, Uncontrolled system, a) $\xi = 0.005$ and b) $\xi = 0.01$.

Figures 2(a) and 2(c) show the energy build up and displacement response respectively, taking into account the following conditions for the non-linear SDOF system: $k_1=k$, $k_2=0.1k$ and yield displacement $u_y=2.7\text{cm}$. It's seen that the energy dissipated by the hysteretic damping of the model is approximately 50% and also the displacements decrease. The inconvenient are that after more inelastic cycles the structure could fail and also the increasing of the input energy.

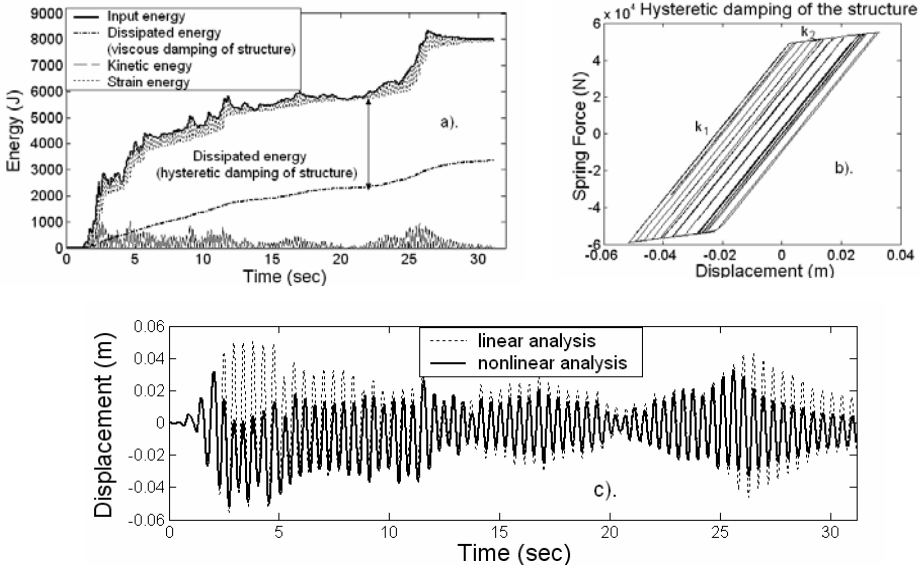


Figure 2: a) Energy balance; b) Force-Displacement (hysteretic damping of structure); c) Comparison of SDOF displacement response between linear analysis case ($\xi = 0.01$) and non-linear analysis case.

Damping devices installed at discrete locations in structures supplement their natural energy dissipation capabilities. Results are show in Figure 3(a), 3(b) and

3(c) supposing that the structure works in elastic domain and it's equipped with a passive hysteretic damper with an elastic-perfectly plastic behaviour. The characteristics of the device are: elastic damper stiffness $k_{dev}=40000$ N/m and yield force $F_{ydev}=4000$ N.

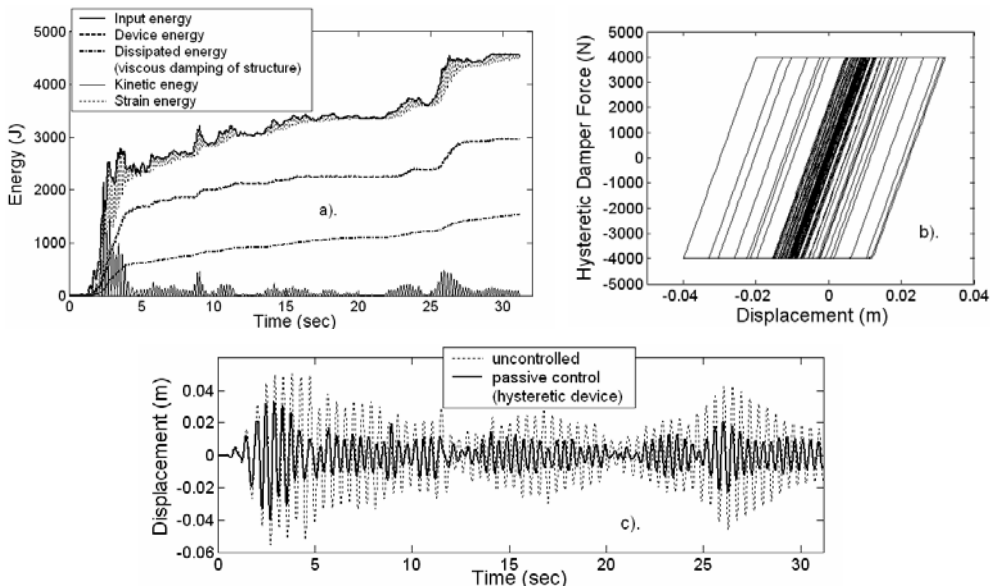


Figure 3: a) Energy balance; b) Force-Displacement (hysteretic passive damper); c) Comparison of SDOF displacement response between uncontrolled case ($\xi = 0.01$) and controlled case with hysteretic passive damper.

In this case the demand of energy absorption capacity on the main structural members and the response of the system is reduced. Thus, the possibility of structural damage is minimized. When the maximum response of the system is achieved, the peak of input energy is decreased approximately with 35%.

For active control purpose, a SIMULINK model was developed for SDOF response. The model is based on physical balance of forces and energies (Figure 4). The figure could seem as a complex model, but in reality it's very simply, there are only the connections among the right input with the right outputs. Some scopes were added to the outputs, which can also be joined with some blocks in order to export variables into the MATLAB workspace for analysis after the simulations. The force signal is the sum of earthquake excitation force and the control force given by an actuator. The response of the structure can be computed in the controlled or uncontrolled case by connecting or disconnecting the input. In this case study, one block was used to model the SDOF structural system.

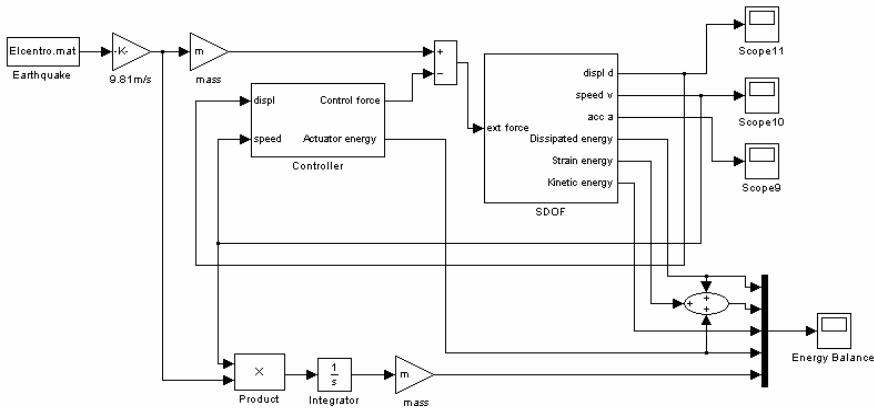


Figure 4: Simulink model of SDOF structural system

It has one input that is external force signal and more outputs, which are energies and displacement, speed and acceleration response. Figure (5) shows the actuator model, which consists of two inputs (the displacement and the speed signal, which are measured by sensors) and two outputs (the actuator force applied on structure and actuator energy added in the structure).

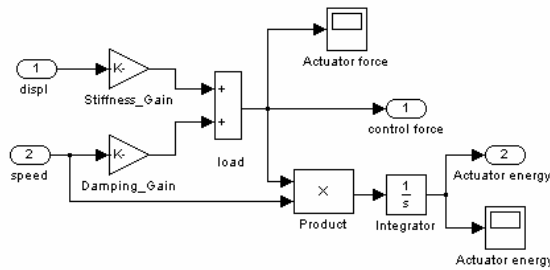


Figure 5: Simulink model of actuator.

Two cases are analyzed for the design of active control system. Both cases take into account only the velocity and for the case A is used a gain $g=20000$ Ns/m and in the case B, $g=65000$ Ns/m. The obtained gains are based on quadratic optimal control. Results are shown in Figure 6, for both cases, when the model is subjected to El Centro's earthquake.

The results in case A can be compared with the results in passive control device case. It's preferable to choose the use of the passive control damper because of the close results regarding the displacement response, stored energy and energy dissipation (viscous damping of structure). This passive mechanism requires no external power energy, whereas the active technique cannot function without an external source of energy. The passive damping device removes energy from

response, and therefore cannot cause the response to become unstable. Since an active control needs by an external power source to control the actuator force applied on structure, there is the potential for introducing instability in the system. In case A, the actuator must be able to produce a maximum force of 9000 *N*.

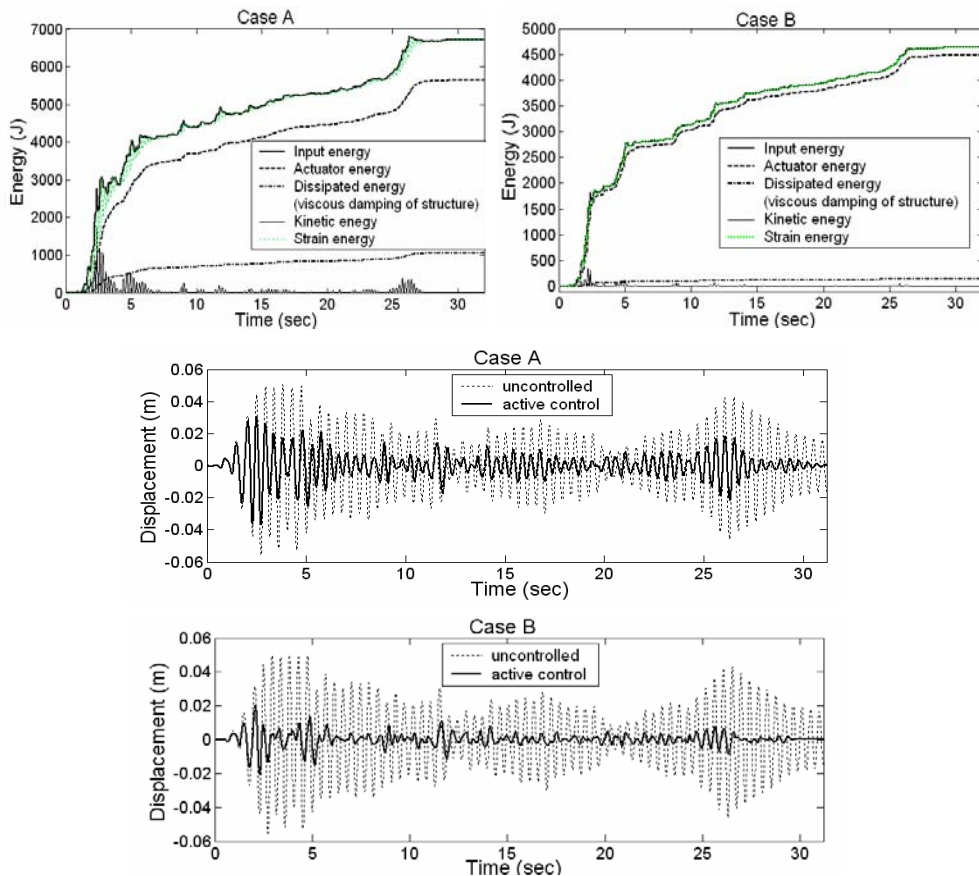


Figure 6: Energy Balance: case A and case B; Comparison of SDOF displacement response between uncontrolled case ($\xi = 0.01$) and controlled case with active system: case A and case B.

A reduction of the stored energy is achieved for a factor around 3.5 in passive case and active case A for this particular system and seismic excitation.

If we want to have a greater decreasing of the displacements, the input energy and the stored energy, the case B is preferable. Thus, the requirement of the power source increases and the actuator will have to be able to produce a maximum force of 20000 *N*.

Semi-active control device have, in fact, the behaviour of passive mechanisms but they require a small amount of power energy to change the stiffness or damping of

the device. In most design cases of semi-active techniques the control forces track the forces that could be applied by an active control [2]. Therefore, a semi-active control device could achieve the performance of an active control system [1].

4. Conclusion

From point of energy balance view, the control strategy for a particular structure subjected to a dynamic excitation, involves a number of decisions as follows:

1. What is the admissible level with respect to the structure for the energy storage and the energy dissipated by viscous damping (E_{da})?
2. Which strategies should be implemented? Passive, active or semi-active system or a combination among these.
3. The type and mechanical properties of passive energy dissipation devices, which are appropriate for structural system and their locations.
4. If semi-active or active control mechanisms are used instead of passive devices or to supplement them, the type and capacity of control forces need to be specified and compared for certain cases. Also, there must be decided on the locations for the semi-active and active systems.

After the choice of a control mechanism, an experimental campaign must be conducted in order to find its real behavior. If unexpected characteristics of the device are seen, the control law must be modified in accordance. Once the control law is done and the mechanical properties of the device are known, the numerical simulations of the whole system (structure and control devices) must be performed.

The fundamental step is to conduct a specimen test with all the mechanical, electrical and structural limitations or problems that could be met in practical case.

The final step will be the implementation of the control strategy in real structure.

References

1. Marazzi, F. (2003). *Semi-active Control of Civil Structures: Implementation Aspects*. Phd thesis, University of Pavia, Structural Mechanics Department.
2. Preumont, A. (2002). *Vibration Control of Active Structures: An Introduction* 2nd Edition, Kluwer Academic Publishers.
3. Soong, T.T. and Spencer, B.F. (2002). *Supplementary Energy Dissipation: State-of-the-Art and State-of-the-Practice*. In *Engineering Structures*, Vol. 24, pp. 243–259.

PROBLEME SPECIFICE PRIVIND STABILITATEA CAII FARA JOANTE

Gavril KÖLLÓ¹, Mădălina CIOTLĂUȘ²

Rezumat

Calea este supusă unei varietăți de eforturi, complexitatea elementelor care compun cadrul șină-traversă, imperfecțiunile și neomogenitatea patului de piatră spartă fac dificilă determinarea atât pe cale experimentală cât și pe cale statistică a parametrilor necesari diferitelor metode de calcul.

Studiul comportării căii fără joante la temperaturi ridicate devine o necesitate din cauza faptului că în șină pot apărea tensiuni și fenomene cu caracter spontan și cu rezultate negative asupra siguranței circulației.

Rezistența căii la deplasarea transversală este dată de reacțiunea prismului de piatră spartă. În cazul unei căi bine întreținute, reacțiunea este suficient de mare ca să preia, fără deplasări, eforturile transversale la care este supusă în mod normal șina.

Stabilitatea căii în plan orizontal trebuie studiată în special în cazul curbelor unde tendința de pierdere a stabilității este favorizată de însăși geometria căii în plan. O cale supusă eforturilor de compresiune nu va fi niciodată perfectă, întotdeauna vor exista mici imperfecțiuni și defecte accentuate în timp de acțiunea materialului rulant.

În lucrarea de față sunt tratate câteva aspecte specifice privind stabilitatea căii sudate în aliniament punându-se accent pe rezistența laterală asigurată de prisma de piatră spartă pentru diferite tipuri de traverse utilizate.

1. Introducere

Stabilitatea șinei în planul orizontal trebuie studiată în special în curbe unde tendința de pierdere a stabilității spre exteriorul curbei este favorizată de însăși geometria căii în plan. O cale supusă eforturilor de compresiune nu va fi niciodată perfectă, existând întotdeauna mici excentricități și defecte agravate în timp de acțiunea materialului rulant.

¹ Prof, Universitatea Tehnica din Cluj-Napoca, kollo@yahoo.com

² Preparator, Universitatea Tehnica din Cluj-Napoca, ciotlaus_madalina@xena.utcluj.ro

2. Parametri de calcul

Efortul de compresiune din șină datorat temperaturilor ridicate, poate atinge valori apreciabile, moment în care se pune problema stabilității șinei.

Considerând intervalul temperaturilor de fixare ($17^{\circ}\div 27^{\circ}\text{C}$) corespunzător țării noastre, temperatura maximă care poate apărea în șină (60°C), în zona centrală a căii fără joante se poate dezvolta un efort considerabil :

$$P_{\max t} = \alpha \cdot E \cdot A(60^{\circ} - 17^{\circ}) = 1038.45 \cdot A \quad (1)$$

$$A = 2A_s \quad P_{\max t} = 2076.90A_s \quad (2)$$

Este necesar să se determine elementele de calcul ale căii fără joante pentru a putea preveni instabilitatea căii și a putea menține siguranța circulației.

Cu cât șina este mai grea (aria secțiunii transversale este mai mare), cu atât efortul crește mai mult. La eforturi mari, în anumite condiții, calea își pierde stabilitatea prin șerpuirea căii în planul de rezistență minimă (la suprastructurile moderne – planul orizontal).

Calea fără joante este considerată un cadru orizontal, înglobat în prismul de piatră spartă, fără a fi fixat, având o geometrie aparte (aliniamente și curbe spațiale).

Fenomenul de pierdere al stabilității este împiedicat atât de rigiditatea cadrului șine-traverse, cât și de rezistența dată de prismul de piatră spartă la deplasarea în plan transversal și longitudinal a căii.

Influența prismului de piatră spartă a fost determinată cu relația :

$$q = q_0 + C \times y \quad \text{dacă } y \leq y_0 \quad \text{și } q_p = q$$

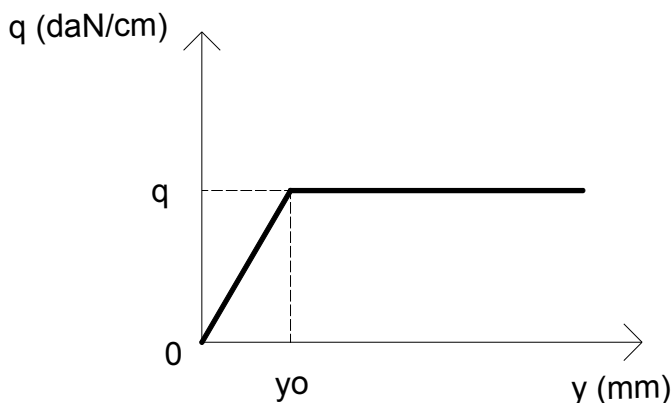


Fig.1 Rezistența laterală q la variația deplasării y

Forța critică de pierdere a stabilității a fost calculată folosind metoda energetică. Pentru cazul general (în curbă), forța critică de pierdere a stabilității este :

$$P_{cr} = \frac{K_1 \frac{EI}{l^2} + K_2 q_0 \frac{l^2}{f} + K_3 Cl^2 + \frac{2r}{a}}{1 + K_5 \frac{l^2}{fR}} \quad (3)$$

Pentru $R \rightarrow \infty$ (aliniament):

$$P_{cr} = K_1 \frac{EI}{l^2} + K_2 q_0 \frac{l^2}{f} + K_3 Cl^2 + \frac{2r}{a} \quad (4)$$

Unde:

K_1 - K_5 - constante pentru diferite tipuri de imperfecțiuni;

l – lungimea imperfecțiunii geometrice;

f – săgeata imperfecțiunii geometrice;

C – coeficient de proporționalitate a prismului de piatra spartă;

E – modulul de elasticitate al oțelului;

α – coeficient de dilatație liniară a oțelului;

A – aria secțiunii transversale a șinei; $A=2A_s$;

q – rezistența prismului de piatră spartă la deplasarea transversală a căii;

m – momentul distribuit; $m = \frac{2 \cdot M_r}{a}$

a – distanța dintre axele traverselor ;

r – coeficient ce caracterizează prinderea șinei pe traversă;

Forța critică P_{cr} depinde de constantele mai sus amintite și de două variabile : l și f :

Unde:

$f = \{f_1, f_2, \dots, f_m\}$ săgețile imperfecțiunilor geometrice

$l = \{l_1, l_2, \dots, l_n\}$ lungimile imperfecțiunilor geometrice

Forța critică de pierdere a stabilității căii depinde de rezistența la deplasarea laterală a cadrului șină – traversă (q). Ponderea acestei rezistențe este hotărâtoare pentru păstrarea stabilității căii.

În continuare se va prezenta comparativ pentru calculul simplificat (cu formula aproximativă a forței critice), ponderea procentuală a diferitelor componente ale forței critice pentru o suprastructură alcătuită din șine tip 60 și 65.

	f_1	f_2	.	f_i	.	f_m	
P_{cr}	P_{cr11}	P_{cr12}	.	P_{cr1i}	.	P_{cr1m}	l_1
	P_{cr21}	P_{cr22}	.	P_{cr2i}	.	P_{cr2m}	l_2

	P_{crk1}	P_{crk2}	.	P_{crki}	.	P_{crkm}	l_k
.	
.	
P_{crn1}	P_{crn2}	.	P_{crni}	.	P_{crnm}	l_n	

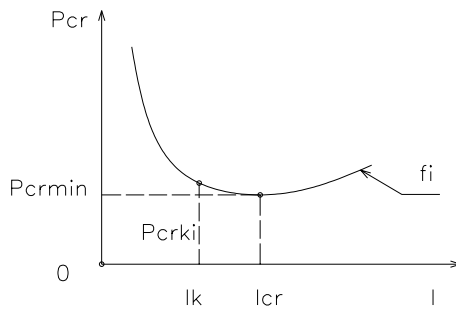
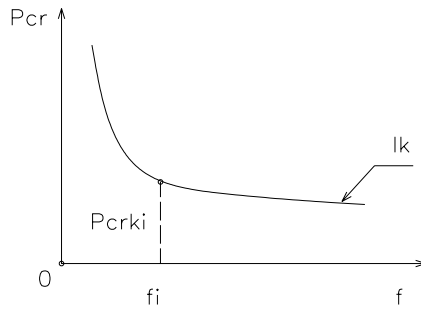


Fig. 2 Matricea forței critice de pierdere a stabilității

$r = 2 \cdot 10^6 \text{ daNcm}$ (în cazul buloanelor strânse la moment prescris)

$r = 0.3 \cdot 10^6 \text{ daNcm}$ (în cazul prinderilor slăbite),

$a = 0.65 \text{ m}$, $q = 7 \text{ daN/cm}$.

$$P_{crA} = 40 \frac{EI}{l^2} + \frac{2r}{a} + \frac{l^2}{10f} q$$

$$P_{crB} = 80 \frac{EI}{l^2} + \frac{2r}{a} + \frac{l^2}{39f} q$$

Tabel nr.1

Suprastructura	Tip defect	$\alpha \frac{EI}{l^2}$	$\frac{2r}{a}$	$\frac{l^2}{f} q$	$(\sum) P_{cr}$	Exprimare procentuala		
						1	2	3
60	E	9822	61538	787500	858860	1.1	7.2	91.7
	A	39289		630000	730827	5.4	8.4	86.2
	B	78578		161538	301654	26.1	20.4	53.5
65	E	10889	61538	787500	859927	1.3	7.2	91.5
	A	43556		630000	735094	5.9	8.4	85.7
	B	87112		161538	310188	28.2	19.8	52

Tabel nr. 2

Suprastructura	Tip defect	$\alpha \frac{EI}{l^2}$	$\frac{2r}{a}$	$\frac{l^2}{f} q$	$(\sum) P_{cr}$	Exprimare procentuala		
						1	2	3
60	E	9822	9230	787500	806552	1.22	1.14	97.64
	A	39289		630000	678519	5.79	1.36	92.85
	B	78578		161538	249346	31.5	3.70	64.78
65	E	10889	9230	787500	807619	1.35	1.14	97.51
	A	43556		630000	682786	6.38	1.35	92.27
	B	87112		161538	257880	33.8	3.58	62.64

Se poate observa ponderea importantă (peste 50%) a componentei care reprezintă rezistența prisme de piatră spartă la deplasarea transversală a căii $\frac{l^2}{f} q$. Din aceste considerente rezultă că utilizarea traverselor care asigură o rezistență transversală sporită este o necesitate obiectivă. Aceste traverse sunt traversa bibloc, traversa cadru din beton armat sau traversa metalică în Y.

Caracteristicile geometrice ale traversei metalice se prezintă în figura nr. 3.

Din cauza faptului că o cale alcătuită din traverse metalice în formă de de Y are o rezistență mai mare datorită rezistenței prismului de piatră spartă la deplasare transversală, se consideră :

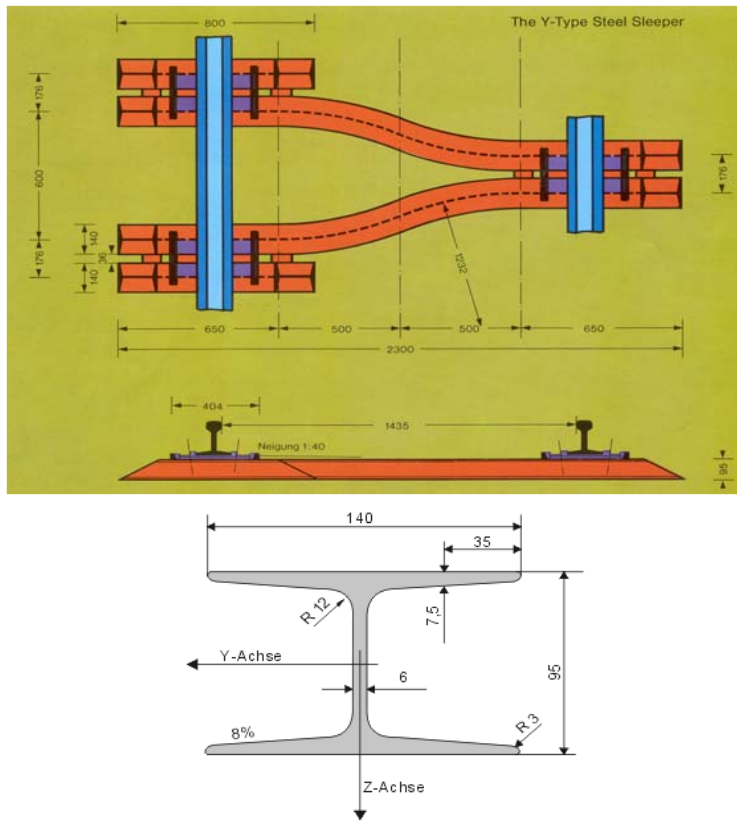


Fig. 3. Caracteristicile geometrice ale traversei metalice Y.

Tabel nr. 4

Traversă din beton	Traversă metalică Y
$q_0=3$	$q_0=4.5$
$C=3$	$C=6.5$
$r=0.3 \times 10^6$	$r=3 \times 0.3 \times 10^6$

Exemplu:

Pentru tipurile de imperfecțiuni B în aliniament și C în curbă, avem următoarele rezultate:

Forța critică de pierdere a stabilității pentru $f = 1.25$ cm, imperfecțiune tip B și C, șină tip 65

Tabel nr. 4

L(cm)	P _{cr} (daN)			
	TIPUL IMPERFECTIUNII: B		TIPUL IMPERFECTIUNII: C; R=1000M	
	Traversă din beton	Traversă metalică Y	Traversă din beton	Traversă metalică Y
100	20367278	20386604	48302106	48321430
500	849656	889740	12066725	12088628
1000	317381	422332	5360761	5386946
1500	335011	548075	4018705	5050845
2000	478443	842865	4940125	8979858

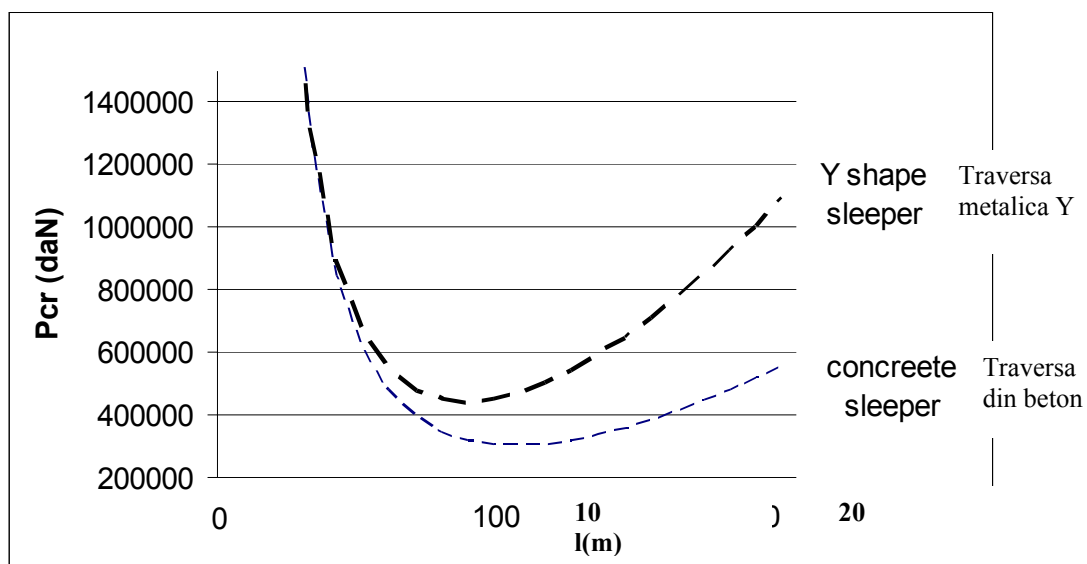


Fig. 4 Forța critică de pierdere a stabilității pentru traversa din beton și traversa metalică Y, pentru $f=1.25$ cm, tip imperfecțiune: B; șină tip 65.

3. Concluzii:

Traversa metalica Y are o rezistență mai mare la delapsarea laterală decât o traversă din beton. Un cadru format din șine și traverse metalice în formă de Y este de aproximativ 5 ori mai rigid decât un cadru format din șine și traverse din beton, rezultatul fiind un cadru mai rigid în special la stabilitate decât unul clasic compus din traverse din beton. Forța critică minimă de pierdere a stabilității este, în cazul unei suprastructuri clasice cu aproximativ 25% mai mică decât la o suprastructura cu traverse metalice în Y.

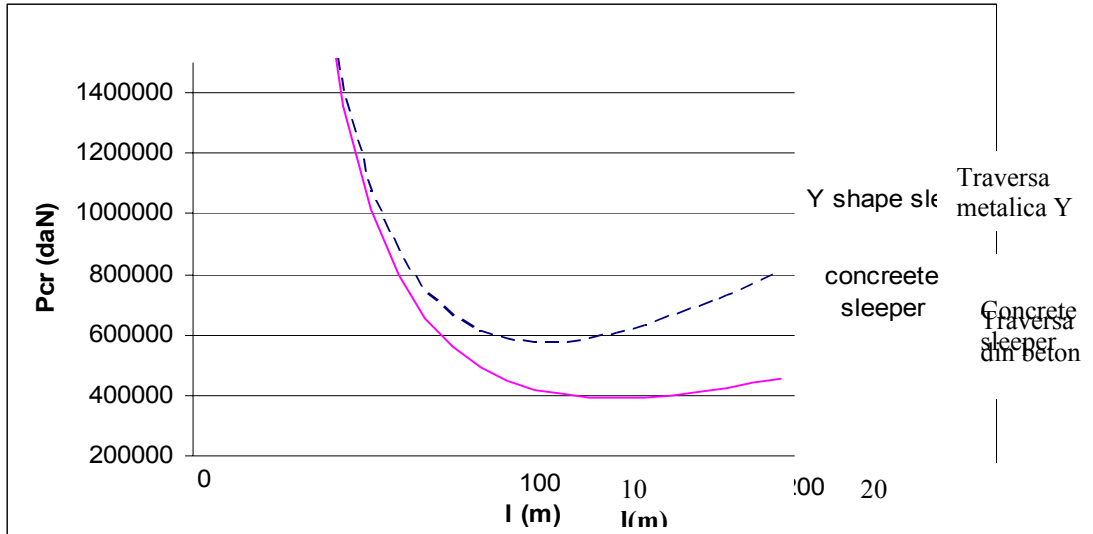


Fig. 5 Forța critică de pierdere a stabilității pentru traversa din beton și traversa metalică Y, pentru $f=1.25$ cm, tip imperfecțiune: C; șină tip 65.

Bibliografie:

1. Köllő Gavril - Considerente asupra stabilitatii caii sudate, Consfătuire pe țară a lucrărilor de căi ferate, drumuri și poduri, vol. 2, 1982
2. Köllő Gavril - Studiul stabilității căii fără joante in curbe cu raze mici, Sesiunea stiințifică jubiliară " 40 de ani de învățământ superior de construcții la Iași", 1981

ISBN 973-7962-50-8



MANIFESTARI STIINTIFICE